Determination of Dissolved Iron Speciation in the North East Atlantic Ocean by Flow Injection Chemiluminescence

by

Simon James Ussher

A thesis submitted to the University of Plymouth in partial fulfilment for the degree of

DOCTOR OF PHILOSOPHY

School of Earth, Ocean and Environmental Sciences

Faculty of Science

March 2005

Dedicated to Cécile and my family

Authors Declaration

At no time during the registration for the degree of Doctor of Philosophy has the author been registered for any other University award without prior agreement of the Graduate Committee,

The study was financed with the aid of a studentship from the Natural Environmental Research Council and funding from the EU registered IRONAGES Project (EVK2-CT1999-00031). A programme of advanced study was undertaken and relevant scientific seminars and conferences were regularly attended at which work was presented; external institutions were visited for consultation purposes and several papers were prepared for publication.

The work presented in this thesis was primarily the work of the author unless acknowledged otherwise. The method development for Fe(II) determination in seawater using Flow Injection Chemiluminescence was led by A. R. Bowie and supervised by E. P. Achterberg and P. J. Worsfold (Chapter 2) and all secondary author publications resulted from collaborative projects with the authors listed. All first author journal publications are indicated by the name of the author of this thesis being present first in the list of authors. Data from the thesis has been archived at the University of Plymouth and can be viewed by contacting the author (sussher@plymouth.ac.uk).

Word Count of main body of thesis

45,200 words

Signed:.....

Date.....13/12/05.....

Determination of Dissolved Iron Speciation in the North East Atlantic Ocean by Flow Injection Chemiluminescence

Simon James Ussher

The knowledge of iron biogeochemistry is constrained by paucity in the understanding of its uptake, transport and the partitioning of the element between different phases, redox states and coordination sites. The work presented in this thesis describes the optimisation and evaluation of a Flow Injection Chemiluminescence (FICL) method for the shipboard determination of dissolved Fe(II) species (< 0.2 μm) in seawater. This includes results from two ship-board trials and a study of the effects of model ligands on iron redox speciation measurements in natural waters. The method was also used to determine the distribution of dissolved iron species (< 0.2 μm) in two contrasting study areas in the North East Atlantic Ocean and for a study of aerosol iron dissolution in seawater.

The FI-CL method was evaluated and was found to be robust and sensitive, to have low limits of detection (5–12 pM) and short analysis times (~ 3 min) suitable for the high resolution spatial and temporal sampling required for shipboard analysis of Fe(II). A study of the effects of model ligands on Fe(II) determination revealed no conclusive evidence for significant interference from organic molecules on the method but Fe(III) in the presence of certain organic molecules had the potential to cause positive and negative interference in aqueous samples.

Field survey results obtained for a transect between the Bay of Biscay to the coast of the Netherlands, showed enrichment of dissolved iron (0.7 – 2 nM) on the European continental shelf in March 2002. Near the shelf break, the iron enriched shelf waters were separated from low iron open ocean surface waters (0.15 – 0.4 nM) by a well-defined mixing gradient. Elevated dissolved Fe(II) concentrations (> 100 pM) were observed at the shelf break and during a solar radiation maximum in the coastal waters of the southern North Sea. These features were attributed to the dissolution of Fe(II) from anoxic sediments and photoreduction of iron from dissolved and suspended particles, respectively.

In the surface waters of the Canary Basin in October 2002, low Fe(II) concentrations that varied from below the limit of detection of the FI-CL method (< 5 pM) to 60 pM were determined. A horizontal dissolved iron gradient (0.1 – 1.0 nM) inversely related to distance from the North West African coast was observed. It was hypothesised that the gradient was caused by the advection of enriched coastal and upwelled water, rather than by spatial variation in aerosol deposition. Preliminary aerosol iron dissolution experiments demonstrated the significance of the effect of dust loading and variation in seawater matrix on iron solubility.

In conclusion, continental margins were found to be a highly significant source of dFe in both study areas and evidence was found that a major portion comes from the reductive dissolution of iron in sediments. However, the flux of iron from shelf waters to the open ocean is likely to be dependant on several factors, such as the direction and magnitude of lateral and axial advection and the efficiency of scavenging and biological uptake in the surface waters.

Acknowledgements

I am indebted to my supervisors Paul Worsfold and Eric Achterberg for their superb guidance and vision, without whom, this work would not have been possible.

For field training, I would like to thank the 'iron gurus' Andy Bowie and Peter Sedwick for teaching me the ways of 'contamination free' sampling and analysis as well as other techniques such as "flow injection 'til you chuck" and the "hammer and chock method".

A big thank you to all our European friends involved in the 'Ironages' cruises, in particular; Patrick Laan, Hein de Baar, Klaas Timmermans, Stephan Blain, Agate Laes, Geraldine Sarthou, as well as Jurjen, Micha, Louis and Damiano, and the crews, officers and engineers who worked on-board the RNIOZ research ship "The Pelagia" during the cruises. I also wish to acknowledge external collaborators: Fauzi Mantoura, Tim Jickells, Alex Baker and Peter Statham.

Finally, I thank all my past and present colleagues at the University of Plymouth, especially; Martha Gledhill, Malcolm Nimmo, Geoff Millward, Alan Tappin, Charlotte Braungardt, Paul McCormack, Richard Sandford, Ian Doidge, Andy Arnold, Andrew Tomkin, Angie Milne, Mohammed Yaqoob, Utra Mankasingh, Laura Gimbert, Ndukaku Omaka, Vincenzo Cannizzaro, Paulo Gardolinski, Kate Howell and Grady Hanrahan, for contributing to the solid research base and friendly atmosphere found in the SEOES department and I wish everyone well for the future.

The funding for the work conducted here was provided as a part of the European Union 'Ironages' project (EVK2-CT1999-00031).

Posters and Oral Presentations

Primary author presentations:

'Monitoring iron in coastal and oceanic waters using an automated flow injection system with chemiluminescence detection' poster presented at:

Analytical Research Forum (RSC), UEA, July 2001

Progress in Chemical Oceanography (PICO) conference, Bangor, Wales, September 2001

'Shipboard monitoring of iron(ii) in coastal and oceanic waters using an automated flow injection analyser with chemiluminescence detection' poster presented at:

Analytical Research Forum (RSC), Kingston, July 2002

Challenger Centenary Conference: Marine Science 2002, Plymouth, September 2002.

'Redox speciation of dissolved iron in the North East Atlantic Ocean' poster presented at:

AGU Fall Meeting, Moscone Centre, San Francisco. December 2002.

'Speciation of dissolved iron in the North East Atlantic Ocean' oral presentation at:

EGS-AGU-EUG Joint Assembly, Nice, April 2003

'Effect of model ligands on iron redox speciation in natural waters using flow injection manifolds with luminol chemiluminescence detection' poster presented at:

Analytical Research Forum (RSC), Preston, July 2004

Secondary author presentations:

'Iron in the Sargasso Sea during summer: aeolian imprint, spatiotemporal variability, and ecological implications'

P. N. Sedwick, T. M. Church, A. R. Bowie, C. M. Marsay, S. J. Ussher,

Poster presentation at ASLO meeting, Hawaii, USA, 2005.

'Influence of high atmospheric inputs on the iron distribution in the water column of the North Atlantic Ocean'

G. Sarthou, P. Laan, S. Ussher, J.Kramer, K. R. Timmermans, S. Blain,

Poster presentation at EGS-AGU-EUG Joint Assembly, Nice, France, April 2003.

Journal Publications

'High temporal and spatial resolution environmental monitoring using flow injection with spectroscopic detection', G. Hanrahan, S. Ussher, M. Gledhill, E. P. Achterberg and P. J. Worsfold, *TRAC-Trends in Anaytical Chemistry,* **21(4),** (2002), 233.

'Real-time Monitoring of Picomolar Concentrations of Iron(II) in Marine Waters Using Automated Flow Injection - Chemiluminescence Instrumentation', A. R. Bowie, E. P. Achterberg, P. N. Sedwick, S. Ussher, P. J. Worsfold, *Environmental Science and Technology,* **36,** (2002) 4600.

'Direct Determination of Iron(II) in Seawater using a Matrix Matched Flow Injection Manifold with Chemiluminescence Detection', M. Yaqoob, S. J. Ussher, A. Nabi, E. P. Achterberg and P. J. Worsfold *Journal of Flow Injection Analysis,* **20,** 183-186 (2003).

'Detection of siderophores produced by mixed bacterioplankton populations in nutrient enriched seawater incubations' Martha Gledhill, Paul McCormack, Simon Ussher, Eric P. Achterberg, R. Fauzi C. Mantoura and Paul J. Worsfold, *Marine Chemistry,* **88,** (2004) 75– 83

'Marine Biogeochemistry of Iron – A Review', Simon J. Ussher, Eric P. Achterberg, Paul J. Worsfold, *Environmental Chemistry,* **1(2),** (2004), 67, doi: 10.1071/EN04053

'Design of an automated FI-CL instrument incorporating a miniature photomultiplier tube for monitoring picomolar concentrations of iron in seawater', A.R. Bowie, E.P. Achterberg, S. Ussher and P.J. Worsfold, *Journal of Automated Methods and Management in Chemistry,* (in press).

'Dissolved iron in the Sargasso Sea (BATS region): Seasonal aeolian imprint, small-scale spatiotemporal variability, and ecological implications', P. N. Sedwick, T. M. Church, A. R. Bowie, C. M. Marsay, S. J. Ussher, K. M. Achilles P. J. Lethaby1, R. J. Johnson, and D. J. McGillicuddy, *Global Biogeochemical Cycles,* 2005, (accepted).

'Effect of Model Ligands on the determination of Fe(II) in Natural Waters Using Flow Injection with Luminol Chemiluminescence Detection', S. J. Ussher, M. Yaqoob, E. P.Achterberg, A. Nabi and P. J. Worsfold, *Anaytical Chemistry,* (accepted January 2005).

List of Abbreviations

Speciation

Fe'	Labile inorganic iron species
FeL	Organically complexed iron species
dFe	'Dissolved iron', iron species that have passed through a 0.2 - 0.45 µm pore size filter (both Fe(II) + Fe(III)) and have been determined after acidification (pH ~ 2).
dFe(<0.02 µm)	'Soluble Iron', iron species passing through a <0.02 µm pore size filter (Fe(II) + Fe(III)), analysed after acidification (pH ~ 2)
TD-Fe	Total Dissolvable Iron, unfiltered, acidification after collection (pH ~ 2)
dFe (0.02-0.2 µm)	'Small Colloidal Iron', fraction determined by the difference between dFe and dFe(<0.02 µm).
Fe(II)	Dissolved Iron(II), <0.2 µm, analysed immediately after in-line filtration.
%Fe(II)	percentage fraction of Fe(II) in the dissolved iron (<0.2 - 0.45 µm) pool (e.g. %Fe(II) = [Fe(II)/(Fe(II) + Fe(III)] x 100%)
dAl	Dissolved aluminium species passing through a 0.2 - 0.45 µm pore size filter, analysed after acidification (pH ~ 2)
DOM	Dissolved organic matter
LFSE	Ligand Field Stabilisation Energy
ATP	Adenosine Triphosphate

Analytical / Experimental

FI	Flow Injection
CL	Chemiluminescence
FI-CL	Flow Injection Chemiluminescence
DI method	Determination of analyte by direct injection of sample into a reagent stream
ICP-MS	Inductively Coupled Plasma Mass Spectrometry
GF-AAS	Graphite Furnace Atomic Absorption Spectrometry
LOD	The limit of detection (3 x standard deviation of the blank)
nM	nmol L^{-1}

pM	pmol L^{-1}
VI	Virtual instrument (Labview™)
8-HQ	8-hydroxyquinoline
DMS	dimethyl sulphide
DMG	dimethylglyoxime
PTFE	poly(tetrafluoroethene)
Luminol	5-amino-2,3-dihydro-1,4-phthalazinedione
UHP water	Ultra High Purity water (18.2 MΩ cm^{-1})
Q- (e.g. HCl, HNO_3)	High purity, quartz distilled reagents
LISW	Low iron seawater
LNS	Low nutrient seawater
CASS	Coastal Atlantic Surface Seawater (certified sea water NRCC Canada)
NASS	North Atlantic Surface Seawater (certified sea water NRCC Canada)
Filtered	refers to filtration through 0.2 or 0.4 μm pore size filter
Ultrafiltered	refers to filtration through <0.02 μm or < 30 kDa pore size filter

Oceanographic

HNLC	High-nutrient, low-chlorophyll
ITCZ	Intertropical Convergence Zone
AABW	Antarctic Bottom Water
AAIW	Antarctic Intermediate Water
LNADW	Lower North Atlantic Deep Water
LSW	Labrador Sea Water
MNADW	Mid North Atlantic Deep Water
MOW	Mediterranean Outflow Water
NEADW	North East Atlantic Deep Water
SAF	Sub-Antarctic Front
SPMW	Sub Polar Mode Water
UNADW	Upper North Atlantic Deep Water

List of Contents

Title *Page*

Chapter 1.
Marine biogeochemistry of iron

1.1 Introduction 2
1.2 The significance of iron in the oceans 2
1.3 Iron speciation in seawater 6
1.3.1 The crustal abundance of iron 6
1.3.2 Dissolved inorganic iron speciation 8
1.3.3 Dissolved organic iron complexes in seawater 11
1.3.4 Dissolved iron complexation and redox transitions 12
1.3.5 The kinetics of iron(II) oxidation 15
1.3.6 Reduction of iron(III) in seawater 17
1.4 Iron inputs to the oceans 18
1.4.1 Fluvial inputs 19
1.4.2 Atmospheric inputs 20
1.4.3 Hydrothermal inputs 24
1.4.4 Sediment inputs 24
1.5 Iron cycling in the oceans 25
1.5.1 Vertical distribution 25
1.5.2 Iron uptake by marine organisms 27
1.5.3 Additional sources of bioavailable iron 30
1.6 Conclusions 31
1.7 Aims and objectives 33

CHAPTER 2.
Flow injection chemiluminescence methods for the determination of iron redox species in seawater

2.1 Introduction 35
2.2 The use of flow injection analysis in the marine environment 35
2.3 Determination of iron(II) and dissolved iron species in seawater using flow injection chemiluminescence (FI-CL) 39

2.3.1 Operationally defined iron fractions 39
2.3.2 Shipboard iron determination by Flow Injection - Chemiluminescence (FI-CL) 41
2.4 Automated FI-CL instrument for monitoring picomolar concentrations of dissolved iron and iron(II) in seawater **43**
2.4.1 Reagents and standards 44
2.4.2 FI analyser 45
2.4.3 Interface 48
2.4.4 Detector performance 50
2.4.5 Analytical figures of merit and blank measurement for dissolved iron 51
2.4.6 Dissolved iron determination in the field: Trial hydrocast 53
2.5 Automated monitoring of picomolar concentrations of dissolved iron(II) in surface seawater: field trials **55**
2.5.1 Sampling 56
2.5.2 Method chemistry 57
2.5.3 Blank measurement and calibration 58
2.5.4 System operation 59
2.5.5 Results and discussion 60
2.6 Direct determination of iron(II) in seawater using a matrix matched flow injection manifold with chemiluminescence detection **65**
2.6.1 Reagents and standards 65
2.6.2 FI manifold 66
2.6.3 Optimisation of FI manifold 67
2.6.4 Calibration and blank protocol 70
2.6.5 Interferences 71
2.6.6 Accuracy 71
2.7 Conclusions **72**

CHAPTER 3.

Effect of model ligands on iron redox speciation in natural waters using flow injection with luminol chemiluminescence detection

3.1 Introduction **76**
3.2 Experimental **78**
3.2.1 Reagents and solutions 78
3.2.2 Methods 80

3.2.3 Calibration 83
3.2.4 Blank measurements 83
3.2.5 Seawater samples 83
3.3 Results and discussion 84
3.3.1 Kinetic and equilibrium considerations for the complexation of nanomolar concentrations of Fe(II) and Fe(III) with organic compounds in high-purity water. 84
3.3.2 Effect of organic compounds on observed Fe(II) concentrations in water 86
3.3.3 Effect of organic compounds on observed Fe(II) concentrations in aqueous solutions containing Fe(III) 88
3.3.4 Effect of sample pH on Fe(III) interference for the DI method 89
3.3.5 Effect of organic compounds on the observed redox speciation in seawater 90
3.3.6 Effect of strong ligands on the determination of dissolved iron 91
3.3.7 Kinetics of sulphite reduction of iron in filtered (<0.2 μm) and ultrafiltered (<0.02 μm) coastal seawater 93
3.4 Conclusions 95

CHAPTER 4.
Iron speciation in the North East Atlantic Ocean

4.1 Introduction 99
4.2 Redox chemistry and Fe(II) measurements in the open ocean 99
4.3 Iron redox speciation models 101
4.3.1 Thermodynamic equilibrium model for oxic waters 102
4.3.2 Kinetic steady state model for oxic waters 103
4.4 Dissolved iron distributions in the North Atlantic Ocean 105
4.4.1 Hydrography 105
4.4.2 Surface waters 106
4.4.3 Intermediate waters 109
4.4.4 Deep waters 110
4.4.5 Residence time and transport 111
4.5 Conclusions 113

CHAPTER 5.
Redox speciation and distribution of dissolved iron on the European Continental Shelf

5.1	**Introduction**		**116**
5.2	**Sampling and methods**		**118**
	5.2.1	Cast samples	118
	5.2.2	Surface water sampling	119
	5.2.3	Operationally defined redox and size species	120
5.3	**Dissolved iron distribution**		**121**
	5.3.1	Vertical distribution of dissolved iron – Deep casts off the shelf	121
	5.3.2	Vertical distribution of dissolved iron on the shelf slope	123
	5.3.3	Horizontal distribution of dissolved iron along a transect between shelf waters and North East Atlantic surface waters	125
5.4	**Dissolved iron redox speciation**		**128**
	5.4.1	Vertical changes in iron redox speciation - off the shelf	128
	5.4.2	Vertical section of iron redox speciation on the shelf slope	131
	5.4.3	Surface redox speciation between shelf waters and North East Atlantic surface waters	133
5.5	**Conclusions**		**136**
	5.5.1	Dissolved iron distribution	136
	5.5.2	Dissolved iron redox speciation	137

CHAPTER 6.
Redox speciation and distribution of dissolved iron in the Canary Basin

6.1	**Introduction**		**140**
6.2	**Sampling and methods**		**141**
6.3	**Distribution of dissolved iron species in intermediate and deep waters**		**144**
6.4	**Distribution of dissolved iron and dissolved aluminium in intermediate and deep waters**		**147**
6.5	**Distribution of dissolved iron species in the euphotic zone**		**149**
	6.5.1	Hydrography	149
	6.5.2	Variation in the size speciation of dissolved iron	150

6.5.3 Effect of photosynthetic organisms on iron redox speciation in the euphotic zone 151

6.6 Distribution of dissolved iron species in near surface waters 153

6.6.1 Hydrography 153

6.6.2 Redox speciation and distribution of dissolved iron in surface waters 154

6.6.3 Distribution of dissolved iron in surface waters versus distance from the Western Saharan coast 155

6.6.4 Distribution of dissolved iron and dissolved aluminium in surface waters 156

6.7 Dust dissolution experiments 159

6.7.1 Experiment 1 – The kinetics of Fe(II) and dFe dissolution in seawater from atmospheric dust 160

6.7.2 Experiment 2 – Dissolved iron concentrations seawater equilibrated with dust 162

6.7.3 Experiment 3 – Dissolved iron concentrations in unfiltered and ultra-filtered seawater equilibrated with dust 164

6.8 Conclusions 166

CHAPTER 7.

Conclusions and suggestions for future work

7.1 Conclusions 170

7.1.1 Optimisation, trials and evaluation of an FI-CL method for the ship-board determination of dissolved Fe(II) in seawater. 171

7.1.2 Potential interferences from dissolved organic molecules to the FI-CL method. 171

7.1.3 Distribution of dissolved iron and redox speciation in two study areas in the north east Atlantic Ocean. 172

7.1.4 The significance of small colloidal iron (0.02 - 0.2 μm) in the dissolved iron pool of the euphotic zone of the Canary Basin. 175

7.1.5 Potential variables that affect the dissolution of iron from aerosol dusts in seawater. 176

7.2 Future work 176

REFERENCES 181

PUBLICATIONS 197

List of Figures and Tables

Figure no.	*Figure Title*	*Page*
Fig. 1.1	Gibbs free energies of formation ($-\Delta G_f$) for common inorganic iron compounds.	7
Fig. 1.2	Phase transfers of iron and related processes in seawater.	8
Fig. 1.3	Inorganic speciation model of dissolved Fe(III) species in seawater.	9
Fig. 1.4	Inorganic speciation model of dissolved Fe(II) species in seawater.	10
Fig. 1.5	Standard redox potentials of well-known iron complexes and redox buffering reactions that occur in oxic waters.	14
Fig. 1.6	Global iron transport.	19
Fig. 1.7	Dissolved iron (< 0.2 µm) profiles from the North-East Atlantic Ocean.	26
Fig. 1.8.	Free ion model for iron uptake by phytoplankton.	29
Fig. 2.1	FI analyser in the laminar flow hood of a ship clean container.	38
Fig. 2.2	The free radical oxidation pathway of luminol.	42
Fig. 2.3	FI-CL manifold for the determination of iron in seawater.	45
Fig. 2.4	Block diagram of the automated FI-CL instrument incorporating the main control unit and PMT interface.	47
Fig. 2.5	LabVIEW graphical user front panel for the automated virtual instrument.	49
Fig. 2.6	Wiring diagram showing the graphical code for instrument control and data acquisition.	49
Fig. 2.7	Effect of changing the PMT gain on the CL background emission, CL background peak-to-peak noise, analyte signal and signal-to-noise ratio with the instrument in direct injection mode.	51
Fig. 2.8	Shipboard calibration peaks and corresponding standard additions plot for iron over the range 0.2-1.0 nM.	52
Fig. 2.9	Typical depth profile of dFe and temperature in the upper water column of the Southern Ocean south of Australia.	54

Figure no.	*Figure Title*	*Page*
Fig. 2.10	Concentration of 8-HQ-reactive iron(II), dFe and the iron(II)/dFe ratio during a 10 h shipboard deployment in the Atlantic Ocean over the period 10:00-00:00 (UTC) on 20th October 2000.	62
Fig. 2.11	Concentration of 8-HQ-reactive iron(II), dFe and the iron(II)/dFe ratio during a 5 h shipboard deployment in the Southern Ocean over the period 21.00 on 10th December 2001 to 05.00 (UTC) on 11th December 2001.	64
Fig. 2.12	Flow injection with chemiluminescence detection (FI-CL) manifold for the determination of Fe(II).	67
Fig. 2.13	Effect of borate buffer pH on the peak response of the luminol CL reaction.	68
Fig. 2.14	Effect of luminol concentration on the determination of Fe(II).	69
Fig. 3.1	Flow Injection manifolds used for iron(II) determination.	81
Fig. 3.2	Calculated complexation of free metal ions (2 nM) with ligands versus first stability constant (K1)	85
Fig. 3.3	Iron(II) detected by the DI method and the 8-HQ column method after the reaction of inorganic Fe(II) with organic compounds in water after 4 h and 24 h.	87
Fig. 3.4	Iron(II) detected by the DI method and the 8-HQ column method after the reaction of inorganic Fe(III) with organic compounds in water after 4 h and 24 h.	89
Fig. 3.5	Fe(II) detected in aged Northeast Atlantic surface water after the addition of inorganic Fe(III) (20 nM) and organic compounds (200 nM).	90
Fig. 3.6	Fe(II) recovered over time from 2 nM Fe(III) solutions containing strong iron ligands after acidification (pH 2, HCl) and sulphite reduction (100 µM), using the 8-HQ method.	92
Fig. 3.7	Comparison of Fe(II) recovered from control solutions after 72 hours, using the DI method and the 8-HQ column method.	93
Fig. 3.8	Fe(II) detected after acidification and reduction of filtered and ultrafiltered coastal seawater.	94
Fig. 4.1	Summary of possible reactions of iron in surface waters.	104
Fig. 4.2	The Atlantic Ocean.	106
Fig. 5.1	Study area for the 'Iron from Below', Ironages Cruise March 2002.	117
Fig. 5.2	Schematic of ship-board sample processing.	120
Fig. 5.3	Salinity and dissolved oxygen versus potential temperature for deep water cast southwest of La Chapelle Bank (station 28).	121
Fig. 5.4	Vertical profiles showing the distribution of dFe and major nutrients off the European Continental Shelf in the NE Atlantic Ocean.	122
Fig. 5.5	Dissolved iron distribution over the south west European Continental Shelf	124
Fig. 5.6	Variation of surface dFe and salinity for a transect between the open ocean (8.0 °W, 35.9 °N) and the coast of the Netherlands (3.9°W 27.6°N).	126
Fig. 5.7	Effect of depth on surface dFe concentrations.	126

Figure no.	*Figure Title*	*Page*
Fig. 5.8	The influence of the continental shelf slope on the variation of dFe and salinity between the English Channel and open ocean surface waters.	127
Fig. 5.9	dFe versus salinity for surface waters between the English Channel (1.2 °E, 50.4 °N) and the North East Atlantic Ocean (8.0 °W, 35.9 °N).	128
Fig. 5.10	Vertical profiles showing the redox speciation of dFe near the European Continental Shelf in the NE Atlantic Ocean.	129
Fig. 5.11	Equilibrium model predicting dFe redox speciation assuming the free aqua ions and physicochemical data from station 28 (46.0 °N, 8.0 °W).	130
Fig. 5.12	Calculated Fe(II) fraction for varying standard reduction potential for surface (40 m 12.6 °C) and deepwaters (3000 m, 2.7 °C) at pH 8.0.	130
Fig. 5.13	Iron redox speciation and physico-chemical variables over the European Continental Shelf.	132
Fig. 5.14	Iron redox speciation, salinity and photosynthetic active radiation (PAR) in the European Continental Shelf surface waters.	134
Fig. 6.1	Study area for the 'Iron from Above', Ironages Cruise October 2002.	141
Fig. 6.2	World Aerosol optical depths for summer 2002 (0.47 microns, monthly means).	143
Fig. 6.3	Salinity versus potential temperature for a deep-water cast at Station 10 in the Canary Basin.	144
Fig. 6.4	Dissolved iron (dFe) and nutrient profiles for Station 10 (31.7 °N, 22.0 °W).	145
Fig. 6.5	Dissolved iron (dFe) redox and size speciation for Station 10 (31.7 °N, 22.0 °W).	147
Fig. 6.6	Vertical profile of dissolved iron (dFe) and aluminium (dAl) concentrations at station 10.	148
Fig. 6.7	Correlation between dissolved Fe and Al for station 10	148
Fig. 6.8	Salinity versus potential temperature for the euphotic zone (20 - 150 m) in the study area	149
Fig. 6.9	Histograms showing the frequency distribution of size fractionated dissolved iron species in the euphotic zone of the Canary Basin.	150
Fig. 6.10	Redox and size speciation of iron in the euphotic zone in relation to phytoplankton cell numbers and chlorophyll a concentrations	152
Fig. 6.11	Underway surface temperature and salinity data for the 'Iron From Above' cruise	153
Fig. 6.12	Dissolved iron and Fe(II) concentrations in the surface mixed layer of the study area	154
Fig. 6.13	Relationship between dFe concentrations in surface waters (3 - 6 m depth) versus the distance from the North West African coast.	155
Fig. 6.14	Relationship between dFe concentrations in the euphotic zone (0 – 150 m depth) versus the distance from the Western Saharan coast.	156
Fig. 6.15	Contour map showing sea-surface dissolved Al concentrations during the 'Iron from Above' cruise.	157

Figure no.	*Figure Title*	*Page*
Fig. 6.17	Dissolution of dFe and iron(II) from Turkish atmospheric dust into ultra-filtered (<30 kDa) and unfiltered surface seawater.	161
Fig. 6.18	Correlation between Fe(II) determined in ultra-filtered (<30 kDa) and unfiltered surface seawater.	162
Fig. 6.19	Variation in the solubility of iron (<0.2 mm) in unfiltered seawater with dust concentration	163
Fig. 6.20	Variation in the % soluble iron (<0.2 mm) in unfiltered seawater with dust concentration	164
Fig. 6.21	dFe concentrations in ultra-filtered and unfitered surface seawaters (D1 and D2) equilibrated with Turkish dust	165

Table no.	*Table Title*	*Page*
Table 1.1	Reported half-lives for iron(II) oxidation in natural and artificial seawater at 25°C.	16
Table 1.2	Percentage soluble iron in collected aerosols.	21
Table 1.3	Percentage soluble iron in collected precipitation.	22
Table 1.4	Redox speciation of iron in collected precipitation.	23
Table 2.1	Attractive features of FI for in situ environmental monitoring.	36
Table 2.2	Shipboard and submersible deployment of flow injection instrumentation with spectroscopic detection for monitoring marine environments.	37
Table 2.3	Operationally defined iron fractions used in this study.	40
Table 2.3	Specifications of miniature photon counting head.	46
Table 2.4	Timing sequence for one analytical cycle.	48
Table 2.5	Effect of various parameters on the CL peak response for the determination of 100 nM Fe(II).	70
Table 2.6	Calibration data.	71
Table 2.7	Effect of foreign ions on the CL peak response for the determination of Fe(II).	72
Table 2.8	Shipboard evaluation of automated FI-CL method.	73
Table 3.1	Classification of model organic compounds used in this study.	79
Table 3.2	Analytical parameters for the direct injection (DI) and 8-HQ column methods.	82
Table 4.1	Characterised surface and intermediate waters of the North East Atlantic.	107
Table 4.2	Characterised deep waters of the North East Atlantic.	110

Table no.	*Table Title*	*Page*
Table 4.3	Reported iron concentrations in Atlantic waters.	111

CHAPTER 1.

Marine biogeochemistry of iron

1.1 Introduction

The importance of the role of iron as a limiting micronutrient for primary production in the World Ocean has become increasingly clear following large-scale in situ iron fertilization experiments in high-nutrient, low-chlorophyll (HNLC) regions. [1] This has led to intensive international research with the aim of understanding the marine biogeochemistry of iron and quantifying the spatial distribution and transport of the element in the oceans. Recent studies have benefited from improved trace metal handling protocols and sensitive analytical techniques, but uncertainties remain concerning fundamental processes such as redox transfer, solubility, adsorption, biological uptake, and remineralization.

This chapter summarizes our present knowledge of iron biogeochemistry. It begins with a discussion of the effects of the physicochemical speciation of iron in seawater from a thermodynamic perspective, including important topics such as inorganic and organic complexation and redox chemistry. This is followed by an overview of the fluxes of iron to the ocean interface and a description of iron cycling within the open ocean water column. Current uncertainties of iron biogeochemistry are highlighted and suggestions of future work provided.

1.2 The significance of iron in the oceans

An estimated 40% of photosynthesis on Earth occurs in aquatic environments [2] and the turnover time for marine plant biomass is nearly three orders of magnitude faster than that of terrestrial biomass. [3] Hence, the nutrients that regulate primary production in the marine environment have a significant effect on the global carbon cycle and consequently play a key role in controlling the world's climate.

Protein-bound iron complexes act as vital electron mediators for many metabolic processes in living systems. Iron complexes have important functions in intracellular respiration, oxygenic and non-oxygenic photosynthesis, and the element is further utilized by respiring higher organisms for oxygen transport. [4] Within aquatic photosynthetic organisms, iron is found as an essential component in photosynthetic apparatus (i.e. photosystems (PSI, PSII) and cytochromes) and for ATP synthase. [3] It is also required for nitrogen fixation and reduction of nitrate, nitrite, and sulphate.

In most oceanic regions, primary production is limited by light and macro-nutrients (i.e. nitrate, phosphate, and silicate) but approximately 40% of the world's surface waters are replete with major nutrients. [5] These regions have been named HNLC areas, the most important regions being the Southern Ocean, the Equatorial Pacific, and the Subarctic Pacific.

The observation that neritic waters near these regions often sustained far greater phytoplankton communities compared to the nearby open ocean waters led early workers to hypothesize that trace elements are essential for phytoplankton growth. [6] For example, Harvey [7] suggested that iron and manganese could become growth-limiting to phytoplankton, based on experiments that showed increased growth of diatoms and dinoflagellates after additions of iron and manganese to Southern Ocean seawater that was rich in phosphate and nitrate. Despite these early observations, there were few major advances in the knowledge of the significance of iron in these areas until the late 1980s when the first reliable iron determinations were made in the Pacific Ocean as part of the VERTEX programme. [8-10] These measurements were made possible by the sampling and analytical techniques previously developed by Bruland et al. [11]

In addition to the vertical concentration profiles obtained at this time, ship-board experiments using iron additions to fresh seawater samples revealed that iron-limited regimes existed in the nutrient-rich, upwelling areas of the Subarctic and Equatorial Pacific. [12] Using the same methodology, it was also confirmed that there was a definite relationship between ambient iron concentrations and

phytoplankton growth in the Southern Ocean, when neritic (coastal) and pelagic (open ocean) waters were compared. [13]

In accordance with this, Martin published the 'Iron Hypothesis' in 1991. [14] This was based on an inverse correlation found between carbon dioxide and iron concentrations (inferred from aluminium data) in the Vostok ice cores. It was found that the trends corresponded with glacial and interglacial transitions. Martin proposed that an increase of iron input to HNLC oceanic regions, by means of higher dust loading, could stimulate primary production. Furthermore, it was suggested that this phenomenon had the potential to cause intense drawdown of carbon dioxide, reduce atmospheric temperatures, and hence cause significant global climate change.

The validity of this hypothesis has since been contested. Models based on global iron data and data from fertilization experiments estimated that realistic iron forcing could cause a maximum of ~50% of the CO_2 change expected during glacial–interglacial periods [15,16] but the remaining change was predicted to be due to other mechanisms, such as changes in ocean circulation and sea-ice extent. In addition, examination of sediment cores in the North Atlantic Ocean indicated that dust deposition fluxes in the Northern Hemisphere at the time of the penultimate deglaciation do not correlate with the change in CO_2 concentration in the Vostok ice cores. [17] However the affirmation of iron-limited HNLC areas, combined with the correlations observed in the Vostok ice cores, provide evidence that iron distribution is at least potentially an important control for global primary productivity and climate.

The fact that deck incubation experiments did not represent large-scale biological processes in the ocean, along with the development of artificial conservative tracers (i.e. SF_6) led to the instigation of in situ iron fertilization experiments. These have now been conducted in the Equatorial Pacific (e.g. IronEx I and IronEx II [1,18–20]), the Southern Ocean (e.g. SOIREE [21] and SOFeX [22]) and the Subarctic Pacific (e.g. SEEDS [23]), showing that primary productivity is iron-limited in these areas. In recent years, it has also become apparent that iron may play a vital intermediary role in nutrient cycling in low and mid-latitudes due to its involvement in nutrient cycling processes, such as nitrogen fixation. Iron-

limited growth has been found in coastal upwelling areas [24-27] and iron co-limitation has been observed in areas such as the Northeast Pacific Ocean [28] and the Northwest Indian Ocean. [29]

General conclusions about HNLC waters drawn from these experiments were:

1. The long-term fate of sequestered carbon remains uncertain, i.e. no evidence of significant carbon export to deep waters has been observed.
2. The efficiency of iron cycling depends on the conditions and ecology of the area. [30]
3. Zooplankton grazers were often quick to respond to increased numbers of phytoplankton.
4. Certain phytoplankton species benefited more from iron addition (usually large diatoms and flagellates).

There is increasing evidence that the extent of iron limitation in a given water mass is likely to vary according to the species of organisms present in natural assemblages. This variation contributes to the increasing complexity of defining 'nutrient limitation' when discussing marine ecosystems.

Following the success of iron fertilization experiments, the possibility of industrial-scale iron fertilization of the oceans has been discussed as a means of reducing atmospheric CO_2 concentrations. [31] However, a number of possible ecological effects caused by large-scale iron fertilization have been predicted, such as denitrification and nitrate reduction, production of climate changing gases, and anoxia. [32] Furthermore, although CO_2 drawdown has been observed in many of the iron fertilization studies mentioned above, there is at present no conclusive evidence that fertilization increases carbon burial fluxes over long timescales.

Recent attempts to implement international emission targets (such as the Kyoto Agreement) have created the potential for an industry based on the reduction of greenhouse gases. This controversial industry would allow emission targets to be exceeded by a country if it could prove that the excess gases, such as CO_2, were actively being removed from the atmosphere. Due to this, certain organizations, which have foreseen the economic gain from ocean fertilization, have been requesting

authorization to begin regular large-scale fertilization [31,33] even though there is no proof that fertilization will cause long-term drawdown of CO_2. The possibility of industrial-scale ocean fertilization has initiated considerable response from the scientific community, including public warnings of the unknown ecological effects and protests against countries assuming the right to 'use the world's oceans to resolve its domestic problems'. [34]

Clearly, the study of iron and macronutrients in marine biogeochemical cycles has become of great scientific, ecological, and political significance. It follows that to improve our understanding of important issues, such as the physicochemical transformations of iron occurring in seawater and the large-scale biological feedback mechanisms that may influence global climate, a detailed knowledge of iron biogeochemistry, transport, and distribution is required.

1.3 Iron speciation in seawater

1.3.1 The crustal abundance of iron

Iron is the fourth most abundant element in the Earth's crust, exceeded only by oxygen, silicon, and aluminium. Its high relative abundance of 5.6% [35] in the Earth's crust can be attributed to the highly stable ^{56}Fe nucleus. This is the largest nucleus formed exothermically by nuclear fission during planetary formation and is known to have the highest nuclear binding energy per nucleon of all nuclei. [36] Iron has six known isotopes, from ^{54}Fe to ^{59}Fe. The percentage abundances of the more common isotopes ^{54}Fe, ^{56}Fe, and ^{57}Fe are 5.82, 91.66, and 2.19% respectively, resulting in a relative atomic mass of 55.847 amu. [37] Due to its high crustal abundance, iron compounds make up a large proportion of the Earth's rocks and soils. Iron forms salts with most inorganic anions in the solid phase but exists predominantly as oxides and carbonates, stabilized by their negative Gibbs free energies of formation (Fig. 1.1).

The most commonly occuring compounds in iron ores are haemetite (Fe_2O_3), magnetite (Fe_3O_4), limonite ($2Fe_2O_3 \cdot 3H_2O$), siderite ($FeCO_3$), and pyrite (FeS_2). [38] Due to the high stability of these compounds, efficient separation of iron from its ores requires highly energetic and strongly reducing conditions. Further still, it goes some way in explaining why, despite being ubiquitous in the Earth's crust, iron is found at trace concentrations within many aqueous environments.

Figure 1.1. Gibbs free energies of formation ($-\Delta G_f$) for common inorganic iron compounds. Plotted using tabulated values from Stumm and Morgan.[39]

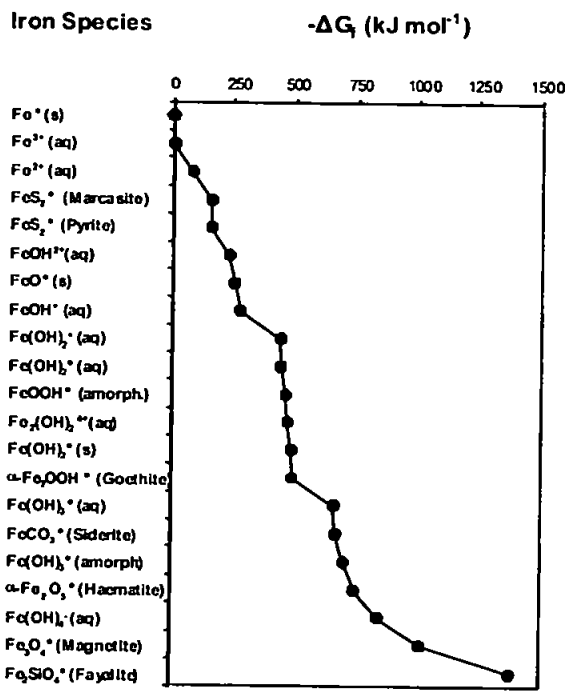

The physicochemical speciation of iron in seawater is dependent on the heterogeneous equilibrium between various particulate and dissolved phases (see Fig. 1.2). The concentration of iron in the solid and particulate phases is therefore dependent on the rate of each process and the composition of the seawater. These processes are further complicated by the existence of redox transitions between the ferric and the more soluble ferrous forms.

In order to understand the processes that control iron marine biogeochemistry, the species that are investigated must be clearly defined. Size fractionation is particularly important due to the broad variety of iron species that are thought to exist in seawater, including colloidal phases and macromolecules. Historically, dissolved iron has been defined as iron which passes through a 0.4 μm pore size filters and the recent development of ultra-filtration techniques allows improved characterization of different size fractions. [40,41]

Figure 1.2. Phase transfers of iron and related processes in seawater.

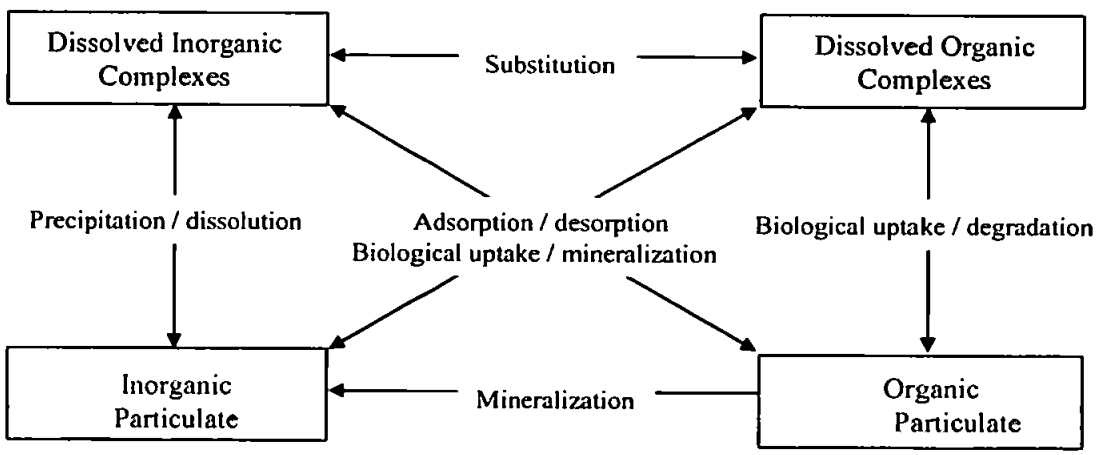

1.3.2 Dissolved inorganic iron speciation

Under most natural conditions, iron is found in the +2 and +3 oxidation states and forms salts with the majority of common anions. In aerated aqueous solutions at circum-neutral pH the hexa-aqua iron(III) cation becomes hydrolyzed, followed by the formation of polynuclear oxy-hydoxides. As a result, when the pH of an acidic solution is increased the solubility of the ions decreases, reaching a minimum at around pH 8. A solubility value of $\sim 10^{-11}$ M has been reported for 0.7 M NaCl solutions (pH 8.1,

25°C) where soluble iron was defined as that which passed through a 0.02 μm filter. [42] The solubility of iron(II) far exceeds that of iron(III). Under anoxic conditions, iron(II) is often found at millimolar concentrations but in air-saturated solutions and at high pH (> 5) it becomes unstable and oxidizes rapidly.

Figure 1.3. Inorganic speciation model of dissolved Fe(III) species in seawater. Calculated using the hydrolysis stability constants of Liu and Millero[47] measured in seawater and the chloride stability constants of Millero et al.[44]

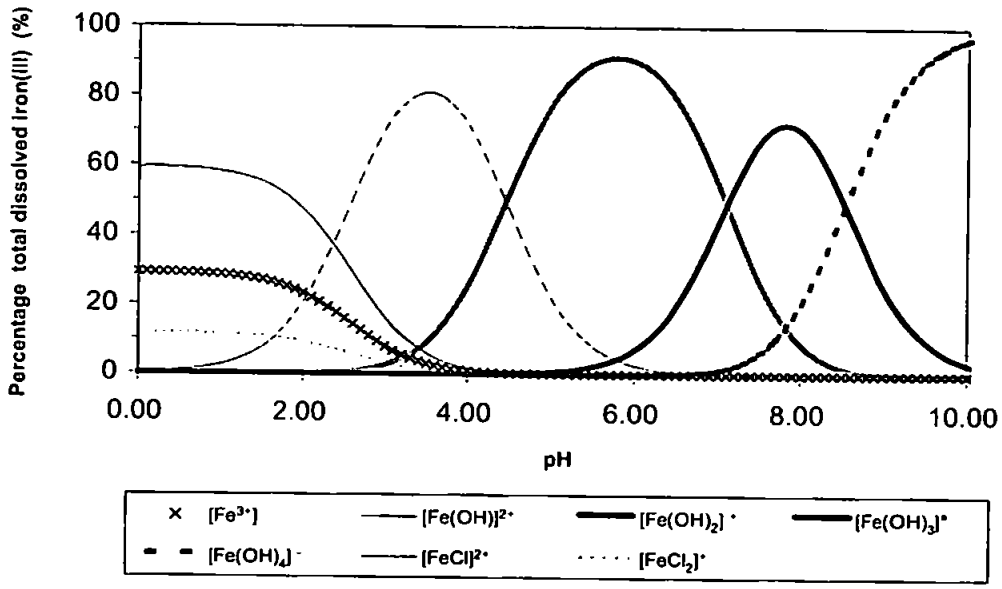

The dissolved inorganic speciation of iron in seawater can be estimated using experimentally determined equilibrium constants (conditional stability constants), found for the most common inorganic iron species in seawater. [43–47] The speciation diagrams (Figs 1.3 and 1.4) show the calculated proportions of inorganic iron(III) and iron(II) species in seawater at 25°C; recently reported hydrolysis constants were used.

Figure 1.4. Inorganic speciation model of dissolved Fe(II) species in seawater. Calculated using the hydrolysis stability constants of Millero et al.[44] measured in seawater. Dissolved inorganic carbon modelled as an open system in equilibrium with the atmosphere under ambient conditions.

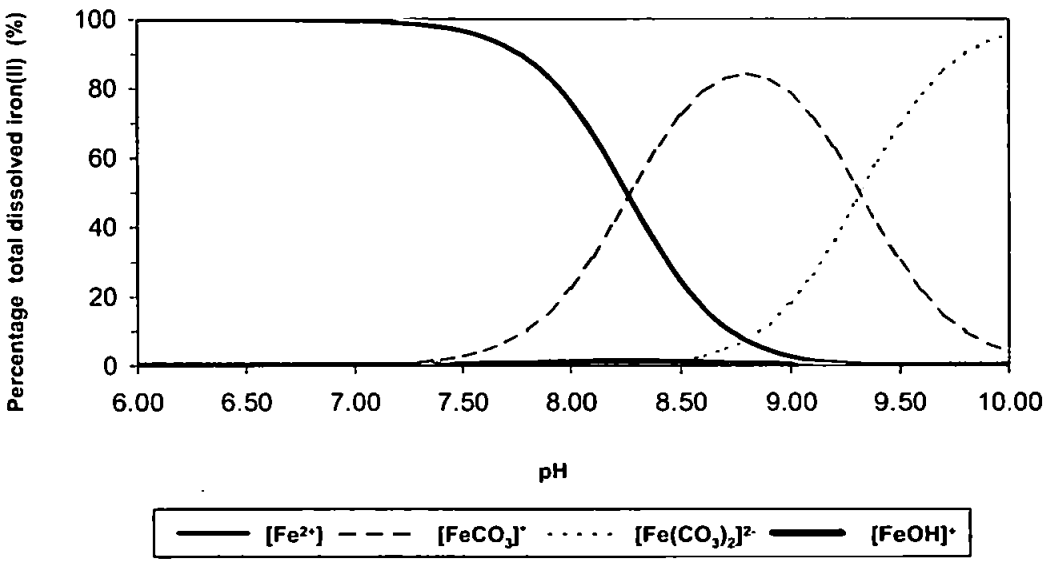

An ambient seawater chloride concentration (0.55 M) was used in the iron(III) model (Fig. 1.3) to represent an example of one of the simple anions that exist at high concentrations in seawater and associate with iron(III). At low pH, sulphate and fluoride behave in a similar manner. The most important trend to note is that the hydrolysis species are predicted to dominate when the pH value of the solution is greater than 4. This is due to the increase in activity of hydroxide anions at higher pH and the strong affinity of iron(III) for charged oxygen species as ligands.

Iron(II) behaves very differently, having relatively weak associations at pH values less than 7. At higher pH, inorganic complexation occurs when carbonate and hydroxy anions are more abundant. Interestingly, the solubility of iron(II) is predicted to be dependant on whether the seawater is in equilibrium with the atmosphere due to the formation of the insoluble $FeCO_3$ (siderite) species. Fig. 1.4 shows an open system in which there is considered to be continuous CO_2 exchange.

1.3.3 Dissolved organic iron complexes in seawater

Iron(III) has been found to be > 99% complexed by strong organic ligands in seawater, even in intermediate and deep waters, [48-52] and two classes of strong iron-binding ligands (L_1, L_2) have been characterized and determined in open ocean seawaters. The complexing ability of iron-binding ligands is measured under ambient conditions and is expressed using conditional stability constants $K_{Fe^{3+}L}$ from the equilibrium of Eqn (1.1):

$$K_{Fe^{3+}L} = \frac{[FeL]}{[Fe^{3+}][L]} \qquad (1.1)$$

A recent study of iron binding ligand stability constants in seawater summarized constants for all classes of ligands obtained in nine different oceanic regions. [53] The overall mean ($\pm 1\sigma$) $\log K_{Fe^{3+}L}$ for all the data reported was 21.4 ±1.5 and the range of ligand concentrations [L] was 0.31–39.2 nM. All workers used similar methodologies; therefore it can be assumed that these values are representative iron-binding ligands in most oceanic regions. The consistency of these values with other thermodynamic data can be validated with the inorganic iron speciation model (e.g. Fig. 1.3). For example, if a theoretical ligand concentration [L_1] of 1 nM and the mean reported value of $\log K_{Fe^{3+}L}$ (shown above) are used, 99.8% of the total iron(III) is predicted to be bound by organic ligands at pH 8.0, similar to that observed in seawater samples (> 99%). Therefore the presence of strong organic chelation has a significant effect on the speciation and solubility of iron in seawater.

Evidence that organic complexation increases iron solubility in seawater has been reported for 0.7 M NaCl solutions after the addition of humic acid and EDTA [42] and for seawater exposed to ultraviolet (UV) light. Furthermore, Kuma et al. [54] found that the solubility of iron in oceanic water exposed to UV for 3 h was reduced by one order of magnitude. A comparison of the effect of UV treatment on

coastal and open ocean waters as well as surface waters and deep waters was also described. The results indicate that although the binding constants of strong organic iron ligands are similar, some are more resistant to UV radiation.[45,54]

1.3.4 Dissolved iron complexation and redox transitions

The chemistry of the ferrous and ferric cations is extensive and a broad range of stereochemistries have been observed for natural and synthesized iron(II) and (III) complexes with coordination numbers from four to ten.[38] Iron(II) and (III) cations share similar characteristics but the effect of the difference of a single electron on the chemistry of both cations is considerable (i.e. difference in d^5 and d^6 configurations). One example is the effect on the size of their ionic nuclei; iron(II) has reported ionic radii of 0.75–1.06 Å whereas iron(III) is 0.63–0.92 Å. [56] Furthermore, the differences in their aqueous chemistry are best explained in terms of the free energies of the cations themselves and the ligand field stabilization energies (LFSE) of their bonding orbitals.

With a few exceptions (such as distorted complexes found with some stronger ligands) both cations are most often found in high- and low-spin octahedral states. The importance of the variation in LFSE should be emphasized as it can be used to explain the stability of oxidation states in different ligand fields. This is particularly true when comparing high- and low-spin compounds. For example, iron(II) in a high-spin state has a relative LFSE of $\Delta° = 2/5$, whereas in a low spin state it has a LFSE of $\Delta° = 12/5$, therefore gaining considerable stability in higher ligand fields where the effect of spin-pairing energy becomes less significant.

Iron(III) retains a high-spin, octahedral configuration in most of its complexes except with ligands that are high in the spectrochemical series. The high LFSE generated when bonding with ligands of this kind can cause spin-pairing in the t_{2g} orbitals (e.g. with bipyridyl and cyanide anions). [56] Iron(III) is a hard metal ion, acidic in nature, and forms its strongest complexes with O, N, and F donor ligands, particularly when they are negatively charged. Most iron(III) complexes absorb photons in the UV end

of the spectrum and are often colourless due to the spin-forbidden nature of the d–d transitions. Iron(III) also forms strong chelates and a large variety of cluster compounds either with other iron(III) atoms or other transition metals directly or through oxo and hydroxo bridges.

Iron(II) is a borderline metal ion, between hard and soft cations, and forms complexes that are often coloured. It therefore gains stability in complexation with both soft bases, such as P or S ligands, as well as the stronger electron-pair donating ligands that bind strongly with iron(III). Similar to iron(III), iron(II) is most commonly found in the high-spin state but forms fewer complexes with O-donor ligands. Iron(II) gains the greatest LFSE in low-spin octahedral complexes with strong π-acceptor ligands such as cyanide and 1,10-phenanthroline.

To understand the redox equilibrium between aqueous inorganic iron species in seawater, both redox states must be considered with varying pH and electron activity (pE). [57] Oxic inorganic solutions at seawater pH, are predicted to contain negligible iron(II) concentrations at equilibrium. [39] However, due to the high percentage of organically complexed iron species in seawater, the dissolved iron redox speciation may not be controlled by the pH-dependant equilibria of free hydrolysis species but by the effect of pH and pE on the organic complexes formed in seawater. This type of thermodynamic control would mean that the iron redox speciation in seawater is dependant on the physicochemical properties of the organic complexes present.

The reduction potentials of individual iron complexes can be used to estimate the equilibrium ratio of iron(II) and (III) species under different conditions. Complexes with high reduction potentials will favour iron(II) whereas those with low reduction potentials will favour iron(III) (see Fig. 1.5). The redox speciation of individual iron species under oxic conditions can be calculated using Eqn (1.2):

$$pE_{O_2/H_2O} = pE^{\circ}_{Fe(II)/Fe(III)} - \log\frac{[Fe(II)]}{[Fe(III)]} \qquad (1.2)$$

Where pE_{O_2/H_2O} is the pE of the water and oxygen couple and $pE^{\circ}_{Fe(II)/Fe(III)}$ is the standard reduction potential of defined Fe(II) and Fe(III) complexes. Using equation 1.2 and a pE range for oxic seawater of between 13–14.5, (assuming pH 7.6-8.1 and temperature 2-15 °C, see section 5.4), the standard reduction potential (E_H°) required to give an equilibrium ratio of 0.01 for [Fe(II)]/[Fe(III)] in seawater would be greater than 0.65 V, which is higher than the reduction potentials of most natural iron-binding chelates (e.g Fig.1. 5).

Figure 1.5. Standard redox potentials of well-known iron complexes and redox buffering reactions that occur in oxic waters.

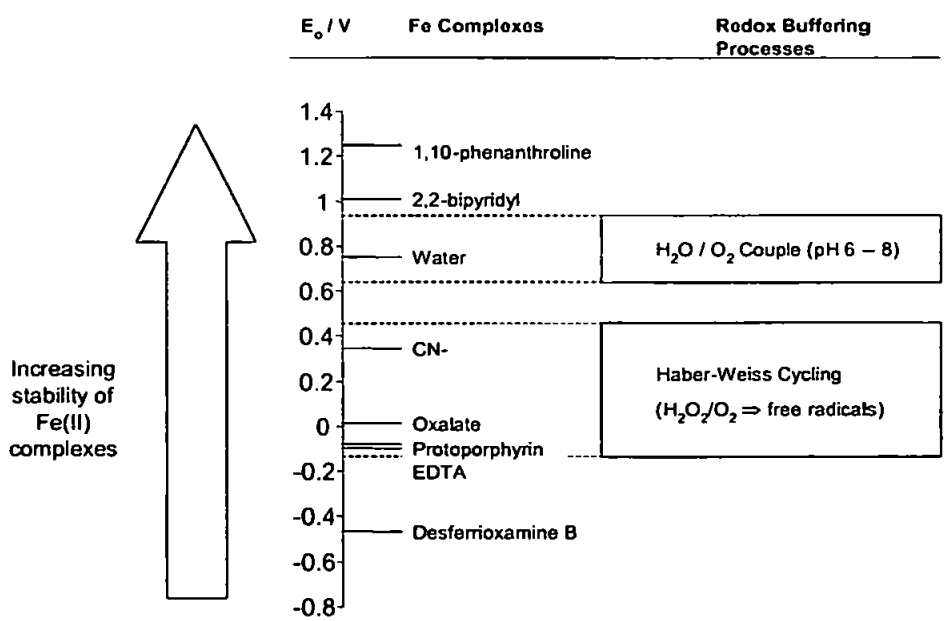

Indeed, recent thermodynamic data have shown that a large proportion of naturally occurring strong iron-binding ligands (such as porphyrins and siderophore–iron complexes) have reduction potentials that are significantly lower than 0.65 V [58,59] and are unlikely to stabilize iron in the ferrous form in

oxygenated seawater. However many of these complexes are more reactive and soluble than the inorganic hydrolysis species, and therefore may be reduced by processes such as Haber–Weiss cycling and photoreduction, hence kinetic models are often adopted to estimate iron redox speciation.

1.3.5 The kinetics of iron(II) oxidation

The kinetics of oxidation of iron(II) have been investigated in natural [60–64] and artificial seawaters. [65] Millero and coworkers [61] confirmed that oxidation rate constants have a positive relationship with pH and temperature, and all workers have found the pseudo-first-order half-life of iron(II) in natural and artificial seawater at ambient conditions (pH 8, 25°C) to be in the order of minutes (see Table 1.1).

The oxidation of iron(II) is reported to proceed predominantly according to the Haber–Weiss mechanism,

$$Fe(II) + O_2 \xrightarrow{k_1} Fe(III) + O_2^{\bullet -} \qquad \textit{step 1}$$

$$Fe(II) + O_2^{\bullet -} + 2H^+ \xrightarrow{k_2} Fe(III) + H_2O_2 \qquad \textit{step 2}$$

$$Fe(II) + H_2O_2 \xrightarrow{k_3} Fe(III) + HO^{\bullet} + OH^- \qquad \textit{step 3}$$

$$Fe(II) + HO^{\bullet} \xrightarrow{k_4} Fe(III) + OH^- \qquad \textit{step 4}$$

for which Eqn (1.3) expresses the rate equation for a solution of defined pH, temperature, and salinity:

$$\frac{-\,d[Fe(II)]}{dt} = 2\,k_1[O_2][Fe(II)] + 2k_3[H_2O_2][Fe(II)] \qquad (1.3)$$

The Haber–Weiss mechanism illustrates the importance of dissolved oxygen and hydrogen peroxide on iron(II) oxidation rates. Other inorganic side reactions, such as those of superoxide and redox-active transition metals (e.g. copper), have also been shown to be important but the most significant rate-determining step in the oxidation mechanism remains the reaction of inorganic and organically complexed iron with molecular oxygen. [63]

Table 1.1 Reported half-lives for iron(II) oxidation in natural and artificial seawater at 25°C

Medium	pH	$t_{1/2}$ [min]	Ref.
North Sea Seawater	8.0	1.5	[60]
Gulf Stream Seawater	8.0	1.2	[61]
Australia (NSW), Coastal Water	8.09	3.5	[63]
0.7 M NaCl	7.83	~1	[65]

The relationship between the speciation of iron(II) and its oxidation rate has gained considerable attention. King et al. [66,67] and Millero et al.[61,62] have described the effects of inorganic speciation, focussing mainly on the common inorganic iron complexes in seawater. Results show that species such as $FeCl^+$ alter the oxidation rate but the most striking observation was the increase in the rate for carbonate and hydroxy species, which form a significant fraction of the inorganic ferrous species at higher pH (> 7). Similar to the thermodynamic treatment above, an estimation of whether a complexed ligand will decrease or increase the oxidation rate of iron(II) can be estimated by comparing the equilibrium constants, ΔG_F values, or reduction potentials of the iron(II) and (III) species.

In accordance with this, organic ligands have been found to both stabilize and promote the oxidation of iron(II). Generally, oxygen ligands that form highly stable iron(III) complexes (e.g. EDTA, NTA, citric acid, desferrioxamine) are found to increase the rate of iron(II) oxidation whereas nitrogen or sulphur ligands inhibit it. [68] At circum-neutral pH, organic compounds commonly found from biological decay

have been seen to retard the oxidation of iron(II) for up to several days.[69,70] A study of the effects of some common amino acids on iron(II) oxidation at pH 6–8, revealed cysteine to be among these compounds,[71] whereas naturally occurring strong iron-binding ligands such as fulvic acid and oxalate have shown an accelerating effect.[63,72]

1.3.6 Reduction of iron(III) in seawater

Despite thermodynamic redox speciation calculations predicting negligible concentrations of iron(II), the dynamic and variable chemistry of seawater means that this is not always the case. Physicochemical reduction processes of iron in seawater have been observed to cause significant pseudo-steady-state concentrations of Fe(II) to persist under natural oxic conditions.

The most studied physicochemical process of iron(II) production in surface seawater is photoreduction. This occurs when UV irradiation causes direct and indirect photoreduction of colloidal and dissolved ferric species. Indirect photoreduction results from the reaction of iron(III) with reducing species produced during irradiation, whereas direct photoreduction refers to ligand–metal charge transfer (LMCT) reactions caused by photon absorption by iron complexes. Direct photoreduction is known to reduce the monohydroxide ferric species [73] and a number of organically complexed dissolved species via LMCT reactions (see ref. [74] and references therein), including certain siderophore chelates. [75]

Reduction of iron complexes is important in surface seawater as most of the dissolved iron is organically complexed, and reductive dissociation in the presence of phytoplankton may provide a source of bioavailable iron to phytoplankton. [50,75] In addition, several studies have shown the importance of the photoreduction of colloidal iron in seawater [76–79] although the nature of the colloids that promote photoreduction in seawater is unknown.

Diel variations of subnanomolar (0.1–1 nM) concentrations of iron(II) in naturally irradiated coastal water have been observed. [81] However, according to the model formulated by Johnson et al.,[80] photo-produced concentrations of iron(II) in fully irradiated surface waters of open ocean gyres are likely to be in the picomolar range or less (assuming dFe concentrations) are ~0.15 nM, which is typical in the Equatorial Pacific).

Biomediated reduction is another process that can generate iron(II) in seawater, although it is unlikely to be as efficient as photoreduction in surface waters. The bioreduction of ferric species is a well-known phenomenon of subsurface bacteria found in terrestrial and marine sediments. Laboratory studies using cultured bacterial strains (e.g. *Shewanella putrefaciens* [82,83] and *S. alga* [84]) have shown significant reduction rates of ferric colloids under anaerobic conditions. In addition, recent evidence of cell surface reduction has been found for several species of marine phytoplankton (see below) and the chemical reduction of iron by natural organic matter (NOM) has also been observed at pH 3–6, in the absence and presence of light [85] and in the presence of bacteria. [83] Further laboratory and in situ studies are required to confirm whether or not the chemical and biomediated processes mentioned above produce iron(II) at rates that are rapid enough to maintain significant steady-state concentrations of iron(II) in oxic seawater.

1.4 Iron inputs to the oceans

Iron is transported to the ocean via three major pathways: fluvial (riverine) input, atmospheric deposition, and processes occurring on the sea floor such as hydrothermal venting, sediment resuspension, and diagenesis (see Fig. 1.6).

To be transported by any of these pathways, iron must firstly become mobilized from the lithosphere by either mechanical action (i.e. erosion) or by thermal and chemical reactions (i.e. leaching, anoxia, or

geothermal activity). Once in a mobile phase, many physicochemical processes can occur, altering properties such as solubility and chemical speciation, between the source–ocean interface. Further understanding of the global iron cycle will be gained by determining fluxes of iron to/in the water column of the open ocean and by assessing its transport in marine ecosystems.

Figure 1.6. Global iron transport. Ambient concentrations of dissolved iron (dFe) and particulate iron (Fe) are in white boxes, and approximate annual fluxes are shown in black and white arrows. Approximate values are deduced from refs [86–90,94-96]. Riverine flux is estimated on the basis of 90% loss from estuarine mixing.

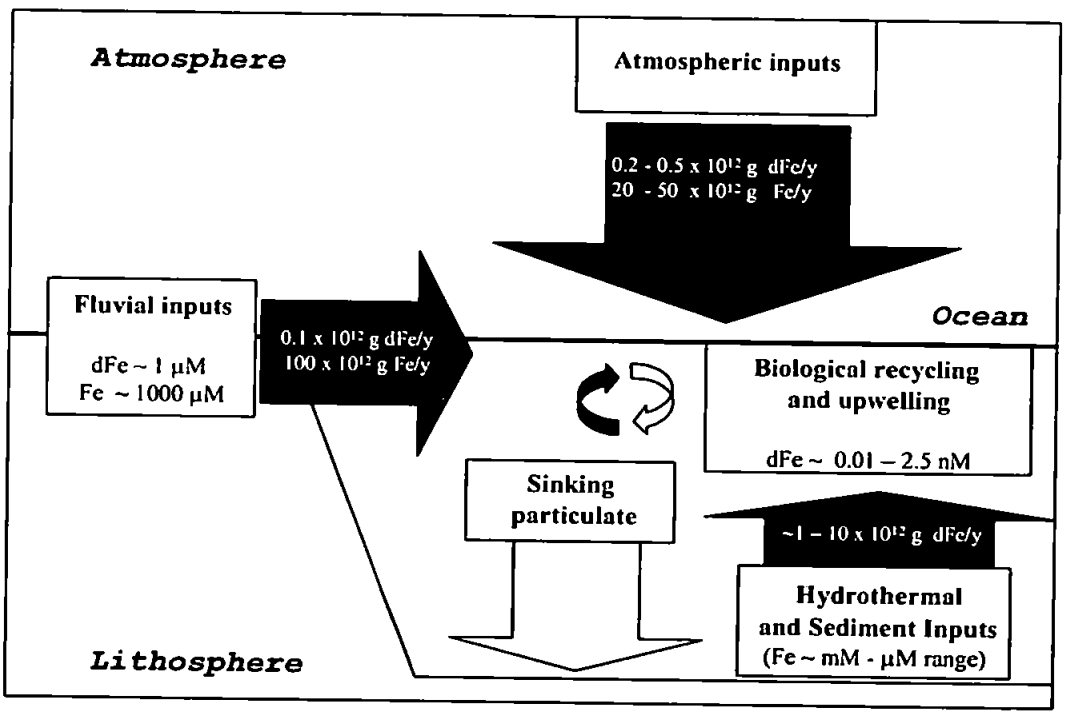

1.4.1 Fluvial inputs

Fluvial inputs transport iron to the coastal zone, following mobilization from soils and rocks. Particulate and dissolved iron concentrations in rivers are typically in the order of 1 mM and 1 μM

respectively (the estimated global mean for dFe in major rivers is 0.7 μM [86]). Upon mixing with seawater, the speciation of dissolved and particulate iron are greatly altered and both species are scavenged when flocculation occurs within the salinity/pH gradient. [90–93] Estuarine mixing reduces the global dissolved iron flux to the ocean by about 70–95%. [94] Rivers and land run-off are estimated to deliver approximately half of the surface global iron input to the oceans (see Fig. 1.6), despite a high percentage of mobilized iron being lost in estuaries. Riverine inputs of iron to the oceans are extremely variable and dominated by occasional flood events. Although this pathway is likely to provide the main source of bioavailable iron to many coastal and shelf waters, it remains unknown what proportion of suspended/soluble iron originating from land run-off is transported to open ocean gyres.

1.4.2 Atmospheric inputs

The importance of the transport of atmospheric iron to the ocean surface is high. Firstly, because it accounts for a major portion of the global iron input to the World Ocean (see Fig. 1.6) but also because this pathway is considered the principle source of soluble and bioavailable iron to remote open ocean surface waters, often thousands of miles from the aerosol origin. [89] The majority of aeolian iron received by the ocean arrives via wind-transported dust originating from arid and semi-arid landmasses, important areas being North Africa, the Asian deserts, and the Middle East. Due to their dependence on meteorological events, rates of dust production and wet/dry deposition to the ocean are sporadic.

Approximate models for global and regional aerosol iron fluxes have been calculated using available field data. [5,96] These demonstrate the magnitude of dust flux to the ocean and the large-scale regional effects of the aforementioned arid areas. The overall annual dust flux to the oceans using the data compiled by Duce et al. has been estimated to be in the region of 500×10^{12} g yr^{-1}. [89] The atmospheric flux of iron to surface waters and its oceanic residence time depend on several factors, the most important being the percentage iron content of the mineral aerosols (for crustal aerosols this is usually

assumed to be its abundance in soils and rocks, about 3.5%) and the soluble percentage of iron in aerosols.

At present, a representative global average for the fraction of soluble iron (i.e. < 0.2 or < 0.45 μm filtered) from aerosols has not been reported, although a value of 2% was used for a recent global biogeochemical model. [5] Laboratory protocols (i.e. leaching conditions) used for dissolution experiments are often different, making results difficult to compare. However, there are trends seen in the data such as the apparent lower solubility of crustal aerosols in comparison with marine and anthropogenic aerosols (see Table 1.2).

Table 1.2. Percentage soluble iron in collected aerosols

Percentage solubility [%]	Dissolution medium	Aerosol	Ref.
		Marine aerosols	
5–50	Seawater, pH 8.11	Central Pacific Islands marine aerosols	[97]
~10	Seawater, pH 5.4–8	Nova Scotia, Canada marine aerosols	[113]*
		Crustal origin	
~0.05	Water, pH 3.8–5.3	Capo Verdi, North East Atlantic (Sahara, Niger)	[114]
~0.4	Seawater, pH 8.11	Saharan soil, small grain size	[98]
< 0.013–0.2	Water, pH 8	Laboratory acid-cycled Saharan dust	[115]

* First to recognise the significance atmospheric iron input

Particulate loading is known to affect iron solubility in seawater. Leaching experiments using marine aerosols in North Pacific surface water gave saturation concentrations of 10–17 nM (dFe). [97] More

recently, supporting evidence for this phenomenon was an observed relationship between dust concentration and percentage iron solubility for Saharan dust dissolution in Mediterranean surface water. [98] The authors of this study reported higher solubilities for lower dust inputs and by modelling the relationship they were able to estimate iron solubility for the low ambient dust concentrations in their study area.

The solubility of iron in wet precipitation collected from different study areas (mean values of each data set) varies within the range of 5–50% (see Table 1.3). Aerosol iron solubility is dependent on dust composition, [99] meteorological phenomena, [100] and the degree of cloud processing that the aerosol undergoes. Considerable differences have been seen between trace metal enrichment for aerosols of crustal and anthropogenic origin, [101,102] and simulated atmospheric conditions have been observed to cause chemical and photoinduced dissolution of aerosol iron. [103]

Table 1.3. Percentage soluble iron in collected precipitation

Percentage solubility [%]*	Medium	Location of precipitation	Ref.
9.6	Rainwater, pH 3–8	Erdemli, Turkey	[116]
26	Rainwater	Wilmington, USA	[100]
37.8	Rainwater	Dunedin, New Zealand	[108]
41	Snow	Eastern Antarctica	[117]

*Results are averages of several measurements

Redox speciation changes during the lifetime of wet and dry aerosols are known to enhance iron solubility. This is due to the high solubility of iron(II) compared to iron(III) and the subsequent oxidation of iron(II) to more labile amorphous species on the surface of aerosols. [104] At cloud/rainwater pH values, chemical- or photoproduced iron(II) has been observed to have a half-life in

the order of hours to days, and it has been postulated that iron(II) in aerosols is stabilized by organic complexation, [105,107] although little evidence has been reported to confirm this. However, there is increasing evidence that a major portion of dissolved iron in rainwater is organically complexed with ligands such as oxalate. [106]

Table1. 4. Redox speciation of iron in collected precipitation

Percentage Fe(II) in dissolved Fe fraction [%]	Medium	Details of precipitation	Ref.
24*	Rainwater	Coastal: Dunedin, New Zealand	[108]
60*	Rainwater	Coastal: Wilmington, USA	[100]
25–55	Rainwater	Coastal: Boston, USA	[118]
25–74	Snow		[118]
2–55	Fog, pH 2.2–7.1	Coastal and inland: Los Angeles, Bakersfield, and Delaware Bay, USA	[109]

*results averages of several measurement

Due to scavenging, total iron concentrations in wet deposition can be relatively high and are usually between 5–1500 nM (see ref. [100] and references therein). Reported iron(II) percentages of the dissolved iron in precipitation also show high variability (see Table 1.4). The broad range of iron(II) fractions can be explained in terms of the variables discussed above for total iron dissolution (i.e. aerosol origin, cloud processing). In addition, there is strong proof that iron photoreduction in atmospheric water is closely related to light-induced diurnal cycling, including the redox cycling of other species such as copper, acetate, oxalate, sulphur (IV)/(VI), and hydrogen peroxide. [72,109-111] The reactions with sulfur are considered particularly important due to the link with dimethyl sulphide (DMS) production as a potential feedback mechanism for atmospheric exchange with phytoplankton. [112]

1.4.3 Hydrothermal inputs

In the past few decades, high- and low-temperature hydrothermal systems have been identified at spreading centres of mid-ocean ridges. The physicochemical effects of these sources are localized (e.g. high temperatures, low pH, enrichment and depletion of different elements) but seawater endmembers produced by these systems are known to have very high iron concentrations, in the region of 1 mM. [119-120]

The global flux of dissolved iron from hydrothermal activity is estimated to be in the region of 1–10×10^{12} g yr^{-1}. This indicates that this pathway is potentially the largest supplier of dFe to deep waters. Nevertheless, it should be noted that sediments in the vicinity of hydrothermal areas have been found to be highly enriched in iron, suggesting that the a high percentage of the dFe precipitates and therefore is not transported away from these areas.

1.4.4 Sediment inputs

Within marine sediments, iron is generally found to have an abundance of 1–20% (by weight) with the highest enrichment found near hydrothermal areas and ferromanganese nodules. [121] The upper sediments of coastal, shelf and open ocean regions are often found to be areas of high chemical activity where early diagenesis occurs, causing the oxidation of organic matter and, consequently, the utilization of oxidants. The resulting chemical and biologically mediated conditions mean that most particulate iron species are potentially reducible and therefore can be reintroduced into the overlying waters in a more bioavailable form. [121] Recent studies have shown that even highly refractory iron species are reducible by certain bacteria. [122]

As a result of these redox reactions, solubilized iron(II) is often found to accumulate in marine sediments and pore waters under anoxic conditions, often at micromolar concentrations. An example of

this was seen over the tan-green colour change in pelagic sediment cores collected from the Peru Basin, [123] which contained iron(II) at 10–40% of the total iron content. However, on account of the rapid oxidation of iron(II) in oxic seawater, it is unlikely to be released into the overlying waters in an inorganic form unless the bottom water is anoxic or there is only a short oxygen penetration depth. [121] Hence dissolved iron(II) and iron(III) inputs from sediments are only expected to be important in anoxic areas, in areas where there is significant turbidity or pressure, or if there is a gradual release of iron in a chemically stabilized form (e.g. organically complexed).

1.5 Iron cycling in the oceans

1.5.1 Vertical distribution

The vertical distribution of iron is controlled by variation in biogeochemical and physical processes occurring throughout the water column. Covariance between dFe and nutrient concentrations have been observed by some workers (e.g. Martin et al. [10]) suggesting the occurrence of a nutrient type mechanism caused by biological uptake in near surface waters and regeneration at depth in oxygen depleted waters. However, due to the low solubility of iron and its affinity for particles it is also scavenged efficiently by sinking lithogenic particles and detritus. Hence vertical differences in concentration are also likely to be related to variation in particle flux and the physicochemical properties of the water column.

In open ocean HNLC waters, depleted dFe concentrations of less than 0.3 nM often exist in surface waters, increasing to 0.4–1.5 nM below 500 m depth. Whereas surface and intermediate waters of areas that receive lateral inputs from continental margins or high atmospheric iron fluxes, often contain higher and more variable iron concentrations (e.g. see Fig. 1.7).

Interestingly, similar deep water dissolved iron concentrations have been reported for a number of ocean basins (average concentration of 0.76 nM, $n = 30$) and these show little inter-ocean fractionation. [124] This phenomenon is surprising, considering the variability in iron sources and a relatively short residence time in deep waters (~70–200 yr). The consistent solubility observed may be controlled by either equilibrium between dissolved and suspended particulate and/or by the association of iron with strong organic ligands (see above). A model fitted to global datasets has been reported and supports the latter hypothesis, [125] but for it to be valid the complexation reactions must be rapid ($> 10^{-4}$ M^{-1} s^{-1}) and the dissociation slow ($< 10^{-4}$ M^{-1} s^{-1}). [126] Further open ocean studies are required to validate this hypothesis, and hence steady-state control of dissolved iron by association and dissociation of dissolved iron from particles should not be disregarded as an important mechanism for controlling iron solubility in deep waters. [127]

Figure 1.7. dFe profiles from the North-East Atlantic Ocean (IRONAGES Cruises II and III, 2002).

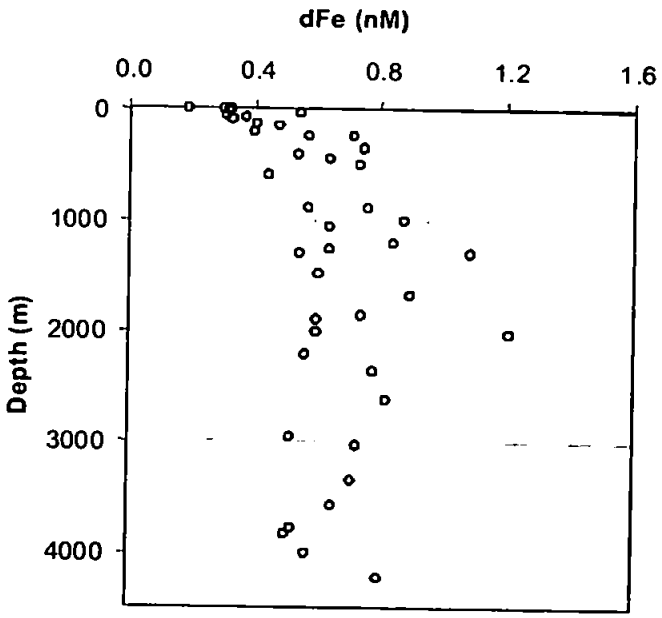

Iron transport in the upper water column is far more dynamic due to intensified biological activity and mixing processes [128] and the estimated residence times for iron reflect this. For example, residence

times for dissolved and particulate iron in the upper 100 m of the Sargasso Sea have been calculated to be about 250 and 18 days, respectively. [105]

The recent global model of Moore et al. [5] indicates that the main processes exporting dissolved iron from the mixed layer in the open ocean to be entrainment and sinking detritus, whereas the main inputs are entrainment and atmospheric deposition, although it should be noted that regional processes such as upwelling are highly significant in certain areas. Within the euphotic zone, iron is also cycled within the biological pool. This has a significant effect on iron transport through the upper water column, and rates of iron uptake by marine organisms and remineralization are estimated to be of the same order as the input and export fluxes, where surface mixed layer global fluxes are in the order of 10^{12} g(Fe) yr^{-1} ($\equiv 2\times10^{10}$ mol(Fe) yr^{-1}). [5]

1.5.2 Iron uptake by marine organisms

Marine microorganisms acquire iron by either ion membrane transporters or siderophore systems. Siderophore systems have been observed for terrestrial bacteria and fungi [129] and, more recently, for marine bacteria. They function by the excretion of low molecular weight (300–1000 Da) iron chelators, often found to have hydroxamate or catecholate functional groups, which selectively bind iron(III) and are then transported back into cells via chelate specific transport proteins. Siderophore production is known to be used as an iron uptake mechanism for heterotrophic and cyano bacteria but at present there is no conclusive proof that these systems are used by eukaryotic marine phytoplankton although they have been observed to utilize siderophore-bound iron. [130,131]

There is growing evidence that siderophore compounds excreted by marine bacteria form a major component of the strong iron-binding ligand pool. For example, production of two classes of ligands (L_1, L_2) were observed during the IronEx II mesoscale iron enrichment experiment following iron addition. [132] These had conditional stability constants in the order of $K_{Fe'L_iL} = 10^{12}$ M^{-1} and 10^{11} M^{-1},

respectively (where the constant is calculated for all inorganic iron (Fe′) rather than free Fe^{3+}). The binding constants of these ligands were similar to the binding constants of catecholate and hydroxamate marine siderophores produced by laboratory cultures and low molecular weight ligands extracted from coastal seawater ($K_{Fe'L,Fe} = 10^{11.5}$–$10^{12.5}$ M^{-1} [133–135]). The presence of these compounds and their high affinity for iron has been predicted to have significant effects on dissolved iron speciation, such as increased dissolution rates and solubilities of ferric hydroxides. [136]

Marine siderophores that have been characterized are reported to have high cellular membrane affinities or are produced by bacteria associated with particles. [137–140] Repressed siderophore production has been observed under iron-replete conditions [141] but production of characterized siderophores have also been observed in iron-rich coastal waters [142] Thus, the significance of siderophore production in different regions is unknown, although it is hypothesised to be favoured in low turbulence areas with high concentrations of biomass. [143]

Ion membrane transporters are used by both marine bacteria and phytoplankton but unlike siderophore species, iron uptake is considered to be directly related to the concentration of free inorganic iron species ([Fe′]) in solution. These free species represent labile hydrolysis and mono-substituted inorganic species which are in equilibrium with strong organic complexes (FeL). It is uncertain whether specific free iron species are preferentially utilized by ion membrane transporters (i.e. free iron(II) or (III)). Furthermore, there is evidence that cell surface mechanisms increase [Fe′] by accessing organically complexed iron (see below). Nevertheless, workers investigating iron uptake by cells often use the 'free ion model', Fig. 1.8, [144] to interpret data.

In this model, it is assumed that a steady state concentration of free inorganic ions (M'_{inorg}) exists from the dissociation of strong organic complexes (ML_{org}). k_1 and k_2 are the association and dissociation rate constants, respectively, for binding with trans-membrane ligands, and k_{in} is the rate constant for uptake across a cell membrane. The model also assumes that only free inorganic iron becomes bound to

transport proteins on the cell membrane, from where it either dissociates back into solution or is transported into the cell. Iron membrane transport is thought to be driven by ATP or electrochemical gradients. [145]

Figure 1.8. Free ion model for iron uptake by phytoplankton (Hudson [144])

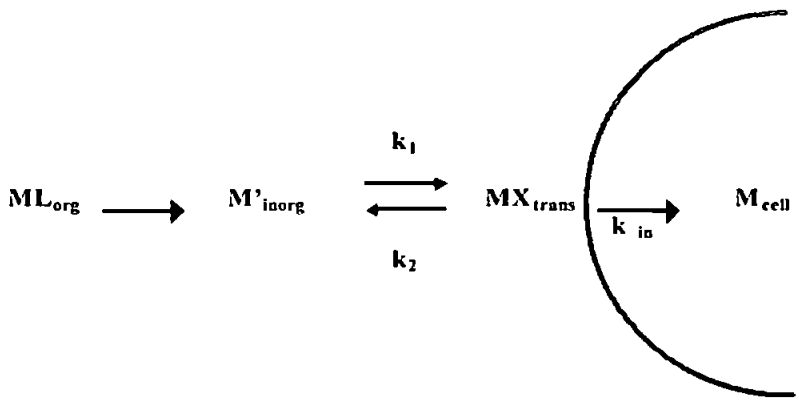

The rate of iron uptake can operate under equilibrium or kinetic control. The former implies that k_1 and $k_2 >> k_{in}$, whereas kinetic control implies that k_2 is slow and k_1 and k_{in} are fast. Based on experiments on coastal phytoplankton, the rate-determining step is kinetically controlled by the binding of Fe′ to the transporter site. This is ultimately dependent on the loss of water from the Fe′ inner coordination sphere. [144,146,147]

Comparisons of several phytoplankton species revealed that, when normalized to cell surface areas, they all had a similar maximum limit of iron uptake based on the kinetics of iron exchange with transport proteins and the space available on the cell membrane. [147,148] Further interpretation of this phenomenon shows that the surface area to volume ratio of cells becomes important with regards to iron uptake, when diffusion limitation ceases to dominate (cell diameters less than 60 μm). [143]

In situ studies have shown that the uptake of iron by smaller cells is far more efficient when normalized to unit cell volume. In addition, open ocean phytoplankton are able to reduce their cell sizes to cope with iron limitation and even adapt their metabolism to cope with lower cellular iron requirement for growth. [76,149] Furthermore, variation in cellular iron concentrations can also vary depending on growth rate, cell volume, light limitation and the nitrogen source utilised by the cell. [145]

1.5.3 Additional sources of bioavailable iron

Ferric reduction is an important process for organisms that use ion membrane transporters, as it provides a further source of bioavailable Fe′ species for marine organisms and can recycle otherwise refractory iron species. Reduction occurs in marine waters via physicochemical processes (such as photochemical and thermochemical reduction of particle-bound iron or iron chelates) and various forms of biological reduction (see above). However, there is growing evidence that in the absence of sufficient external sources of Fe′, iron-deficient phytoplankton are able to reduce iron(III) chelates, including siderophores, using trans-membrane reductases (e.g. NADH, NADPH). Models relating cell surface reduction to cell radius show that, unlike siderophore systems, larger cells benefit more from this process whereas small cells benefit from the resulting increase of Fe′ in the bulk seawater. [143]

Cell surface reduction of iron chelates has been observed for several species of marine diatoms including *Thalassiosira oceanica*, [150,151] *T. weissflogii*, [152] and *Phaeodactylum tricornutum*. [153] In the case of *T. oceanica*, evidence suggests that iron(II) production can be faster than the cell uptake rate (allowing for a large proportion to diffuse away from the cell) and that it is the resulting oxidized Fe(III)′ species that is taken up by the cell.. Furthermore it was observed that the reduction rate was proportional to the logarithm of the ratio of the ferric and ferrous binding constants for individual complexes, i.e. $\log (K_{Fe(III)L}/K_{Fe(II)L})$. [151]

Particulate iron is another source of Fe′ that can be used by certain marine organisms to satisfy their iron requirements. It has been demonstrated that Fe′ can be obtained by phytoplankton from

amorphous iron hydroxides [154,155] and iron bound to natural marine colloids. [83] This can occur either by thermal- or siderophore-mediated dissolution and by plasma membrane reductase mechanisms, such as those described above. Another important pathway for the creation of bioavailable iron is the digestion of colloids and biogenic particles. It has been estimated that the production of bioavailable iron from ingested colloids during protozoan grazing exceeds that of photoreduction when the entire water column is considered. [156] In addition, mixotrophic flagellates can also obtain iron through ingestion of bacteria and this pathway has been estimated to account for to up to ~50% of the total iron uptake by autotrophs in the Equatorial Pacific.[157]

1.6 Conclusions

Iron plays a critical role as a limiting micronutrient for primary production in the World Ocean. This review considers the marine biogeochemistry of the element in relation to modelling iron transport and biological utilization in the marine environment. Specific issues that need to be addressed to improve our understanding include the following five subjects.

Analytical Constraints. In the past decade analytical techniques with picomolar detection limits have been developed for the determination of dissolved iron, but inconsistencies remain between reported dissolved iron datasets (e.g. for aerosol iron solubility and open ocean concentrations). This demonstrates a clear need for a sub-nanomolar iron certified reference materials and more reliable protocols for sample collection and filtration, pre-treatment (e.g. acidification), and storage. Consistency between workers will only be achieved by continued international collaboration and rigorous intercomparison exercises, both at sea and in the laboratory.

Sources and Fate of Marine Iron. To improve regional and global iron flux estimates, further temporal and spatial studies of iron distribution and speciation in the open ocean are required. These should

include surveys that ascertain the sources and magnitude of iron inputs, e.g. by determining aerosol input fluxes, isotopic abundances and elemental ratios (Fe/Al for example), as well as tracer studies that target specific processes that transport the element in the water column.

Significance of Iron-Binding Ligands. Speciation studies and global models highlight the importance of experiments that characterize and quantify iron-binding ligands in seawater. Organic complexation strongly influences the thermodynamics of iron and hence its redox state and solubility. In addition, it is predicted that the kinetics of important processes, such as phase transitions, biological uptake, and scavenging, are perturbed by organic complexation. Hence, further laboratory and in situ studies that investigate the effects of complexation on all of these processes are required. In particular, there is a need for data relating to iron(II) complexation.

Kinetics of Complexation. Reported conditional stability constants for natural ligands are becoming more available but there is also a need for conditional kinetic constants for the complexation of iron(II) and (III) with dissolved organic and particle-bound ligands in seawater. This will help to determine the timescales of such reactions and whether they can compete with important mesoscale processes such as precipitation and biological uptake.

Bioavailability and Phase Transitions. Current iron bioavailability models are constrained by the lack of well-defined iron speciation data. Most iron uptake models consider only 'free iron species' (i.e. truly dissolved, unbound species) or biologically produced siderophore species that are targeted by membrane receptor sites, but iron concentrations determined during field and laboratory studies are operationally defined fractions. Therefore obtaining near real-time data describing the fractionation of the iron pool (qualified by size and complexation coefficients) will help to integrate theoretical uptake models with experimental data and better describe the chemistry of iron at cell membranes.

1.7 Aims and objectives

The main aims of the work reported in this thesis were to refine and optimise techniques for the determination of dissolved iron speciation in seawater and to investigate iron biogeochemistry in two study areas in the north east Atlantic Ocean. The key objectives were as follows:

1. Optimise, trial and evaluate a Flow Injection Chemiluminescence (FI-CL) method for the ship-board determination of dissolved Fe(II) in seawater.

2. Assess potential interferences from dissolved organic molecules to the FI-CL method.

3. Determine the dissolved iron redox speciation in two study areas in the north east Atlantic Ocean.

4. Interpret the data in relation to hydrographic and geographic features, investigate the variance of dissolved iron concentration with nutrients and other trace metal data and identify possible sources, sinks and controlling variables.

5. Determine dissolved iron in different size fractions in the euphotic zone of the Canary Basin to assess whether small colloidal iron (0.02 - 0.2 μm) is a significant proportion of the dissolved iron pool in this region.

6. Investigate potential variables that affect the dissolution of iron from aerosol dusts in seawater.

CHAPTER 2.

Flow injection chemiluminescence methods for the determination of iron redox species in seawater

2.1 Introduction

The Flow Injection Chemiluminescence (FI-CL) techniques optimised and used in this study are described in this chapter. It includes descriptions/illustrations of:

1. Flow injection analysis as a tool for the shipboard determination of dissolved chemical species in the marine environment and the application of this methodology for determining operationally defined iron species in seawater.

2. A description of the automated analyser used to determine dFe (Fe(II) + Fe(III)) and Fe(II). This includes an assessment of the suitability of the instrument to determine Fe(II), based on field trials in open ocean regions.

3. The optimisation of a simple luminol chemiluminescence method for Fe(II) using the direct injection of sample into the reagent stream (i.e. no preconcentration column).

2.2 The use of flow injection analysis in the marine environment

The technique of flow injection (FI) is now an established analytical tool for automating wet chemical analyses and facilitating on-line sample treatment (physical and chemical) for a range of detection systems. It is used for process analysis [158] but is also well suited for *in situ* environmental monitoring. The attractive features of FI for this purpose are shown in Table 2.1.

Analytical techniques are required for mapping nutrient and trace element distributions across ocean and local scale transects, determining their chemical speciation (e.g. redox states) and

studying their interactions with living organisms. The recognition that many trace elements are often present at sub-nanomolar concentrations in the ocean has necessitated the development of contamination free sample handling methodologies and very sensitive analytical techniques.

Table 2.1. Attractive features of FI for *in situ* environmental monitoring.

- High temporal and spatial resolution
- Robust, portable, automated instrumentation
- Contamination free enclosed environment
- Sensitive and selective detection
- In-line removal of matrix interferences e.g. sea salts
- Long term stability (reagents, standards, pumps, detector)
- In-line filtration to remove suspended particulate matter
- In-line treatment (e.g. acid wash) to prevent internal biofouling
- On-board calibration and quality control (for accuracy)
- Simple and rapid field maintenance

Highly sensitive, laboratory based destructive techniques, such as inductively coupled plasma mass spectrometry (ICP-MS) and graphite furnace atomic absorption spectrometry (GF-AAS) have been adapted to provide accurate and sensitive methods for trace element determination but cannot be used on-board ships. Furthermore, the kinetics of marine biogeochemical processes are often rapid and thus the chemical speciation in a sample can be greatly modified by storage. Therefore, many chemical speciation measurements can only be made in the field using reliable shipboard analytical techniques.

With analysis times in the order of minutes/seconds, the high temporal resolution of FI is an attractive feature for studying dynamic marine processes and open ocean environments e.g. mapping of oceanic biogeochemical provinces. Furthermore, the portability and spatial resolution capability of FI make it highly suitable for shipboard deployment. This is particularly important

when the analyte speciation is likely to change after collection e.g. Fe(II)/Fe(III) redox states. [162-165]

Table 2.2 Shipboard and submersible deployment of flow injection instrumentation with spectroscopic detection for monitoring marine environments.

Analyte	Location	Limit of Detection* (nM)	Detection	Comments	Ref.
Al(III)	Open ocean	0.15	Fluorescence	Lumogallion, Brij-35	[159]
Co(II)	Open Ocean	0.5	Chemiluminescence	Gallic acid, hydrogen peroxide	[160]
Cu(II)	Coastal waters	0.1	Chemiluminescence	Hydrogen peroxide, 1,10-phenanthroline	[161]
Fe(II)	Open ocean	0.45	Chemiluminescence	Brilliant sulfoflavin, hydrogen peroxide	[162]
Fe(II)	Open ocean	0.04	Chemiluminescence	Luminol, dissolved oxygen	[163]
Fe(III)	Open ocean	0.02 - 0.01	Chemiluminescence	Hydrogen peroxide, luminol	[164] [165]
Mn(II)	Coastal waters	0.1	Chemiluminescence	7,7,8,8-Tetracyano-quinodimethane	[166]
Zn(II)	Open ocean	0.1	Fluorescence	P-tosyl-8-aminoquinoline	[167]
H_2O_2	Open ocean	10.6	Chemiluminescence	Cobalt(II), luminol	[168]
$NO_{x\,(aq)}$	Open ocean	100	Spectrophotometry (with LED)	N1NED,suphanilimide, cadmium reduction, submersible	[169]
NO_2^- NO_3^-	Open ocean	4.6	Fluorescence	Aniline, imidazole, cadmium reduction	[170]
NH_3	Open ocean	1	Fluorescence	OPA, dialysis temperature controlled	[170]
$Si(OH)_4$	Coastal waters	300	Spectrophotometry	Ammonium molybdate, tin chloride, submersible analyzer	[171]
pH	Open ocean	-	Spectrophotometry	m-Cresol purple, temperature controlled	[172]
pH	Open ocean	-	Spectrophotometry	Phenol red, temperature controlled	[173]

*as defined by investigator

In addition, contamination from the field environment is minimised using an FI analyser housed within a portable laminar flow hood and manipulating the sample within the confines of the narrow bore (0.7 mm) manifold tubing (Figure 2.1.). Other important attributes of FI shipboard monitoring are low reagent consumption, waste containment, high reliability and ease of maintenance.

Current shipboard flow systems use a variety of detection methods in order to maximise sensitivity, precision and selectivity for individual trace elements and nutrients. Table 2.2 lists FI methods that have been used for shipboard measurements of trace metals, nutrients and inorganic ions in marine waters. Spectrophotometry, fluorescence and chemiluminescence have been used for detection and a common feature of many of the reported methods is the incorporation of a solid phase micro-column containing an immobilised chelating ligand for preconcentration of the analyte and matrix removal (e.g. the major sea salt ions). One of the most documented extraction columns for trace metal analysis is the immobilised 8-hydroxyquinoline column (8-HQ). [159,161-167] Direct spectrophotometric methods (i.e. no micro-column) require careful optimisation to minimise refractive index (Schlierren) effects. [171]

Figure 2.1. FI analyser in the laminar flow hood of a ship clean container

Typical on-line treatments used with shipboard FI methods include reduction columns for redox speciation e.g. NO_2^-/NO_3^- and specific filtration techniques to remove suspended particulate matter and/or colloidal fractions. On-line seawater supplies from towed fish can be coupled with filtration units and FI to provide near real-time analysis, e.g. of dissolved or total nutrient concentrations in surface waters. [159,165] Another option, particularly for transient species, is the deployment of a submersible FI analyser. [169,171]

Shipboard FI techniques are not restricted to measuring trace elements and nutrients. Methods for determining other inorganic species that require high temporal and spatial resolution measurements, e.g. pH, pCO_2, TCO_2 [172,173] and H_2O_2 [168] have also been adapted for high precision shipboard use in a FI system. The small size and weight of FI instruments also permits simultaneous multi-analyte measurements. [170, 174]

2.3 Determination of iron(II) and dissolved iron species in seawater using flow injection chemiluminescence (FI-CL)

2.3.1 Operationally defined iron fractions

Trace metal species in seawater samples are generally operationally defined by the pre-treatment and method of analysis used. Details of the iron species that were determined during this study are listed in Table 2.3. The dissolved iron (dFe) fraction was chosen to mimic traditional pre-treatments used by other workers (e.g. <0.2 - <0.4 μm filtration followed by acidification to pH 2 and several months storage [11]) and hence allows comparison of the dFe data with historical dFe data. Since this fraction may contain small colloids, some of the later studies reported here (Chapter 6) also include dFe data for a <0.02 μm fraction, which has been used by other workers to define 'soluble' iron in seawater. [42] Further information on the total acid labile iron in open ocean

regions can also be obtained by the analysis of unfiltered acidified samples or total dissolvable iron (TD-Fe). However, iron concentrations in these samples are likely to be more variable due to the lack of homogeneity of particles and organisms in seawater.

Table 2.3 Operationally defined iron fractions used in this study.

Fraction	Abbreviation	Filtration	Pre-treatment
Total Dissolvable Iron	TD-Fe	Unfiltered	Acidification after collection (pH 2, HCl). Sulphite reduction before analysis.
Dissolved Iron	dFe	<0.2 µm	Filtered immediately after collection. Acidified and stored for 3 months (pH 2, HCl). Sulphite reduction before analysis.
Soluble Iron	dFe(<0.02 µm)	<0.02 µm	Filtered immediately after collection. Acidified and stored for 3 months (pH 2, HCl). Sulphite reduction before analysis.
Small Colloidal Iron	dFe (0.02-0.2 µm)	-	See note[a]
Dissolved Iron(II)	Fe(II)	<0.2 µm	Analysed immediately after in-line filtration.
Percentage iron(II)	%Fe(II)	<0.2 µm	See note[b]

[a] value obtained by subtracting dFe(<0.02 µm) from dFe
[b] percentage fraction of dFe e.g. %Fe(II) = [Fe(II) / dFe] x 100

Redox speciation measurements were made by determining dissolved iron(II) (i.e. Fe(II)) *in situ* by immediate analysis using FI-CL with in line filtration (<0.2 µm)). Data is often presented as %Fe(II) which denotes the percentage fraction of Fe(II) in the 'total' dFe pool (e.g. %Fe(II) = [Fe(II)/(Fe(II) + Fe(III)] x 100%) An investigation into the accuracy of this technique and the

possibility of interferences caused by organic molecules in the sample matrix is given in Chapter 3. Practical details of all filtration and sample pre-treatment are described in Chapters 5 and 6.

2.3.2 Shipboard iron determination by Flow Injection - Chemiluminescence (FI-CL)

DFe in seawater can be determined in the laboratory using ICP-MS with isotope dilution [175] or solid phase extraction, [176] GFAAS after solvent extraction, [11] FI with chemiluminescence (CL), [163, 165] spectrophotometric detection [177] or cathodic stripping voltammetry. [178] However, current oceanographic studies require the determination of iron at sea in near real-time and this necessitates the use of portable, shipboard instrumentation, for which FI techniques are ideally suited.

Flow Injection Chemiluminescence (FI-CL) can be defined as a flow injection technique that quantitatively determines an analyte following its reaction with a chemiluminescent dye. The light emitted during the reaction is therefore relative to the quantum yield of photons emitted from the electronically excited state of the dye to its ground state after reacting with the analyte. FI using luminol (5-amino-2,3-dihydro-1,4-phthalazinedione) chemiluminescence is among the most sensitive ship-board FI-CL methods, capable of determining picomolar concentrations of dFe in seawater. [179]

The proposed reaction pathway for the oxidation of luminol followed by chemiluminescence has been determined [180] and is shown in Figure 2.2. [181] The important conditions of the reaction are firstly, that the initial one-electron oxidation reaction (reaction 1) requires the presence of reactive oxidants such as transition metals (e.g. Fe, Co, Cu and Mn) or free radical moieties. Secondly, that the efficiency of the chemiluminescence emission in the final decomposition step (426 nm, reaction 3) is dependent on the deprotonation of the α-hydroxy-hydroperoxide species (pKa = 8.2 [180]). Due to this, the reaction has an optimum chemiluminescence at a pH of ~10.5. [182]

The type of oxidant used with luminol influences the iron redox species determined in seawater. Obata *et al.* [164,183] used hydrogen peroxide as an added oxidant to determine iron(III) following

acidification to pH 3.0 and selective preconcentration on an 8-HQ column. Using this methodology, determination of iron(II) required initial removal of iron(III) from the sample using the 8-HQ column and increasing the sample pH to 6 in order to preconcentrate iron(II) in addition to iron(III).

Figure 2.2 The free radical oxidation pathway of luminol [180, 181]

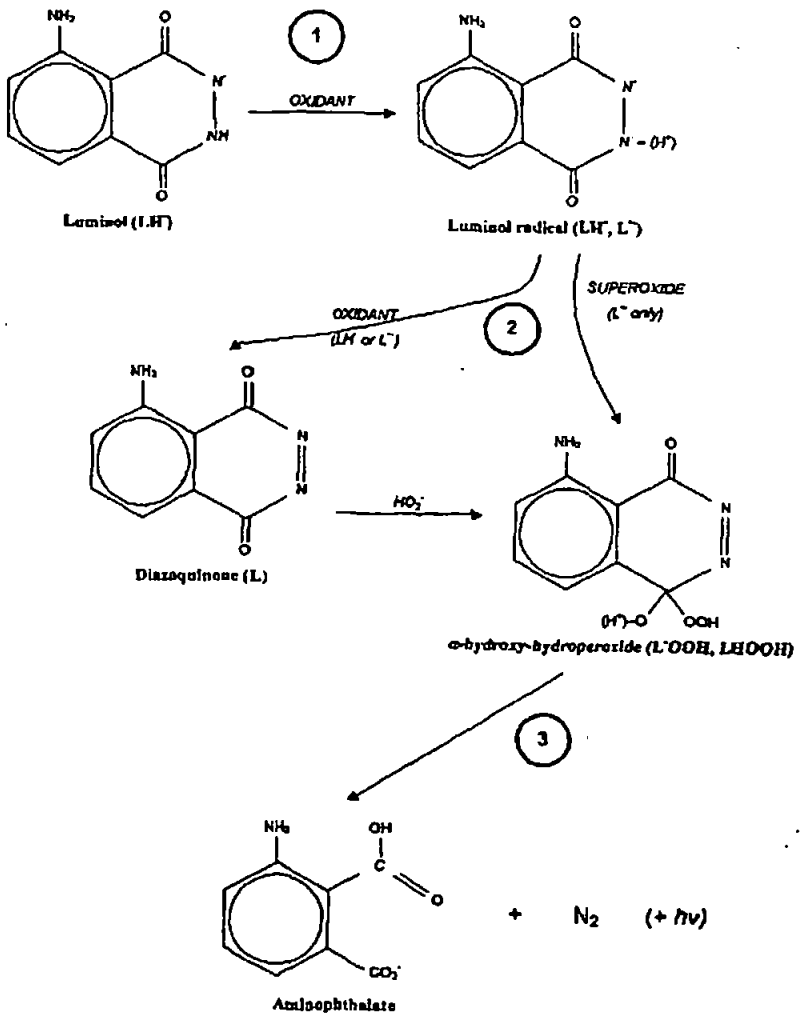

Alternatively, the oxidation of luminol in the presence of dissolved oxygen has been used to selectively determine iron(II). [184-187] The use of this reaction for determination of iron(II) in seawater using FI analysis was initially investigated using a stopped flow technique without

preconcentration (O'Sullivan *et al.* [182]). This method was later developed and used for measurement of total dissolvable iron in unfiltered samples by reducing iron(III) to iron(II) using sulphite and preconcentration on to an 8-HQ microcolumn [163,188] and in recent years, it has been applied for direct Fe(II) measurements in surface waters. [189,190]

In addition to luminol chemiluminescence, the iron(II) specific reagent brilliant sulfoflavin (4-amino-*N*-*p*-tolyl)-naphthalimide-3-sulfonate) has been used to determine subnanomolar iron(II) following preconcentration (Elrod et al. [162] and Hirata et al. [191]). Total dFe was measured using this technique by adding a reducing agent (ascorbic acid [162] or hydroxylammonium chloride [191]) to samples prior to analysis.

2.4 Automated FI-CL instrument for monitoring picomolar concentrations of dissolved iron and iron(II) in seawater [192]

The fully automated and portable FI instrument that was used for real time monitoring and off-line determination of dFe species in this study is described below. The system incorporated a low power (5 V) PMT, an immobilised chelating resin for analyte preconcentration and luminol chemistry for detection. The automated virtual instrument used flow injection with luminol CL detection (with no added oxidant) for the determination of iron in seawater.

The method is an inexpensive, portable and robust system suitable for shipboard deployment. The detection limit of ~21 pM allows the determination of iron in all marine environments, including remote, iron-limited open-ocean regions. Iron(II) can be determined directly by its enhancing effect on the luminol reaction and total iron(II+III) can be determined after acidification and sample reduction steps. A graphical programming environment (LabVIEW® [193]) facilitated the design of a virtual instrument with a fully flexible user interface for instrument control and data acquisition.

In addition, the use of off-the-shelf components and industry standard graphical programming software makes the instrument readily adaptable to related analytes (e.g. cobalt [194], copper [195]) using well-documented chemiluminescence reactions. This instrumentation should be easily transferable between laboratories, thus 'facilitating the harmonisation of analytical methods for the determination of iron in seawater', a current initiative of the Scientific Committee for Oceanic Research (SCOR) Working Group 109 (Biogeochemistry of Iron in Seawater). [196]

2.4.1 Reagents and standards

All chemicals were obtained from VWR, unless otherwise stated. Labware was cleaned by soaking in successive baths of 5% (v/v) micro-detergent (Decon) for 24 h, 6 M HCl (AnalaR) for 1 week and 2 M HNO_3 (AnalaR) for 1 week, and rinsed thoroughly with double deionised water (ultra high purity (UHP) water, 18.2 MΩ cm^{-1}) between each step. Sample handling was carried out in a class-100 laminar flow hood. High purity quartz distilled (Q-) HCl, HNO_3, ammonia and acetic acid were purified by quartz sub-boiling distillation.

Iron(II) standards were prepared daily in 0.1 M Q-HCl from $Fe(NH_4)_2(SO_4)_2.6H_2O$. Luminol (Sigma) ($1x10^{-5}$ M) was prepared in 0.1 M Na_2CO_3 by dilution of a 0.01 M stock and adjusted to pH 12.2 with 2 M NaOH, and passed through a Chelex-100 (Sigma) chelating resin column just prior to use. Ammonium acetate sample buffer (0.4 M) was prepared from a 2 M stock and adjusted to pH 5.5 with Q-acetic acid. An iron(III) reducing agent of 100 μM Na_2SO_3 (extra pure) was prepared from a 0.4 M stock pre-cleaned through an 8-HQ column. The eluent was 0.05 M Q-HCl and the acid wash was 0.6 M Q-HCl. Low iron seawater (LISW) obtained from the open-ocean was used as the carrier stream to transport sample from the holding loop to the preconcentration column in the FI manifold.

2.4.2 FI analyser

Figure 2.3 shows the automated FI-CL system. Pumps A, B and C were 4-channel peristaltic pumps (Gilson Minipuls 3, Anachem, Luton, UK). Injection valves 1 and 2 were ¼"-28, 6-port, low pressure valves (Cheminert C22, Valco, Houston, USA) with two position micro-electronic actuation. A ¼"-28, 10-port, low pressure selection valve (Cheminert C25, Valco, Houston, USA) with multi-position micro-electronic actuation was used to switch between standards and sample. Switching valves were PTFE 3-way, two position solenoids (EW-01367-72, Cole-Parmer, Hanwell, UK).

Figure 2.3 FI-CL manifold for the determination of iron in seawater

(a) Shipboard flow diagram

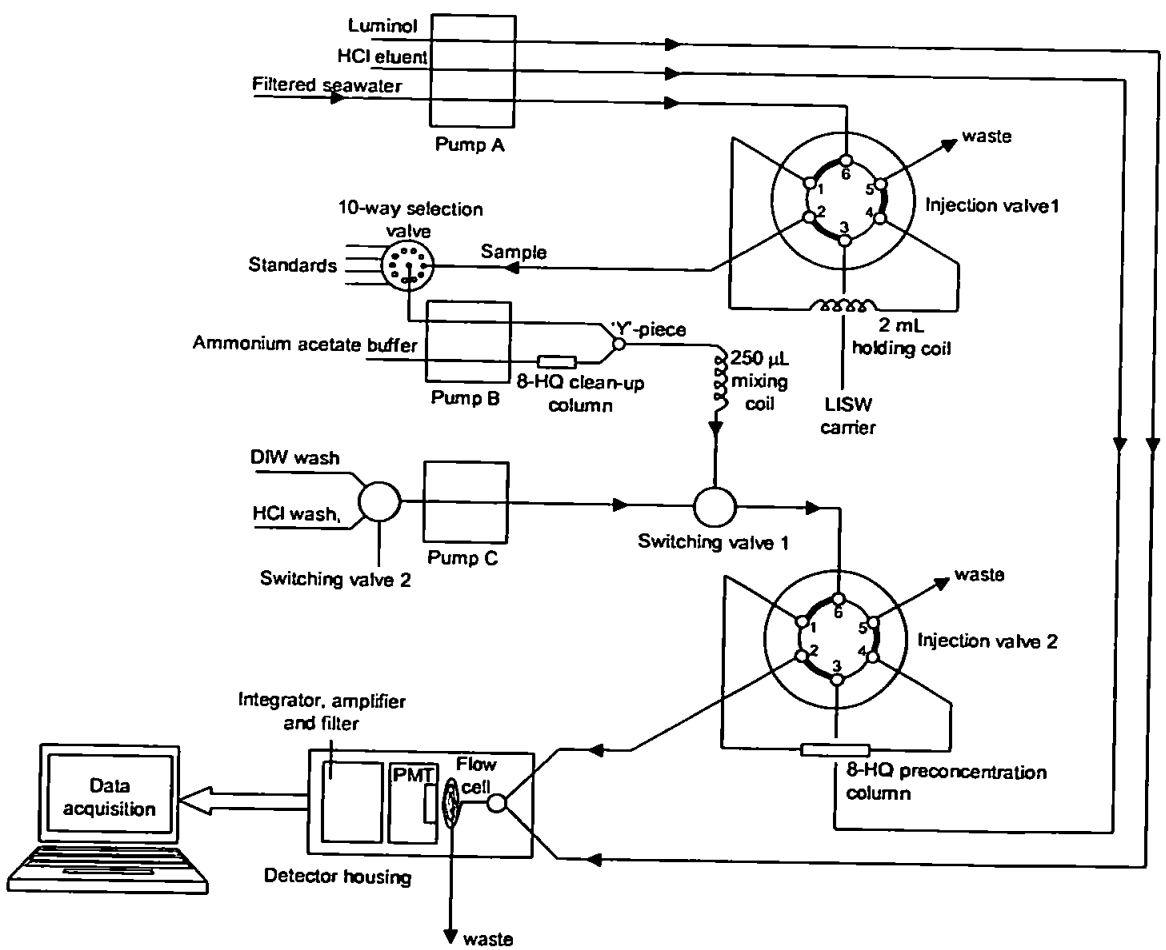

(b) Automated system

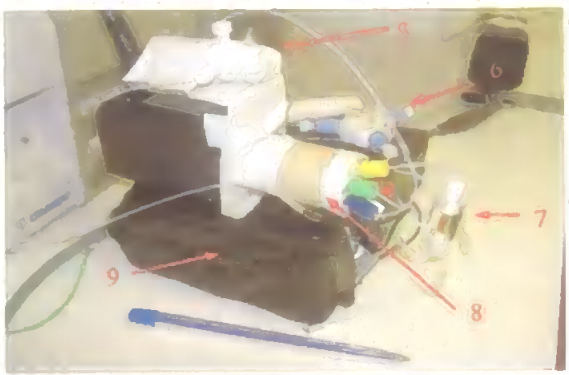

1. Laptop with DAQCard™ PCMCIA interface

2. Main control unit

3. 4-channel peristaltic pumps (A-C)

4. FI-CL manifold

5. 2-position PTFE solenoid valve (V1)

6. Y-piece and mixing coil with manually operated valves for buffer and sample flows

7. 8-HQ preconcentration column

8. 6-port injection valve (I2)

Table 2.3 Specifications of miniature photon counting head.

MAXIMUM RATINGS

Parameter	*Value*	*Unit*
Supply voltage	+6	V dc
Operating temperature range	+5 to 40	°C
Storage temperature range	-20 to 50	°C

SPECIFICATIONS AT 25 °C

Parameter		*H6240-01*	*Unit*
Effective area		4 x 20	mm^2
Spectral response		185 to 850	nm
Dark count	Typical	80	cps
	Maximum	200	cps
Counting linearity		2.5	Mcps
Pulse pair resolution		35	ns
Output pulse width		30	ns
Output logic		TTL, positive	
Input voltage		+5	V dc
Input current at 2.5 Mcps output		Maximum 80	mA

Pumps and valves were operated at 5 V dc (TTL) and switches at 12 V dc. A power saver relay reduced the solenoid input voltage to 8 V dc when energising for extended periods. The detection system was a coiled transparent PVC flow cell (1.0 mm i.d.) side mounted on the window of a 5 V dc photon counting head (model H6240-01, Hamamatsu Photonics, Welwyn Garden City, UK). Detector specifications are given in Table 2.3. The TTL pulse train from the photon counting head was integrated, amplified and filtered prior to data acquisition (Figure 2.4).

Figure 2.4 Block diagram of the automated FI-CL instrument incorporating the main control unit and PMT interface (integrator, amplifier and filter are shown on PMT 1 only).

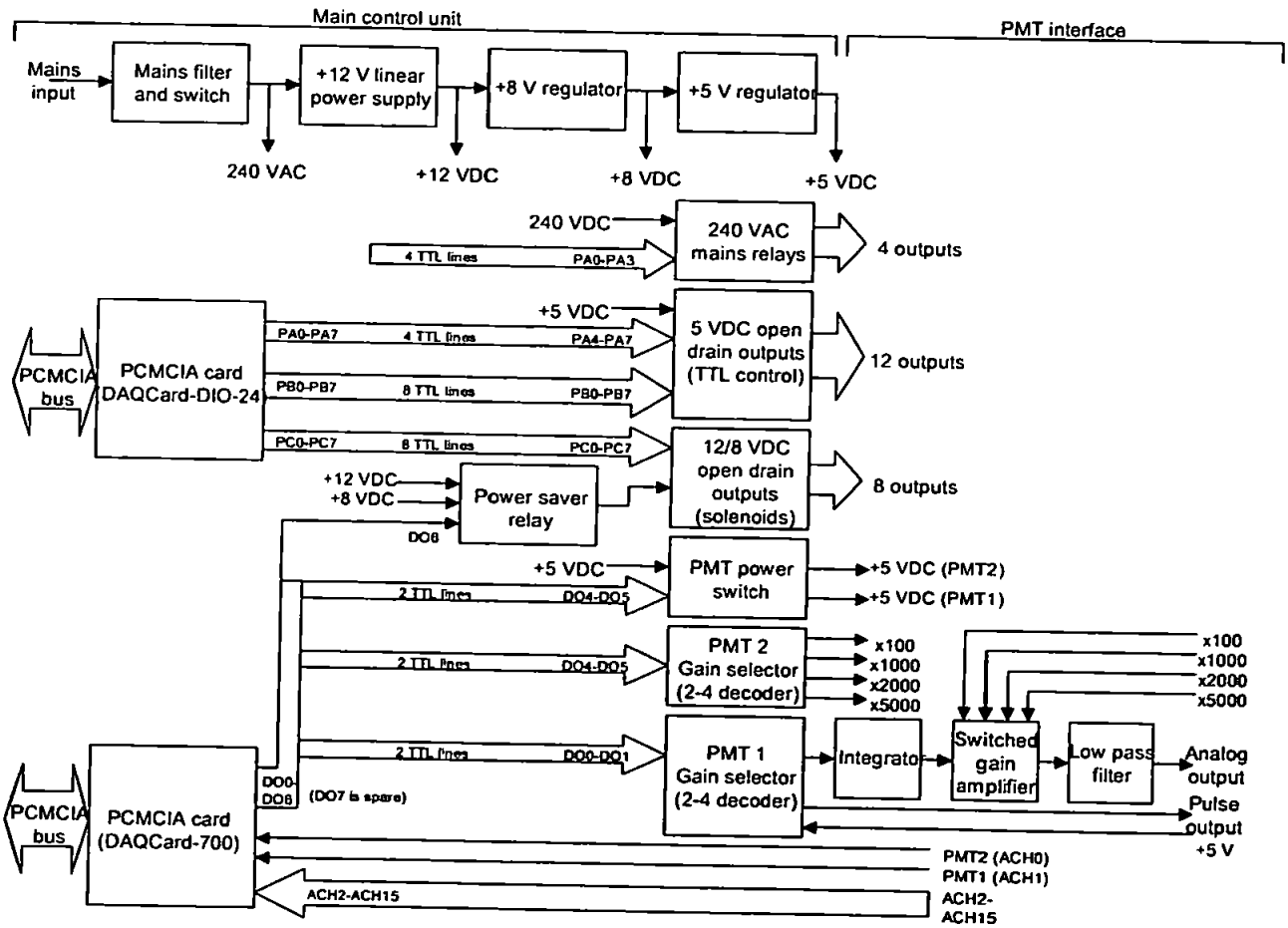

Flow lines, fittings and connectors were cleaned for 1 day with 0.5 M Q-HCl and UHP water prior to use. Manifold tubing was 0.75 mm i.d. PTFE (Fisher Scientific, Loughborough, UK). Peristaltic

pump tubing was flow-rated PVC (Elkay, Basingstoke, UK). Preconcentration, matrix elimination and sample buffer clean-up was performed in-line using 8-HQ immobilised on a vinyl co-polymer resin packed into 50 µL micro-columns. [163] One complete analytical cycle, consisting of sample load, rinse and elution, took 3 min. The operation, state of each component (on or off for switching and injection valves; position for selection valve) and associated timing parameters during each cycle are shown in Table 2.4.

Table 2.4 Timing sequence for one analytical cycle.

Elapsed time (s)	Pumps			Injection valves [a]		Switching valves		10-way selection valve position [c]	Operation
	A	B	C	1	2	1	2 [b]		
0	ON	ON	OFF	ON	OFF	ON	OFF	1	Load
60	ON	OFF	ON	OFF	OFF	OFF	OFF	1	Wash
100	ON	OFF	OFF	OFF	ON	OFF	OFF	1	Elute
160	ON	OFF	ON	OFF	OFF	OFF	OFF	1	Rinse
180	Cycle back to line 1								

The pump and valve numbers refer to those shown in Figure 2.3. [a] Injection valves: OFF=LOAD sample and ON=ELUTE sample. [b] Switching valve 2 is ON only when an acid wash solution is passed over the 8-HQ column. [c] 10-way selection valve remains in position 1 (sample port). For calibration this valve switches to positions 2-10 (depending on the number of standards to be run).

2.4.3 Interface

Instrument control was achieved via a DAQCard-DIO-24 card (National Instruments Corp., Newbury, UK) with 24 digital input/output TTL lines, and signal acquisition was via a DAQCard-700, with 16 channel, 12-bit A/D conversion. This card was also used for changing PMT gain. Virtual instrument (VI) software (Ruthern Instruments Ltd., Bodmin, UK) was written in LabVIEW® version 5.1 (National Instruments Corp.).

Figure 2.5 LabVIEW® graphical user front panel for the automated virtual instrument.

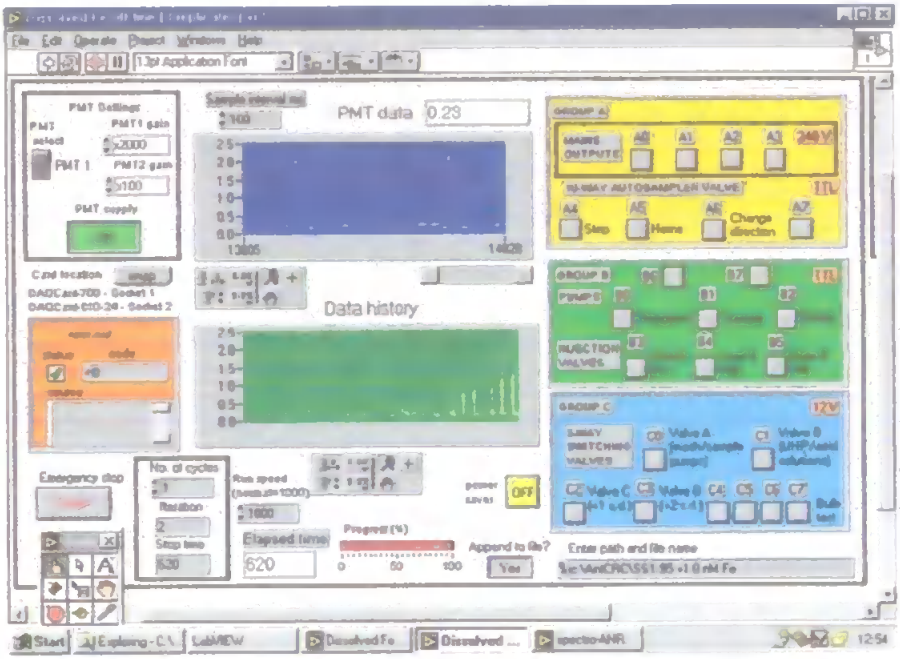

Figure 2.6 Wiring diagram showing the graphical code for instrument control and data acquisition. This code drives the functions shown on the *Front Panel* in Figure 2.5.

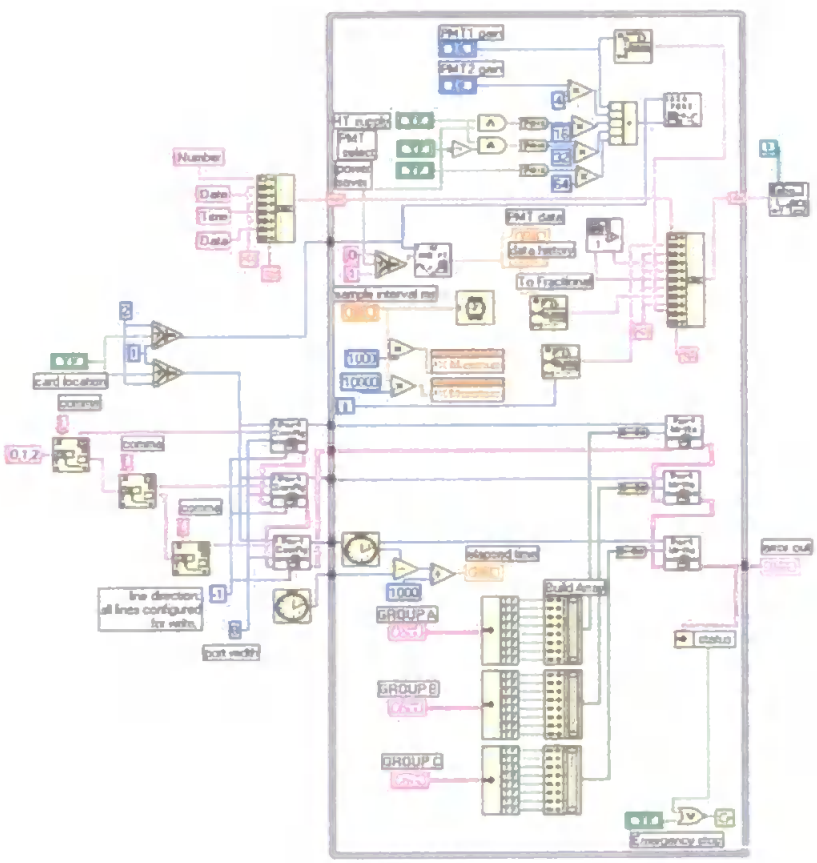

The interface had two units, one for controlling pumps and valves and one for the PMT and signal processing (Figure 2.4). The LabVIEW® VI front panel contained ready-to-use switches, buttons, controls and graphical displays of detector readings (Figure 2.5). Each element in the front panel was connected via the wiring diagram (Figure 2.6), which included functions for signal processing, timing of operations and file management.

2.4.4 Detector performance

The PMT interface contained a 4-position switched gain amplifier (Figure 2.4). This provided settings of x100, x1000, x2000 and x5000, selectable by the control VI software, which allowed the sensitivity to be adjusted to suit the variable concentrations of iron found in seawater. The effect of each of these settings on the CL background emission, background noise and analyte signal for a 2.0 nM iron(II) standard was investigated in direct injection mode (i.e. no preconcentration column), and the results are shown in Figure 2.7.

The CL background noise (peak-to-peak) showed no change with gain setting, but both the CL emission for iron and the background CL emission both increased linearly with respect to PMT gain. The maximum signal-to-noise ratio was obtained at the highest gain setting (x5000), which was therefore most suitable for iron depleted open-ocean measurements. For environments with higher iron concentrations (such as coastal and estuarine waters), a lower gain setting can be used to provide an expanded linear range.

Instrumental drift was monitored during the Atlantic Ocean shipboard trials by regularly measuring the CL background emission and background peak-to-peak noise, blank signals and calibration slopes. Sensitivity variations may result from temperature fluctuations (affecting both the PMT detector and CL chemistry), differences in reagent composition between batches, reagent ageing and degradation of pump tubing (affecting flow rates).

Figure 2.7 Effect of changing the PMT gain on the CL background emission, CL background peak-to-peak noise, analyte signal and signal-to-noise ratio with the instrument in direct injection mode (no preconcentration).

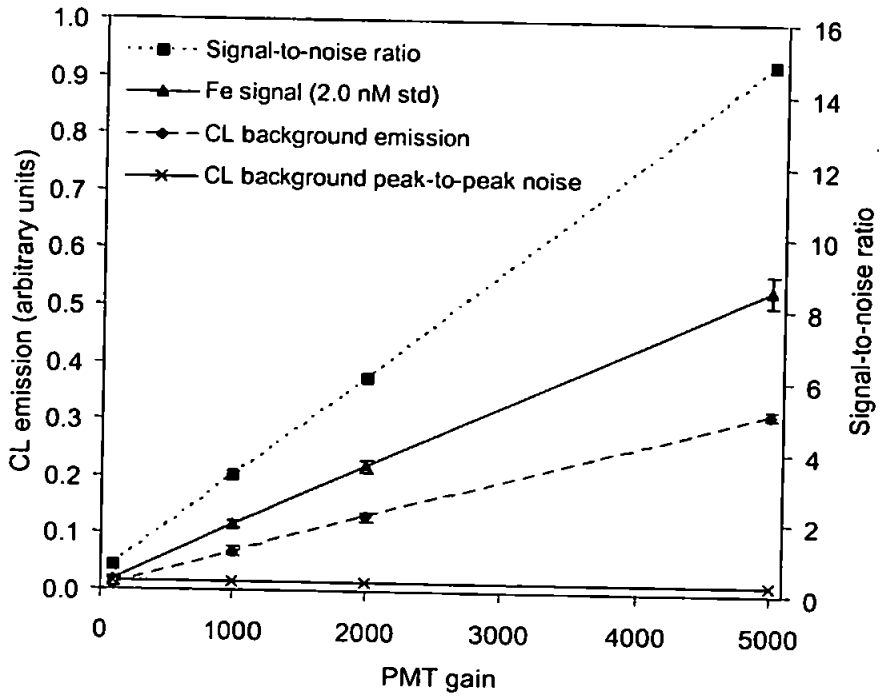

The effect of temperature on the CL background noise and analyte signal generated using a 2.0 nmol l^{-1} iron(II) standard prepared in UHP water with the FI system in direct injection mode (i.e. 8-HQ microcolumn removed; see 2.5.2) was studied over a 24 h period. No significant changes in CL background noise (<2 % drift, one measurement made each second, n > 80,000) or analyte signal (<6 %, 86 ± 5 mV, n = 36) were observed, despite a 5.5 °C change in laboratory temperature. However, to minimise the risk of possible changes in sensitivity with temperature, the complete system was housed in an air conditioned clean air laboratory container.

2.4.5 Analytical figures of merit and blank measurement for dissolved iron

Figure 2.8 shows a typical FI trace for the blank, sample and standard additions of 0.2 – 1.0 nM iron(II) spikes to a seawater sample. The mean repeatability and standard deviation for 4 replicates over this range was 5.9 ± 3.2 %. The standard addition plot showed excellent linearity (R^2 =

0.9979) over this range. The iron(II) blank during the trial was typically 24 ± 7 pM (n = 4), resulting in a limit of detection of 21 pM (defined as three times the standard deviation of the blank). The major contributions to the blank signal were from iron impurities in the ammonium acetate sample buffer, UHP water used for column washing, and (for iron(II+III) determinations) the acid and sulfite used for sample pre-treatment. [163] For Fe(II) measurement, the limit of detection can be reduced by placing an 8-HQ cleaning column on the UHP water line to clean up the water wash. [64]

Figure 2.8 Shipboard calibration* peaks and corresponding standard additions plot for iron over the range 0.2-1.0 nM.

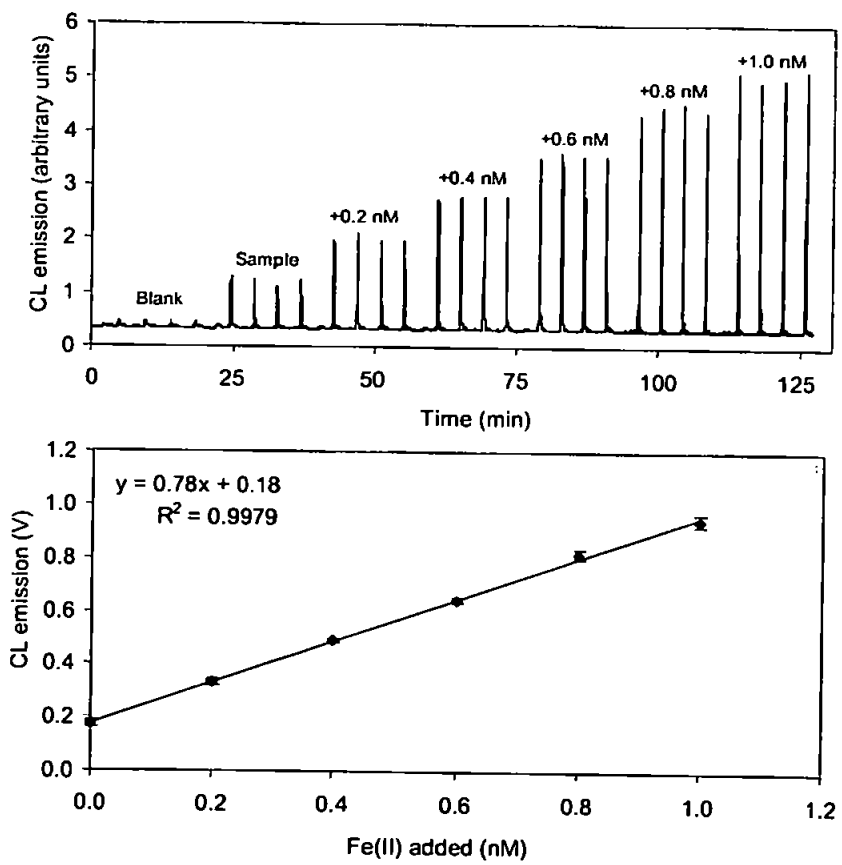

*20 mL sample aliquots were spiked with varying volumes of Fe(NH4)2(SO4)2.6H2O, shaken well and equilibrated for 20-30 min and then analysed within a 1h period.

Blank determination for dFe was achieved by finding the sum of three components; Reagent and injection blank (B_{RI}), acid blank (B_{HCl}) and sulphite blank ($B_{Sulphite}$), i.e.:

$$B_{Total} = B_{RI} + B_{HCl} + B_{Sulphite}$$

The reagent and injection blank was determined before and after each batch of sample measurement whereas B_{HCl} and $B_{Sulphite}$ were determined by separate standard addition analysis. B_{RI} was measured by finding the mean of >3 injections after ammonium acetate sample buffer and UHP water were loaded onto the 8-HQ column and eluted into the reagent stream. To achieve this, the seawater sample line was disconnected and the lines were equilibrated with ammonium acetate buffer before commencing the measurement.

B_{HCl} was found by spiking two aliquots of UHP water with HCl to give solutions of 0.005 and 0.015 M HCl. Standard additions of Fe(II) (0 – 0.5 nM) were later made to each aliquot and B_{HCl} was quantified (pM) as the difference between the intercept of the two linear plots. Similarly $B_{Sulphite}$ was found after two aliquots of UHP water were spiked with sodium sulphite to give 100 and 300 μM concentrations. After Fe(II) standard additions, the blank was measured as half of the difference between the intercepts. Generally B_{HCl} and $B_{Sulphite}$ were both < 20 pM and B_{RI} was < 50 pM.

2.4.6 Dissolved iron determination in the field: Trial hydrocast

The optimised FI-CL instrument was tested at a hydrocast station close to the Antarctic continent during a Southern Ocean expedition (November 2001) along the CLIVAR SR3 line (~141°E). Clean surface seawater was supplied to the FI manifold at sea using a high volume peristaltic pump (7591-00, Cole Palmer Instrument Co.) connected to a torpedo-shaped fish, which was towed alongside the research vessel at a depth of 1-2 m below the surface, 5 m from the ship's hull.

For water column samples, seawater was collected in acid-washed polycarbonate samplers suspended off Kevlar hydroline, following standard trace metal sampling methods. [197] Seawater was filtered in-line through a 0.4 μm cellulose acetate membrane contained in a polypropylene cartridge unit (Sartorius, Epsom, UK). Samples for iron(II) determinations were fed directly to the analyser at ambient seawater pH. Samples for iron(II+III) were acidified to pH ~2 with Q-HCl and reduced off-line using 100 μM Na_2SO_3 (12 h) prior to analysis.

Figure 2.9 Typical depth profile of dFe and temperature in the upper water column of the Southern Ocean south of Australia.

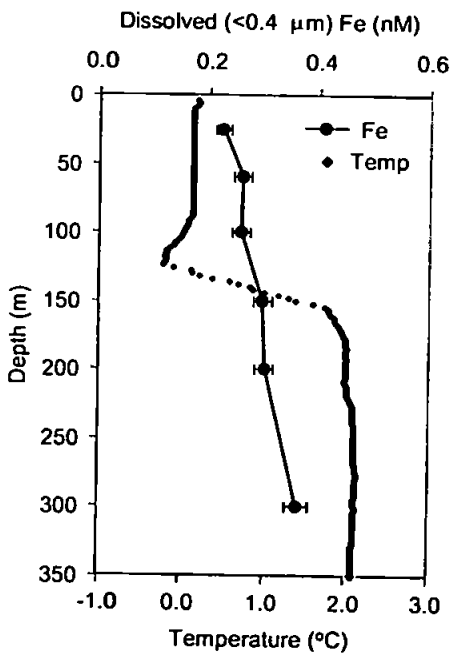

Figure 2.9 shows the profiles of dFe and temperature in the upper water column (25 – 300 m). Iron concentrations were between 220 and 360 pM at this location, consistent with literature data. [198] At sea, the instrument was totally reliable over 50 days of near continuous use for surface transects and depth profiling, with no downtime in spite of the harsh conditions experienced in this

environment. A report on the environmental significance of the complete dataset, obtained using this instrumentation, for the 2001 CLIVAR SR3 expedition will be presented elsewhere.

2.5 Automated monitoring of picomolar concentrations of dissolved iron(II) in surface seawater: field trials [189]

To test the capability of the FI-CL system to determine Fe(II) in surface waters, shipboard trials were conducted during expedition AMT XIII/1 (September 29th – October 23rd 2000) aboard PS *Polarstern*. A north-south transect of the Atlantic Ocean was undertaken during the cruise from Bremerhaven (Germany) to Cape Town (South Africa). The regions of the open Atlantic Ocean covered during this voyage receive trace metal inputs dominated in the tropics and sub-tropics by wet and dry atmospheric deposition, predominantly due to episodic, long-range transport of Saharan dust, and precipitation through the migrating Inter-Tropical Convergence Zone. Moreover, high daytime irradiance levels experienced through large sections of this transect meant that this was an interesting area in which to study the possible effects of photochemistry on iron redox speciation.

A second shipboard trial was conducted in a contrasting environment aboard RSV *Aurora Australis* as part of the CLIVAR SR3 expedition in the Southern Ocean south of Australia (October 28th – December 12th 2001). Cold seawater temperatures and low H_2O_2 concentrations may lead to extended iron(II) oxidation half-lives in these waters. [197, 199] During the return voyage to Hobart (Australia) a north-south transect was undertaken across a filament of the Sub-Antarctic Front (SAF). In contrast to the open Atlantic Ocean, this is an area of extremely low atmospheric iron deposition and long summer daylight periods, although irradiance levels are variable due to persistent cloudy skies, even during the austral summer.

2.5.1 Sampling

Continuous underway sampling of surface (1-2 m) seawater was performed using a towed torpedo-shaped fish deployed off the crane arm of a hydrographic winch at a distance of ~5 m from the ship's starboard side. [165, 199] For the Atlantic Ocean survey, seawater was pumped on-board using a variable speed high volume peristaltic pump (model 7591-00, Cole Palmer Instrument Co.), fitted with silicone pump tubing and filtered through a Sartobran-P polypropylene cartridge unit with a 0.2 μm cellulose acetate filter membrane (Sartorius Ltd., Epsom, UK). For the Southern Ocean survey, seawater was pumped on-board using a pneumatic PVDF double-diaphragm pump (model P.025, Wilden) and filtered through a Whatman Polycap (model 150TC) filter with 0.2 μm polyethersulfone filter membrane. Water from the sampling tubing entered a clean container laboratory positioned on the ship's aft deck, passed through a flow regulator and was split into two channels. Seawater from one line was fed directly to the FI-CL iron(II) analyser (Figure 2.3) whilst the other line provided a collection point for discrete samples which were later analysed for dissolved iron(II+III) by FI-CL.

Elevated signals were observed for the first few (5-6) sample injections of each automated run of the iron(II) analyser. This phenomenon was believed to be due to either low level contamination from the Cheminert injection valves or photoreduction of iron in seawater sitting in the transparent PTFE flow lines contained within the laboratory van. Thus data from the initial peaks for each run are not considered. The timing of each sample injection was determined by back calculation from the time (in UTC, Co-ordinated Universal Time) each data file was written to disk, and this time was adjusted for lag time delays due to surface water pumping and analysis (5.5 min on the Atlantic Ocean survey, 13.0 min on the Southern Ocean survey). The iron(II) concentration data were then combined with the ship's position and underway surface water parameters recorded on the ship's data logger.

2.5.2 Method chemistry

In-line adjustment of sample pH was necessary to ensure optimum preconcentration of iron(II) species onto the 8-HQ resin, whilst minimising the effect of any interfering species which bind to 8-HQ at higher pH (e.g. Mn). [183] Many other species are also known to catalyse the luminol reaction in the absence of selective analyte extraction and preconcentration. [200] As such, these iron(II) measurements represent the operationally defined fraction that is extracted onto an 8-HQ microcolumn after short (1 min) in-line buffering of sample to pH 5.5. It is recognised that the iron(II) oxidation rate will be retarded and stability enhanced at lower pH (see Chapter 1). Ideally, iron(II) measurements should follow a sampling and pre-treatment protocol that maintains speciation integrity as closely as possible (as discussed in Chapter 3).

The iron(II) detected using this approach was not thought to be an artefact of the analytical method as the residence time of the sample in the 8-HQ microcolumn is short (<1.7 s). No significant reduction of inorganic iron(III) was observed in aged, filtered Southern Ocean seawater solutions spiked with up to 5.0 nmol L^{-1} iron(III), although a signal statistically higher than the blank was observed for the larger Fe(III) additions (<7 % of analyte signal obtained for equimolar spiked iron(II) standards, discussed in Chapter 3).

Direct injection iron(II) measurements without the preconcentration protocol (and hence not operationally defined) are also possible by removing the 8-HQ microcolumn and sample buffer line. To achieve this, the 8-HQ column within injection valve I2 is replaced with a sample loop (typically 100-150 µl), UHP water is used as carrier instead of an HCl eluent stream, and the column wash step (see Figure 2.3) is eliminated. In this manifold, injection valve I1 is not required, as seawater is fed directly to the loop within valve I2. The detection limit of this method (found during these trials) is an order of magnitude higher than with the 8-HQ column manifold (~0.2 nmol L^{-1}), and thus unsuitable for open-ocean iron(II) measurements where dissolved iron(II+III) concentrations are extremely low (<0.1 nmol L^{-1}). However, this no-preconcentration version of the

iron(II) system is particularly useful as a tracer for rapid underway mapping during iron fertilisation experiments although it is important that the protocols described below are followed when determining the analytical blank. Positive interference from pM concentrations of Co(II) [163] can be removed for all these methods, by adding dimethylglyoxime (20 μM) to the luminol stream. [64]

2.5.3 Blank measurement and calibration

The blank measurement for on-line Fe(II) determination was defined as the mean CL signal of >6 injections after ammonium acetate sample buffer and UHP water were loaded onto the 8-HQ column and eluted into the reagent stream (Reagent and injection blank (B_{RI})). To achieve this, the seawater sample line was stopped at the 'Y'-piece (to the right of pump B in Figure 2.3) and the associated pump tubing disconnected. The lines were then equilibrated with ammonium acetate buffer before beginning the measurement. B_{RI} was generally of the same order as the sample Fe(II) signal, thus >6 replicates were taken before and after on-line seawater analyses to accurately determine the mean blank (that was to be extracted from the signals detected from each batch of samples) and limit of detection (3s).

System calibration was performed as follows: Low-iron seawater, which had been previously collected and allowed to age in the dark, was adjusted to pH 2.0 with triple quartz-distilled hydrochloric acid (Q-HCl) and 100 μM sodium sulphite added to ensure the iron in the sample was present in the reduced, ferrous form. Standards prepared at pH 2.0 in the presence of a reducing agent were necessary in order to prevent re-oxidation of iron(II) which may have occurred at a higher pH. After a >8 h reduction period, standard additions of iron(II) in the range 0-1.0 nmol l^{-1} were made to this solution and immediately introduced into the FI-CL analyser. The sensitivity of the system to iron(II) was ascertained from the slope of the standard curve.

2.5.4 System operation

Prior to use, the PTFE flow lines, fittings, connectors and 8-HQ microcolumns of the FI manifold were cleaned with 0.5 M Q-HCl and UHP water for >8 h. The system was calibrated at the start and end of each batch of reagents and also after any change in sensitivity (e.g. after change in temperature). For sample analysis, filtered (0.2 μm) ambient pH seawater was continually pumped from the towed torpedo fish into a 5 m (2.2 ml) holding loop (Figure 2.3) contained within injection valve I1. If air bubbles form in the holding loop (e.g. due to the de-gassing that may occur when very cold seawater enters a warm container laboratory) the injection valve I1 can be replaced by a polyethylene bottle or PTFE de-bubbling vial that temporarily stores a small volume (e.g. 2 ml) of seawater pumped from the tow-fish for subsequent sub-sampling using a PTFE tube from the FI system. On switching I1 to the elute position, 1.6 ml of sample was drawn into the FI manifold where it was buffered in-line to pH 5.5 on passing through a 0.57 m (250 μl) mixing coil.

The iron(II) in the buffered sample was preconcentrated and separated from the seawater matrix as it passed for 1 min over the 8-HQ microcolumn contained within injection valve I2 (see section 2.5.2). A distribution valve allows the system to be switched from sample analysis mode to calibration mode whereby up to 9 flow lines may be fed to spiked standard solutions. During calibration, seawater from the fish is continually pumped through the holding loop in injection valve I1 and to waste.

One complete analytical cycle was completed within 3 min. During this time, injection valve I1 was returned to the load position and seawater continually pumped through the holding loop ready for the next sample load. Using one batch of reagents, two blank measurements (in triplicate), two calibration curves (seawater standard plus two additions, in triplicate), and up to 8 h (160 peaks) of continuous on-line determination of iron(II) can be performed. With a sampling and analysis sequence taking place every 3 min, a measurement is made every 0.9 km of the ship's track if the cruising speed is ~10 knots (18 km h^{-1}).

2.5.5 Results and discussion

Analytical performance

Instrumental drift was monitored during the Atlantic Ocean shipboard trials by regularly measuring the CL background emission and background peak-to-peak noise, blank signals and calibration slopes. Sensitivity variations may result from temperature fluctuations (affecting both the PMT detector and CL chemistry), differences in reagent composition between batches, reagent ageing and degradation of pump tubing (affecting flow rates). The effect of temperature on the CL background noise and analyte signal generated using a 2.0 nmol l^{-1} iron(II) standard prepared in UHP water with the FI system in direct injection mode (i.e. 8-HQ microcolumn removed; see section 2.5.2) was studied over a 24 h period. No significant changes in CL background noise (<2 % drift, one measurement made each second, n > 80,000) or analyte signal (<6 %, 86 ± 5 mV, n = 36) were observed, despite a 5.5 °C change in laboratory temperature. However, to minimise the risk of possible changes in sensitivity with temperature, the complete system was housed in an air conditioned clean air laboratory container.

The sensitivity of the system was evaluated by comparing the slopes of calibration curves for standards prepared in low iron seawater (LISW), collected from the Southern Ocean Iron RElease Experiment (SOIREE) site (61°S 140°E) at a depth of approximately 500 m. [30] Standard additions of 0.2, 0.4, 0.6, 0.8 and 1.0 nmol L^{-1} iron(II) were made. System sensitivity varied <5 % on a single day (800 ± 40 mV per nmol L^{-1}, $r^2 = 0.998$), but up to 10 % between days (typically 775 ± 73 mV per nmol L^{-1}, $r^2 = 0.995$). The precision for the standard addition solutions was in the range 0.9 - 6.2 % RSD (n=4). The iron(II) blank was typically 24 ± 4 pmol l^{-1} (n = 4), resulting in a limit of detection of 12 pmol L^{-1} (defined as three times the standard deviation of the blank). Shipboard calibrations were performed at the beginning and end of each reagent batch (10 h periods). Four replicates of each solution were made. The CL background noise showed good stability and reproducibility between replicate (n=4) injections was typically <3 %.

Atlantic Ocean survey

Figure 2.10 shows the results from the continuous determination of iron(II) in surface waters of the south-east Atlantic Ocean during one 10 h day-night period. Concurrent sea-surface temperature, salinity and incident solar radiation are also shown. The on-line system was calibrated prior to switching to fully automated mode at 12:40 UTC on 20th October 2000. Continuous analyses were conducted until 22:34, except between 17:33 and 18:03 when a flow problem through the filtration cartridge needed to be rectified. The ship travelled between 23°17' S, 8°39' E and 24°48' S, 9°59' E during the trial. During daylight hours, light cloud cover was present and dusk occurred between 17:45-18:15 UTC. Sub-samples were also taken hourly from the on-line system during the trial, acidified and reduced (0.01 M Q-HCl, 100 μM Na_2SO_3), and analysed at sea by FI-CL for dissolved iron(II+III). [163]

The results (Figure 2.10) for iron(II) showed concentrations in the subtropical, oligotrophic Atlantic Ocean ranging from below the detection limit (<12 pmol l^{-1}) during darkness up to 45 pmol l^{-1} at 12:50 UTC, at which time the solar intensity was close to the maximum experienced during the trial. The concentration of dFe(II+III) in surface waters generally increased during the survey, but was low compared to other data [198] for the Atlantic Ocean (164 ± 35 pmol l^{-1}, n=10). Dissolved iron(II) or dFe distributions are not correlated with subtle changes in temperature and salinity. Interestingly, the iron(II) to iron(II+III) ratio decreased steadily from 37 % at 13:05 to 3 % at 21:07, suggesting that the iron(II) concentration was independent of changes in water mass. These data are consistent with earlier work that suggests photochemical reduction of iron(III) to be the dominant mechanism for iron(II) production in the Southern Ocean, [30, 199] offshore waters of Peru [200] and northern Australian shelf waters. [81] Our data also support previous results demonstrating diurnal cycling between total "reducible" (dissolved/bioavailable) and "non-detectable" (colloidal/particulate) iron concentrations in natural seawater incubations spiked with added iron. [80] The reduction of iron(III) to transient iron(II) species, either photochemically or involving marine microorganisms, may increase the solubility and bioavailability of iron in seawater.

Figure 2.10. (a) Concentration of 8-HQ-reactive iron(II), dFe and the iron(II)/dFe ratio during a 10 h shipboard deployment in the Atlantic Ocean, (b) surface temperature and salinity (10 min resolution), and (c) global solar radiation (10 min resolution) over the period 10:00-00:00 (UTC) on 20th October 2000. A typical error bar (1s) for the iron(II) concentrations is shown. The horizontal black bar represents the dark period during the survey.

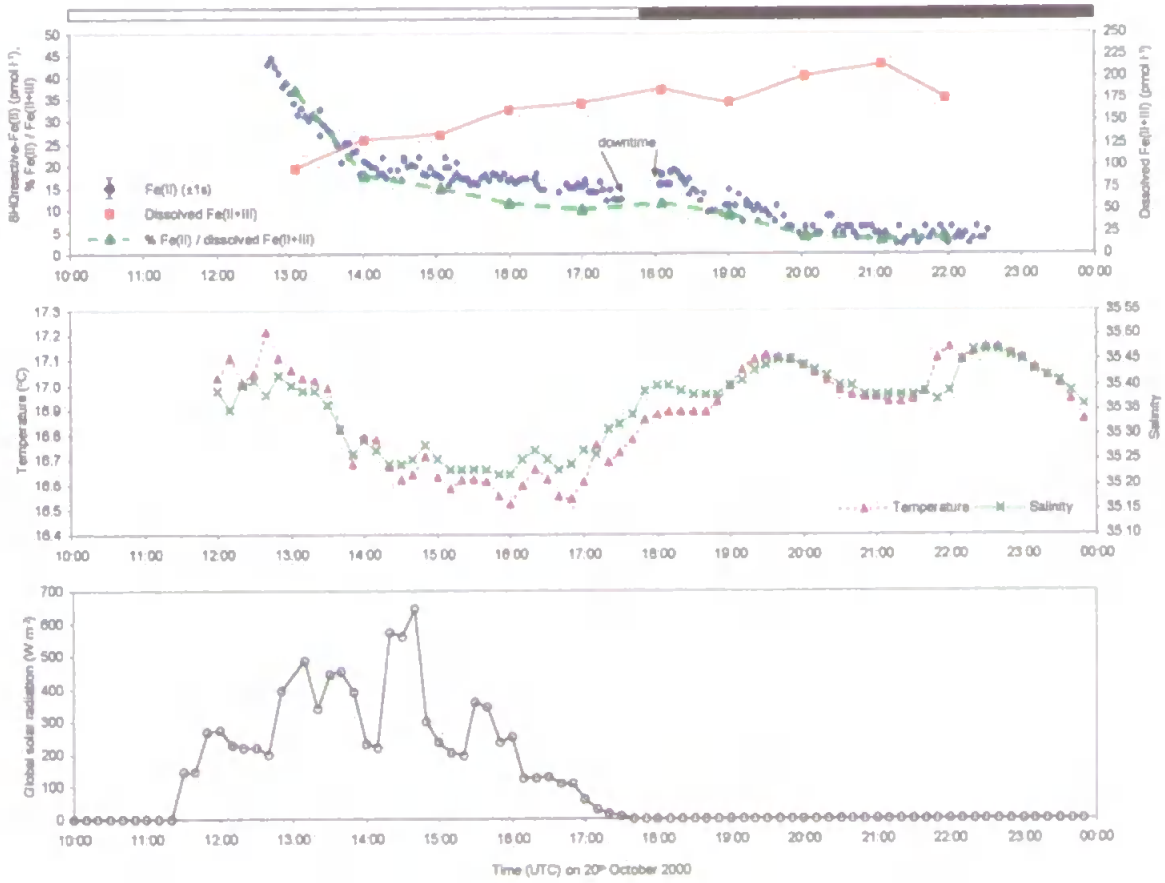

Southern Ocean survey

A short (5 h) trial was also undertaken in the Australian sector of the Southern Ocean between 50°92' S, 143° 38' E and 51°25' S, 143°03' E, in the Sub-Antarctic Front (SAF). The objective was to demonstrate the generic capability of the instrumentation by deploying it in a contrasting marine environment. Iron(II) was measured from 21.00 on 10th December 2001 to 05.00 UTC on 11th December 2001 (local daytime) during austral summer. Conditions were partly overcast. Calibration standards were prepared as described above, and three replicates of each solution were made. The mean detection limit from daily shipboard calibrations was 8.7 pmol l^{-1} and reproducibility between replicate (n=3) blank injections was RSD <7.6 % A 'de-bubbler' polyethylene sub-sampling bottle replaced injection valve I1 during this survey (see Section 2.5.2). Unfortunately, there are several short periods where no data were recorded. This was due to a problem with the continuous supply of surface water from the tow-fish, which was a deployed in increasingly rough seas.

The results (Figure 2.11) show concentrations ranging from below the detection limit up to 29 pmol l^{-1} for iron(II). dFe concentrations generally increased during the transect from 99 pmol l^{-1} at 22:06 to 257 pmol l^{-1} at 03:03 UTC, although total dissolvable iron (i.e. unfiltered and acidified, TDFe) levels (not shown) were fairly constant (399 ± 33 pmol l^{-1}, n=16).

These data are consistent with the low surface dFe concentrations (0.1-0.2 nmol l^{-1}) observed in previous studies of this region. [197,201] In the period 00:40 to 03:10, a significant shift in temperature (1.0 °C) and salinity (0.2 units) was observed, suggesting the intrusion of a different water mass, although this resulted in no clear trend in iron(II), dFe or TDFe concentrations. The iron(II) to iron(II+III) ratio was variable and ranged from 4 to 13 %. The Southern Ocean iron(II) concentrations are also in the same range as the south-east Atlantic data, but are closer to the detection limit, have greater temporal variation, and are out of phase with the variable solar irradiance profile, suggesting that photochemically-mediated reduction of iron(III) to iron(II) was not dominant.

Figure 2.11 (a) Concentration of 8-HQ-reactive iron(II), dFe and the iron(II)/dFe ratio during a 5 h shipboard deployment in the Southern Ocean, (b) surface temperature and salinity (5 min resolution), and (c) global solar radiation (portside, 5 min resolution) over the period 21.00 on 10th December 2001 to 05.00 (UTC) on 11th December 2001.

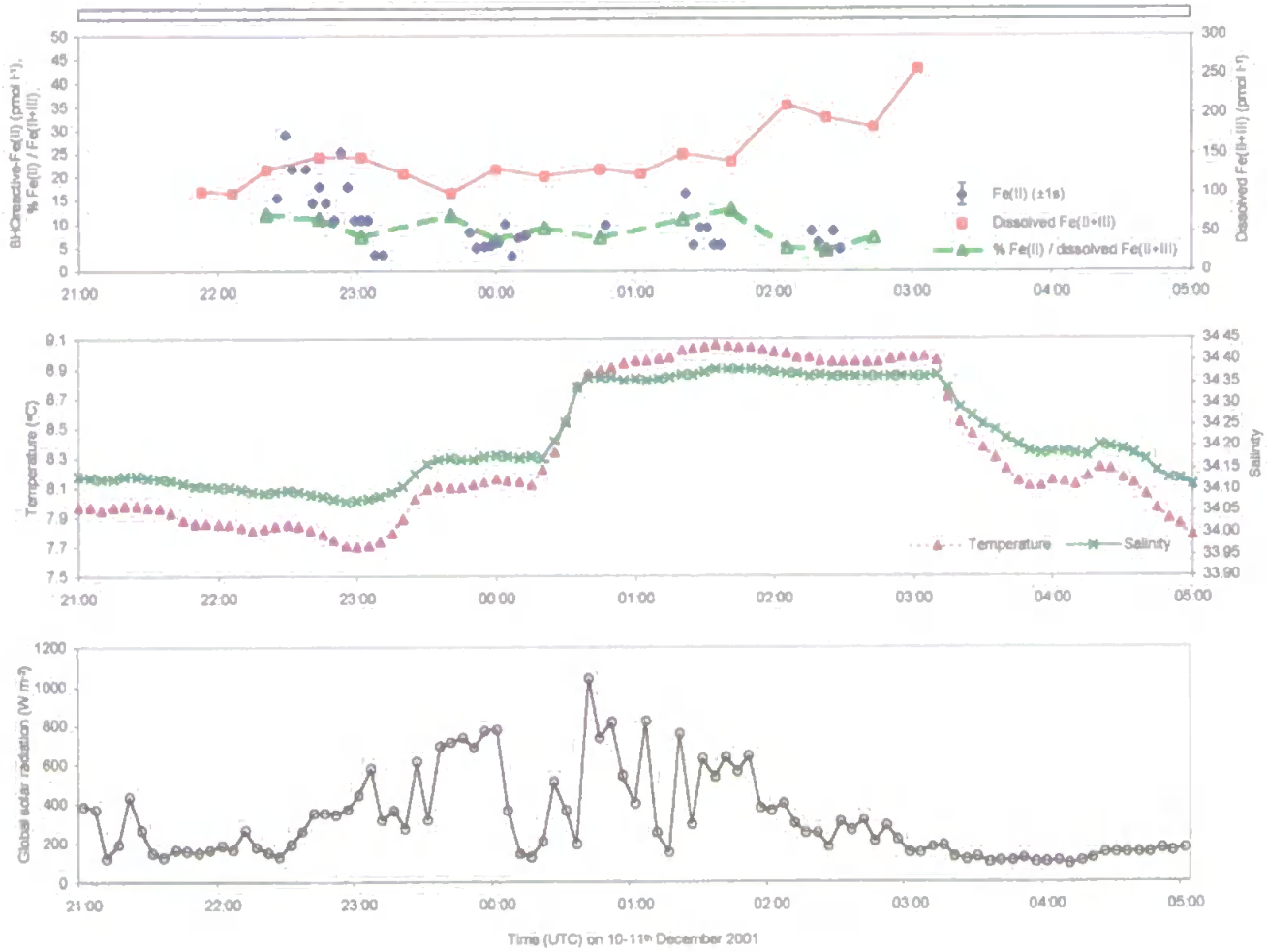

2.6 Direct determination of iron(II) in seawater using a matrix matched flow injection manifold with chemiluminescence detection [202]

The aim of this work was to develop and optimise a flow-injection method based on selective luminol chemiluminescence detection with no added oxidant or preconcentration column for the determination of iron(II) in natural waters. A further requirement was that the manifold could use the sample matrix as the carrier in order to eliminate the possibility of speciation changes caused by adding buffer or removing the analyte by solid phase extraction. The rationale was that the resulting method could then be compared to the FI-CL system described above (which includes buffer addition and a preconcentration step) to separate and assess the interferences and analytical artefacts individually associated with the luminol chemiluminescence reaction and use of the 8-HQ column. Furthermore, using the two systems simultaneously allowed real-time comparisons of their analytical attributes.

In this study, an FI-CL method is described for the rapid and selective determination of Fe(II) in acidified seawater by its catalytic effect on the oxidation of luminol in the absence of added oxidant and without a preconcentration column. The manifold used is similar to previously reported methods [66, 190] but uses a seawater carrier stream (rather than 0.7 M NaCl at pH 7.0 or ultra-pure water). Manifold parameters have been optimised, several buffers have been investigated and the method applied to the determination of Fe(II) in a coastal seawater certified reference material.

2.6.1 Reagents and standards

All plastic ware used during the experiments and for storage of reagents and standards was cleaned with 50% HCl for 48 h, thoroughly rinsed with ultra high purity (UHP) deionised water (18.2 MΩ

cm^{-1}, Elgastat, Maxima, England) and stored in re-sealable plastic bags to prevent contamination. All reagents and standards were of analytical grade (supplied by VWR unless stated otherwise), were prepared in UHP water and further diluted immediately prior to use. Low nutrient seawater (LNS, salinity 35) was obtained from Ocean Scientific International, Petersfield, England.

An iron(II) stock solution (0.01 M) was prepared by dissolving 0.196 g of $Fe(NH_4)_2(SO_4)_2.6H_2O$ in 50 mL of HCl (0.01 M, prepared every 15 days). The standards were prepared daily in LNS adjusted to pH 3.0 to prevent oxidation of Fe(II). Standard solutions of Mn(II), Cu(II), Ni(II), Zn(II), Pb(II), Co(II) and Cr(III) were prepared from atomic absorption standards (Spectrosol, BDH, England) in LNS (pH 3.0). Iron(III) standard was prepared directly from $NH_4Fe(SO_4)_2.12H_2O$.

Luminol stock solution (0.01 M) was prepared by dissolving 0.089 g of luminol (5-amino-2, 3-dihydro-1, 4-phthal-zinedione, Fluka) in 50 mL of borate buffer followed by sonicating for 30 min. A working luminol solution (1×10^{-3} M) was prepared by diluting 10.0 mL of the stock solution in 100 mL of borate buffer (0.1 M) and adjusting to pH 10.4 with sodium hydroxide (2 M). The following buffer solutions were used for luminol solution preparation; NH_3/NH_4, Tris/NaOH, carbonate/NaOH and borate/NaOH (all 0.1 M, pH 10.5).

2.6.2 FI manifold

The FI-CL manifold used for the determination of Fe(II) is shown in Fig. 2.12. A 4 channel peristaltic pump (Minipuls 3, Gilson, France) was used to propel the sample carrier and reagent solutions at a flow rate of 2.0 mL min^{-1}. A rotary injection valve (Rheodyne 5020, UK, 270 µL sample loop) was used to inject Fe(II) standards into the LNS (pH 8.0) stream and was merged at a T-piece with the CL reagent stream. The merged streams travelled 3.0 cm before passing through a quartz glass spiral flow cell (1.1 mm i.d., 130 µL internal volume) placed directly in front of an end window photomultiplier tube (PMT, Thorn EMI, 9798QA).

The PMT, quartz glass coil and T-piece were enclosed in a light tight housing and aluminium foil was placed behind the coil to reflect light onto the photo-cathode. The PMT was attached to a 1 kV power supply (Thorn EMI, PM20NS, England) and an integral amplifier was powered from an independent 15 V power supply (BBH Power Products, England). The detector output was recorded using a chart recorder (Kipp & Zonen, Delft, The Netherlands).

Figure 2.12 Flow injection with chemiluminescence detection (FI-CL) manifold for the determination of Fe(II).

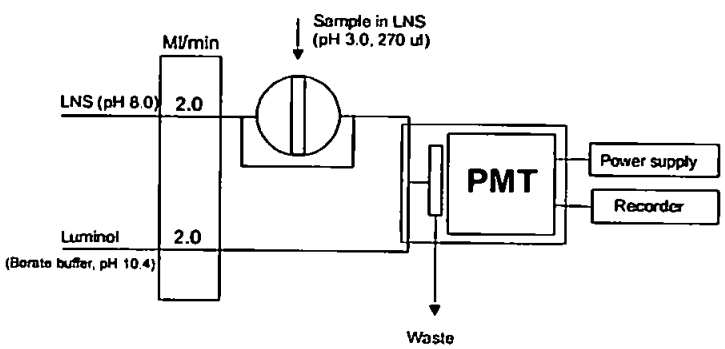

2.6.3 Optimisation of FI manifold

In order to establish optimum conditions for the determination of Fe(II), various parameters were investigated including buffer concentrations and pH, reagent concentrations, sample volume, reagent flow rates and photomultiplier voltage. All these studies were performed using a 100 nM Fe(II) standard. A univariate strategy was deliberately adopted in order to understand the effect of each variable on the reaction chemistry and the system response.

The efficiency of luminol chemiluminescence is particularly dependent on reaction conditions. In the proposed FI-CL system, different buffers were investigated (NH_3/NH_4, Tris/NaOH, carbonate/NaOH and borate/NaOH; 0.1 M, pH 10.5). The CL responses for 100 nM Fe(II) using these buffers were 5.0, 15.0, 20.0 and 350 mV (n =4) respectively. LNS formed a precipitate with the carbonate buffer and CL signals were irreproducible with an unsteady baseline. The CL responses were very small when using ammonia and Tris-HCl buffers and maximum CL response was obtained with borate buffer. The optimum pH for the luminol reaction with borate buffer was therefore investigated in the range 9.8 – 10.8. Maximum CL emission was observed at pH 10.4, as shown in Fig. 2.13, and was therefore used for all subsequent studies.

Figure 2.13 Effect of borate buffer pH on the peak response of the luminol CL reaction.

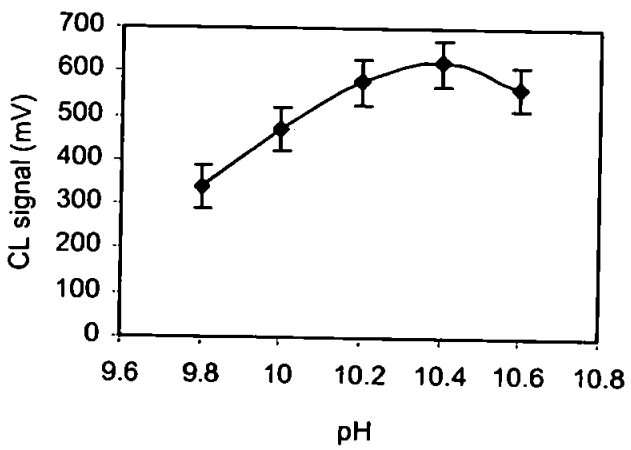

The effect of the luminol concentration was then studied over the range $1x10^{-2} - 1x10^{-6}$ M using the optimised buffer conditions. As shown in Fig. 2.14, the CL response increased up to $1x10^{-3}$ M luminol (used in all subsequent experiments), above which the response decreased due to photon quenching. Variation in reagent sensitivity was observed over time as the luminol solution aged, as found by other workers, [66] and therefore it was always prepared 24 h before use.

Figure 2.14 Effect of luminol concentration on the determination of Fe(II).

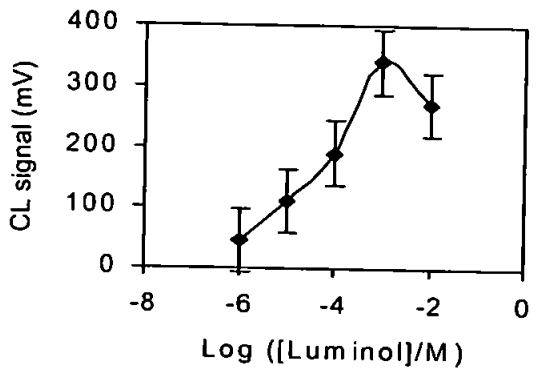

The effect of the flow rate of the carrier and reagent streams was studied over the range 1.0 – 3.0 mL min^{-1} in terms of CL response, speed of analysis and reagent consumption (where the flow rates of the two streams are matched). At a flow rate of 2.0 mL min^{-1} (for both individual channels), maximum CL intensity was observed with a steady base line and reproducible peak heights (Table 2.5). Hence this flow rate was used for all subsequent experiments The effect of the sample volume on CL response was studied in the range of 45 – 450 μL. Maximum CL response was obtained at 270 μL (Table 2.5) and was selected for all subsequent experiments.

The effect of LNS pH on the determination of Fe(II) was investigated in the range 1.0 – 5.0. There was an increase in CL intensity up to pH 3.0 but a higher pH decreased the CL intensity (Table 2.5). Therefore, LNS at pH 3.0 was used for the preparation of all Fe(II) standard solutions to prevent oxidation of iron(II). The effect of PMT voltage over the range 900 – 1300 V was optimised for maximum CL signal-to-noise (Table 2.5). CL response increased linearly with PMT voltage but 1050 V was used for all subsequent studies because it gave the best signal-to-noise ratio.

Table 2.5 Effect of various parameters on the CL peak response for the determination of 100 nM Fe(II)*

Flow Rate (mL/min)	1.0	1.5	2.0	2.5	3.0
CL signal (mV)**	300	450	760	755	750
Sample volume (μL)	90	180	270	360	450
CL signal (mV)**	250	460	510	500	500
PMT voltage (V)	900	1000	1100	1200	1300
CL signal (mV)**	32	90	250	580	1400
LNS pH	1.0	2.0	3.0	4.0	5.0
CL signal (mV)**	390	410	450	430	400

*For each parameter the following conditions for all other parameters were used, i.e. flow rate 2.0 mL/min; sample volume 270 μL, PMT voltage 1050 V, LNS pH 3.0.

** Mean of four injections

2.6.4 Calibration and blank protocol

Using the optimum conditions described above, the calibration data of CL response versus Fe(II) concentration using acidified LNS (pH 3, 2.0 – 10 nM Fe(II)) is shown in Table 2.6 The correlation coefficient was 0.993 (n=5) and the regression equation was $y = 2.65x - 2.10$ [y = CL response (mV), x = concentration (nM)]. The relative standard deviation of the method was 1.0 – 3.7 % (n=4) over the range studied. The limit of detection (3 x standard deviation of the blank) was 0.1 nM Fe(II). The time between injection and detection with the optimised system was 12 s, which makes the method suitable for high resolution shipboard monitoring of Fe(II) in marine waters.

To obtain an analytical blank for the calibration graph, LNS (pH 5.0) was first passed through a pre-cleaned 8-hydoxyquinoline column (8-HQ, 2.5 mm x 3.0 cm, washed with HCl (0.5 M) for 24

h, followed by a UHP water rinse) [163] at a flow rate of 0.3 mL min^{-1}. Thereafter, the LNS was adjusted to pH 3.0 with HCl (2.0 M) and used as a blank for the proposed FI-CL system. The blank signal was reduced by approximately 50% compared with the signal from untreated LNS (pH 3.0).

Table 2.6 Calibration data

Iron Standards (nM)	2.0	4.0	6.0	8.0	10.0
CL intensity (mV)*	4.0	8.0	13.0	19.0	25.0
RSD (%)	3.7	2.7	3.7	1.0	1.3

- Mean of four injections, blank value 3 mV; all data are blank subtracted.

2.6.5 Interferences

The effect of foreign metal ions on the determination of Fe(II) was studied by preparing standards at elevated concentrations (compared with typical seawater) in LNS (pH 3.0). The results are shown in Table 2.7. Mn(II), Cu(II), Ni(II), Pb(II), Zn(II) and Cr(III) had no effect and Fe(III) and Co(II) had only a slight effect at concentrations of 100 nM and 170 nM respectively. However, the maximum Co(II) concentration in open sea waters typically range between 100 – 300 pM. [160] If necessary, Fe(III) and Co(II) can be masked by adding desferrioxamine B (1.0 μM, in UHP water) [191] and dimethylglyoxime (100 μM in methanol), [64] respectively, to the luminol stream.

2.6.6 Accuracy

The accuracy of the proposed method was ascertained by analysing CASS-3 (Coastal Atlantic Surface Seawater) certified sea water obtained from the National Research Council of Canada

(Marine Analytical Chemistry Standards Program). This solution was analysed using the proposed FI-CL system after addition of a 100 μM solution of high purity sodium sulphite for 1 h to reduce Fe(III) into Fe(II). A value of 18.5 ± 5.2 nM was obtained for Fe, as Fe(II), which is in good agreement with the certified value of 22.56 ± 3.04 nM. CASS-3 was also analysed without the reduction step and gave a result of 16.8 ± 4.5 nM Fe(II) which shows that the majority of the iron in the CRM is in the reduced Fe(II) form.

Table 2.7 Effect of foreign ions on the CL peak response for the determination of Fe(II).

Metal ions	Concentration (nM)	CL signal (mV)*
LNS Blank	–	3.0
Fe(II)	10	18.0
Ni(II)	17,000	0.5
Pb(II)	5,000	0.2
Zn(II)	15,300	0.2
Mn(II)	18,000	0.0
Cu(II)	16,000	0.0
Cr(III)	10,000	0.3
Fe(III)	100	2.5
Co(II)	170	7.5

* Mean of four injections

2.7 Conclusions

A fully automated FI-CL analyser was assembled and optimised to determine picomolar concentrations of dFe in seawater. The original method was developed and validated by previous workers [163] and incorporated a preconcentration step using an 8-HQ column followed by elution and luminol chemiluminescence detection. The method is specific to Fe(II) under the conditions

described (i.e. no added oxidant), hence acidification of the sample and a sulphite reduction step (converting dissolved Fe(III) to the ferrous form) allows the determination of dFe (Fe(II) + Fe(III)). The optimised FI-CL instrument was tested at sea (Southern Ocean) and was reliable over 50 days of continuous use. Iron concentrations determined at an open ocean hydrocast station were found to be consistent with literature data (220 - 360 pM) and the sensitivity and consistency of the FI-CL analyser was found to be satisfactory when tested during two shipboard trials in the eastern Atlantic Ocean and the Southern Ocean (see Table 2.8).

Table 2.8 Shipboard Evaluation of Automated FI-CL method with 8-HQ preconcentration

PARAMETER	RANGE
Time for one analytical cycle	180 seconds
Calibration	
Range	0 – 2 nM
Linearity (R^2)	R^2 = 0.990 –0.998
Sensitivity variation over 10 hours	<5 %
Sensitivity variation over 24 hours	10 %
Precision (RSD, n=4)	
range	0.9 - 6.2 %
mean ± 1s	5.9 ± 3.2 %.
Blank for Fe(II) measurement	24 ± 7 pM* (n = 4)
Limit of detection (3σ of blank)	21 pM*
Instrumental drift (24 hours ± 5°C)	
CL background noise n > 80,000	<2 %
Analyte signal 86 ± 5 mV, n = 36	<6 %

* Equivalent Fe(II) concentration.The blank and limit of detection were later reduced by placing an 8-HQ cleaning column on the UHP water line reducing contamination from the water wash. [84] This resulted in a limit of detection range of 5-15 pmol L^{-1} (defined as three times the standard deviation of the blank). Note: S is used in this table to represent the standard deviation of the measurement.

The method was modified to determine ambient Fe(II) in surface seawater, delivered via an underway sampling system, by buffering and preconcentrating the seawater sample inline and omitting the acidification and reduction steps. Data showing Fe(II) concentrations in surface waters of the equatorial Atlantic Ocean and the Southern Ocean were collated and indicated Fe(II) concentrations from 100 pM to below the limit of detection of the system (~12 pM). Although all possible interferences were not examined, slight increases in the operationally defined iron(II) concentration were detected in separate seawater solutions spiked with iron(III) up to a concentration of 5.0 nmol L^{-1} (<7 % of signal obtained for equimolar spiked iron(II) standards), indicating further interference studies were required.

In order to investigate the possible interferences of other components contained within the seawater matrix on the Fe(II) preconcentration and chemiluminescence reaction, a second manually controlled FI-CL analyser with no preconcentration column was developed, optimised and evaluated. This method also used luminol chemiluminescence detection with no added oxidant. However, the sample matrix was used for the carrier stream; potentially reducing analytical artefacts and possible changes in iron speciation when preconcentration is used (e.g. pH changes, mixing gradients at the sample/carrier stream interface). In addition it has the potential to be used for real time Fe(II) monitoring in the field.

The manual FI-CL method was found to be simple and rapid, with an analysis time of 12 s and a limit of detection of < 0.1 nM for Fe(II) in acidified seawater. The method was validated by quantifying total dFe (Fe(II) +Fe(III)) in a certified reference coastal seawater (CASS-3) after reduction with sulphite. The result, 18.5 ± 5.2 nM, was in good agreement with the certified value 22.56 ± 3.

CHAPTER 3.

Effect of model ligands on iron redox speciation in natural waters using flow injection with luminol chemiluminescence detection

3.1 Introduction

To improve our understanding of the role of iron in biogeochemical cycles, it is necessary to make consistent and accurate measurements of aqueous dFe species. Several analytical methods that can determine subnanomolar concentrations of dFe in seawater have been developed, [203] but to determine Fe redox speciation, detection must be redox selective (i.e., determine either Fe(II) or Fe(III)) and samples must be analysed in situ to avoid speciation changes during storage.

A limited number of laboratory techniques meet these criteria, including competitive ligand cathodic stripping voltammetry, [204] flow injection spectrophotometry [205-207] and flow injection chemiluminescence (FI-CL). [162,189,190] These methods also have limits of detection in the picomolar concentration range, are relatively free from interferences, have short analysis times (of the order of minutes), and are designed to minimize sample alteration.

There is, however, increasing evidence that a significant fraction of dissolved Fe (<0.2 or 0.45 μm) is complexed by strong organic ligands in natural waters, e.g., >99% in seawater [48,50,51,208] and Fe-oxalate complexes in rainwater, [107] and the sensitivity of these analytical techniques to organically complexed Fe(II) and Fe(III) is not well documented. All of the methods cited above involve at least one chemical reaction with Fe(II) such as the complexation of Fe(II) with an excess of 2,2-dipyridyl [204] or ferrozine ligands [205-207] or the free radical redox reaction with luminol. [162,189,190] Consequently, it is possible that these methods alter the Fe redox speciation during the measurement process.

Luminol chemiluminescence is induced following the oxidation of Fe(II) by oxygen, hydrogen peroxide, or both. This creates superoxide and hydoxyl radicals, which initiate the three-step oxidation of luminol (see Figure 2.2). [63, 180] Using this reaction, Fe(II) determination is achieved by the detection of light emitted during the final oxidation step in the pH range 9-11. Some transition metal cations (e.g. Co(II), Zn(II), Mn(II), Cu(II)) are known to interfere with the Fe(II) luminol CL reaction, and

interferences due to changes in salinity, dissolved gases (e.g., carbon dioxide), hydrogen peroxide, and organic compounds have also been reported. [184,182,185,209,210]

When Fe(II) determinations are conducted with FI-CL, the changes in sensitivity associated with these potential interferences can be minimized using standard additions to the sample matrix and/or in-line microcolumns with strong transition metal chelating ligands such as 8-hydroxyquinoline (8-HQ) bound to a solid phase. Signals derived from other free transition metal ions can then be determined with and without preconcentration columns and their effect minimized by altering the reaction conditions (e.g., pH) or by adding masking agents (e.g., dimethylglyoxime for Co(II)).

Interpretation of Fe(II)-related CL signals is complicated by the presence of organic compounds, particularly those complexed with Fe(II). Organic compounds can alter the efficiency of both the chemiluminescence reaction (by making Fe(II) "unavailable", quenching, or charge-transfer reactions) and any competitive extraction process that is used.

The aim of this study was to assess the accuracy of in situ methods for determining Fe(II) by luminol FI-CL in the presence of selected organic compounds. Experiments were conducted using high-purity water and seawater matrices (pH 5-8), and Fe(II) was determined using two luminol-based FI-CL methods. The Direct Injection (DI) method was used to examine the signal produced when a sample is injected directly into a luminol reagent stream without pre-treatment (see Section 2.6), whereas the 8-HQ column method used initial preconcentration onto an 8-HQ micro-column followed by elution with acid into the reagent stream (see Section 2.4). Parallel experiments were made using these two methods in order to investigate and decouple the effects of organic compounds on the solid-phase chelation step and the luminol CL reaction.

The organic compounds included natural reducing agents (e.g., ascorbic acid), nitrogen σ-donor/π-acceptor compounds (e.g., 1,4-dipyridine, protoporphyrin IX), aromatic compounds (e.g., 1,4-dihydroxybenzene), synthetic iron chelators (e.g., EDTA), and natural iron binding compounds (e.g.,

desferrioxamine B, ferrichrome A). Fe(II) determinations for both luminol FI-CL methods were affected by submicromolar concentrations of redox-active compounds, strong iron binding ligands (i.e., log K_{FeL} > 6), and compounds with electron-donating functional groups in both high-purity water and seawater. This was due to reactions between organic molecules and iron species before and during analysis, rather than chemiluminescence caused by the individual organic compounds.

In addition, the effects of strong ligands and size speciation on Fe(II) recoveries from seawater following acidification (pH 2) and reduction (100 μM sodium sulphite) were investigated.

3.2 Experimental

3.2.1 Reagents and solutions

All reagents were obtained from VWR, and solutions were prepared in ultrahigh purity (UHP) water (18.2 MΩ cm^{-1}, Milli-Q water, Millipore), unless stated otherwise. Solutions were stored at 20-25 °C in the dark in poly(tetrafluoroethene) (PTFE) or low-density polyethylene containers (Nalgene) that had been acid washed (1 week, 20% HCl) and rinsed thoroughly with UHP water before use. Hydrochloric and acetic acids (Aristar grade, VWR, Poole, England) were purified by quartz finger distillation whereas ammonia (Aristar grade, VWR) was purified by isothermal distillation. All solution transfers were made in a clean room under a class-100 laminar flow hood (Bigneat Ltd.).

Separate Fe(II) and Fe(III) standard solutions (0.02 M) were prepared by dissolving 0.784 g of ammonium ferrous sulfate ($Fe(II)(NH_4)_2(SO_4)_2,6H_2O$) and 0.964 g of ammonium ferric sulfate ($NH_4Fe(III)(SO_4)_2,12H_2O$) in 100 mL of 0.1 M HCl. The stock solutions were then spiked with sodium sulphite (Ultrapure, VWR) for Fe(II) and hydrogen peroxide (Aristar grade, VWR) for Fe(III) (final

concentrations 100 μM) and refrigerated at 4 °C. Working standards (<40 μM) were prepared daily by dilution in 0.01 M HCl solution.

Table 3.1 Classification of model organic compounds used in this study

Compound Number	Compound	Supplier	Classification	Binding constant ($logK_1$) Fe(II)*	Binding constant ($logK_1$) Fe(III)*
1	ascorbic acid	VWR	Reducing	-	-
2	citric acid	VWR	Compounds	4.4[a]	11.4[a]
3	glucose	VWR		-	-
4	ammonia	VWR	Compounds	-	-
5	urea	Sigma	with Nitrogen	-	-
6	thiourea	VWR	Functional	-	-
7	2,2-dipyridine	Sigma	Groups	4.2 [a]	-
8	1,10-phenanthroline	Aldrich		5.9 [a]	6.5 [a]
9	benzoic acid	VWR	Aromatic	-	-
10	quinol (1,4 dihydroxy-benzene)	VWR	Compounds	-	-
11	humic acid	Aldrich	Natural Iron	-	-
12	protoporphyrin IX	Frontier Scientific	Binding	-	22[d]
13	rhodotoluric acid	Frontier Scientific	Compounds	10.6[e]	31.2[e]
14	desferrioxamine B	Sigma		16.2 (β_{FeHL}) 21.2 (β_{FeH2L})[c]	29.6 (β_{FeL}) 29.9 (β_{FeHL})[c]
15	ferrichrome A	Sigma		9.91[e]	29.1 FeL[a]
16	8-hydroxyquinoline	VWR	Synthetic	8.0[a]	14.52[a]
17	(ethylenedinitro)-tetra-acetic acid (EDTA)	VWR	Iron Chelators	14.3[b]	25.1[b]

[a] Sillen, L. G.(1971) [213] ; [b] Martell and Smith (1982) [214] ; [c] calculated from Smith and Martell [211] ; [d] Rue and Bruland 1995 [50] ; [e] Calculated from Boulkhafa and Crumbliss (2002) [58] and Spasojevic (1999). [215]. Hyphens (-) represent unknown constants.

Luminol (5-amino-2,3-dihydro-1,4-phthalazinedione) (Sigma) solutions were prepared by dilution of a 0.01 M stock solution into a solution of borate buffer (0.1 M; Aristar grade, VWR) for the DI method, and into 0.1 M Na_2CO_3 (Aristar grade, VWR) for the 8-HQ column method. These solutions were adjusted with a 2 M NaOH solution, to give a pH of 10.5 after mixing with the carrier stream in the FI-CL manifold. The resulting reagent solutions were stored in the dark and equilibrated overnight. A 2 M ammonium acetate sample buffer was prepared from purified acetic acid and ammonia. Both the working ammonium acetate buffer (pH 5.5) and the purified reducing agent (0.1 M sodium sulphite,

pH 5.5) were made as described by Bowie et al., [25] and hydrogen peroxide dilutions were made when required from a refrigerated stock solution (30% v/v).

Stock solutions (0.1-0.01 M) of organic compounds (**1-17**, see Table 3.1) were made in UHP water, except for the siderophores, dipyridine, protoporphyrin, and benzoic acid, which were dissolved in HPLC grade methanol. A 1 g L^{-1} humic acid (sodium salt, Aldrich) stock solution was made in dilute NaOH solution and filtered through an Acrodisc syringe filter (Gelman, PTFE membrane, 0.2 μm pore size) and this was assumed to be a 1 mM solution for the sake of comparison. Minor pH adjustments were made to other organic compound stock solutions (such as EDTA and protoporphyrin solutions) using NaOH and HCl in order to solubilize the compounds. The dilution of these solutions to 100 nM in UHP water (1 mg L^{-1} for humic acid) and seawater did not alter the reaction pH.

3.2.2 Methods

The DI method (Figure 3.1a) was adapted from the flow injection method reported by King et al. [205,212] and is described in detail in Section 2.6. The manifold consisted of a constant flow of luminol reagent and carrier solution, both propelled by a four-channel peristaltic pump (Minipuls 3, Gilson, Villiers le Bel, France). These solutions mixed at a T-piece connected to a quartz spiral flow cell that was mounted on the end window of a photomultiplier tube (PMT; 9789QA, Electron Tubes Ltd., Ruislip, U.K.). The PMT was attached to a 1-kV power supply (PM 20SN, Electron Tubes Ltd., Middlesex, U.K.), and an integral amplifier was powered from an independent 15-V power supply (BBH Power Products, England). The detector output was recorded using a chart recorder (Kipp & Zonen Ltd., Lincoln, U.K.). A 270 μL sample loop connected to a rotary injection valve (Rheodyne 5020, PerkinElmer LAS Ltd.) was used to inject samples into the carrier stream.

The 8-HQ column method (Figure 3.1b) used an automated flow injection analyser for Fe(II) determination, [189] which provided control of three peristaltic pumps (Minipuls 3, Gilson), a threeway,

two-position solenoid valve (EW-01367-72, Cole-Parmer Instrument Co., Hanwell, U.K.), and a six-port injection valve (C22, Valco Instruments Co., Houston, TX) while simultaneously powering and acquiring measurement data from a photon counting head (H6240-01, Hamamatsu Photonics, Welwyn Garden City, U.K.).

Figure 3.1 Flow Injection manifolds used for iron(II) determination

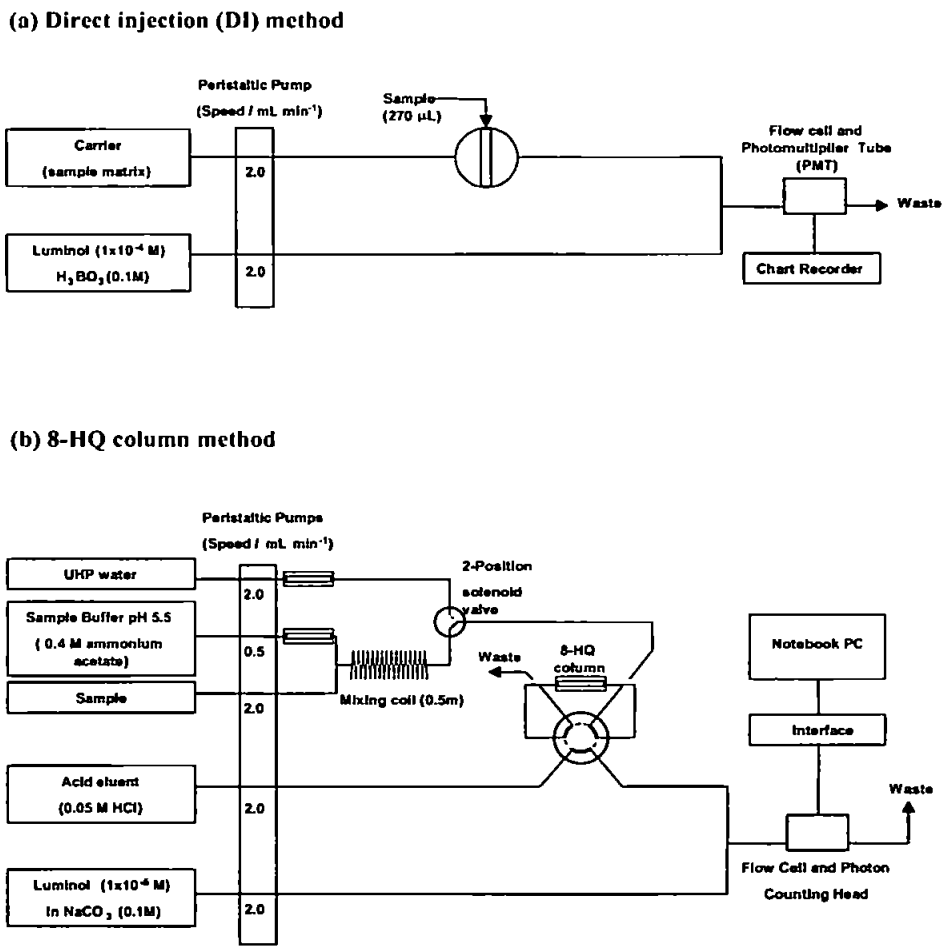

Instrument control and data acquisition were performed using a notebook computer (Travelmate 201T, Acer, Slough, U.K.) via two PCMCIA DAQCards (National Instruments Corp., Newbury, U.K.), and all software was written in LabVIEW version 5.1 (National Instruments Corp.). More detail on the system can be found in Section 2.4.

The flow injection manifold was similar to that reported by Bowie et al. for the determination of total dFe. [163] It incorporated an 8-HQ preconcentration column (in place of the sample loop used in the DI method), and consequently, an HCl (0.05 M) carrier was used to elute Fe(II) from the column. An optional buffer line (used only for pH 2 solutions and seawater experiments) mixed ammonium acetate solution with the sample to give a final pH of ~5.5.

Table 3.2 Analytical parameters for the direct injection (DI) and 8-HQ column methods.

Parameter	DI Method	8-HQ column Method
Mean limit of detection (n = 5)	39 ± 17 pM (3 x noise)	9.6 ± 6.8 pM (3s of blank)
Precision (2 nM Fe(II), n = 20)	2.3 %	6.6 %
Analysis time	0.5 minutes	2.5 minutes
1st row transition metal interferences *	Fe(III) (1.3 %), Co(II) (2.5%)	Co(II) (28%) [163]
CASS-3 (22.56 ± 3.04 nM)**	18.5 ± 5.2 nM	22.3 ± 1.8 nM

* In acidified seawater (pH 2) spiked with 2 nM inorganic standards. Results shown are positive interference (when > 1%) shown as relative response to equivalent Fe(II) concentration (%). ** By standard additions after 12 h sulphite reduction

The 8-HQ column was rinsed before each elution (25 s) to remove any unassociated species using a UHP water wash line controlled via the three-way valve. The flow cell was made from coiled transparent PVC tubing (Altec, Hants, U.K.) and mounted on the window of the photon counting head. All measurements reported for both methods are the mean peak heights of three or four replicates, and error bars represent two standard deviations (2σ) unless stated otherwise. A comparison of the analytical figures of merit determined from data obtained during this study is shown in Table 3.2.

3.2.3 Calibration

Experiments conducted with acidified (pH 2) or unbuffered UHP water were calibrated by spiking 20-mL aliquots solution with varying volumes of Fe(II) standard. A different approach was required for seawater calibrations due to the higher pH of the matrix. For the DI method, magnetic stirred seawater aliquots were spiked with varied volumes of Fe(II) standard solution and analysed every 30 s. A first-order kinetic approximation obtained from the oxidation curve was then used to determine the Fe(II) signals at t = 0. [63] The 8-HQ column method used an line sample buffer to alter the pH to 5.5. Therefore, the seawater matrix used for calibration by standard additions was buffered off-line to pH 5.5, which prevented the rapid oxidation of Fe(II). Calibrations in UHP water and seawater were non-linear, and thus, the line of best fit was modelled using quadratic functions whereas acidified UHP water and seawater (pH 2) gave a linear response (0-10 nM Fe(II)) using the 8-HQ column method.

3.2.4 Blank measurements.

The carrier used for the DI method was the original sample matrix of each experiment; hence, no blank injection measurement was required. Injection blanks for the 8-HQ column method were obtained using a matrix blank (i.e. the original matrix without additions of Fe or organic compounds), eliminating the need for further blank measurements. The exception to this procedure was the blank measurement for the seawater experiments where an in-line buffer was used. For these experiments, the blank was defined as the signal caused by the elution of the 8-HQ column without sample introduction (i.e., by passing only the buffer solution over the column followed by a UHP water wash and elution).

3.2.5 Seawater samples.

Open ocean and coastal seawater samples were collected for use in these experiments. The first was a 10-L sample of North Atlantic surface water (NASW) collected using trace metal clean towed fish and

a PTFE diaphragm group in the Bay of Biscay (46.5°N, 7°W), onboard the R. V. Pelagia in March 2002. This was filtered in-line through a 0.2 μm Sartobran cartridge filter (Sartorius) directly into an acid-washed carboy. It was then aged in the dark for 15 months at room temperature 20-25 °C). The second sample was collected from the English Channel at station L4 (50°16' N, 4°13' W) onboard the R. V. Squilla, June 2003. The L4 sample was pumped directly into a 20-L acid-washed carboy, filtered in the shore-based clean room, and used as required. Two in-line sequential filtrations were performed using syringe filters with 0.2 μm (Acrodisc, 25-mm PTFE membrane,Gelman) and 0.02 μm (Anotop, sterilized, aluminum oxide membrane, Anopore) pore sizes. These had been acid washed and rinsed thoroughly with UHP water and sample.

3.3 Results and discussion

3.3.1 Kinetic and equilibrium considerations for the complexation of nanomolar concentrations of Fe(II) and Fe(III) with organic compounds in high-purity water.

Dissolved concentrations of 2-20 nM Fe(II)/Fe(III) and 0.1-0.2 μM organic compounds were chosen for the experiments to mimic concentrations found in natural low-iron waters. Before beginning the experiments, the degree of complexation between Fe(II)/Fe(III) and dissolved organic compounds was calculated using a simple equilibrium model (Figure 3.2). The first stability constants (K_1) of Fe(II) and Fe(III) with each organic compound were used and ionic strength effects were ignored. Results showed that complexation in pure water was negligible unless log K_1 was >6.

In addition to equilibrium calculations, it was also necessary to investigate the reaction kinetics. The second-order kinetics of transition metal (Me) complex formation are described by the Eigen-Wilkins equation:

$$d[Me(H_2O)_{m-1}L^{n+}]/dt = k_w K_{os} [Me(H_2O)_m^{n+}] [L] = k_f [Me(H_2O)_m^{n+}][L] \quad (3.1)$$

Experimental rate constants (k_f) for the complexation of ligands with iron hydrolysis species are often of the same order as the water disassociation constant (k_w), which for $Fe(H_2O)_6^{2+}$ is 4×10^6 s^{-1} and for the dominant Fe(III) hydrolysis species at circum neutral pH is $\sim 10^5 - 10^9$ [27]. However, a recent kinetic study of the complexation of Fe(II) and Fe(III) with a variety of humic compounds in seawater reported estimated rates of $5 \times 10^2 - 7.5 \times 10^4$ M^{-1} s^{-1} for Fe(II) and 2.1×10^5 - 9.6×10^7 M^{-1} s^{-1} for Fe(III), [214] demonstrating the range of complexation rates that can occur with a mixture of humic compounds.

Figure 3.2 Calculated complexation of free metal ions (2 nM) with ligands versus first stability constant (K_1)

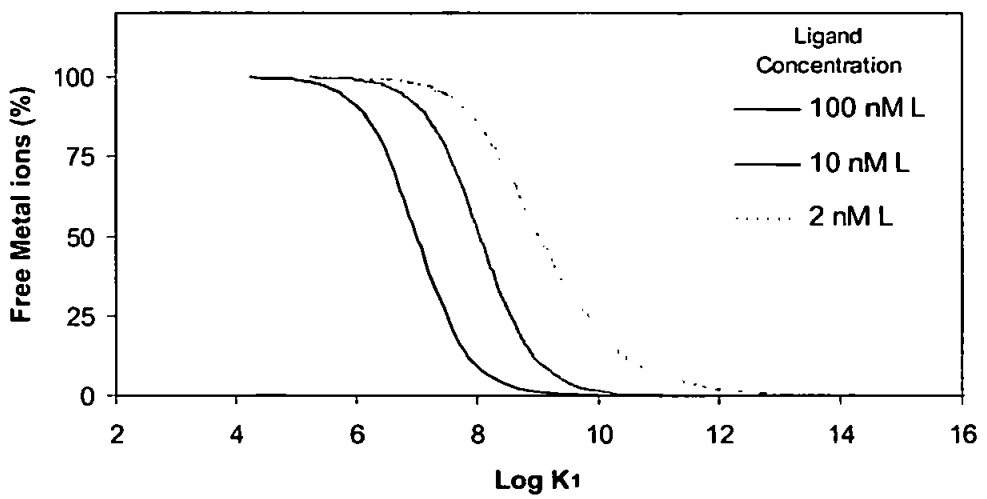

If a minimum rate constant (k_f) of 1×10^2 M^{-1} s^{-1} is assumed for both redox species then the estimated pseudo first order half-life for reactions of 2 nM inorganic iron species with 100 nM ligand is < 24 h (i.e. $\ln 2 / k_f[L]$). Hence, reaction times of 24 - 48 h were chosen for all the experiments reported here. Due to the lack of reported rate constants in the literature, detailed interpretation of the data in terms of the complexation kinetics was not possible unless k_f or the outer-sphere stability constants (K_{os}) were known.

3.3.2 Effect of organic compounds on observed Fe(II) concentrations in water

The determination of Fe(II) in natural waters using luminol CL detection is usually quantified by standard additions of inorganic Fe(II) to the sample matrix followed by subtraction of reagent and injection blanks. However, the sensitivity of the method to naturally occurring Fe(II) associated with inorganic/organic molecules may differ from that of the inorganic Fe(II) standard added. Furthermore, direct interference by organic compounds may occur. [63]

To test these hypotheses, experiments were conducted using UHP water. The rationale was, first, to avoid the interference produced by high ionic strength artificial buffers and, second, to equilibrate solutions at the pH of UHP water (5.3- 5.6). This pH range is similar to rainwater and freshwaters and is low enough for nanomolar concentrations of Fe(II) and Fe(III) to remain in solution. Furthermore Fe(II), although slowly oxidized, remained at detectable concentrations over the time scale of the experiments.

The 17 model organic compounds (ligands) selected all had functional groups that commonly occur within the broad variation of dissolved organic matter found in natural waters. They included the following: natural reducing compounds (**1-3**), aliphatic and aromatic nitrogen-containing compounds (**4-8**), phenolic and benzoic acid aromatic compounds (**9, 10**), humic acid, porphyrin and hydroxamate iron binding siderophores (**11-15**), and synthetic chelating compounds (**16, 17**).

Chemiluminescence signals for solutions of the dissolved organic compounds (100 nM) gave signals below the limits of detection for Fe(II), which were 39 and 10 pM for the DI and 8-HQ methods, respectively (see Table 3.2), indicating that the solutions were uncontaminated and caused no significant quenching or signal enhancement. The exceptions were ascorbic acid and quinol, which both gave 50 ± 9 pM equivalent Fe(II) signals using the 8-HQ column method, and humic acid, which gave a 125 pM equivalent Fe(II) signal with the DI method. EDTA suppressed the CL signal for the 8-HQ column method due to the chelation of trace metal ions in the matrix.

To examine the effects of the organic compounds on Fe(II) determination by FI-CL, an excess of each compound was added (100 nM final concentration) to 2 nM Fe(II) solutions (at t = 0 h). The solutions were stored in the dark in PTFE vials (20-25 °C) and were measured after 4 and 24 h using both methods. An untreated control solution of inorganic iron(II) in the absence of aqueous organic compounds was made for each experiment. The results are shown in Figure 3.3.

Figure 3.3 Iron(II) detected by (a) the DI method and (b) the 8-HQ column method after the reaction of inorganic Fe(II) with organic compounds in water after 4 h (light grey bars) and 24 h (dark grey bars). Solutions contained 2 nM Fe(II) and 100 nM ligands in UHP water (pH 5.5 ± 0.3) and were stored in the dark at 21 - 25 °C. Error bars indicate two standard deviations of four injections. S is the 2 nM iron standard analysed immediately after addition to water, C is the control in which Fe(II) was added at T=0 and 1-17 are the model organic compounds listed in Table 1. Horizontal bars show 15% deviation from the control after 24 h.

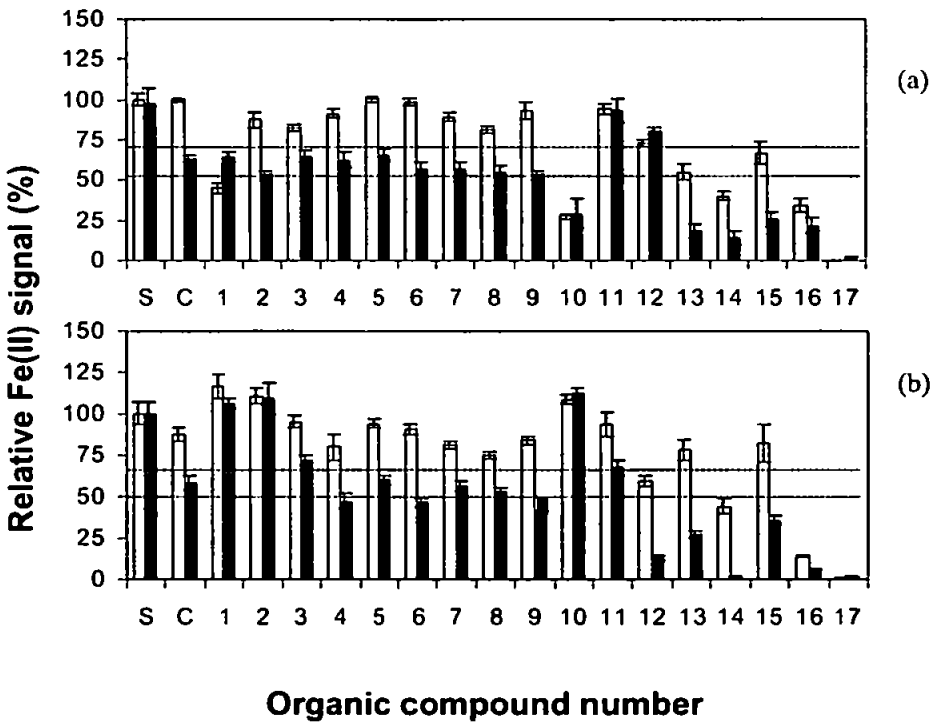

The analytical signals for Fe(II) with compounds **1-9** did not deviate by more than ca.15% from the control signal (2 nM Fe(II) solution made at t = 0) for either method over 24 h (except for the effect of the reducing agents (**1**) and (**2**) on the 8-HQ method). This showed that, under these conditions, Fe(II)

was quantitatively detected in the presence of these compounds and the lack of interference was attributed to the low binding constants (i.e. log $K_1 < 6$) and reactivity of these compounds.

In contrast, EDTA (**17**) caused a 95% reduction in CL signal within 4 h and 8-HQ and siderophore solutions (**13-15**) reduced the Fe(II) signals for both methods by 60-98% within 24 h. EDTA and desferrioxamine are strong iron binding chelators and are known to significantly increase the oxidation rate of Fe(II). [216] Hence, the reduction in Fe(II) detected by both methods can be related to chelation and an increased oxidation rate rather than an artifact of the method.

Significant differences between sample and control signals were also seen for solutions **1**, **2**, and **10-12**. Ascorbic acid (**1**) interfered directly with the redox chemistry of both methods whereas quinol (**10**), humic acid (**11**), and protoporphyrin (**12**) solutions appeared to stabilize Fe(II) signals when analysed directly by CL (DI method). Considering the low thermodynamic stability of Fe(II) in oxic waters, [217] the apparent signal stabilization observed with these compounds was probably due to redox and charge-transfer reactions occurring within the FI-CL manifold. [63]

3.3.3 Effect of organic compounds on observed Fe(II) concentrations in aqueous solutions containing Fe(III)

The effect of Fe(III) (2 nM) in an excess of organic compounds **1-17** (100 nM final concentration) in UHP water (pH 5.3-5.6) was also investigated using both FI-CL methods and the results are shown in Figure 3.4. The control results showed that under these conditions the DI method detected inorganic Fe(III) at ~25% of the equivalent Fe(II) sensitivity whereas no significant Fe(III) signal was observed using the 8-HQ column method. Surprisingly, the presence of organic compounds reduced the high signal observed with the DI method over the 24-h period.

Both methods suffered from positive interference by dissolved Fe(III) species in the presence of the majority of the organic compounds used (1-70% of the equivalent 2 nM Fe(II) signal), but overall the interference was lower for the 8-HQ column method after 24 h (mean 7.4%, n = 18). As in the previous

Fe(II) experiment, enhanced signals (>10% of the equivalent 2 nM Fe(II) signal) were found after 24 h for ascorbic acid (**1**) and quinol (**10**) using both methods and for protoporphyrin (**12**) using the 8-HQ method. Signals for Fe(III) with siderophores and synthetic chelates (**13-17**) after 24 h were generally negligible although signals above the detection limits were detected.

Figure 3.4 Iron(II) detected by (a) the DI method and (b) the 8-HQ column method after the reaction of inorganic Fe(III) with organic compounds in water after 4 h (light grey bars) and 24 h (dark grey bars). Solutions contained 2 nM Fe(III) and 100 nM ligands in UHP water (pH 5.5 ± 0.3) and were stored in the dark at 21 - 25 °C. Error bars indicate two standard deviations of four injections. S is the 2 nM iron standard analysed immediately after addition to water, C is the control in which Fe(II) was added at T=0 and 1-17 are the model organic compounds listed in Table 1.

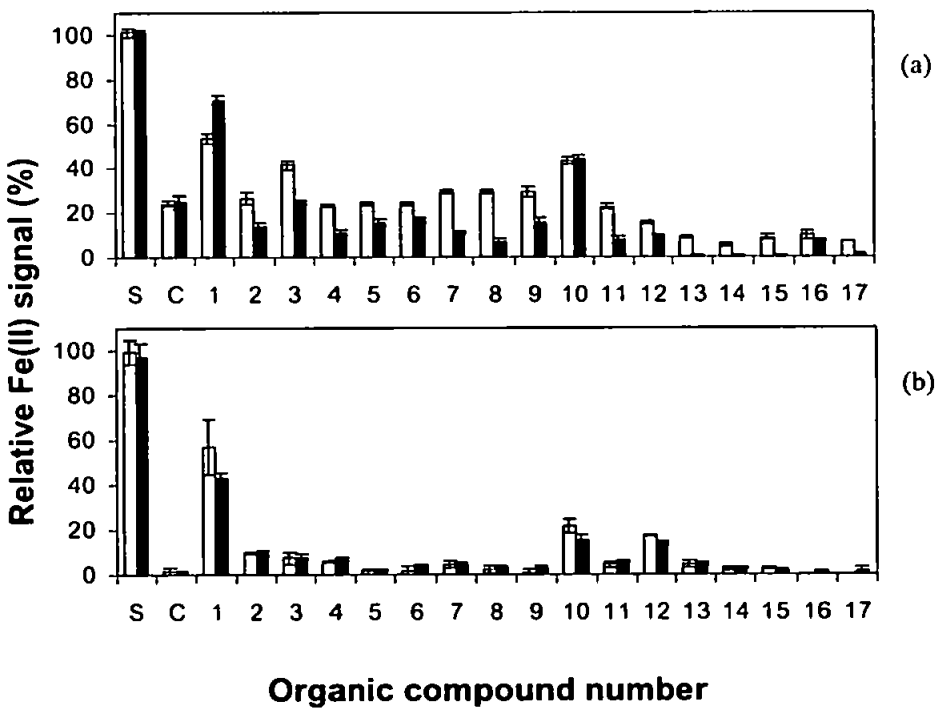

3.3.4 Effect of sample pH on Fe(III) interference for the DI method

The effect of sample pH on the sensitivity of the DI method to inorganic Fe(III) species was investigated by injecting Fe(III) into different carriers of pH 2-8, while the CL reaction pH was

maintained at 10.5 (results not shown). The signal for Fe(III) had a maximum signal at pH ~ 4.5. This interference coincides with the pH range in which the monohydroxy ferric ion ($Fe(OH)^{2+}$) is the dominant species (i.e., pH 4-6). [44]

3.3.5 Effect of organic compounds on the observed redox speciation in seawater

North Atlantic surface water was spiked to give saturated concentrations of 20 nM Fe(III) and 200 nM of each organic compound and stored in the dark for 24 h before analysis. The compounds used included four with nitrogen functional groups (**4**, **7**, **8**, **12**) likely to stabilize Fe(II) as well glucose (**3**), quinol (**10**), and humic acid (**11**). The resulting signals (Figure 3.5) were quantified after calibration with Fe(II) and were <200 pM (equivalent [Fe(II)]). Therefore, <1% of the Fe(III) added was detected as Fe(II) in all the measurements, although the final speciation of the iron was unknown.

Figure 3.5 Fe(II) detected in aged Northeast Atlantic surface water after the addition of inorganic Fe(III) (20 nM) and organic compounds (200 nM). Seawater aliquots were equilibrated for 6 days in the dark at 21 - 25 °C and analyzed using the DI method (clear bars) and the 8-HQ column method (grey bars). SW is untreated seawater and C is the 20 nM iron(III) control. Error bars indicate two standard deviations of four injections. Organic compound numbers are listed in Table 1.

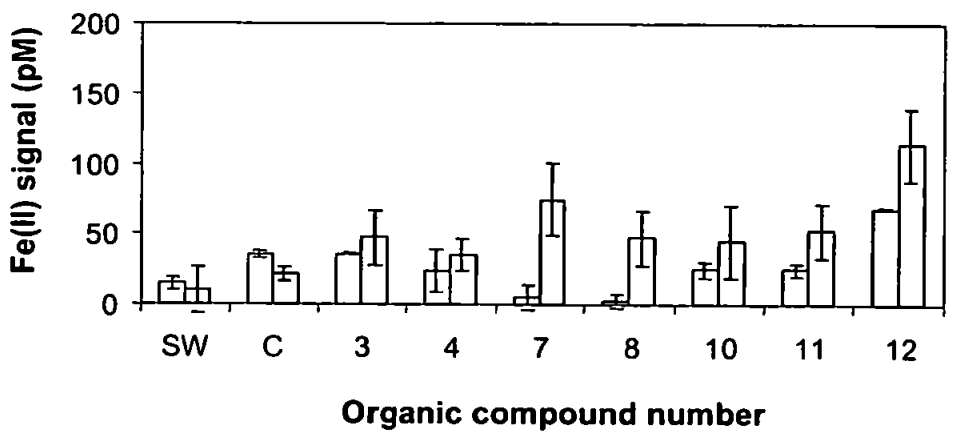

The control (seawater + Fe(III)) gave signals higher than untreated seawater for both methods, and hence, the induced CL must have resulted from either iron complexes formed with natural ligands in the seawater or direct interference from any remaining free inorganic Fe(III). Chemiluminescence induced by filtered seawater spiked with Fe(III) was unlikely to be due to the evolution of Fe(II) as the aged oxic seawater used was stored in the dark with no photochemical or biological source of reduction. Nearly all of the samples spiked with Fe(III) and organic compounds gave positive CL signals, but, as mentioned above, this was not attributed to Fe(II) species because the standard reduction potentials of the majority of iron complexes including many porphyrins) are lower than that of the O_2 / H_2O redox couple, which dominates under oxic conditions (E = +0.74 V at 25 °C, pH 8).

The exceptions were the seawater samples spiked with the Fe(II)-specific ligands 2,2-dipyridine (**7**) and 1,10- phenanthroline (**8**), which have reduction potentials of > 0.74 V. These ligands reduced CL signals to below the LOD for the column method but gave higher CL signals than the control (>25 pM equivalent Fe(II)) for the DI method. This showed that the luminol CL reaction is sensitive to σ-donor/π-acceptor iron chelates. The CL signal for these samples was reduced when extracting onto an HQ column, probably due to competition between the ligands solution and the active sites on the column. The reason for observing any signal from the addition of Fe(III) is due to either shift in Fe redox state or charge-transfer reactions with luminol. One would need additional mechanistic information to determine which of these processes is dominant. However, the aim of this study was to obtain sufficient data to allow a critical comparison of the CL responses from the DI and 8-HQ methods in the presence of a range of organic compounds.

3.3.6 Effect of strong ligands on the determination of dissolved iron

Luminol CL can be used for the determination of dFe (Fe(II) + Fe(III)) using prior acidification and sulphite reduction. [188,211] To examine the effects of strong ligands on the two FI-CL methods, Fe(III)

(2 nM) and organic compounds (**12-17**, 100 nM) were equilibrated in UHP water for 48 h. Aliquots of each solution were then spiked either with HCl (to pH 2) and sulphite (100 μM) or with HCl only (pH 2). In addition, a blank solution was made for each solution that included the organic compound, HCl, and sulphite with no Fe(III) added.

Figure 3.6 Fe(II) recovered over time from 2 nM Fe(III) solutions containing strong iron ligands after acidification (pH 2, HCl) and sulphite reduction (100 μM), using the 8-HQ method. Fe(III) and the organic compounds were added to water and left to equilibrate for 24 hours, before adding the organic compounds. Measurements were made over 72 hours.

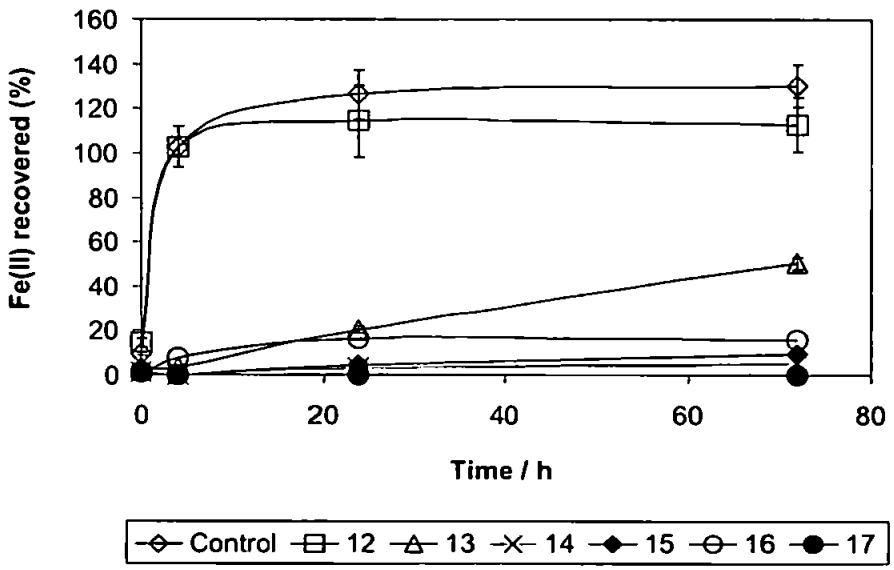

Solutions were then analysed over a period of 3 days. The results (Figures 3.6 and 3.7) for both FI-CL methods showed that for all the test solutions, except the porphyrin solution (**12**), over 40% of the Fe(III) remained undetectable, even after 72 h of acidification and reduction. This has important implications for sample treatment when determining dFe with sulphite reduction with both methods.

Figure 3.7 Comparison of Fe(II) recovered from control solutions after 72 hours, using (a) the DI method and (b) the 8-HQ column method. Fe(III) and the organic ligands were added to water and equilibrated for 24 h before adding the reagents. Clear bars represent 2 nM Fe(III) solutions with organic ligands that were acidified (pH 2, HCl) and reduced with sulphite (100 µM). Grey bars are the same solution without sulphite and black bars are a blank without Fe(III). C was the 2 nM iron(III) control. Numbers on the x axis refer to the organic compounds listed in Table 1.

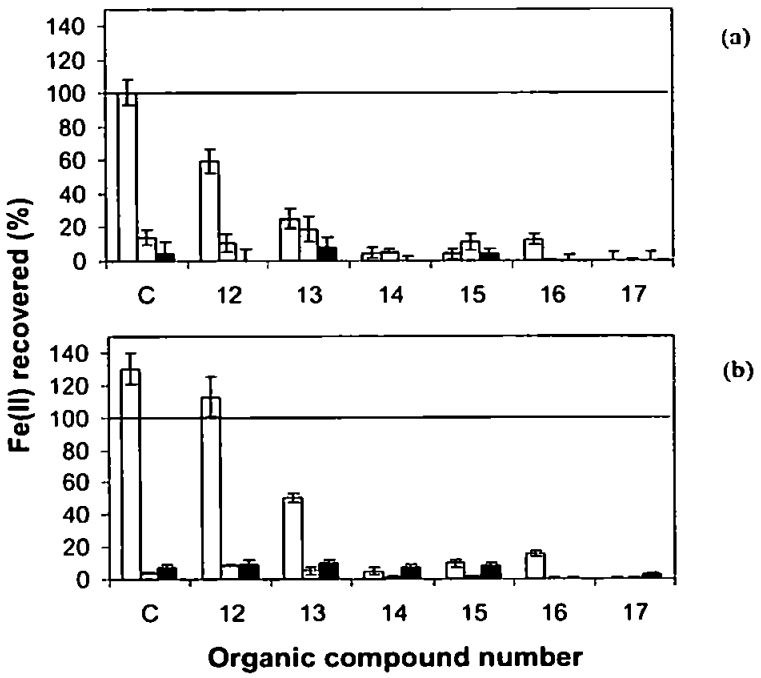

3.3.7 Kinetics of sulphite reduction of iron in filtered (<0.2 µm) and ultrafiltered (<0.02 µm) coastal seawater

An experiment to examine the kinetics of reduction of Fe in a natural sample was conducted using the 8-HQ column method only. Two aliquots of freshly filtered (<0.2 µm) and ultrafiltered (<0.02 µm) coastal seawater were spiked with HCl (pH 2), and one aliquot of each fraction was spiked with sulphite (final concentration 100 µM). These solutions were stored in the dark at 20-22 °C, and Fe(II) was determined periodically over 3 weeks.

The data (Figure 3.8) showed that Fe(II) production in the 0.2 μm filtered samples did not reach a plateau, even after several weeks, whereas the signal for the ultrafiltered samples did so after <24 h. Furthermore, the effect of sulphite was negligible and thus the evolution of the Fe(II) detected must have been due to reductive dissolution of Fe(III) in the acidified seawater. The slower reduction and dissolution of "colloidal" iron in the 0.2 μm filtered sample was attributed to the disassociation of surface-bound iron and iron bound within particles.

Figure 3.8 Fe(II) detected after acidification and reduction of filtered (<0.2 μm, ■) and ultrafiltered (<0.02 μm, X) coastal seawater. Also shown are the results for filtered (◆) and ultrafiltered (▲) coastal seawater after acidification with no reducing agent.

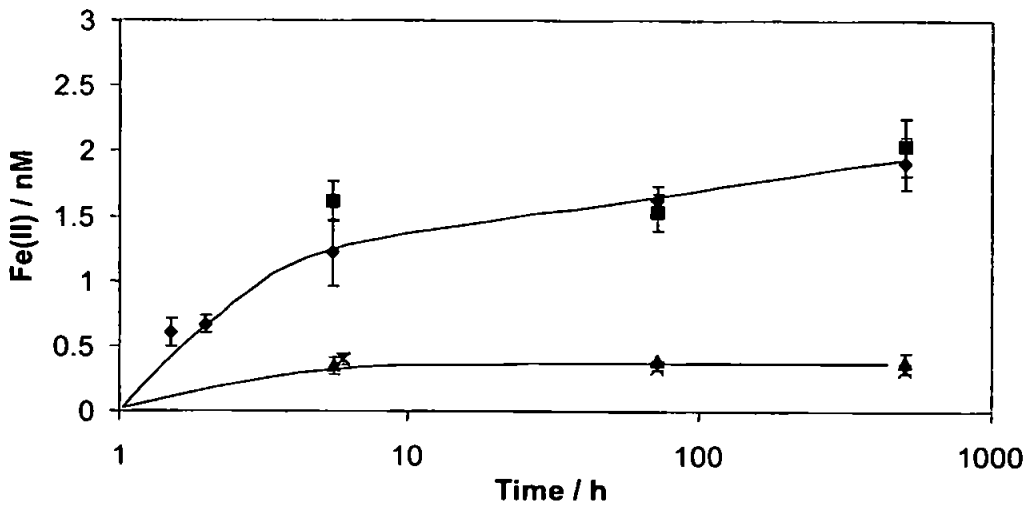

Few iron dissolution studies of natural colloids have been reported. Obata et al. used a similar luminol FI-CL method (using hydrogen peroxide as the oxidant in the luminol reagent stream) determine Fe(III) and reported that the dissolution of Fe from artificial and natural colloids in acidified seawater (pH 3.2) occurred within seconds. [164] The contrasting data shown here are evidence that further investigation of the dissolution and detection dFe is needed to clarify dissolution mechanisms for natural colloids and to determine the dissolved Fe species that are produced.

3.4 Conclusions

1. Differences in iron redox speciation were observed using the two FI-CL methods. Some organic compounds altered the sensitivity of the 8-HQ column method to Fe(II) (e.g., quinol, citric acid), but this method was less sensitive to interference from Fe(III) species in the presence of organic compounds at lower pH (<6), e.g., for rain and freshwater samples. Furthermore, preconcentration using a chelating column may enhance selectivity and minimize the effects of matrix variations produced by dissolved gases, free radicals, and redox-reactive species on the CL reaction. On the other hand, direct injection of the sample into the luminol reagent reduces analysis time and improves the precision of multiple measurements. A disadvantage of the DI method is the difficulty of obtaining a reliable blank signal and hence a reliable LOD for field measurements. Here we used the original matrix as the carrier, and thus, the LOD was defined as 3 times the signal-to-noise ratio, but a realistic blank for field samples would require the selective removal of Fe(II) from the sample matrix preceding injection into the reagent stream.

2. The individual effects of the 17 selected model organic compounds on the CL signals for both FI-CL methods were negligible.

3. Fe(II) signals for both FI-CL methods were enhanced by solutions containing submicromolar concentrations of redox-active compounds (e.g., ascorbic acid) and quinol (1,4-dihydroxybenzene) and masked by strong iron binding ligands (siderophores, 8-HQ, and EDTA) in high purity water at pH 5.3-5.6. Furthermore, CL signals above the LOD of both methods were observed for Fe(III) in the presence and absence of organic compounds at this pH. Thus, significant interference is likely to occur when Fe(II) is determined by FI-CL in waters below circum neutral pH where micromolar concentrations of natural organic compounds are present. This would also affect calibrations when standard additions to the natural matrix are used. Hence, there is a need to develop techniques to

eliminate sensitivity changes that may reduce the accuracy of Fe(II) determination in lake, river, and rainwater by luminol FI-CL.

4. The positive interference from Fe(III) / organic compound mixtures on the Fe(II) signal for both FI-CL methods was lower for seawater (pH 8.1) than for UHP water (pH 5.3 -5.6). Based on the data shown in Figure 3.5, the maximum interference for both FI-CL methods from Fe(III) in the presence of natural organic ligands in seawater is predicted to be <1% of the total iron concentration. The experiments reported here represent extreme conditions in terms of organic speciation as in open ocean environments, dissolved organic carbon concentrations are generally in the micromolar range and compounds are likely to contain a broad range of sizes and functionalities.

5. Siderophores and EDTA iron complexes in UHP water were undetectable under the conditions reported, even after acidification (pH 2) and reduction by sodium sulphite (100 μM). These complexes slow the kinetics of Fe(III) reduction, and therefore, similar ligands present in natural waters may mask the detection of a major fraction of dissolved iron using FI-CL and other techniques. 8-HQ microcolumns have been reported to efficiently extract Fe(II) in an excess of strong ligands (e.g., tartrate, oxalate, fulvic acid, and citrate [218]), but the data reported here is evidence that, even under reducing conditions, strong iron binding ligands can mask Fe(II) from both solid-phase extraction by 8-HQ and the luminol chemiluminescence reaction. However, it is important to note that the concentrations of strong chelators used here were closer to the concentrations found in freshwaters and rainwaters than those found in seawater.

6. Rates of dissolution and reduction of iron in coastal seawater were found to be dependent on the size fraction. The results showed that pre-treatment protocols and intercomparison exercises are still required to minimize any variability in response that may occur between methods for dFe determination.

7. The results reported here show that organic compounds present in natural waters affect the accuracy of Fe(II) determinations. To improve accuracy when using direct FI methods (i.e. direct injection of sample into a reagent stream), a better mechanistic understanding of the Fe(II)-luminol reaction is required. This is a particular challenge for Fe redox speciation measurements because the effects of masking and charge-transfer reactions are difficult to decouple from the analytical signal. The 8-HQ column method is therefore preferred because the Fe species eluted from the column can be constrained, hence removing the effect of the sample matrix on the CL reaction. However, this approach requires an understanding of the solid phase complexation of different Fe species.

CHAPTER 4.

Iron speciation in the North East Atlantic Ocean

4.1 Introduction

This chapter serves as an introduction to the hypotheses investigated during two research cruises in the north east Atlantic Ocean described in Chapters 5 and 6. Firstly, an overview of open ocean iron redox chemistry is presented and processes known to affect redox changes in an oxic marine environment are identified. The variables associated with these processes are described and the thermodynamic models that are subsequently used to rationalise field data are introduced. Finally, a description of the hydrography of the North Atlantic Ocean is given and references made to past studies that report distributions of dFe species in this region. The hypotheses studied in the following Chapters (5 and 6) are summarised in the Conclusions.

4.2 Redox chemistry and Fe(II) measurements in the open ocean

The production of Fe(II) in seawater occurs during biotic and abiotic redox reactions that recycle dissolved and refractory iron species and these mechanisms increase the bioavailability of iron for oceanic microorganisms. [143,219] Kinetically labile inorganic Fe(II)′ and Fe(III)′ species are proposed as the bioavailable Fe forms for eukaryotes. [145,147] Therefore the chemical speciation of iron regulates its biological uptake and utilisation of the element, and as a feedback mechanism, the activity of the biological community also has a profound influence on the speciation and cycling of iron. [220]

Ambient Fe(II) concentrations have been determined *in situ* in Atlantic [221] and Australian [81] shelf waters and the equatorial Pacific. [222] However, due to analytical constraints (techniques require high specificity and low limits of detection, see Chapters 2 and 3) and a lack of kinetic data, our

knowledge of the distribution of Fe(II) in Atlantic waters and its role in global marine biogeochemical cycles is limited. This has resulted in a paucity of redox speciation data for oceanic systems. However, the recent emergence of novel flow injection methods [162,189,190,205-207] with low detecton limits, capable of detecting Fe(II) at picomolar concentrations, means that investigations into oceanic Fe redox processes are now possible.

To investigate iron redox speciation, all the variables that might control or alter the Fe(II) / Fe(III) ratio must be considered. The majority of open ocean waters of the North East Atlantic are oxic and the key variables that might control iron redox speciation in oxic waters are listed below.

Dissolved oxygen and hydrogen peroxide are the dissolved species that are most influential in controlling redox speciation in oxic waters (see Chapter 1). This is due to their control over the kinetics of Fe(II) oxidation (i.e. Haber Weiss mechanism) and the electron activity of seawater.

Temperature is known to alter iron solubility [47] and Fe(II) oxidation rates (Chapter 1). Similarly other reactions and equilibria that affect iron speciation are likely to be altered by temperature.

Electron activity is a controlling variable for redox speciation and hence can be estimated in order to model redox speciation for less dynamic marine waters.

Photoreduction of dissolved and colloidal iron has been shown to maintain significant steady state Fe(II) concentrations in coastal waters (e.g refs [78,81,223,224]) and hence may play an important role in open ocean waters.

Biological redox cycling is used by some marine eukaryotes that directly reduce Fe(III) complexes using membrane bound NAD(P)H oxidase enzymes (or Fe(III) reductase). These enzymes increase concentrations of free Fe(II) and enable subsequent Fe(II)' or Fe(III)' (following oxidation) uptake via metal transport proteins. [225-227] In addition, bacterial oxidation of organic matter is a well-

known process that can produce highly reducing environments capable of reducing iron species (see Chapter 1). However, neither of these processes have yet been reported to cause enhanced steady state Fe(II) concentrations in Atlantic seawater .

Organic speciation. Equilibrium calculations for inorganic species indicate that in oxygenated seawater [Fe(II)/Fe(III)] is of the order of 10^{-10}, with the Fe(II) speciation including Fe^{2+}, $FeCO_3$ and $FeCl^+$ species. [143] However, according to most studies >99 % of dFe is organically complexed in seawater [48-53] and Fe(III)-chelates can be an important source of kinetically labile Fe(II)′. This can occur firstly, when Fe(III)-chelates are subjected to direct and indirect photochemical reduction which typically results in dissociation of Fe(II). [75,223,224,228] Second, Fe(III)-chelate bioreduction, which has been found for diatoms, [150-153] may serve as a mechanism for marine eukaryotes to produce Fe(II)′. Furthermore, complexation can influence redox speciation by altering the free energy of Fe(II)/Fe(III) redox states as well as Fe(II) oxidation rates and the chemistry of natural iron binding ligands remains largely unknown (see Chapter 1).

Particles and colloids. Due to the high solubility of Fe(II) and the high surface area of suspended particles, marine particles such as detritus, atmospheric deposits and faecal pellets may act as sources of Fe(II) via dissolution into the aqueous phase.

4.3 Iron redox speciation models

Redox speciation models can be used to better understand the conditions that control the partition between trace metal redox states in seawater. The value of these models can be increased by the determination of equilibrium and rate constants from laboratory and field data. The models for iron redox species in oxic seawater described below are separated into two categories; thermodynamic equilibrium models and kinetic steady state models.

The thermodynamic equilibrium model presented below includes only physico-chemical variables affecting bulk seawater (excluding light) and may be more representative of deep water chemistry. The kinetic model, however, uses the steady state approximation for known redox reactions in seawater and is representative of more dynamic system such as those found in surface waters.

4.3.1 Thermodynamic equilibrium model for oxic waters

The O_2 / H_2O redox couple has a standard pE that is inversely proportional to temperature:

$$pE^{\circ} = E^{\circ} (F / 2.3RT) \quad (4.1)$$

where E° is the standard electrode potential (V), F is Faradays constant (C mol^{-1}), R is the molar gas constant (J K^{-1} mol^{-1}) and T is temperature (K). Assuming that in oxic waters the O_2/H_2O couple controls the pE of oxic seawater, then the pE can be defined as:

$$pE_{O2/H2O} = pE^{\circ} - \log \frac{1}{P_{O2}^{1/4} [H^+]} \quad (4.2)$$

where P_{O2} is the partial pressure of oxygen in the system and $[H^+]$ is the proton concentration. Thus equation 4.2 shows that the pE of oxic seawater has an inverse relationship with $[H^+]$ and $P_{O2}^{1/4}$, and is most sensitive to pH change. For example, at standard temperature (293 K) a pH change from 7.6 to 8.2 changes the pE of seawater from 13.0 to 12.4 whereas a change in the partial pressure of oxygen from 0.2 to 0.1 atmospheres causes the pE to decrease from 12.58 to 12.50. Hence redox speciation at equilibrium in predominantly oxic seawater is likely to be most sensitive to temperature and pH rather than ambient dissolved oxygen concentrations.

If the redox couple in equation 4.2 controls the pE, then for iron species at equilibrium:

$$pE_{O2/H2O} = pE^{\circ}_{Fe(II)/Fe(III)} - \log ([Fe(II)] / [Fe(III)]) \quad (4.3)$$

Iron redox speciation in oxic waters at equilibrium can be estimated using this model but for qualitative interpretation it must be assumed that a single iron complex species (i.e. a dominant species with a defined binding constant) is present.

4.3.2 Kinetic steady state model for oxic waters

A steady state speciation model for dissolved species in seawater is described by equations 4.4, 4.5 and 4.6:

$$d[Fe(III)L]/dt = k_f [Fe(III)'] [L] - ([Fe(III)L] (k_d + k_{hv} [h\nu])) \quad (4.4)$$

$$d[Fe(II)']/dt = k_{hv} [h\nu] [Fe(III)L] - k_{ox} [Fe(II)'] \quad (4.5)$$

$$d[Fe(III)']/dt = k_d [Fe(III)L] + k_{ox} [Fe(II)'] - k_f [Fe(III)'] [L] \quad (4.6)$$

where Fe(II)' and Fe(III)' are the free inorganic species, L is a ligand and k_f, k_d, k_{hv} and k_{ox} are the formation, dissociation, photo-reduction and oxidation rate constants, respectively. This simple model, proposed by Sunda (2001), [143] uses kinetic approximations for redox and complexation reactions and thus at steady state these all equate to zero. Using this model it was calculated that 4.4% of dissolved iron would be present as kinetically labile Fe(II)' in fully sunlit Pacific Ocean surface waters (pH 8, 25 °C). Using a similar kinetic model that included particulate iron, Johnson *et al.* [80] predicted that maximum Fe(II) concentrations in equatorial surface waters are unlikely to exceed ~ 0.1 % of the total iron concentration (25 m depth, equatorial light regime, 25 °C).

A more detailed model of iron redox cycling derived by Voelker et al. (1997) [85] is summarised in Figure 4.1. This model provides an interpretation of iron redox speciation where both solid and aqueous phase equilibria are considered as well as dynamic processes that occur in seawater. In the majority of the work mentioned above, only photochemical reduction processes for reactions *1* and *2* have been considered but dark reduction (e.g. charge transfer reactions via reactions with organic substrates) and reduction by superoxide were found to be significant in this study. [85]

Figure 4.1 Summary of possible reactions of iron in surface waters (adapted from Voelker *et al.* [85])

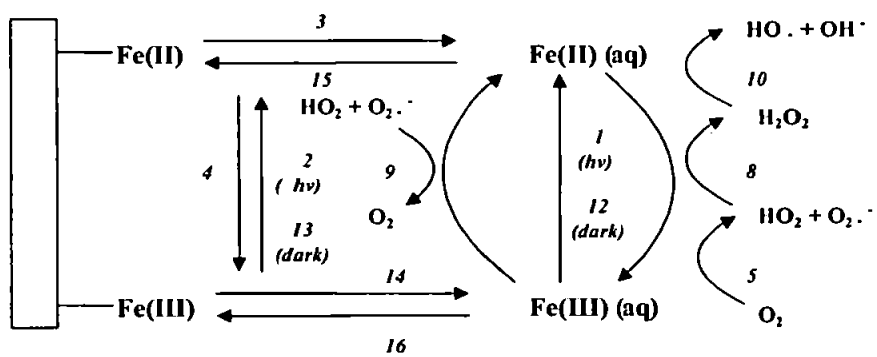

6. $DOM + O_2 \longrightarrow DOM_{ox} + HO_2/O_2^{\cdot -}$

7. $2\ HO_2/O_2^{\cdot -} \longrightarrow H_2O_2 + O_2$

11. $Br^- + HO^{\cdot} \longrightarrow Br^{\cdot} + HO_2/O_2^{\cdot -}$

Key to Reactions (*1*) Photoreduction of dissolved Fe(III) by DOM (*2*) Photoreduction of surface Fe(III) by DOM (*3*) Dissolution of surface Fe(II) (*4*) Reoxidation of surface Fe(II) (*5*) Fe(II) oxidation by O_2 (*6*) HO_2 / O_2^- photoproduction (*7*) Bimolecular dismutation of HO_2 / O_2^- (*8*) Fe(II) oxidation by HO_2 / O_2^- (*9*) Fe(III) reduction by HO_2 / O_2^- (*10*) Fe(II) oxidation by H_2O_2 (*11*) Reduction of $OH^{\cdot}$ accompanied by the oxidation of Br- to Br (*12*) Dark reduction of Fe(III) by DOM (*13*) Dark reduction of surface Fe(III) by DOM (*14*) Non reductive dissolution of Fe(III) oxide (*15*) Sorption of dissolved Fe(II) (*16*) Fe(III) adsorption / precipitation.

The determination of rate constants for iron redox reactions under ambient conditions is challenging due to their fast reaction rates. The use of detailed kinetic models is further limited as the effects of common variables such as temperature, depth, variation in particulate matter, phytoplankton and heterotrophic bacterial communities on steady state iron(II) concentrations have not been examined in detail. Furthermore models only take into account the reactions of Fe with uncharacterised dissolved organic matter (DOM), whereas in natural seawater these redox cycles may be significantly altered by other redox reactions e.g. manganese cycling.

All the models discussed above account for the effects of light as a reducing agent but elevated Fe(II) concentrations are possible where dissolved and particulate Fe(III) species are reduced in sediments and micro-environments (e.g. fecal pellets) by the oxidation of organic matter and during periods of wet and dry atmospheric deposition. [220] Furthermore the models are limited by the assumptions described above and hence accurate *in situ* Fe(II) data are required to validate such models.

4.4 Dissolved iron distributions in the North Atlantic Ocean

4.4.1 Hydrography

The Atlantic Ocean (Figure 4.2) covers an area of nearly 100 million km^2 and occupies approximately one quarter of the total area of the World Ocean. It is contained by the continents of North and South America, Europe and Africa but is connected to the other oceans via the Southern Ocean and the Arctic Ocean, although a large plateau area divides the latter (~1000 m depth near Greenland and Iceland) greatly reducing inter-ocean deep-water circulation at the northern extent.

Figure 4.2 The Atlantic Ocean

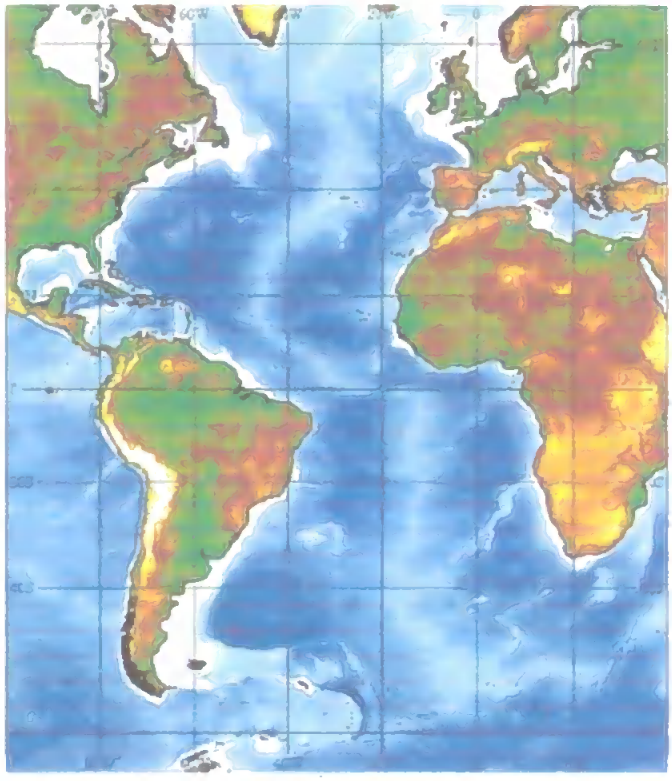

Reproduced from the GEBCO Digital Atlas published by the British Oceanographic Data Centre on behalf of IOC and IHO, 2003'.

The properties and movement of individual water masses are important when considering iron speciation and distribution throughout the water column of the Atlantic Ocean. Despite its relatively short residence time in deep waters (~ 70 – 200 years [124,229,230]) the distribution of dFe is influenced by the movement of water masses through areas that contribute to the dissolved iron pool such as hydrothermal vents, anoxic sediments and areas with high atmospheric deposition fluxes. Tsuchiya et al. [231] reported detailed physical and chemical data for a north-south hydrographic section of the North Atlantic (~20 °W). The different characterised water masses in the North East Atlantic discussed below are summarised in Tables 4.1 and 4.2.

4.4.2 Surface waters

A broad variation in physico-chemical properties of surface waters exists across the North Atlantic. This is due to spatial and seasonal variations in climatic conditions, mixing and ocean-atmospheric

exchange. Consequently, surface water masses are generally not classified in the literature, the exception being stratified, high salinity, sub-tropical and tropical surface waters (see Table 4.1).

Table 4.1 Characterised surface and intermediate waters of the North East Atlantic (adapted from Tsuchiya et al. 1992 [231])

Water Mass	Latitude (°N)	Potential Temperature (°C)	Salinity ($^0/_{00}$)	Potential Density (σ_2, kg m^{-3})	Depth (m)	Characteristics
Sub Polar Mode Water (SPMW)	40 - 50 50+	11 - 12 7.5	~35.5 ~35.15	-	100 - 500 100 - 700	Characteristic temperature and flow (vorticity).
Sub tropical and Tropical High Salinity Waters	0 – 40	~15 – 30	> 36	< 36	0 - 300	Very high salinity with oxygen maximum of 100 –110 %.
Antarctic Intermediate Water (AAIW)	0 – 22	~ 4.5 – 10	< 34.5 - 35	36 – 36.5	600 -800	Salinity minimum (<34.5) increases northwards. High nutrients decreasing >20°N.
Mediterranean Outflow Water (MOW)	~30 - 42	~ 8 – 12	35.6 - >36.1	36.3 – 36.7	~ 800 - 1400	Warm and high salinity. Irregular 'meddies' extending north and south of core.
Labrador Sea Water (LSW)	41 - 65	~ 3.4 – 3.8	34.90 – 34.94	36.85 – 36.90	~1400 - 1800	Salinity minimum and O_2 maximum at 1500m ending abruptly at 41°N.
Iceland-Scotland Overflow Water	60 - 65	< 3	> 34.96	> 37	1500 -2800	High O_2 and nutrient poor water.

Surface water iron concentrations vary considerably throughout the open ocean surface waters of the North East Atlantic (0.02 – 1.5 nM, see Table 4.3), especially near regions of high atmospheric particle flux (e.g. Duce 1991 [96]) and vertical mixing (i.e. upwelling and winter convection). [232] Further variability is caused by short-timescale physicochemical processes (such as diurnal redox cycling), biological recycling and lateral inputs near continental margins from shelf waters and riverine inputs (see Chapter 1).

Observations in the Intertropical Convergence Zone (ITCZ) of the equatorial Atlantic Ocean by Vink and Measures (May/June 1996 [233]) provide an example of the importance of mineral aerosol inputs on dFe concentrations in surface water. The range of dFe concentrations found was 0.4 – 1.4 nM between 15 °S and 5 °N. The data had a strong correlation with dissolved aluminium concentrations and an inverse correlation with salinity, indicating that at the time of the study, wet deposition was the predominant input in this region. A similar positive trend between total dissolvable iron and aluminium was seen by Bowie *et al.* between 50 °S and 50 °N. [232] In contrast, Wu and Boyle [234] reported dFe concentrations of 0.2 – 0.8 nM in surface waters in the Sargasso Sea in March 1998 (26 – 31 °N) where deposition events are less frequent. They proposed that vertical mixing, phytoplankton growth and particle scavenging played more dominant roles in controlling the iron concentrations in this remote area.

The upward flux of macro- and trace metal nutrients to surface waters is most significant in upwelling currents such as the Equatorial, North West African and Benguelan upwelling areas as well as winter mixing in the high latitudes (> 40 °N/S) where surface waters mix with nutrient rich water from below. The effect of the latter is known to have a large scale effect on nutrient concentrations in the Northern Atlantic Ocean due to the existence of a front at ~50 °N (described by Saager *et al.* [235]). North of the front, higher nitrate, phosphate and oxygen concentrations were observed in surface waters due to high winter convection penetrating the nutrient maximum (~ 800 m) whereas to the south, winter convection was only estimated to influence the top 200 m. The surface layer at ca. 40 – 50 °N, 38 °W forms Sub Polar Mode Water (SPMW) and flows eastwards, eventually circulating the northern extent of the subtropical gyre to the North East Atlantic where it constitutes the main body of water at depths of 100 – 700 m north of 40 °N. [236] Thus the seasonal transport of the SPMW and LSW delivers high nutrient surface water to the North East Atlantic.

Dissolved Fe concentrations determined in the SPMW after the spring bloom by Martin *et al.* were relatively low (0.07 – 0.4 nM, 47 °N, 20 °W [237]). Therefore the relatively short residence time of

iron in surface waters (e.g. c.a. 10 – 300 days [105,244]) and its utilisation as a micronutrient reduces the transport of iron in SPMW across the North East Atlantic.

4.4.3 Intermediate waters

Nutrient maxima in lower latitudes (0 – 50 °N) of the North East Atlantic have been found to coincide with the oxygen minima at ~750 – 900 m below the SPMW, as a result of organic matter mineralisation. However, this is not the case in higher latitudes (> 50 °N) where deep winter convection occurs. DFe maxima of 0.5 – 0.6 nM at 700 - 900 m were reported by Martin *et al.* at 47 °N, 20 °W and 59 °N, 20 °W. [237]

Below 1000 m, low salinity and well oxygenated sub-polar LSW flows eastward with its core located at around 1500 m and then extends southward to a front at ~ 40 °N where it meets with Mediterranean Outflow Water (MOW). DFe concentrations of LSW near the western European Shelf were reported by Laes *et al.* as 1.0 – 1.2 nM, indicating that LSW becomes enriched as it travels alongside the European Shelf. [238] South of the frontal extent of LSW, the MOW flows westward from the Strait of Gibraltar (found between 30 - 42 °N at 25 –30 °W) as well as northwards into the Bay of Biscay. [239] DFe concentrations of the northward moving MOW, also near the western European Shelf, were reported to be 0.6 – 0.9 nM. [238]

In the equatorial area, Antarctic Intermediate Water (AAIW) forms a low salinity tongue at 600 – 800 m depth extending from the equator to around 22 °N. This contains high nitrate (30 – 40 μM), phosphate (2 – 3 μM) and silicate (20 – 30 μM) typical of the intermediate waters of the Southern Ocean. At present, there are few water column dFe measurements reported in the equatorial and South Atlantic Ocean. [198] However, average dFe concentrations in the surface waters (0 – 500 m) of the Atlantic section of the Antarctic Circumpolar Current were reported by many workers to be between 0.05 and 0.5 nM [198,240] and hence intermediate waters in the South Atlantic might have lower iron concentrations than those of the northern gyre.

4.4.4 Deep waters

The North Atlantic deep waters, which are clearly characterised at lower latitudes, are known to originate from sinking water that flows south along the Western Boundary Current. A portion of

Table 4.2 Characterised deep waters of the North East Atlantic (adapted from Tsuchiya et al. 1992)

Water Mass	Latitude (°N)	Potential Temperature (°C)	Salinity ($^0/_{00}$)	Potential Density (σ_2, kg m^{-3})	Depth (m)	Characteristics
North East Atlantic Deep Water (NEADW)	41 – 60	~ 2.4 - 3.2	34.94 – 34.96	~37.05 - 36.96	2000 -4000	Deep water salinity maximum ~34.95 with uniform nutrient concentration at ~2700m.
Upper North Atlantic Deep Water (UNADW)*	0 – 21*	3.6-4.6	34.96 – 35.10	36.8 – 36.95	1500 - 1800	Intermediate salinity maximum.
Mid North Atlantic Deep Water (MNADW)**	0 – 41	2.4 – 3.6	34.92 - 35.0	36.94 – 37.05	~2000 - 3000	O_2 maximum Found to be deeper at low and high latitude.
Lower North Atlantic Deep Water (LNADW)	0 – 52	< 2.4	34.86 - 34.94	> 45.8 (σ_4)	~3000 - 4000	Deepest O_2 maximum at ~ 3700, only seen < 10°N.
Antarctic Bottom Water (AABW)	0 - 65	~ 0.2 – 2.2		> 45.85 (σ_4)	< 4000	Low temperature and high silcate (40 –50 μM).

* not including MOW
** not including LSW
σ_4 refers to the use of a different potential density scale for deeper waters

this water is then deflected eastward along the equatorial currents into the southern part of the North East Atlantic. The near-bottom water of the North Atlantic is mainly constituted of cold (0.2 – 2.2 °C) Antarctic Bottom Water (AABW) which becomes warmer as it moves north (2.2 °C at 70 °N). This originates from the sinking and northern movement of nutrient rich Circumpolar Water in the Southern Ocean [241]). Despite the variations in origin and ventilation time of these deep waters,

there is increasing evidence that the dissolved Fe concentrations determined in the deep waters of the northern Atlantic, and indeed other oceans, are very similar. DFe data from stations in the Gulf of Alaska (59 °N, 20 °W) and the northern gyre (47 °N, 20 °W), [237] the Bay of Biscay (46.0 °N, 8.0 °W) [238] and the Sargasso Sea (32 °N, 64 °W) [234] have reported concentrations between 0.5 and 0.8 nM.

Table 4.3 Reported iron concentrations in Atlantic waters

Atlantic Region	Iron Fraction	Surface (0-500 m)	Intermediate (500 -2500 m)	Deepwater (2500 -5000 m)	Reference
Gulf of Alaska 47 and 59 °N, 20°W	<0.4 µm	0.07 – 0.3	0.4 – 0.8	0.5 – 0.8	Martin *et al* [237]
NW (near shelf) 36-38 °N 72-74 °W	<0.2 µm	0.2 - 0.6	0.7 – 0.9	-	Wu and Luther [242]
Sargasso Sea 26 – 31 °N 57 – 65 °W	<0.4 µm	0.2 – 0.8	0.2 – 0.8	0.5 - 0.8	Wu and Boyle [234]
NE 40 °N, 23°W	<0.2 µm	0.5-1.5	0.9 – 1.5	-	de Jong *et al* [243]
NE (near shelf) 45 - 50 °N 4 - 8 °W	<0.2 µm	0.2 – 0.4	0.6 – 1.2	0.75 ± 0.04	Laes *et al.* [238]
Central 19 °S – 27 °N 5 °E – 16 °W	<0.2 µm	0.02 – 1.11	-	-	Sarthou *et al.* [244]
Central 34 °S – 8 °N 20 – 50 °W	<0.22 µm	0.4 – 1.4	-	-	Vink and Measures [233]
N-S Transects 50 °S - 50 °N	TD-Fe (unfiltered)	0.2 – 8.0	-	-	Bowie *et al.* [232]
Central and SE Atlantic	TD-Fe (unfiltered)	0.2 – 10.0	-	-	Powell *et al.* [245]

4.4.5 Residence Time and Transport

To assess the impact of hydrography and water mass transport on iron distributions, accurate residence times are required for dissolved iron. At present these have only been estimated by a few workers (e.g. 10 - 300 days in subtropical surface waters [105,244] and 70 - 200 years in deep waters [124,229,230]).

The main movement of North Atlantic waters above 200 m is the anticyclonic current circulating the northern gyre. The approximate velocity of the upper water column on the edge of the Northern Gyre is ~50 nautical miles day^{-1}. [246] Thus if dissolved iron in surface water had a residence time of only one month, then it could travel 1500 nautical miles in its lifetime. Hence, interpretation of dFe profiles in North East Atlantic surface waters are complicated as they are not only a product of the vertical fluxes in the area sampled but are also a sum of accumulation and depletion occurring in different regions before arriving at the sampling site. Exceptions to this may occur under extreme conditions such as tropical storms and major dust deposition events where rapid and significant changes in dFe concentrations can be directly linked to a particular source.

The processes that control the deep-water dFe concentrations across the Atlantic and other oceans remain unresolved. There is an apparent similarity between reported iron concentrations for deep waters in the largest oceans and hence there is no clear indication of inter-ocean fractionation. [124] The transport of deep waters across the Atlantic occurs over 100 y timescales (i.e ~ 80 years in the north to south flowing western boundary current [246]) and thus ocean cycling timescales are estimated to be in the same order as the dissolved iron residence time (~ 70-200 y [124,229,230]). Therefore the similarity in deep water dFe concentrations of different basins is unlikely to be due to the long-range transport and mixing of iron in these waters. This is supported by observations from a study of the trace metals; Mn, Ni, Cu and Cd, in the deep North East Atlantic which showed that only the distributions of elements with long residence times (i.e. cadmium and nickel) were consistent with the mixing of water masses. [234]

Recent global models have accurately predicted deepwater iron concentrations in the major ocean basins [125,234,248] but still rely on optimised variables to obtain rates for scavenging and other vertical fluxes. More information on the latter processes can be gained by determining the iron fluxes in areas that receive high iron input that provide a strong chemical signal to the water column (e.g. shelf waters, hydrothermal plumes and high dust flux areas). Such studies benefit

from the deployment of sediment traps and high volume filtration devices to allow particulate and colloidal Fe fluxes to be studied. Further evaluation of iron binding ligand concentrations and binding constants in different areas as well as more accurate dFe data will assist in obtaining more realistic models of iron biogeochemistry in ocean basins. Spatial studies of the euphotic zone are also important for determining seasonal distributions of iron in the more dynamic surface and intermediate waters that contain the major phytoplankton populations.

4.5 Conclusions

1. The variables that are known to affect iron redox speciation in oxic seawater are temperature, pH, dissolved oxygen and hydrogen peroxide concentrations, electron activity, photon concentration, organic speciation, biological redox cycling and particle/colloid concentration.

2. Modelling of iron redox speciation is limited by a lack of speciation data and kinetic constants. Field data from the North East Atlantic obtained during this study can be used to assess the validity of models under varied conditions.

3. Open ocean dFe concentrations in the North Atlantic vary from 0.07 – 1.5 nM in the surface waters (0 - 500 m), 0.2 –1.5 nM in intermediate waters (500 – 2500 m) and 0.5 – 0.8 nM in deep waters (2500 – 5000 m).

4. Interpretation of surface dFe data is limited due to the transport and mixing of the element during its residence time. Hence studies are required in open ocean areas where high iron fluxes occur.

5. Historical dFe data allow estimates of concentrations in different water masses but an improved knowledge of iron residence times and scavenging is required for accurate interpretation of basin-scale iron biogeochemistry.

CHAPTER 5.

Redox speciation and distribution of dissolved iron on the European Continental Shelf

5.1 Introduction

Our knowledge of the biogeochemical cycles of iron in the Atlantic Ocean is constrained by a lack of dFe data for different oceanic regions. Spatial and temporal studies are important in areas that receive high iron inputs such as shelf waters, deep waters surrounding hydrothermal plumes and surface waters impacted by high dust fluxes. As a part of the European Commission's Marine Science and Technology Programme, the IRONAGES ("Iron Resources and Oceanic Nutrients – Advancement of Global Environment Simulations") programme was initiated in response to the need for such studies. The work reported hereafter is the result of two collaborative research cruises, both of which took place in 2002, designed to examine shelf ('Iron From Below' cruise, Chapter 5) and atmospheric ('Iron From Above' cruise, Chapter 6) iron inputs into the North Atlantic Ocean.

The results from the investigation of iron speciation in the two study areas chosen are reported in the following chapters along with the joint aims, hypotheses and an account of the work conducted in the North East Atlantic. The shipboard sampling and data collection methods employed during the cruises are included along with details of physicochemical data and nutrient distributions. The iron biogeochemistry of the two study areas is discussed in terms of the geographic and hydrographic features of the North East Atlantic and the dFe distributions found in this region are compared to past studies.

The *'Iron from Below'* cruise took place on the RV Pelagia (The Netherlands) from the 11th March 2002 to the 3rd April 2002 on the European continental shelf and the deep waters of the north of the Bay of Biscay. This area is characterised by a broad continental shelf with a steep slope that extends down to ~ 4500 m. The major water mass transport at the shelf break is caused by a northward slope current which flows at a velocity of ~5 cm s^{-1} and tides cause strong internal waves at the shelf break. [249,250] Processes such as mixing of shelf and open ocean waters and

sediment resuspension are likely to play an important role in iron cycling in this region.

Figure 5.1 Study area for the 'Iron from Below', Ironages Cruise March 2002

a) Study site location

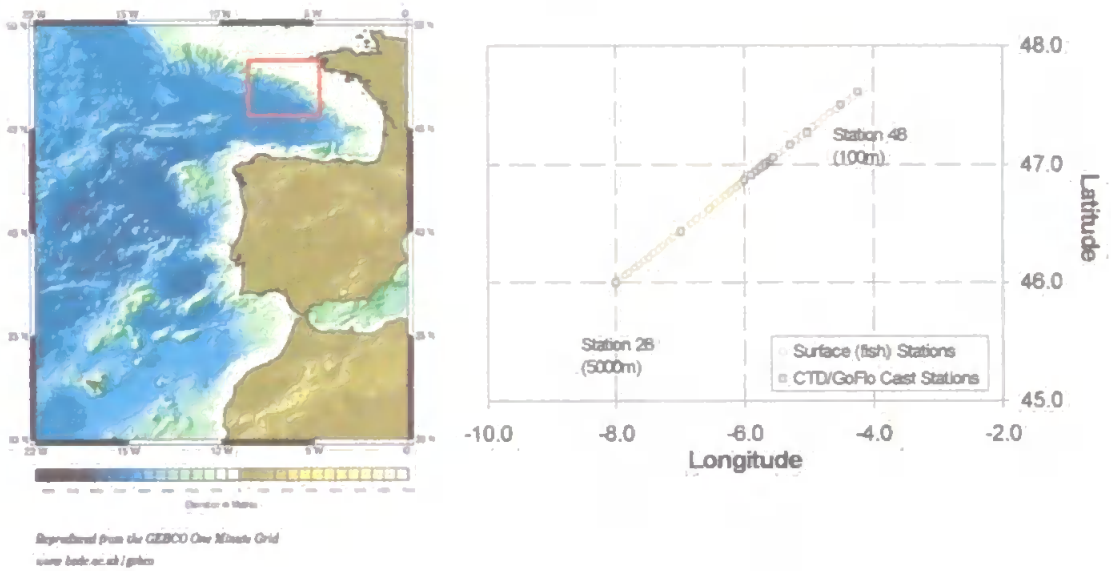

b) Vertical profile of the shelf transect

(vertical lines indicate cast positions)

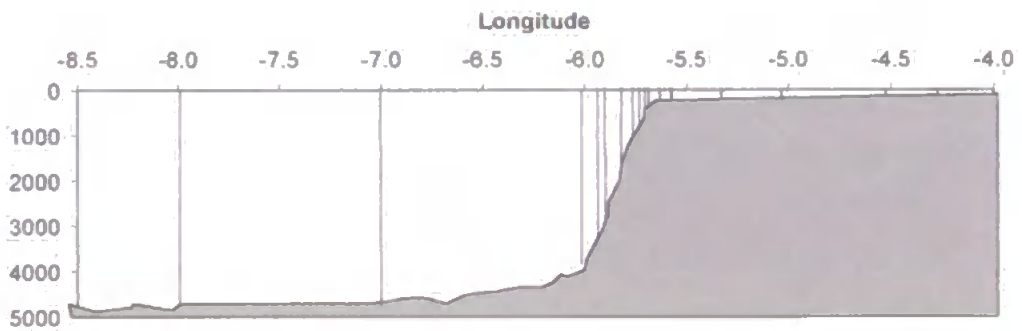

The overall aims of the voyage were 'to define the transport of dissolved iron emanating from the marine sediments into bottom waters' and then evaluate the transport via vertical and lateral mixing into intermediate and surface waters. Supporting data was provided by workers from the Royal

Netherlands Institute for Sea Research (RNIOZ) and included underway and CTD physical data, dissolved oxygen and nutrient data.

Sampling of the water column was conducted over a transect in an area that was considered sufficiently far from the European continent to reduce risk of interference from any major temporal fluctuations from fluvial Fe sources. The transect was approximately perpendicular to the contours of the European Continental Shelf in the Chapelle Bank area. Vertical profiles were sampled at 15 stations positioned along a transect line which extended into the abyssal plane of the Bay of Biscay between 47°61'N, 4°24'W to 46°00'N, 8°01'W, over which the depth of the water column increased from ~100 to 5000 m (see Figure 5.1). Hourly discrete and near real-time underway surface water sampling (~5 min lag time) was conducted between stations using the towed fish, deployed alongside the starboard side of the ship.

Following the vertical section transect, a final surface water transect was carried out over the shelf and through the English Channel (46 °N, 8 °W to 52 °N, 4°W). Similar to the shelf transect, underway filtered surface water samples were taken throughout this transect from the towed fish supply. DFe was determined at the shore-based laboratory using the method discussed in Chapter 2.

5.2 Sampling and methods

5.2.1 Cast samples

A summary of the sample collection and processing is shown in Figure 5.2. Cast samples for Fe(II) and dFe (Fe(II) and Fe(III)) were taken from pre-cleaned, PTFE coated PVC 12 L GoFlo bottles (General Oceanics, FL). These were mounted either on a new stainless steel, epoxy-coated CTD frame with a new stainless steel cable or directly onto a Kevlar wire. After recovery of the bottles they were mounted inside the storage cabinets, placed in the clean air container and a filtered

nitrogen overpressure was used to filter the sample water. Sample processing was completed within 1½ hours of collection.

Discrete cast samples were taken for dFe after filtration through Sartobran™ cartidges (0.2 µm pore size, Sartorius). Ultra-filtered samples (<0.02 µm) were obtained after further in-line filtration through 25mm Anotop™ syringe filters. These had been previously rinsed at 2 mL min^{-1} with 30 mL of 0.1 M HCl, 60 mL of H_2O and 60 mL of sample.

Fe(II) determinations were made immediately after the samples were brought on-deck by pumping fresh unfiltered samples directly through a Gelman™ syringe filter (0.2 µm pore size, PTFE membrane) into the flow injection analyser. This allowed measurements to be made within 20 minutes of sampling. Deep water Fe(II) samples were stable for > 1hour, if kept at their original temperature. DFe (Fe(II) + Fe(III)) in the filtered and ultra-filtered samples was determined in a shore based class 100 clean room after a 3-month acidification period (pH 1.8, quartz distilled HCl in acid washed LDPE bottles) and a 12 h sulphite reduction step.

5.2.2 Surface water sampling

Surface water sampling was conducted whilst the ship was steaming (~12 knots) using a trace metal clean towed fish connected by PTFE tubing to a PTFE bellows pump (Almatec A-15, Germany), which provided a flow rate of approximately 3 L min^{-1}. The pump was driven by a compressor (Jun-Air, Denmark, model 600-4B) operating at 1.5-2 bar pressure located in the clean van. This underway pumping system ran continuously during the cruises. Sample water for dFe analysis was then filtered on-line through a 0.2 µm filter cartidge (Sartobran™, Sartorius) and collected in acid washed LDPE bottles (Nalgene). Sample water for Fe(II) analysis was taken in-line from a supply of unfiltered water delivered directly to the clean room and analysed after filtering in-line via a 0.2 µm pore size, syringe filter (Acrodisc™, Gelman, PTFE membrane)

coupled to the flow injection manifold. This allowed measurements to be made within 5 minutes of sampling.

All sample handling was done using trace metal protocols, either in an over-pressurized class 100 laminar flow hood or beneath filtered air inside a clean container. Samples were analysed using an automated flow injection analyser for Fe(II) determination (detailed in Chapter 2) which was adapted to allow dFe measurements using the method reported by Bowie (1998). [163] All measurements reported for both the Fe(II) and dFe methods are the mean values of 3 or 4 replicates (where peak height has been measured) and error bars represent two standard deviations (2σ) unless stated otherwise.

Figure 5.2 Schematic of ship-board sample processing

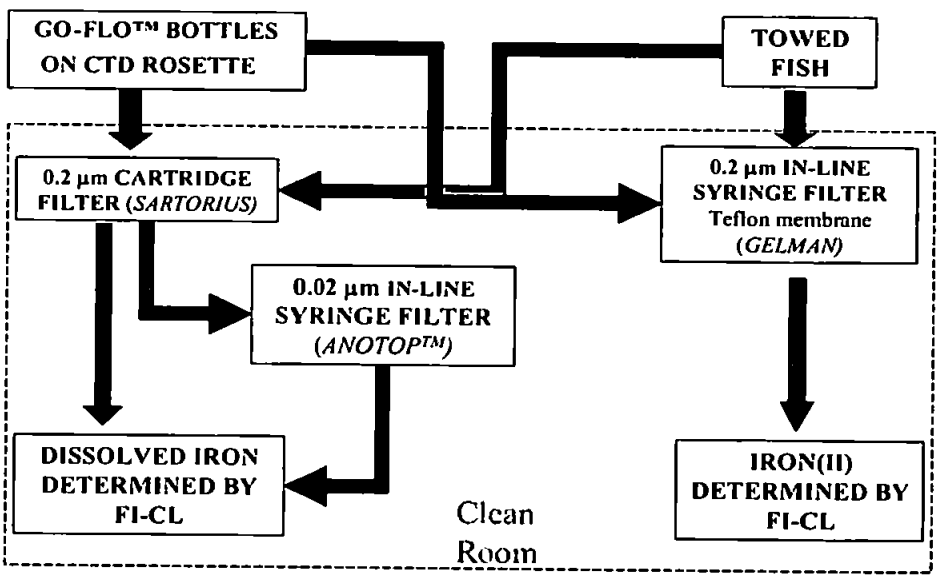

5.2.3 Operationally defined redox and size species

Iron concentrations reported by the marine science community are operationally defined by the pre-treatment that they have undergone before analysis and by the analytical method used. The abbreviations used in the text are described in Table 2.3. Fe(II) is often shown as a percentage fraction of dissolved iron (i.e. (Fe(II) / dFe) x 100%). and abbreviated as ***%Fe(II)***.

5.3 Dissolved iron distribution

5.3.1 Vertical distribution of dissolved iron – Deep casts off the shelf

Deep water casts were made between 8.0 and 6.0 °W to determine the effect of the slope on the iron speciation and dFe concentrations of adjacent waters. The temperature and salinity profiles of the water column in the deep waters adjacent to the shelf (Figure 5.3) indicated intrusions of low salinity, high oxygen Labrador Sea Water (LSW) between 1500 and 2300 m. Whereas a strong oxygen minimum (ca. 185 μM) and high salinity (35.5 – 37.5) Mediterranean Outflow Water (MOW) occurred at 750 – 1000 m. The latter was also observed as a permanent feature in the Goban Spur area from January 1994 to September 1995 by Hydes *et al.* [252] Unstratified surface waters were observed (Figure 5.4) off the shelf due to strong winter mixing caused by high winds and heavy seas at the time of the study.

Figure 5.3 Salinity and dissolved oxygen versus potential temperature for deep water cast southwest of La Chapelle Bank (station 28)

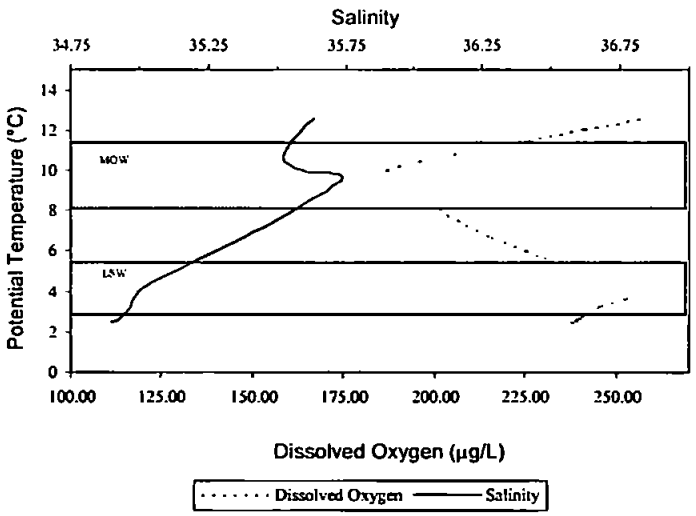

Dissolved iron vertical profiles for cast stations 26 (*46° 52' N, 6° 00' W*), 28 (*46° 00' N, 8° 00' W*) and 44 (*46° 54' N, 5° 54' W*) in the deep waters of the Bay of Biscay are shown in Figure 5.4 along with supporting data. Similar to phosphate and nitrate profiles (Figure 5.4(d)), dFe was depleted in the surface waters of this area and concentrations were generally < 0.6 nM at depths above 500 m.

Figure 5.4 Vertical profiles showing the distribution of dFe and major nutrients off the European Continental Shelf in the NE Atlantic Ocean (Stations 26 (46° 52' N, 6° 00' W), 28 (46° 00' N, 8° 00' W) and 44 (46° 54' N, 5° 54' W))

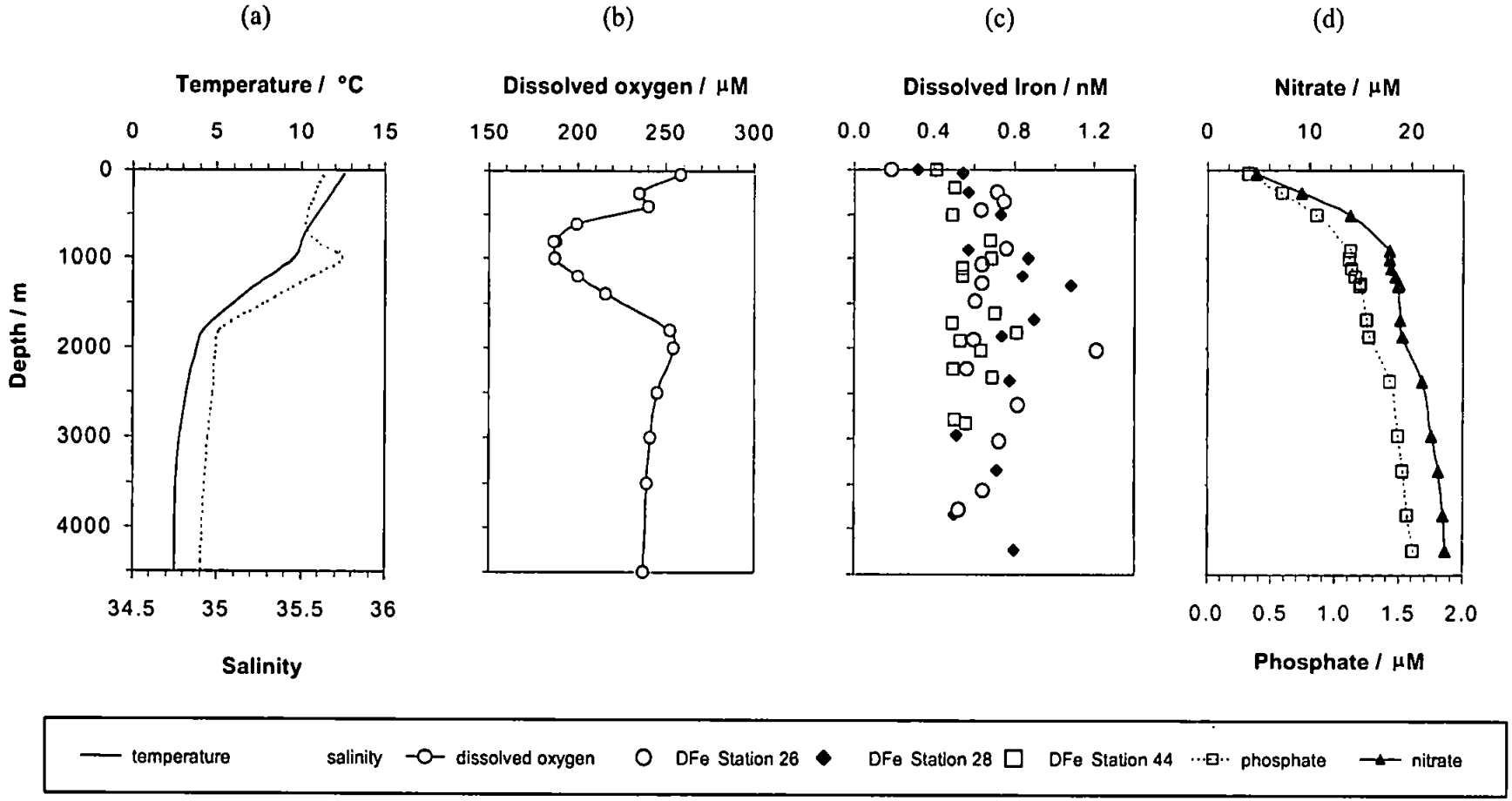

DFe concentrations in intermediate and deep waters ranged between 0.5 and 1.4 nM and showed little oceanographic consistency with other physicochemical parameters. The greatest variability in dFe observed between 1000 and 2500 m. Similar dFe profiles at these depths were reported by other workers using a different FI-CL method, as a part of the same study. [238] These workers hypothesised that the elevated concentrations were due to advection of benthic iron enriched water by the lateral movement of Labrador Sea Water (observed as oxygen maximum at ~1800 m in Figure 5.4(b)) southwards along the shelf. [238] Furthermore, the concentrations and variability seen in these intermediate waters during our study were similar to those reported in the North East Pacific shelf waters for three stations off the west coast of North America (0.6 – 1.5 nM, < 500 m. [9]

Due to the analytical precision of the measurements (ca. 5 %), no other differences in dFe concentrations were distinguishable in the deep-water masses in this area. However, in agreement with the data reported in the literature for other regions in the North Atlantic Ocean (0.5 – 0.8 nM, see Table 4.3), less variability in dFe concentration was observed in deep waters (<2500 m). This is further evidence that an equilibrium between dissolved iron, organic ligands and particles/colloids exists in the deep water column (see Chapter 1, Section 1.4).

5.3.1 Vertical distribution of dissolved iron on the shelf slope

The vertical distribution of dFe on the shelf slope is shown in Figure 5.5. The largest dFe gradient was observed between off shelf surface waters (<0.3 nM) and the shallow well-mixed waters on the shelf (>1.0 nM). Dissolved Fe concentrations below the euphotic zone were between 0.5 and 1.4 nM and the highest concentrations were found in near-bottom samples from the shelf break and in patches within the intermediate waters near to the slope. The high concentrations on the shelf break were considered to be a result of diffusion and sediment resuspension caused by high energy tidal and storm mixing. These results compare well with enhanced dissolved Cd, Mn, Co and Cu

distributions observed at the sea bottom on the Hebridean [254,255] and the Celtic Sea shelf breaks. [256]

Figure 5.5 Dissolved iron distribution over the south west European Continental Shelf (Section Plot, Ocean Data View, Schlitzer (2004) [253]

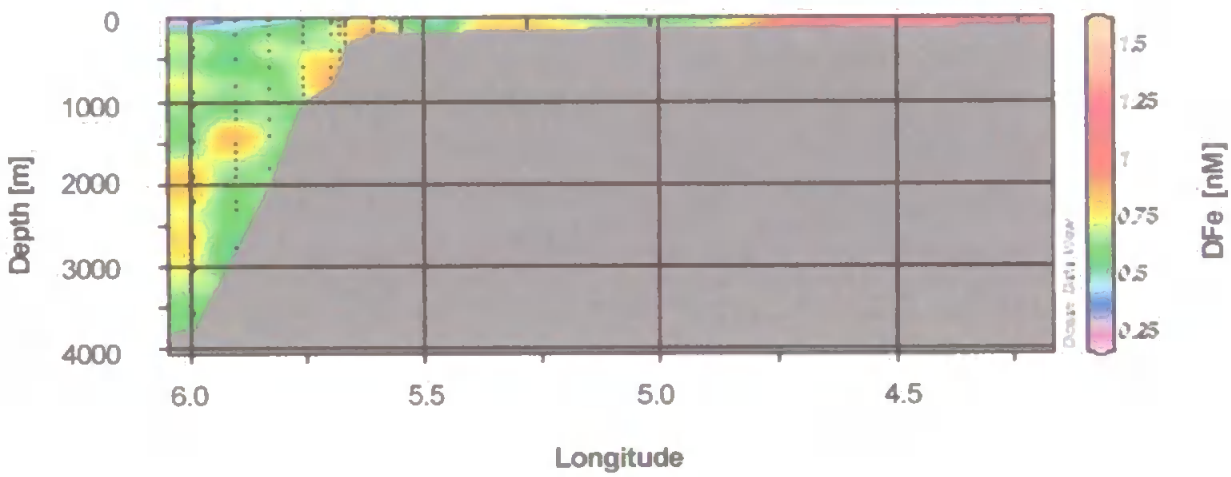

High iron dissolution fluxes (ca. 50 nM m^{-2} s^{-1}) from porewaters in the shelf sediment / seawater interface have been observed on the North East Atlantic shelf slope, [257] hence, this is a likely cause of the enrichment detected near the upper slope (along with Fe(II) data, see Section 5.4). However, the lack of elevated dFe values or concentration gradients found close to the lower shelf slope and in deep waters in this study suggest that this is not the mechanism responsible for higher dFe patches in overlying intermediate waters. Furthermore, no obvious relationships were observed between intermediate and deepwater dFe concentrations and physico-chemical master variables (temperature, salinity and dissolved oxygen).

An increase in particle flux with depth (>1000 m) related to lateral fluxes of resuspended material from the upper slope was observed in the Goban Spur area north of the Ironages study site (1993-1996 [258]). The results showed that the main particle flux occurred from the upper slope and shelf break in a seaward direction to the foot of the slope and varied with topography. Particle flux was

generally as high in the near bottom water at the foot of the slope as it was in intermediate waters. However, particles were reported to be more refractory in the former suggesting chemical processing occurs as the particles move downward through intermediate waters. This is supported by the observation of highly efficient mineralization of organic particles in the water column near the slope. [249]

The high dFe patches observed in this study were considered to be caused by either i) the remineralization of organic matter or dissolution of colloids as they pass through the low oxygen environment (500 – 2000 m) [9] or ii) the sinking and advection of small (<0.2 μm) lithogenic/organic colloids directly from the shelf slope detected as a part of the dissolved iron fraction. Laes *et al.* [238] reported an inverse relationship between dFe concentrations and apparent oxygen utilization in intermediate and deep waters for stations 27, 28 and 47 of this study. Based on these findings these workers suggested that process (ii) (i.e. the sinking/advection of colloids) occurs due to currents moving alongside the shelf that pass through nepheloid layers at intermediate depth.

5.3.2 Horizontal distribution of dissolved iron along a transect between shelf waters and North East Atlantic surface waters

Significant temperature and salinity gradients were observed between the coastal waters of the North Sea, the English Channel and the North Atlantic across the slope into the abyssal plain. The lowest salinity/temperature waters of the English Channel and southern North Sea were due to high riverine and rain inputs typical of early spring. The dFe distribution in the surface waters (2 - 4 m depth) was determined for a transect from station 28 (8.0 °W, 35.9 °N) and the coast of the Netherlands (3.9°W 27.6°N) (Fig. 5.6).

A clear inverse relationship between depth and dFe concentration was observed along a transect from the deep North East Atlantic waters to the English Channel, showing that enhanced dFe

concentrations are maintained in shallow waters as a result of riverine and benthic inputs (Figure 5.7). The highest concentrations (> 2 nM) were observed in the waters near the coast of the Netherlands, where salinity data indicated a strong riverine influence.

Figure 5.6 Variation of surface dFe and salinity for a transect between the open ocean (8.0 °W, 35.9 °N) and the coast of the Netherlands (3.9°W 27.6°N)

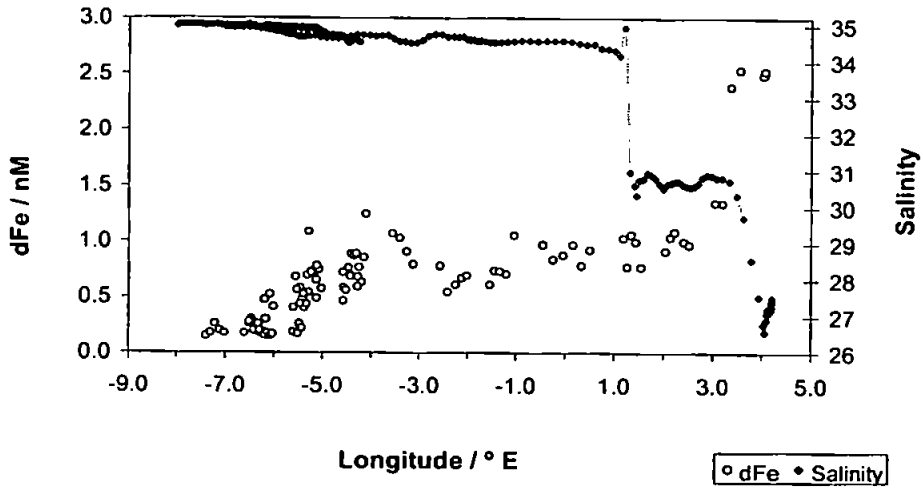

Figure 5.7 Effect of depth on surface dFe concentrations

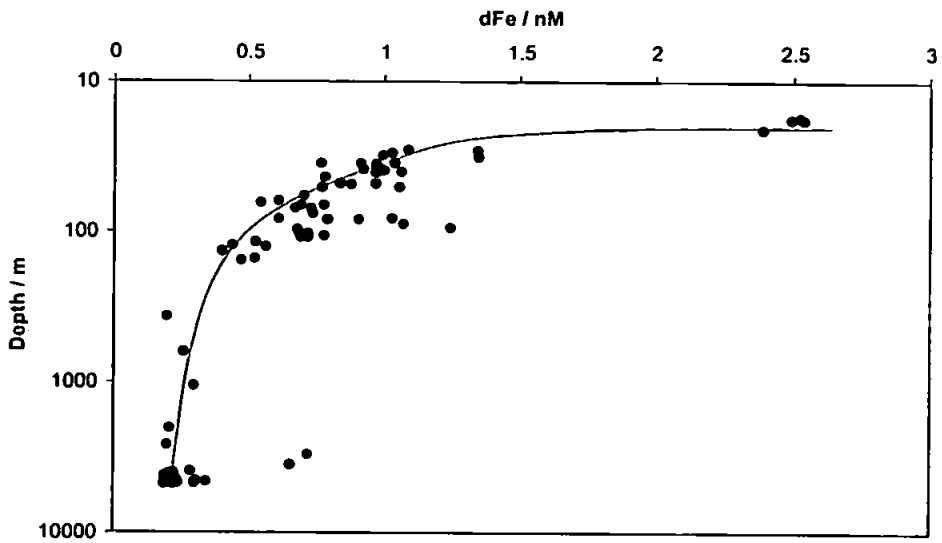

The highest dFe and salinity gradient west of 0.0 ° longitude occurred inshore of the continental shelf break between 4.0 and 7.0 ° W and was a result of mixing of less saline, iron rich English Channel shelf waters with North East Atlantic surface water. A ~5 fold increase in dFe concentrations was seen between open ocean and shelf waters. This was similar to the 1-5 fold enrichments seen for Cd, Ni, Cu and Mn in previous studies of the European Continental Shelf. [254,256,259] This well defined lateral gradient between shelf and open ocean waters for iron on shelf breaks has also been observed for iron distributions on the New Zealand shelf. [260] In addition it supports the data of Hydes *et al.* [252] who did not find large-scale transport of water across the shelf break in this region despite severe winter storms.

Figure 5.8 shows the surface water dFe and salinity data for three repeat transects over the shelf. The position and gradient of the chemical fronts in relation to the shelf break varied spatially, even in the small area covered by these transects, and it is reasonable to assume that these will also vary seasonally as suggested by Le Gall *et al.* [254]

Figure 5.8 The influence of the continental shelf slope on the variation of dFe and salinity between the English Channel and open ocean surface waters

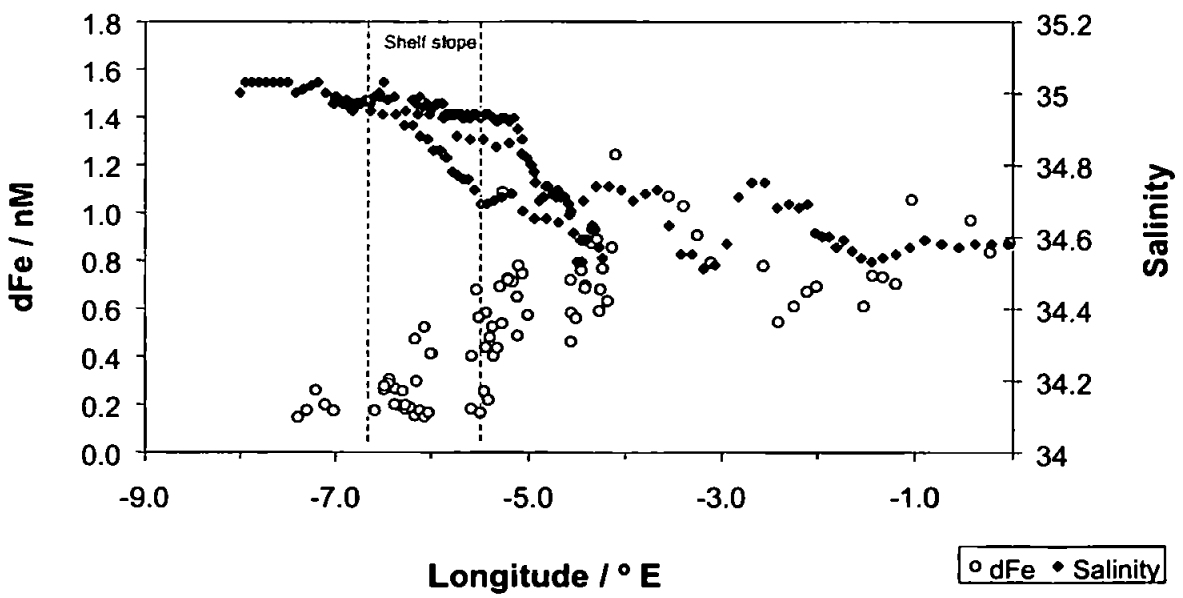

A plot of dFe concentrations versus salinity (Figure 5.9) showed near conservative mixing (R^2 = 0.57) of the element between the English Channel and the open ocean. However, the salinity and dFe data determined in the low salinity coastal waters of the North Sea did not compare well with this relationship (e.g. salinity = 27, dFe = 2.5 nM, data not shown). Similarly, the y-intercept of 40 nM does not compare well with estimated river concentrations (e.g. global mean riverine Fe concentration of ~1 μM). suggests that other physico-chemical factors control dFe concentrations in the eastern English Channel and Southern North Sea waters over the mixing gradient. This is supported by the observations of Tappin *et al.*, [261] who reported a poor relationship between dFe and salinity in the southern North Sea and suggested the variance of dFe concentrations in this region were due to seasonal benthic inputs rather than riverine inputs.

Figure 5.9 dFe versus salinity for surface waters between the English Channel (1.2 °E, 50.4 °N) and the North East Atlantic Ocean (8.0 °W, 35.9 °N)

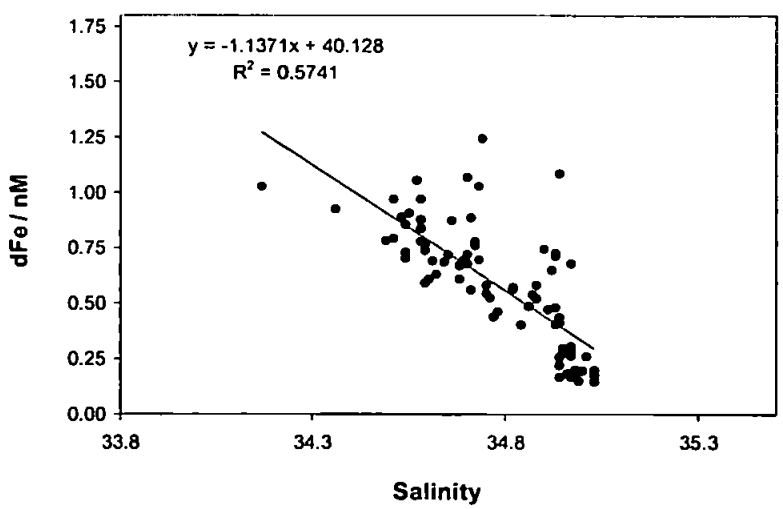

5.4 Dissolved iron redox speciation

5.4.1 Vertical changes in iron redox speciation - off the shelf

The Fe(II) vertical profiles at stations 26 (*46° 52' N, 6° 00' W*), 28 (*46° 00' N, 8° 00' W*) and 44 (*46° 54' N, 5° 54' W*) (Figure 5.10) showed similar trends to the dFe profiles. Low surface water

Fe(II) concentrations (10 – 35 pM) were observed, increasing to ca. 20 - 75 pM in intermediate and deep waters. Fe(II) formed a constant proportion of the dFe fraction (5.6 ±2.5 %) throughout the water column at these stations. No obvious correlation was observed between the %Fe(II) fraction and either dissolved oxygen or temperature, although %Fe(II) decreased marginally with depth.

Figure 5.10 Vertical profiles showing the redox speciation of dFe near the European Continental Shelf in the NE Atlantic Ocean.

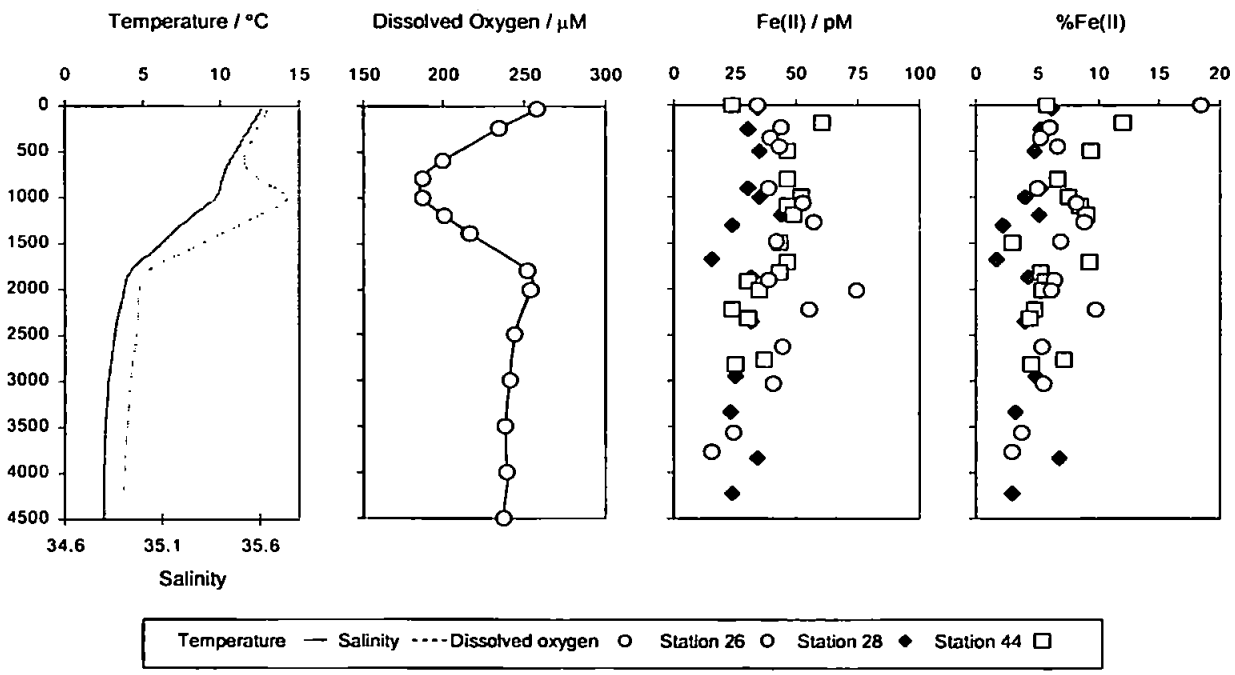

The physicochemical data for the deep-water casts at stations 26, 28 and 44 were used to create an equilibrium model for dissolved iron redox species using equations *4.1 – 4.3* (Chapter 4). No pH measurements of the water column were made during the cruise, so the range of pH 8.0 – 8.2, found for historical pH data measured over the period 1910 – 2000 for this region (45 – 50 °N, 5 – 10 °W, NODC [262]) was used.

Figure 5.11 Equilibrium model predicting dFe redox speciation assuming the free aqua ions* and physicochemical data from station 28 (46.0 °N, 8.0 °W).

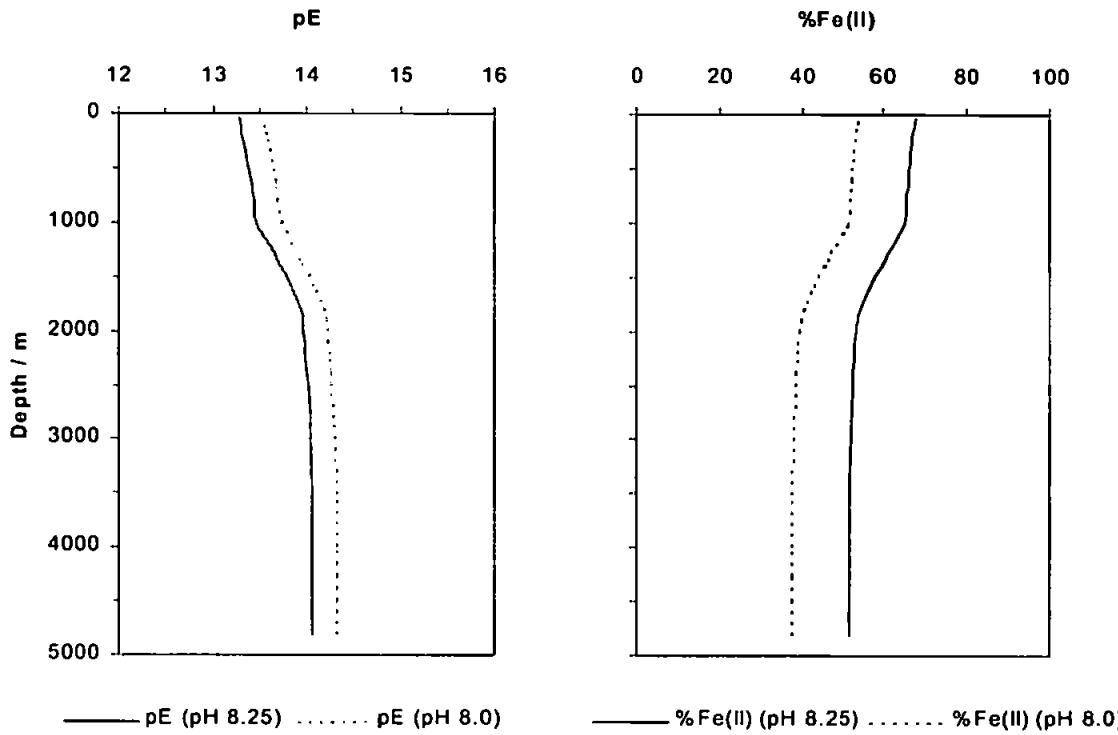

*(Standard reduction potential for free Fe(II) and Fe(III) hexa aqua ions, E° = 0.77 V)

Figure 5.12 Calculated Fe(II) fraction for varying standard reduction potential for surface (40 m 12.6 °C) and deepwaters (3000 m, 2.7 °C) at pH 8.0.

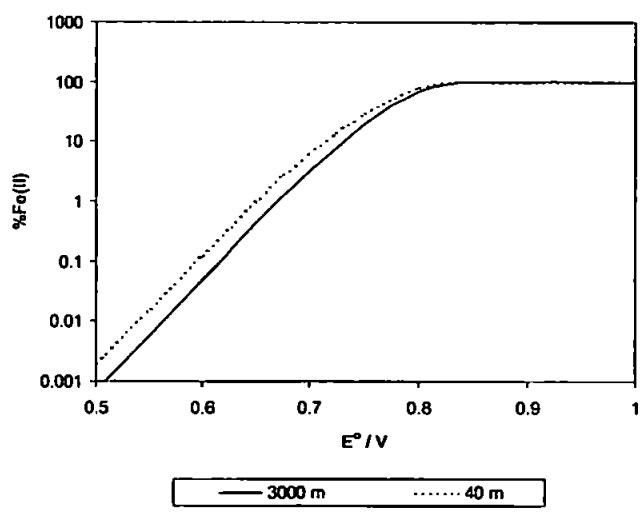

According to the model, the pE of seawater increases from 13.4 ±0.1 to 14.1 ±0.1 between 0 and 5000 m, mainly as a result of decreasing temperature (Fig. 5.11). This caused a decrease in %Fe(II) of between 0 – 40 % of the surface water value (shown in Fig. 5.11 as a maximum decrease from 70 – 40 %Fe(II) where the free aqueous Fe(II) and Fe(III) couple are used). This is similar to the trend observed for the data. The model also demonstrates that complexes capable of stabilising a ~5 % Fe(II)/(Fe(II) + Fe(III)) fraction under these conditions would require a standard reduction potential of > +0.65 V (see figure 5.12). However, the known standard reduction potentials of most natural iron chelates are between –0.5 and +0.2 V [263] (e.g. Fig. 1.5).

This discrepancy can be accounted for by the following three hypotheses: Firstly, the iron redox speciation in deep waters is controlled by solid phase reactions such as physically and biologically mediated dissolution from particles (e.g. steady state Fe(II) concentrations caused by the high solubility of Fe(II) compared to Fe(III) and slowed oxidation kinetics at low temperature). Secondly, the strong complexes that form the major part of the dissolved Fe pool have high reduction potentials (i.e. > +0.65 V) and thirdly, the Fe(II) fraction is misrepresented either by the model or by the analytical method.

5.4.2 Vertical section of iron redox speciation on the shelf slope

Similar to the off shelf data, there was little correlation between %Fe(II) and temperature, salinity and dissolved oxygen was observed near the shelf slope. However, higher Fe(II) concentrations were observed on the shelf break (Fig. 5.13). These results provide strong evidence that intense iron dissolution from sediments occurs in this area. This may be caused by the nature of the benthic boundary layer in the upper slope. Higher flow velocities, bioturbation and anoxic bacterial mineralisation were found as common features for the upper slope sediments (< 1000 m) of the nearby Goban Spur region. [264]

In contrast, deep water samples taken within 50 m of the sea floor in the abyssal plain of the Bay of Biscay (46.0°N, 8.0°W to 46.6°N, 6.4°W) showed no clear enrichment of Fe(II) or dFe. This may be due to low bottom resuspension and deep oxygen penetration in the sediments and consequently low pore water dFe and Fe(II) fluxes.

Figure 5.13 Iron redox speciation and physico-chemical variables over the European Continental Shelf (Section Plot, Ocean Data View, Schlitzer (2004) [253])

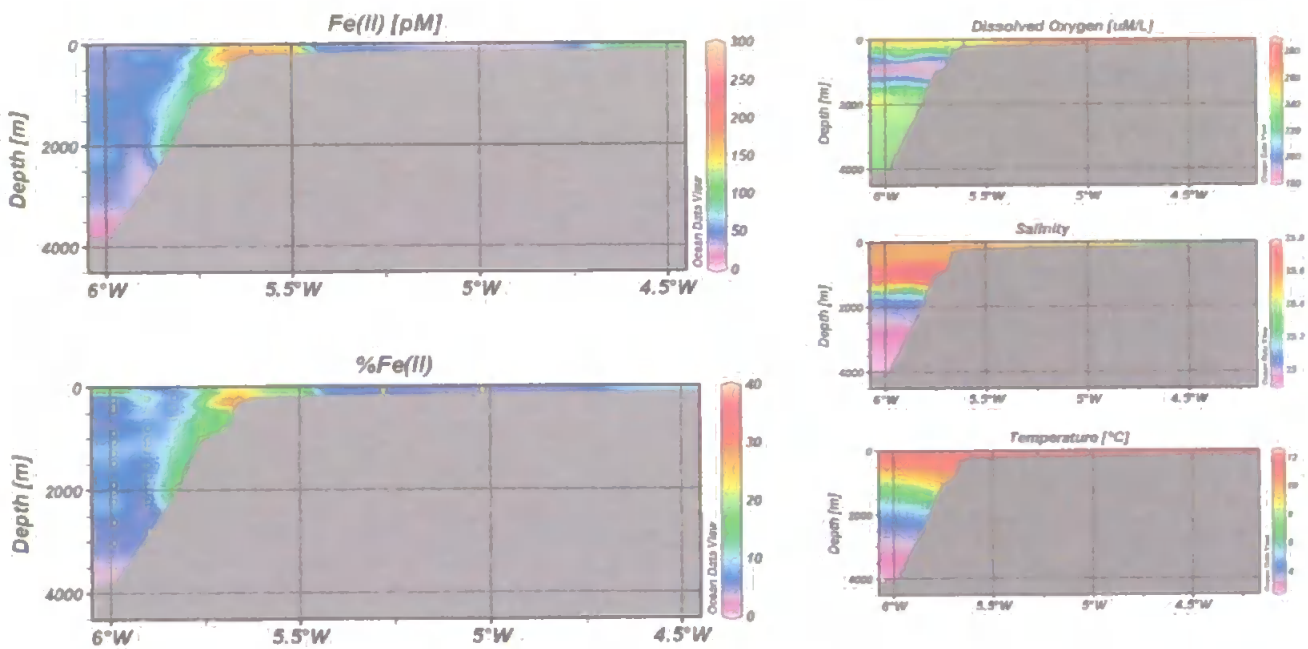

On the shelf break the highest Fe(II)/{Fe(II)+Fe(III)} fraction in the dissolved iron pool was nearly 30 %, a value far higher than would be predicted for most oxic open ocean waters. In order to estimate a minimum rate for Fe(II) production in this area, it was assumed that diffusion, advection away from the shelf break and reduction of dissolved Fe(III) species were negligible. Therefore, if

the interactions between the seawater and suspended sediments were at a pseudo steady state, the following rate equation equates to zero:

$$d[Fe(II)]/dt = k_{sediments} - k_{ox}[Fe(II)] \quad (5.1)$$

where $k_{sediments}$ is the zero order rate constant for the input of Fe(II) from suspended sediments and k_{ox} is the oxidation rate constant. A zero order rate constant is appropriate for this calculation as dFe concentrations in benthic flux chambers have been reported to vary linearly with time (R^2 = >0.7 for 77 % of observations [265]). Therefore, if the Fe(II) concentration in the bottom 1 m^{-3} of the water column was 150 pM and the temperature dependant oxidation kinetics described by Millero et al. [C1] ref are used, the minimum flux of Fe(II) from the bottom sediments at this time would be ca. 12 μM m^{-2} per day. This is not an unrealistic estimate as Fones *et al.* reported sediment surface dFe fluxes as high as 4.3 mM m^{-2} d^{-1} on the slope of the European Shelf [257] and Elrod *et al.* [265] determined mean dFe flux of between 0.5 – 15 μM m^{-2} d^{-1} in benthic flux chambers in Californian Shelf waters.

The long-term fate of the dFe produced from Fe(II) fluxes on the slope is uncertain and depends on whether it is stabilised by complexation or precipitated after oxidation. However, based on these findings, winter mixing on the shelf break is potentially a significant source of dFe to the surface waters of the North Atlantic margins and provides an alternative explanation for the elevated dFe concentrations observed in nearby intermediate waters.

5.4.2 Surface redox speciation between shelf waters and North East Atlantic surface waters

Redox speciation was also examined during the surface transect over the European Continental Shelf (Fig. 5.14) from the north of the Bay of Biscay (46.0 °N, 8.0 °W) to the coast of the Netherlands (52.4 °N, 4.2 °E). The results from this transect show that surface water concentrations of Fe(II) increased simultaneously with dFe over the shelf from the North East Atlantic into the

shelf waters of the English Channel.

The Fe(II) surface data showed a high degree of variability but %Fe(II) was similar to that of deep and intermediate waters (5.0 ± 2.7 %). No correlation was observed between solar radiation and the Fe(II)/dFe ratio for the transect east of the Strait of Dover (2-5 °E) or in the surface waters off the shelf ($R^2 < 0.4$). However, Fe(II) concentrations showed a diurnal trend in the low salinity waters of the Scheldt river plume, where no significant changes in dFe or salinity occurred between 1.5 and 3.4 °E but elevated concentrations of Fe(II) were observed. The most probable cause of this was direct and indirect photochemical reduction of Fe(III) facilitated by high concentrations of dissolved and colloidal organic matter delivered by the river plume.

Figure 5.14 Iron redox speciation, salinity and photosynthetic active radiation (PAR) in the European Continental Shelf surface waters.

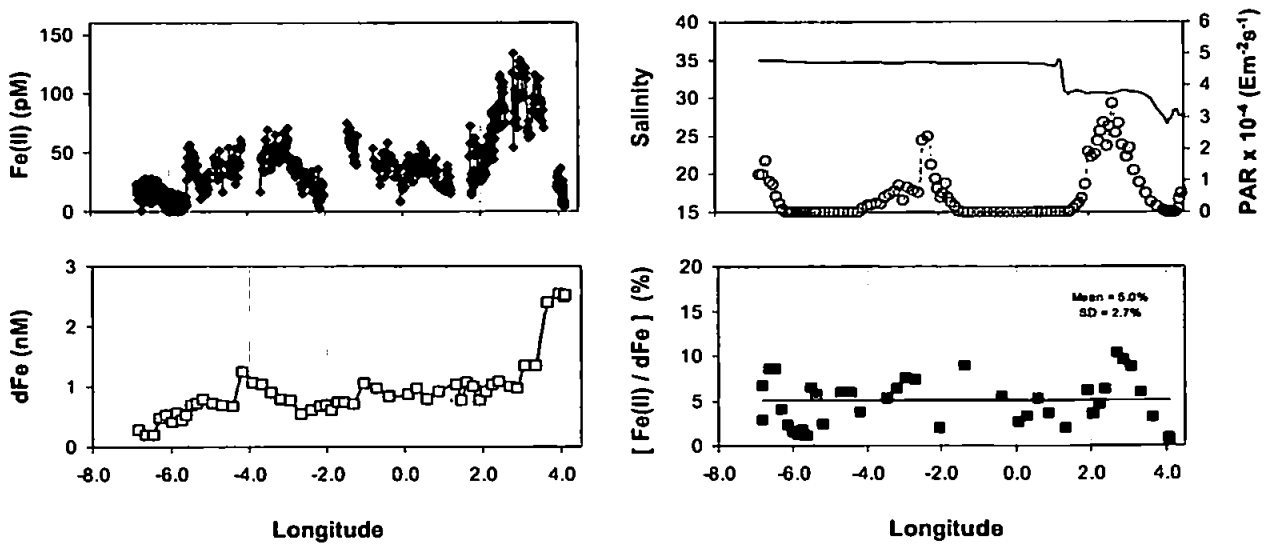

If it is assumed that all the Fe(II) determined between 2.0 and 3.5 °E was due to photoreduction reactions and that {[dFe] - [Fe(II)} represents complexed dissolved iron (Fe(III)L), then a simple rate expression (Equation 4.5) can be used to describe the system (Equation 5.2).

$$k_{hv}^{cond} * = k_{ox}[Fe(II)']/[Fe(III)L] = k_{ox}[Fe(II)]/([dFe] - [Fe(II)]) \quad (5.2)$$

* [*hv*] cannot be determined from PAR measurements

Using the temperature dependant oxidation kinetics described by Millero *et al.*, [61] k_{ox} for the Channel waters in March 2002 was calculated to be 0.027 s^{-1} (temperature = 9.3 °C, salinity = 30.56, dissolved oxygen = 260 μM, pH 8.0). Hence in these waters Fe(II) had a half-life of 25 min. If a steady state Fe(II) concentration of 100 pM is used in the model (Equation 5.2), along with a dFe concentration of 1.10 nM (mid day concentrations found at 2.5 °E), then the upper limit for the conditional first order photo-reduction rate constant (k_{hv}^{cond}) is ~2.5 x 10^{-3} s^{-1}. If the calculated value is extrapolated to estimate photoreduction of dissolved iron in the open ocean surface waters off the shelf where dFe was ~0.3 nM, maximum steady state concentrations of 25 pM would be predicted. This was close to the detection limit of the FI-CL method (5 – 12 pM) and the scatter of the data and thus, together with the lower PAR values seen in these waters (see Fig. 5.14), explains why no clear diurnal trends in the Fe(II) data were seen in these waters.

This k_{hv}^{cond} value found is 1-2 orders higher than previously reported first order photoreduction constants for colloidal iron [266] (e.g. 2.3 x 10^{-4} s^{-1} [80]) and for dissolved iron in coastal seawater (e.g. 6.3 x 10^{-4} s^{-1} [223]). However such differences are expected due to variable seawater speciation, turbidity, operationally defined iron fractions, different light regimes and different treatments of the kinetic model.

5.5 Conclusions

5.5.1 Dissolved iron distribution

1. The off shelf vertical distribution showed depleted dFe in the surface waters (0.1 - 0.6 nM), variable concentrations at intermediate depth (0.5 – 1.4 nM, 1000 – 2500 m) and values in agreement with those reported by other workers [198] for deep waters (0.5 – 0.8 nM).

2. On the shelf slope, elevated dFe concentrations were observed in near bottom waters at the shelf break (0.75 – 1.0 nM) and in patches of intermediate waters (1000 – 3000 m). These higher concentrations on the shelf break were indicative of sediment resuspension and benthic diffusion similar to observations made for New Zealand [260] and Californian [251] shelf waters. Elevated concentrations in intermediate and deep waters are consistent with increased particle fluxes with depth. [258]

3. A 'trace metal front' was observed in the surface waters over the shelf slope (7.0 – 4.0 °W) which had an inverse relationship with salinity (r^2 = 0.57) and was primarily a result of mixing between depleted open ocean surface waters and enriched shelf waters.

4. The relationship between dFe and salinity observed between the North Sea and the European Continental Shelf was non-linear suggesting factors such as benthic inputs and scavenging controlled dFe concentrations in this region, rather than mixing.

Based on these findings and those of other workers mentioned above, [252,254-257] the flux of dFe from the continental shelf to the open ocean is likely to vary temporally and spatially and is not simply sustained by an equilibrium between shelf sediments and the overlying waters. Therefore, further insight into the flux of dFe from shelf waters may be gained by studying iron transport via

particle and colloidal fluxes using particle filtration, sediment traps, benthic flux chambers and moorings near the shelf. If the main enrichment of dFe occurs via advection of colloids then a steady state dissolved/particulate model could be combined with water column downward particle fluxes obtained via field studies. In addition, differences in isotopic ratios may also help to track lithogenic iron originating from the shelf.

5.5.2 Dissolved iron redox speciation

1. Fe(II) concentrations were 10 – 35 pM in the surface waters and 20 - 75 pM in the intermediate and deep waters off the shelf. Surface concentrations of Fe(II) increased over the shelf from the Northeast Atlantic into the shelf waters of the English Channel, where concentrations were 20 – 200 pM. Fe(II) was observed as a constant fraction of dFe in both the surface waters on the shelf (mean = 5.0 %, σ = 2.7 %) and throughout the water column off the shelf (mean = 5.6 %, σ = 2.5 %).

2. A reasonable agreement was found between the trends of %Fe(II) determined in the water column and the predicted %Fe(II) from a thermodynamic equilibrium model that assumed the existence of a dominant class of ligand. However, the model also predicted that to stabilize the observed 5 % Fe(II) fraction in the dissolved iron pool under the conditions found, complexes would require a standard reduction potential of > +0.65 V. Therefore, assuming the Fe(II) concentrations found in these waters were not misrepresented either by the model or by the analytical method, either the Fe(II) fraction in these waters was stabilised by unknown ligands or it was controlled by kinetic processes such as dissolution and remineralization.

3. Elevated Fe(II) concentrations as high as 30 % of the dissolved iron pool were found on the shelf break and were attributed to the dissolution of Fe(II) from anoxic sediments. The minimum flux of Fe(II) released from these waters was estimated to be 12 $\mu M\ m^{-2}\ d^{-1}$. The same high Fe(II)

concentrations were not observed for near bottom samples taken from the lower slope and abyssal plane.

4. A diurnal trend that caused %Fe(II) to be as high as 10% was observed in the Scheldt river plume. An upper limit for a conditional first order photo-reduction rate constant (k_{hv}^{cond}) was calculated as ~2.5 x 10^{-3} s^{-1} for these waters, when Fe(II) had a half-life of ~25 minutes.

The data shown here show the significance of photoreduction and sediment diagenesis as sources of Fe(II) in shelf waters. Based on these findings, winter mixing and dissolution of Fe(II) from sediments on the shelf break are potentially significant sources of Fe(II) and dFe on the North Atlantic margins and provides an alternative explanation for the elevated dFe patches observed in nearby intermediate waters. However the ultimate fate of the Fe(II) and dFe species produced in these waters depends on whether they are stabilised by complexation or precipitated after oxidation.

CHAPTER 6.

Redox speciation and distribution of dissolved iron in the Canary Basin

6.1 Introduction

The Canary Basin is a sub-tropical oceanic region with warm, high salinity, stratified surface waters. The dominant winds in the Canary Basin are the trade winds from the North East and these cause significant upwelling along the North West African coast [267] as well as mobilizing large quantities of dust from arid regions in North Africa across the Atlantic Ocean. [96]

It has been estimated that over a million tonnes of dust (> 40,000 tonnes of Fe) are deposited in the Canary Island region every year. [268] However, deposition is sporadic, occuring in pulses of 3-8 days and is highest during winter and summer (42 and 29 % of the annual deposition occurring between January - March and July – September, respectively). [268] The high aerosol deposition in this area causes elevated fluxes of particulate iron in surface and deep waters, compared to those of other regions of the Northeast Atlantic. [269-271] Indeed, average particulate iron fluxes in the water column of the Canary Basin were reported to be nearly a factor of ~4 higher than those observed in stations between 30 – 55 °N. [269]

The residence time of atmospheric derived dFe in the sub-tropical surface ocean has been estimated to be in the order of weeks (9 – 54 d [244]) to months (60 – 300 days [105,198]). Therefore, despite periods of high atmospheric deposition fluxes, the dominant processes that control iron speciation and distributions in surface waters of this area may vary seasonally.

The *'Iron from Above'* cruise took place on the RV Pelagia (RNIOZ, The Netherlands) from the 2nd October to the 31st October 2002 in the Canary Basin. During the cruise a survey was conducted in an area west of the Canary Islands (see Section 6.2) and biological and physico-chemical measurements were made. In addition, Turkish atmospheric dust (Erdemli, Turkey) was used for solubility experiments in unfiltered and ultra-filtered (<30 kDa) surface water, collected underway. The specific aim of the work reported in this chapter was to determine redox and size-fractionated

iron species in the Canary Basin and relate their distribution to atmospheric, hydrographic and physico-chemical data.

6.2 Sampling and methods

Underway surface water and shallow cast samples (0 – 150 m) were collected along a defined grid (25 – 32 °N and 18 –24 °W) west of the Canary Islands in the Eastern North Atlantic (Fig. 6.1).

Figure 6.1 Study area for the 'Iron from Above', Ironages Cruise October 2002

(a) Geographical setting

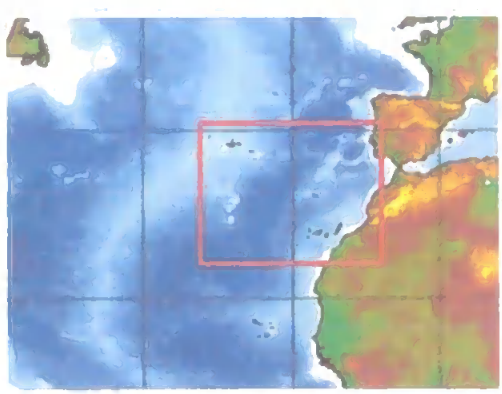

Reproduced from the GEBCO Digital Atlas published by the British Oceanographic Data Centre on behalf of IOC and IHO, 2003'.

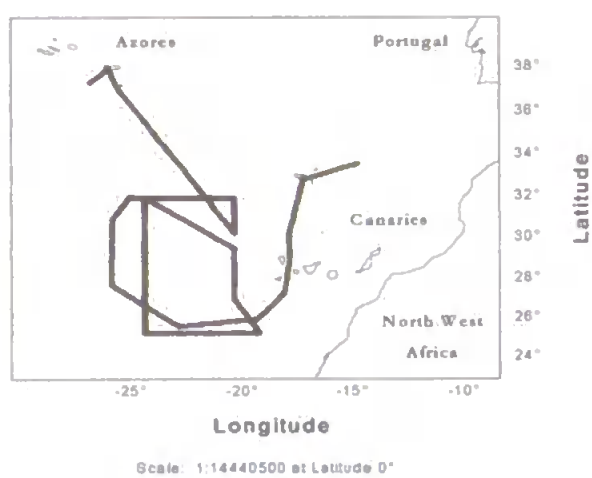

All casts took place between 08:30 and 09:30 am (local time) except for casts 13 and 15, which took place at 13:30 and 15:00, respectively. Underway sampling took place between stations and hence Fe(II) was determined during overnight transects. Samples for dFe and Fe(II) (<0.2 μm) were processed and analysed using the same methods as in the Ironages Research Cruise II (Chapter 5).

(b) Hydrocast station summary

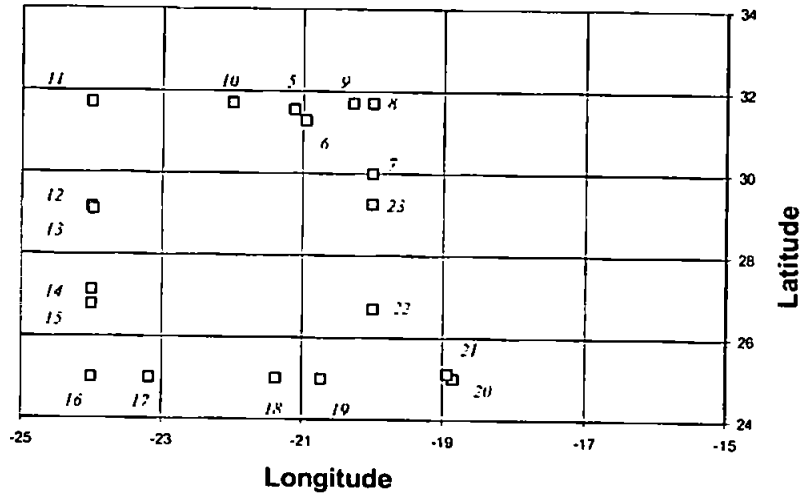

(Numbers in italic blue font denote positions of hydrocast station)

In addition, cast samples were ultra-filtered with in-line, 0.02 μm pore size filters (PTFE membrane, 25 mm diameter, Anotop™, Whatman) to examine a lower molecular weight soluble size fraction dFe(<0.02 μm). Prior to use, these filters were cleaned in-line according to the method of Wu *et al.* [272,273] by washing each filter with 30 mL of 0.1 % HCl followed by 60 mL of UHP water and 60 mL of sample.

Small colloidal iron was determined by calculating the difference between the two filtered fractions (i.e. small colloidal Fe = dFe(0.2 μm) - dFe(0.02 μm)). The sum of the precision on the two analyses was generally between 5 and 20 %, hence the data was used only for qualitative interpretation. The methods used for dust dissolution experiments are described separately in Section 6.7.

The atmospherically processed dust used for all dissolution experiments was a ~2 g homogenised bulk sample collected on the 11th April 2000 in Erdemli, Turkey, using a 1 m^2 nylon mesh screen mounted on the top of a 21 m sampling tower. The dust was reported to have originated from the Saharan Desert [274] and was characterised in terms of particle morphology, size distribution and major minerals. [275] The bulk dust sample was stored frozen (-20 °C) and was weighed into

polypropylene vials for Fe dissolution ship-board experiments using a four figure balance at the land-based laboratory.

Figure 6.2 World Aerosol optical depths for summer 2002 (0.47 microns, monthly means)

Data from http://modis-atmos.gsfc.nasa.gov/IMAGES

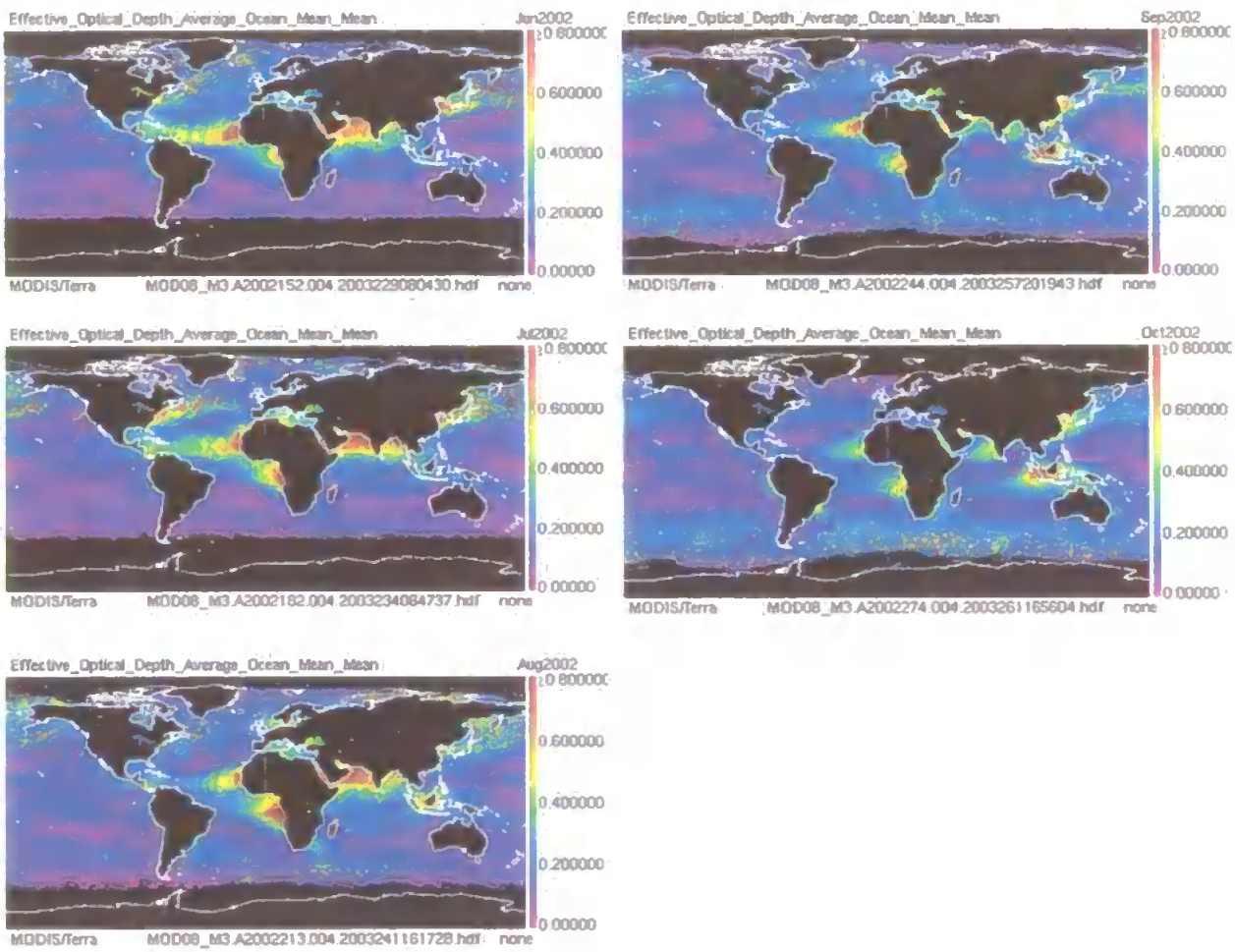

Atmospheric dust deposition events were monitored using meteorological forecasts and satellite imagery of dust storms (using AVHRR, TRMM and SeaWiFS). The aerosol flux to the Canary Basin at the time of the study (October 2002) was low compared with that observed in the summer months (June – September) of 2002. This is illustrated by the satellite data shown in Figure 6.2

where the monthly mean optical depths for the Atlantic Ocean during the summer/autumn period in 2002 are presented. No major aerosol and/or rain events occurred during the study. All supporting data was provided by workers from the Royal Netherlands Institute for Sea Research (RNIOZ) and included underway and CTD physical oceanographic parameters, dissolved aluminium, nutrients (phosphate, nitrate, nitrite and silicate), flow cytometry (FCM), pulse amplitude modulated fluorometry (PAM) and nutrient uptake.

6.3 Distribution of dissolved iron species in intermediate and deep waters

A deep-water cast was conducted at station 10 (31.7 °N, 22.0 °W) at the northern part of the sampling grid. An intrusion of high salinity Mediterranean Outflow Water (MOW, salinity = 35.6, temperature 7-10 °C) was observed at intermediate depth (600-1500m, Fig. 6.3) associated with nitrate, phosphate and silicate maxima. DFe concentrations varied from 0.3 – 0.4 nM in surface waters (0-150 m) to 0.5 – 0.6 nM in deep-waters, with no maximum associated with the MOW water mass (Fig. 6.4).

Figure 6.3 Salinity versus potential temperature for a deep-water cast at Station 10 in the Canary Basin

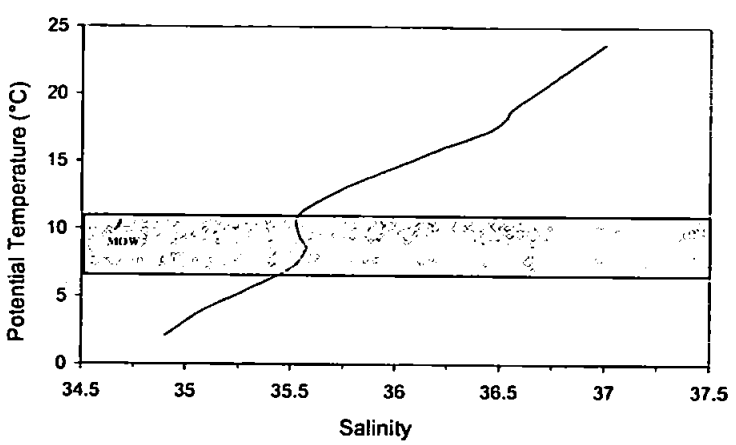

The intermediate and deep water dFe concentrations showed oceanographic consistency and compared well with those reported for a stations located at 47 °N, 20 °W (Martin et al., 0.5 – 0.6 nM, 1000 – 3000 m [237]) and 34.8 °N, 57.8 °W (Wu and Boyle, 0.6-0.8 nM, 1000 – 3000m [234]). The ratio between dFe and nitrate concentrations for the depths sampled (0 – 4000 m) was 0.011 nM dFe / μM NO_3 (R^2 = 0.80) and was similar to the ratio reported by Martin et al. for the Gulf of Alaska (0.014 nM dFe / μM NO_3 [10]). Therefore the profile demonstrates a strong link between both uptake and regeneration (nutrient type biogeochemistry) and scavenging (see dAl data, Section 6.4).

Figure 6.4 Dissolved iron (dFe) and nutrient profiles for Station 10 (31.7 °N, 22.0 °W).

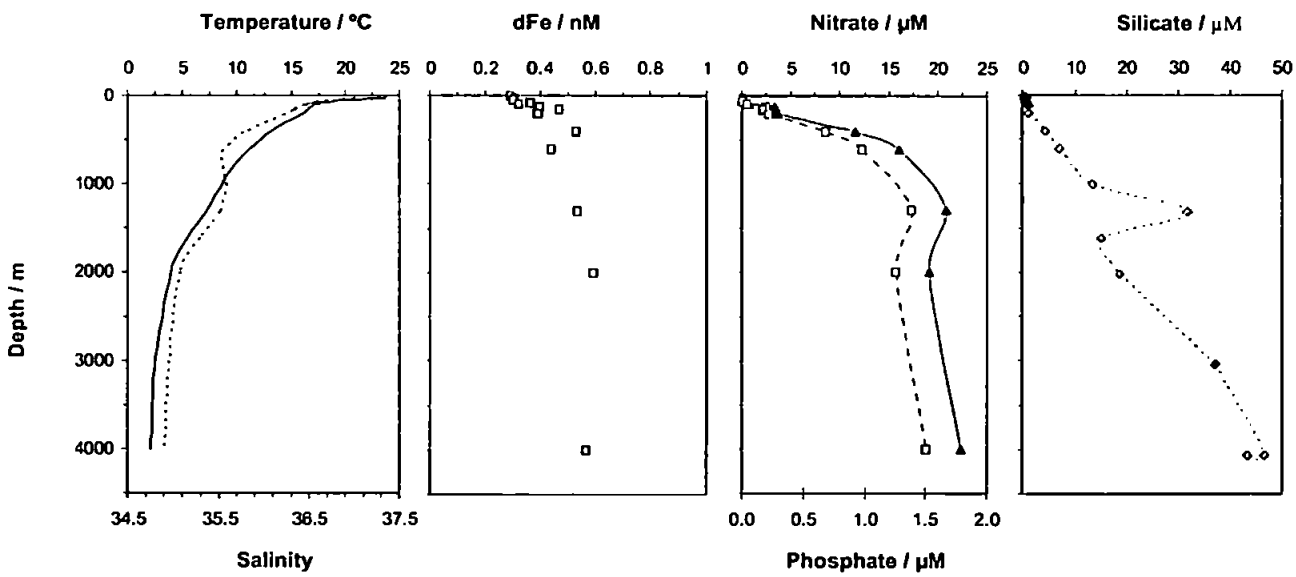

Fe(II) concentrations were lowest in the euphotic zone, between 5 pM (detection limit for these analyses) and 21 pM, and between 10 and 40 pM at depth. The mean %Fe(II) value for all samples in station 10 was 4.1% (σ ±2.5 %). These values were lower than those found in the deep waters of

the Bay of Biscay during the 'Iron From Below' cruise (10 – 35, 20 - 75 pM and 5.6% (σ ±2.5 %) respectively).

Determination of soluble (dFe <0.02 μm) and small colloidal (dFe 0.02-0.2 μm) size fractions showed that depletion of dFe at the surface coincided with low soluble iron (<0.02 μm) concentrations which increased by a factor of ca. 2 with depth (0.14 nM at the surface to 0.32 nM at 1300 m) (Fig. 6.5). Soluble Fe concentrations were similar to those reported by Wu *et al.*,[272] who observed dFe (<0.02μm) concentrations of 0.05 – 0.15 nM in surface waters and 0.2 – 0.4 nM below 1000 m for two stations in the North Atlantic (22.8°N, 36.8°W and 34.8 °N, 57.8°W) and one in the North Pacific Ocean (22.8 °N, 158.8 °W).

The increase in soluble iron concentrations with depth observed at station 10 may reflect the preference of phytoplankton and bacteria for the soluble Fe fraction, as the most significant change with depth was observed at the base of the euphotic zone (100 – 200 m). However, Wu *et al.* [272] also determined soluble (<0.02 μm) iron binding ligand concentrations for the stations mentioned above and found a dramatic increase in soluble ligand concentration from surface waters (~0.1 nM) to a maximum at ~1000 m (0.8 – 1.4 nM). Although no iron binding ligand data was available for station 10, an additional explanation for the increase in soluble iron concentration with depth is that soluble ligand concentrations (and hence also soluble dFe) are depleted at the surface, due to processes such as photodegradation, and enhanced at depth due to regeneration below the euphotic zone.

Small colloidal iron concentrations (0.02 – 0.2 μm) did not vary significantly between 0 – 1300 m depth (mean ± σ = 0.18 ±0.06 nM) and constituted a major portion of dFe (ca. 25 – 60%) in these waters. The small colloidal Fe fraction was similar to those reported for the water column of Northeast Pacific and North Atlantic oceans (e.g. 13 – 50%, 200-600 m [41]) and 30 – 70 %, 200-6000 m [272]).

Figure 6.5 Dissolved iron (dFe) redox and size speciation for Station 10 (31.7 °N, 22.0 °W).

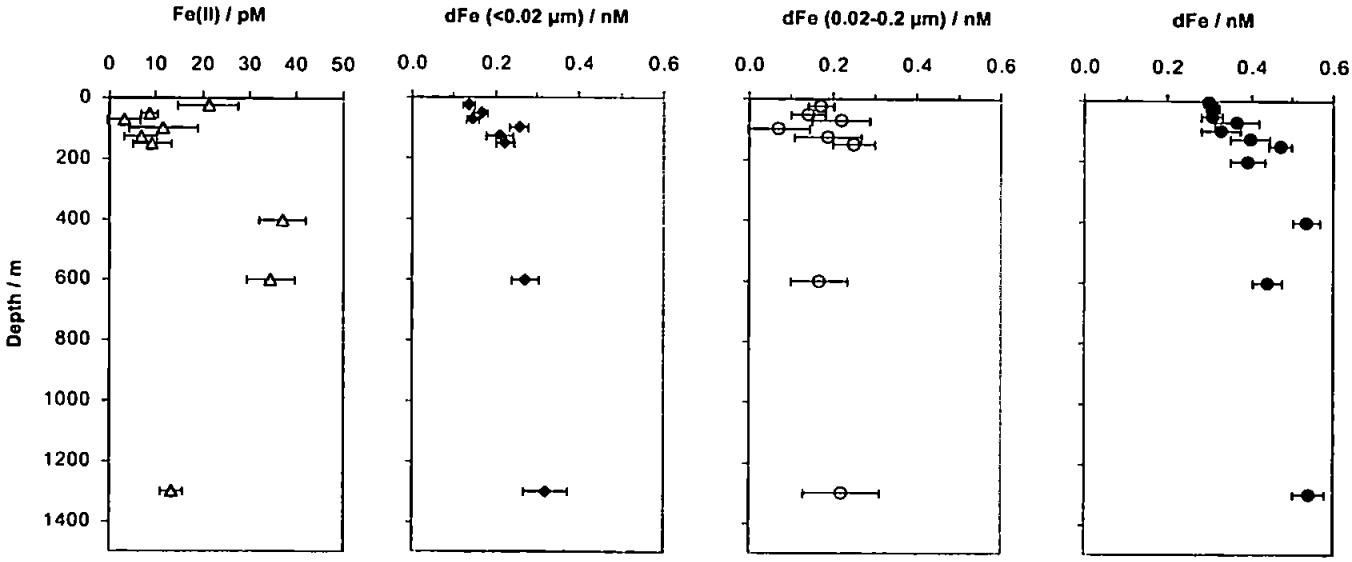

6.4 Distribution of dissolved iron and dissolved aluminium in intermediate and deep waters

A comparison of dFe and dissolved aluminium (dAl) concentrations (dAl data from Kramer *et al.* [276]) for station 10 are presented in Figure 6.6 and a reasonable linear correlation was observed (R^2 = 0.74, Fig. 6.7). It has been hypothesised that the chemistry of both elements below the euphotic zone is very similar and that this correlation is due to the similar residence times of these metals in the intermediate and deep waters of this region (i.e 100 - 200 y for dAl [277] and 70 – 200 y for dFe [124,230]). Assuming aluminium is not taken up by cells, the profile demonstrates the close link between the scavenging of Fe and Al and the transport of biogenic matter controlled by nutrient cycling. However, if uptake was occurring then there was no clear selective uptake of dFe over dAl. The former hypothesis seems more viable particularly as low levels of primary productivity were observed at this oligotrophic station.

Figure 6.6 Vertical profile of dissolved iron (dFe) and aluminium (dAl) concentrations at station 10

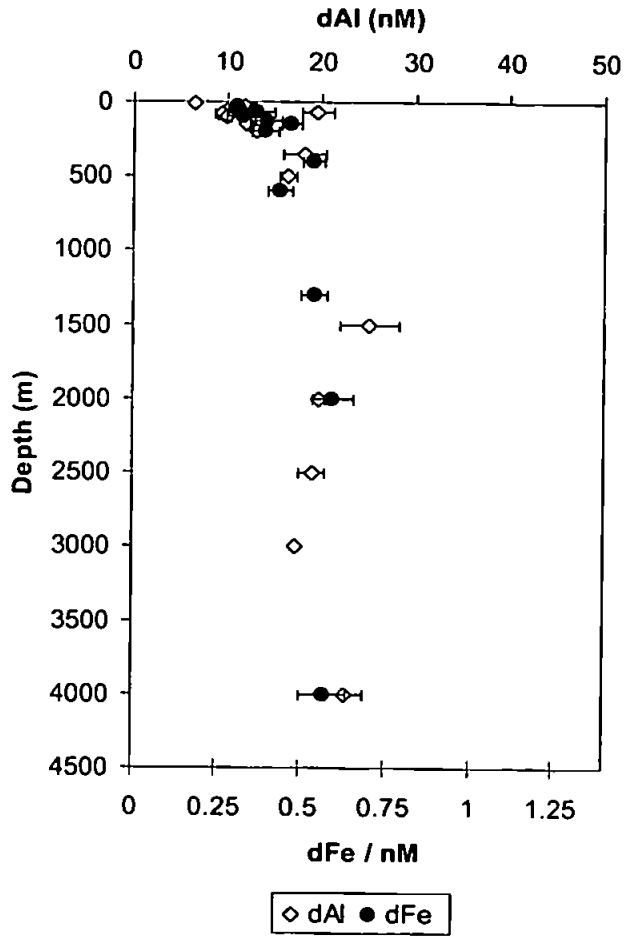

Figure 6.7 Correlation between dFe and dAl for station 10

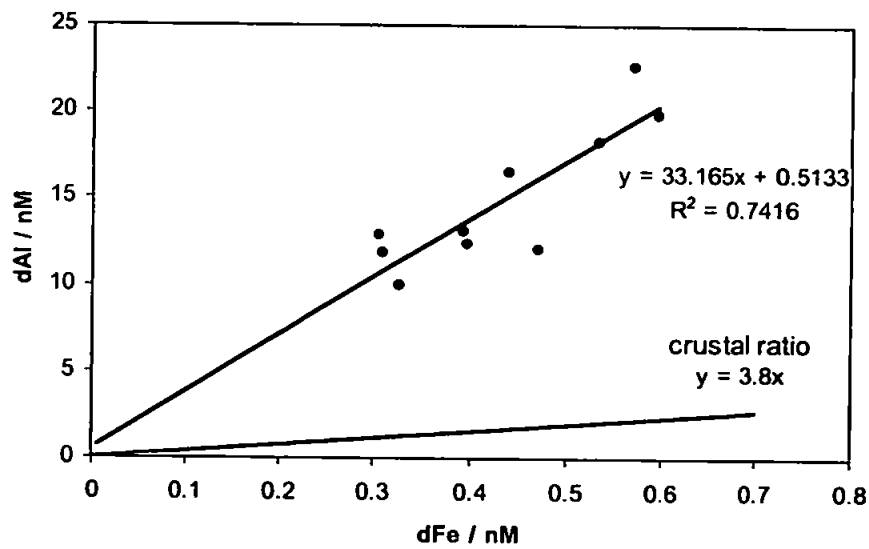

If it is assumed that Fe and Al fluxes in this area are predominantly atmospheric and the deep water residence times of Al and Fe are approximately the same, then the data also show that the solubility of Al in intermediate and deep waters is ca. 10-fold higher than that of iron (when the solubility ratio is defined as the Al/Fe ratio divided by the estimated Al/Fe crustal ratio of 3.8 [278]). It is unknown whether this is constant ratio throughout the Atlantic and indeed, other ocean basins.

6.5 Distribution of dissolved iron species in the euphotic zone

6.5.1 Hydrography

The upper water column in this area was well stratified with high temperatures (18 - 26 °C) and high salinities (36 – 37.5) in the euphotic zone, typical of the North Atlantic Central Water (NACW, as defined by Sverdrup (1942) [279]). The highest salinities (>37) in the upper mixed layer where found in the western part of the grid.

Figure 6.8 Salinity versus potential temperature for the euphotic zone (20 - 150 m) in the study area

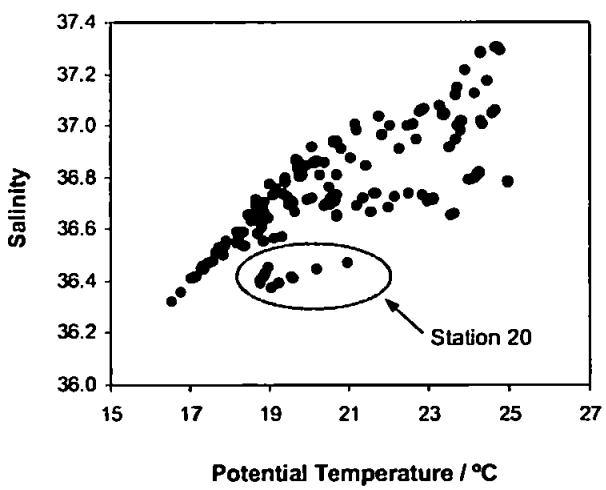

Mixed layer depths varied between 30 and 60 m, with the shallowest (<50 m) observed in the northern (stations 8, 10 and 11) and south eastern part (station 20) of the sampling grid. A

relationship between temperature and salinity was observed when all the data were compared (Figure 6.8). Anomalous low salinity data were observed at Station 20 (~ 4 °W) near the North West African coast (i.e. the data circled in Fig. 6.8) and these were attributed to upwelling conditions.

6.5.2 Variation in the size speciation of dissolved iron

DFe concentrations in the euphotic zone ranged between 0.1 and 1.0 nM (see Fig. 6.9) with a mean concentration of 0.42 nM (n = 71). Soluble iron and small colloidal iron concentrations varied between 0.05 and 0.7 nM. Small colloidal iron was a major portion of dFe in the euphotic zone of this region (mean ± standard deviation = 38.9 ± 20%). The variation of soluble and small colloidal iron data showed a skewed distribution towards lower concentrations (0 – 0.3 nM) with mean values of 0.281 and 0.170 nM respectively (n = 60).

Figure 6.9 Histograms showing the frequency distribution of size fractionated dissolved iron (dFe) species in the euphotic zone of the Canary Basin (18 –24 °W and 25 – 32 °N, October 2002).

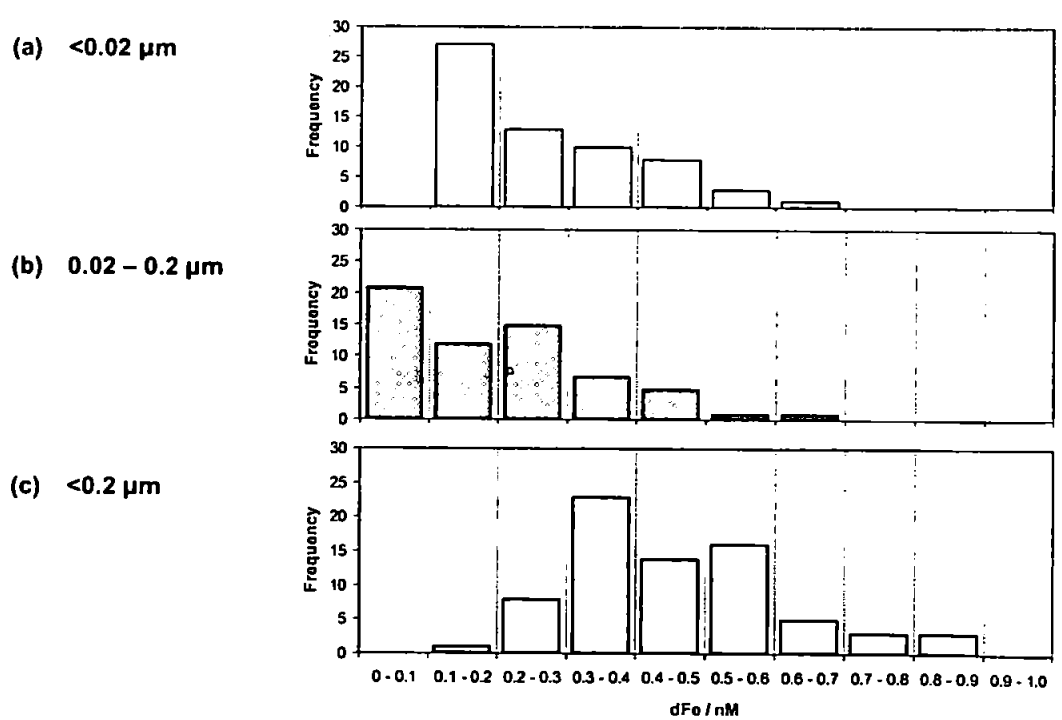

Nishioka *et al.* [41] reported much lower concentrations of small colloidal Fe (200 kDa – 0.2 μm) in the mixed layer of Northeast Pacific waters (0.01 - 0.06 nM). However Wu *et al.* observed higher and more variable concentrations (0.1 – 0.8 nM) in the euphotic zone for two stations in the North Atlantic (22.8 °N 36.8 °W, September 1999, 34.8 °N 57.8 °W, July 1998) and a station in the North Pacific near Hawaii (22.8 °N 158.8 °W). Hence the small colloidal Fe fraction appears to vary considerably in the euphotic zone of other regions as well as the study area of the 'Iron from Above' cruise. This is likely to be related to the aerosol fluxes to surface waters but may also reflect the variation in iron bound to colloidal organic matter. Further work is required to determine the significance of these variables and their effects on the small colloidal iron pool.

6.5.3 Effect of photosynthetic organisms on iron redox speciation in the euphotic zone

The surface waters in the study area were stratified to a depth of ~50 m (except at station 20) and chlorophyll and cell population maxima occurred at the top of the nutricline. At the chlorophyll maxima of ca. 50% of the stations in the study area, Fe(II) concentrations were < 5 pM (limit of detection), presumably due to the rapid uptake or oxidation of dissolved Fe(II) species, whereas detectable concentrations were often present in the mixed layer (0-50 m) and/or at the base of the euphotic zone (150 m).

An inverse relationship between Fe(II) and chlorophyll *a* concentrations was found in the euphotic zone at stations 13, 18, 20 and 23 (10 – 150 m, Fig. 6.10). This relationship showed that the interaction between photosynthetic cells and Fe(II) may have caused a depletion of ambient Fe(II) concentrations in these stratified waters. Linear correlations with chlorophyll *a* were determined for all dFe species (data not shown) but R^2 values were generally below 0.2. Hence the trends seen in the vertical profiles were probably dependant on other conditions such as the populations and classes of phytoplankton and bacteria, hydrography and variable iron fluxes.

Figure 6.10 Redox and size speciation of iron in the euphotic zone in relation to phytoplankton cell numbers and chlorophyll a concentrations

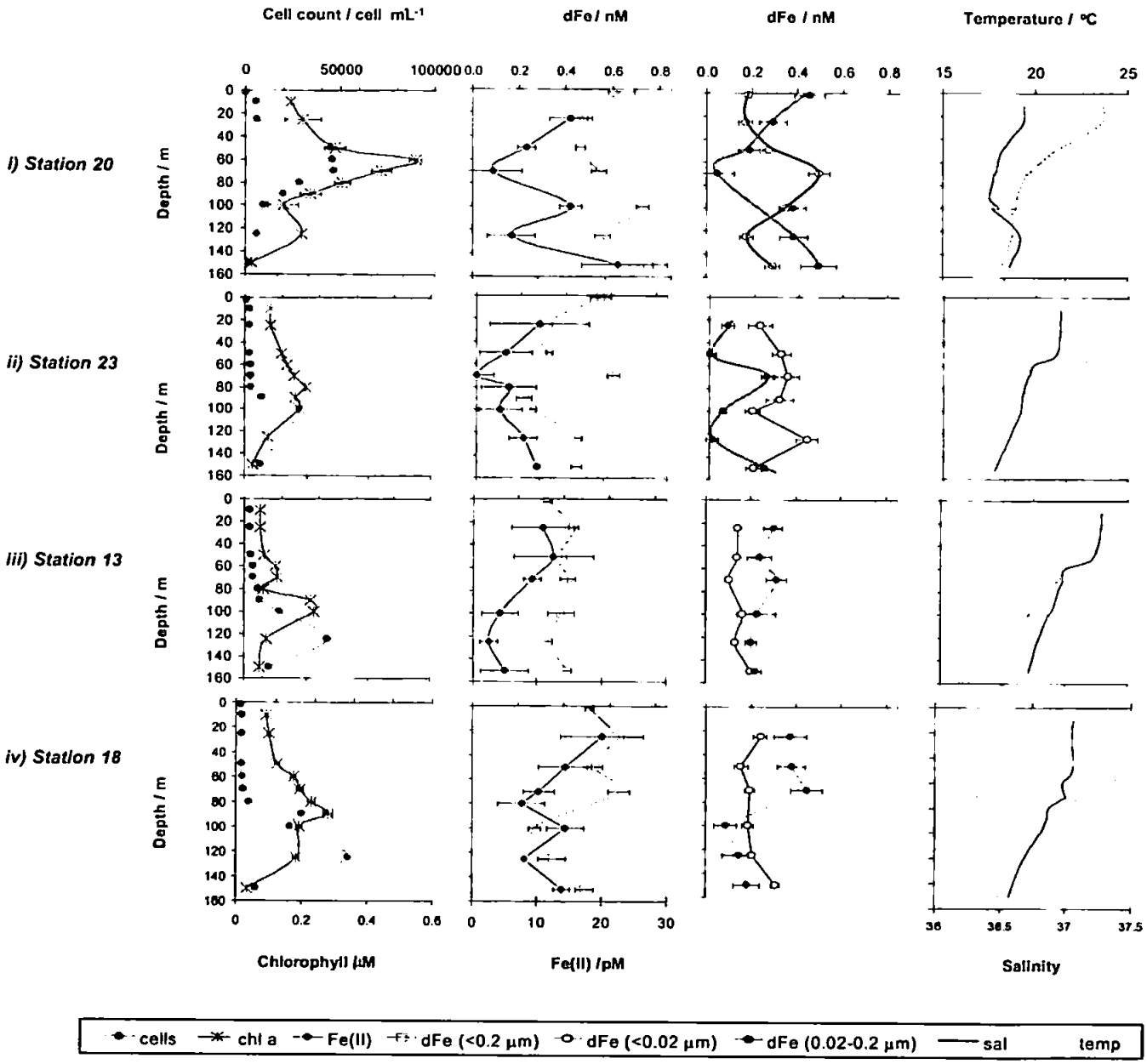

6.6 Distribution of dissolved iron species in near surface waters

6.6.1 Hydrography

The underway temperature and salinity data for the surface waters (5 m depth) of the study area are shown in Figure 6.11.

Figure 6.11 Underway surface temperature and salinity data for the 'Iron From Above' cruise

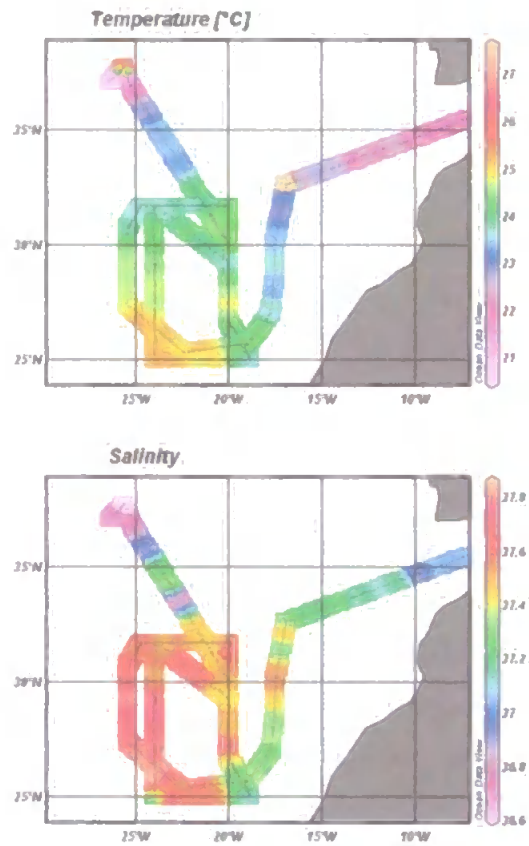

Seawater temperature varied from 21 °C, north of 30 °N to 25 °C in the south west of the study area. Similar to the cast data, the highest salinity water (<37.6) was located between 23 – 26 °W, whereas the lowest salinity water (~36.6) was found near the Azores in the north of the study area. Indication of upwelling affecting the surface waters was observed in the south east corner of the

study area, near the coast of North West Africa, where a sharp decrease in surface salinity and temperature and a decrease in the mixed layer depth were observed.

6.6.2 Redox speciation and distribution of dissolved iron in surface waters

dFe and Fe(II) data for the surface water of the sample grid are shown in Figure 6.13. Generally, Fe(II) concentrations in near surface waters did not vary enough to observe spatial and temporal changes over the sampling grid (i.e. between 5 pM (LOD) and 20 pM). However, elevated concentrations of 30 – 60 pM were observed on several occasions such as at 20.7 °W on the northern transect, following a rain shower, and during a diurnal study in the southern transect between 11.00 and 14:00 h (local time, 20.5 – 21.0 °W).

Figure 6.12 Dissolved iron (dFe, black squares) and Fe(II) (grey triangles) concentrations in the surface mixed layer of the study area

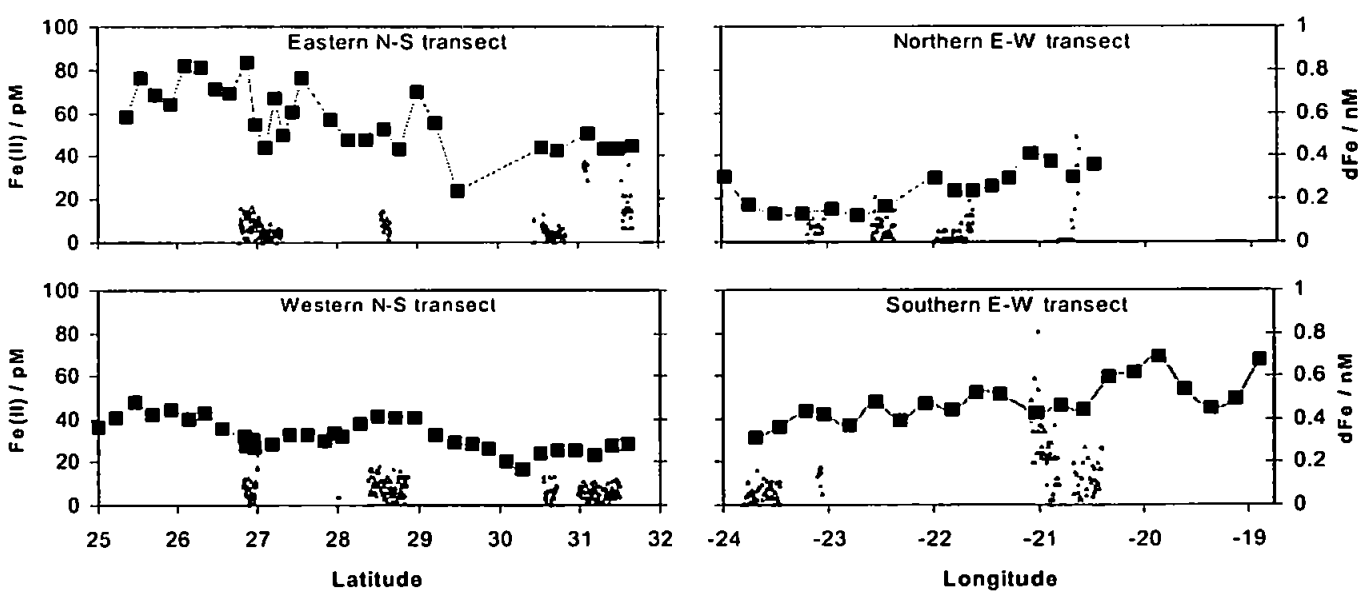

Surface dFe concentrations varied between 0.15 and 0.95 nM over the sampling grid and the range of data compared well with those reported by Sarthou *et al.* (2003) for the same area in October 2000 (0.2 – 1.2 nM [244]). Lower and less variable concentrations were observed in the northern and western transects indicating the influence of the proximity of the North West African continental

margin. The highest concentrations (0.5 – 0.9 nM) were found in the south western corner of the grid near to the coastal upwelling area.

6.6.3 Distribution of dissolved iron in surface waters versus distance from the Western Saharan coast.

An inverse logarithmic relationship between dFe concentrations in surface waters (3-6 m) of the sampling grid and the distance from the North West African coast was observed ($R^2 = 0.66$, Figure 6.13). A similar relationship was also found for concentrations integrated between 0 – 150 m depth (trapezium intergration) (see Figure 6.14) and distance from the coast, although the negative gradient for these data was approximately half of that found for the surface waters (-0.31 as opposed to -0.16 for surface waters).

Figure 6.13 Relationship between dFe concentrations in surface waters (3 - 6 m depth) versus the distance from the North West African coast.

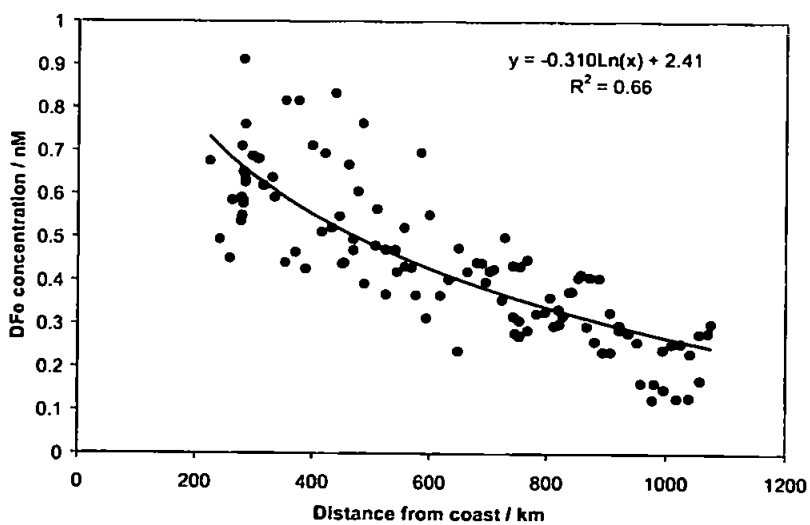

The difference in gradient is hypothesised to be due to the different biogeochemistry and residence times of dFe in surface waters compared with the whole euphotic zone. In the more productive coastal areas, where chlorophyll concentrations and cell numbers were highest, it is likely that a greater proportion of the iron pool, between 50 and 150 m depth, was incorporated into cells.

Higher concentrations of dFe in the euphotic zone compared to the near-surface waters in the north eastern part of the study area may result from a lower Fe residence time in the mixed layer compared to the whole euphotic zone.

Figure 6.14 Relationship between dFe concentrations in the euphotic zone (0 – 150 m depth) versus the distance from the Western Saharan coast.

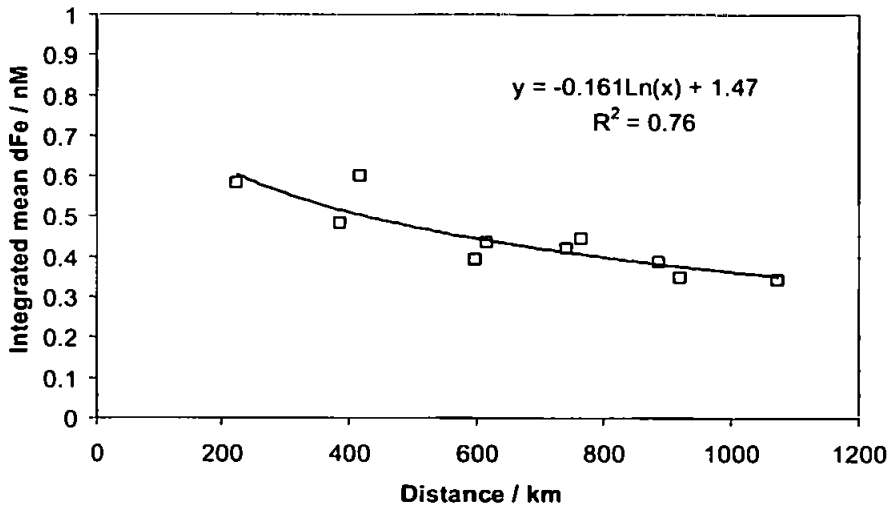

6.6.4 Distribution of dissolved iron and dissolved aluminium in surface waters.

A significant correlation between atmospheric flux and dFe was found in October 2000 during a transect south of our study area (30 °N and 20 °S, Sarthou *et al.* 2003 [244]). However, a direct comparison of dFe concentrations with aerosol flux was not possible during the 'Iron from Above' cruise as no atmospheric deposition flux measurements were made. It has been hypothesised by several workers [281-284] that the primary source of dAl to the Atlantic ocean is the dissolution of aeolian dust of continental origin. Therefore, dAl is often used as a tracer for atmospheric dust deposition in the North Atlantic Ocean. DFe and aluminium ratios have been reported for the

surface waters of the equatorial Atlantic by Vink and Measures (2001). [233] These authors found significant covariance between dAl and dFe but more variation was observed for dAl concentrations (10 – 60 nM) compared to dFe concentrations (0.4 – 1.4 nM). They hypothesised that the expression of dFe from dust inputs is less than that of dAl due to the more constrained solubility range of iron in seawater and its removal by biological export.

Fig. 6.15 Contour map showing sea-surface dAl concentrations during the 'Iron from Above' cruise. All stations are labelled as stars in the figure. (Kramer *et al.* 2004 [276])

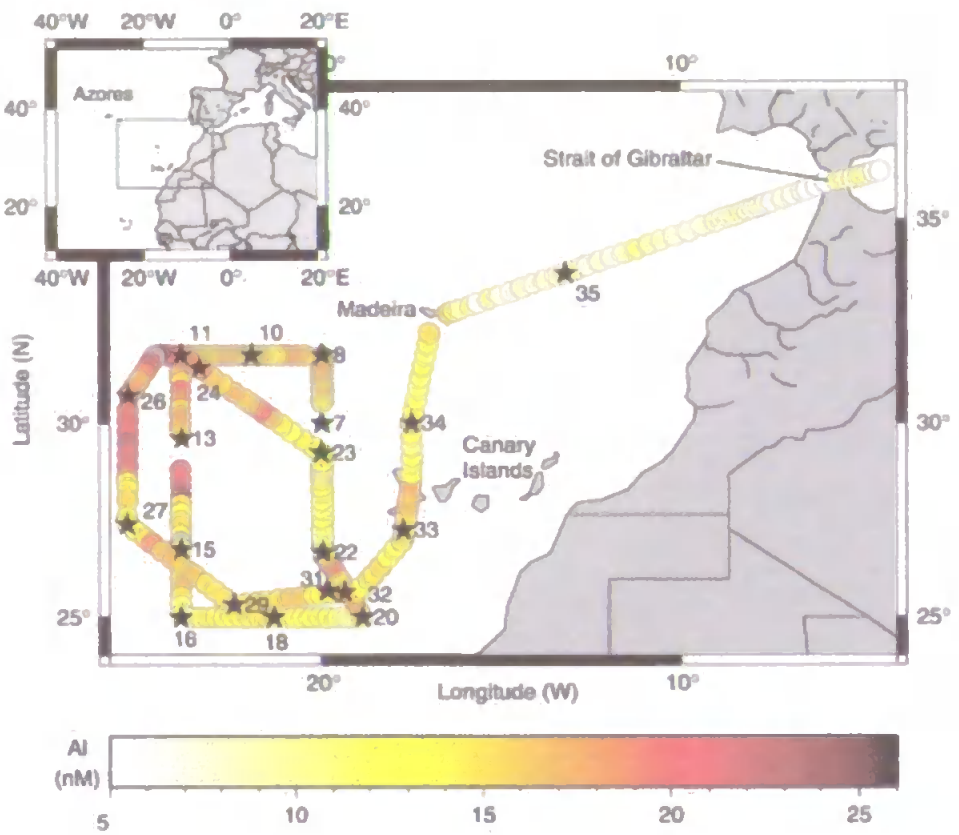

In this study, the dAl distribution in the surface waters of the Canary Basin study area was reported to have higher concentrations in the north western part of the grid (22 – 25 nM) and lower concentrations in the south east (12 – 14 nM) (see Fig. 6.15), with a positive relationship with salinity. [276] The authors attributed this gradient to the mixing of two water masses (NACW and Canary Current) rather than a direct result of atmospheric deposition.

The dAl and dFe data had opposing lateral gradients in the surface waters of the sampling grid (i.e. dAl increased from south east to the north west, while dFe decreased). This was a dissimilar trend to the intermediate and deep waters discussed in Section 6.4, where a vertical correlation was observed. The striking difference between the distribution of both dissolved elements is further evidence that their residence times are significantly different in surface waters (e.g. 3-5 yr for dAl [285] and < 1 yr for dFe [105,198,244]).

The highest aerosol fluxes for the North Atlantic Ocean (20 – 30 °N) occurred during the summer (June – August 2003) and were mostly south of the Canary Islands (see Figure 6.2) and it is assumed that any dFe and dAl enriched water, caused by atmospheric deposition, would have been entrained by the southerly flowing Canary Current within a few months (assuming a minimum velocity of ~0.5 m s^{-1}). Hence it was concluded that the dFe gradient observed was not due to a gradient of atmospheric flux and that the biogeochemistry of the NACW at the time of the study may have had little impact from the summer dust storms.

A similar trend to the data reported here was observed in the North West Pacific Ocean by Johnson *et al.* [286] for a transect from California to Hawaii (March, 2001). In this study, dAl concentrations were reported to be ca. 6 nM at the western end of the transect and decreased to <1 nM towards the east, whereas dFe decreased from ca. 1 nM at the coast to 0.2 - 0.3 nM west of 130 °W. Therefore these opposing trends may be a common feature of eastern upwelling margins when no recent large-scale atmospheric deposition events have occurred.

Near the North West African coast, upwelling is reported to occur throughout the year between 20 and 30 °N, with peak intensity in July/August, and upwelling filaments have been reported that extend as far as 500 km offshore. [267] During this study, upwelling was only clearly detected in the south western part of the sampling grid and due to the southward movement of the Canary Current, this feature alone was unlikely to be the cause of the dFe gradient observed. However, it is

hypothesised that the dFe gradient was a result of the continuous mixing of NACW with iron enriched shelf and coastal waters of the Iberian and North West African margin, transported offshore by upwelling and advection and entrained into the Canary Current.

6.7 Dust dissolution experiments

The lack of data describing the dissolution of Fe from aerosol particles into seawater has meant that estimates of dFe fluxes to the surface ocean are used for global iron cycling models. Indeed most global models extrapolate the quantity of dFe delivered to ocean regions by assuming a mean soluble percentage of Fe for aerosols based on a limited data set (see Section 1.3). However, it has become clear in recent years that the soluble Fe fraction in aerosols can vary spatially and according to the degree of atmospheric processing that aerosols are exposed to. [103,287] In addition, although our knowledge of aerosol Fe solubility is expanding, the use of solubility data is further limited by the lack of dissolution kinetic experiments conducted for natural aerosols in seawater. Without these data it is not possible to ascertain the impact of atmospheric deposition on the euphotic zone, especially when the residence time of particulate iron in surface waters is estimated to be of the order of days. [105,198,244]

The experiments reported here were designed to examine the dissolution of redox and size fractionated iron species from dust and the physico-chemical effects of the natural assemblage of micro-organisms and particles in open ocean seawater. Initially, the kinetics of dissolution of Fe species in filtered and unfiltered surface seawater were investigated over a period of 12 h (Experiment 1). Subsequently, seawater samples with varying concentrations of added dust (5 – 100 mg L^{-1}) were equilibrated for a period of 6 months (in the dark, 20 – 25 °C) to examine the effects of dust loading and marine particles/organisms on iron solubility (Experiments 2 and 3).

Recent studies of iron dissolution from dusts in seawater have been conducted using natural loadings in order to mimic the sea surface deposition of aerosols at ambient concentrations (e.g. 0.01 – 10 mg L^{-1}, Bonnet and Guieu [288]). However, the concentrations of dust used in these studies (5 –100 mg L^{-1}) were far higher than those that are found in the open ocean, as it was expected that processes such as bacterial growth and bottle wall adsorption / desorption could occur during the experiments. Hence interpretation and extrapolation of these data is limited.

6.7.1 Experiment 1 – The kinetics of Fe(II) and dFe dissolution in seawater from atmospheric dust

Experimental

A 20 L unfiltered surface seawater sample (D1) was collected from the underway trace metal clean supply pumped from the towed fish at 29.2 °N, 25.5 °W. 10 L of this sample was then filtered using a Vivaflow™ cross flow filtration (CFF) system (<30 kDa permeate, Vivaflow™, Vivascience, Hannover, Germany) and collected in an acid washed carboy. The CFF system had been washed previously with 5 L of 0.5 M HCl followed by 40 L of UHP water and seawater. Both the ultra-filtered and original unfiltered samples were then stored in the dark and allowed to equilibrate for 24 h.

Following this, 2L of each sample was transferred into an acid washed polyethylene bag and 40 mg of dust was added to each. The motion of the ship agitated the samples sufficiently during the experiment to ensure complete mixing. Both Fe(II) and dFe sub-samples were filtered in-line using a syringe filter (0.2 μm, PTFE membrane, Acrodisc™, Gelman) coupled to the FI-CL manifold. Over a period of 12 h, Fe(II) was determined in near real time (~ 30 s delay before preconcentration on 8-HQ column) while 10 mL aliquots were simultaneously filtered and

collected for dFe. The dFe samples were then acidified (pH 2, high purity HCl) and stored for 3 months before being analysed on land using FI-CL after sulphite reduction.

Results and discussion

Following the addition of the dust, Fe(II) concentrations increased from <15 pM, reaching a plateau of approximately 30 pM after 6 – 8 h (see Figure 6.16). There was no statistical difference ($P < 0.05$) between the concentrations of Fe(II) in ultra-filtered and unfiltered seawater (see Figure 6.17), suggesting that cells and particles in the surface seawater did not play an active role in the dissolution of these species. The increased Fe(II) concentrations found after dust addition were thought to represent a steady state between dissolution and oxidation rather than Fe(II) stabilised after dissolution from the dust.

Figure 6.16 Dissolution of dFe and Fe(II) from Turkish atmospheric dust into ultra-filtered (<30 kDa) and unfiltered surface seawater*.

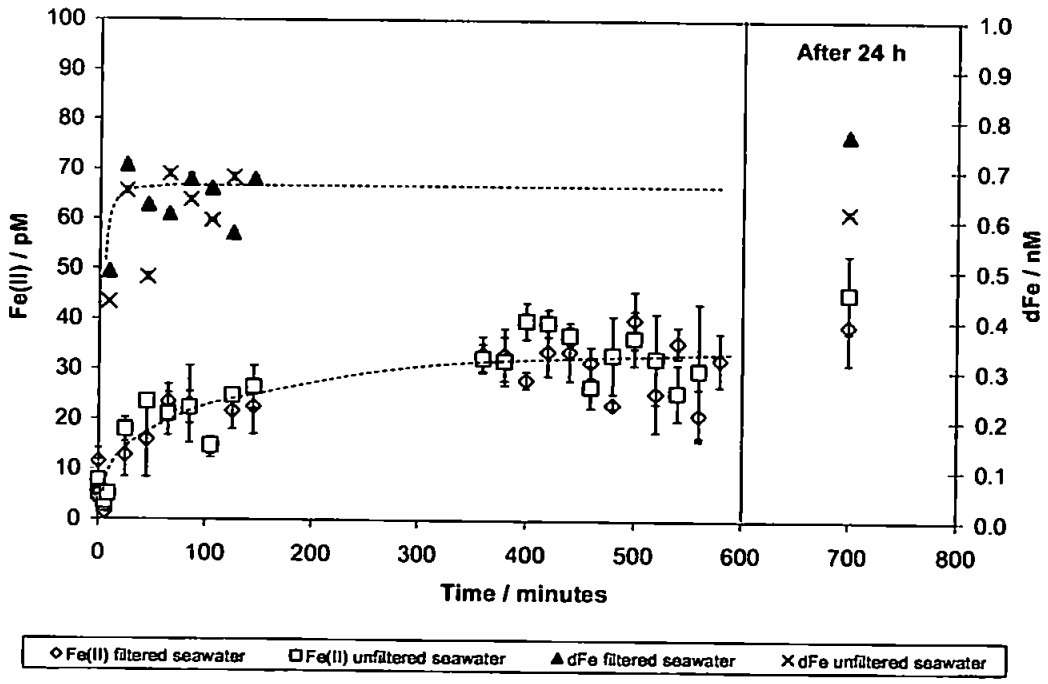

*Curves were fitted by eye to define the trends

During the experiment, dFe increased from ca. 0.45 to 0.7 nM and reached a pseudo steady state concentration in less than one hour (Figure 6.16). Using a value of 3.2 % abundance of Fe in the dust (Orif 2005), [289] the solubility of Fe in the Turkish dust was 0.002 %. This percentage is more than an order lower than reported Fe solubilities for crustal aerosols, found from laboratory experiments (0.013 –0.4 %, see Table 1.2). Such variation in solubility was not unexpected due to the use of different experimental conditions by other workers, the loss of dFe to the walls of the reaction containers, variations in the structure and content of the crustal dust, and variation in the seawater matrix (i.e. solubility limited dissolution in seawater).

Figure 6.17 Correlation between Fe(II) determined in ultra-filtered (<30 kDa) and unfiltered surface seawater.

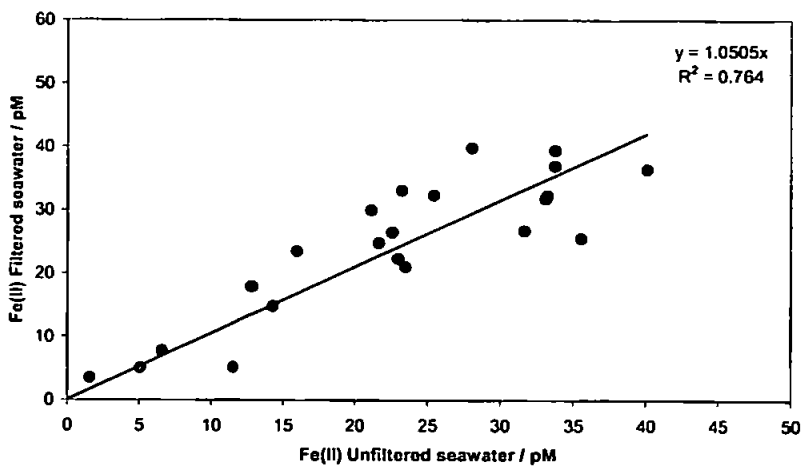

6.7.2 Experiment 2 – Dissolved iron concentrations seawater equilibrated with dust

Experimental

A second bulk surface seawater sample (D2) was taken at 21.8 °N, 25.4 °W using the same sampling and protocol as mentioned above. Unfiltered sub-samples (5 x 2L) were transferred into

acid washed LDPE bottles and a range of different quantities of dust (0 – 200 mg) were added to them. The samples were stored in the dark at 20 – 25 °C for ~ 6 months. Following this time they were filtered through either 0.2 μm (PTFE membrane, Acrodisc™, Gelman) or 0.02 μm (Anotop™, Whatman) pore size filters and analysed for dFe, after 2 weeks acidification (1 mL HCl / L sample).

Results and discussion

The results (Figure 6.18) showed that the highest dFe(<0.02 μm) and dFe(<0.2 μm) concentrations were 0.89 and 1.82 nM respectively, caused by varying the dust concentrations from 5 to 100 mg per litre. Seawater dFe concentrations increased linearly with particle concentration (R^2 = 0.9934 and 0.9929, for dFe(<0.2 μm) and dFe(<0.02 μm), respectively). The range of % soluble iron from the Turkish dust was between 0.002 - 0.006 %. This is within the range reported by Bonnet and Guieu [288] for the dissolution of a Saharan soil in seawater (0.001 – 1.6 %). These authors also observed a good linear correlation for dFe versus particle concentrations (0.01 –10 mg L^{-1}).

Figure 6.18 Variation in the solubility of iron (<0.2 μm) in unfiltered seawater with dust concentration

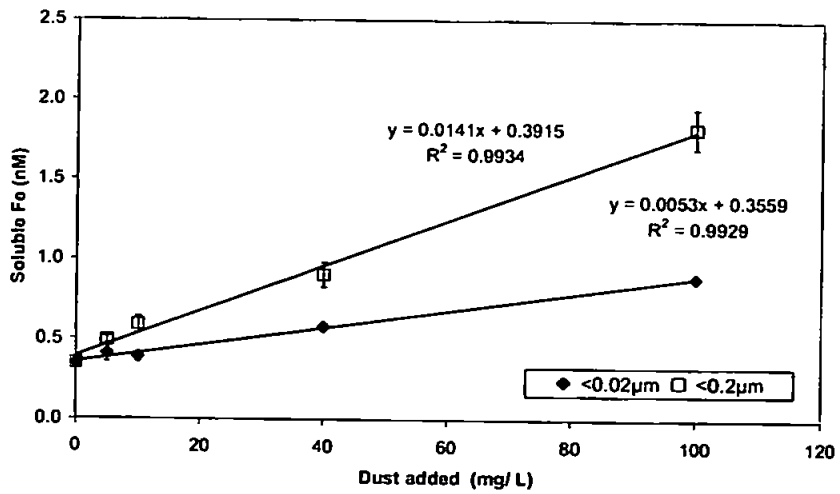

The % soluble iron was calculated for each sample and the data plotted versus the amount of dust added (Figure 6.19) and a negative relationship between particle loading and % soluble iron was observed. Similar negative logarithmic relationships showing higher dissolution for lower dust concentrations have been reported for dissolution experiments by previous workers (Guieu *et al.*(2001), [98] Bonnet and Guieu (2004) [288]).

Figure 6.19 Variation in the % soluble iron (<0.2 μm) in unfiltered seawater with dust concentration

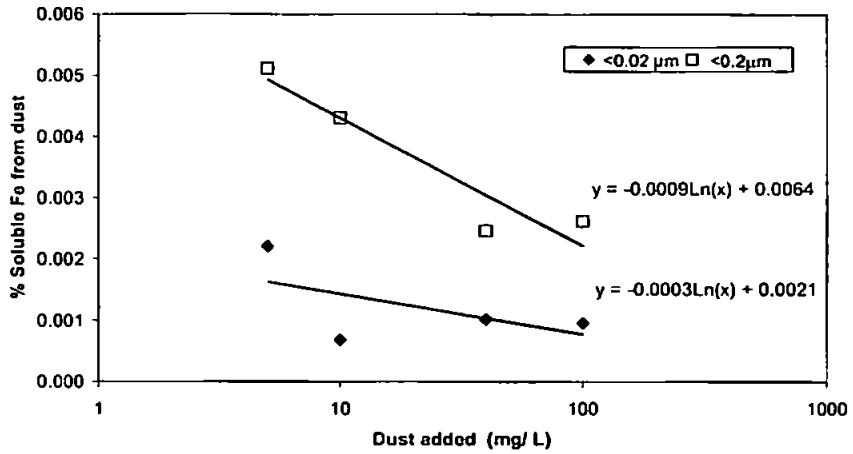

6.7.3 Experiment 3 – Dissolved iron concentrations in unfiltered and ultra-filtered seawater equilibrated with dust

Experimental

2 L subsamples of unfiltered and ultra-filtered (<30 kDa) seawater from both bulk samples (D1 and D2) were equilibrated with 40 mg of dust in the dark for ~ 6 months in the dark (20 – 25 °C). These

were then filtered through 0.2 μm (PTFE membrane, Acrodisc™, Gelman) pore size filters and dFe was determined after 2 weeks acidification (1 mL HCl / L sample).

Results and discussion

Figure 6.20 dFe concentrations in ultra-filtered and unfitered surface seawaters (D1 and D2) equilibrated with Turkish dust (dust concentration = 40 mg L^{-1}, equilibration time = 6 months, error bars = 1 standard deviation of 4 replicate analyses).

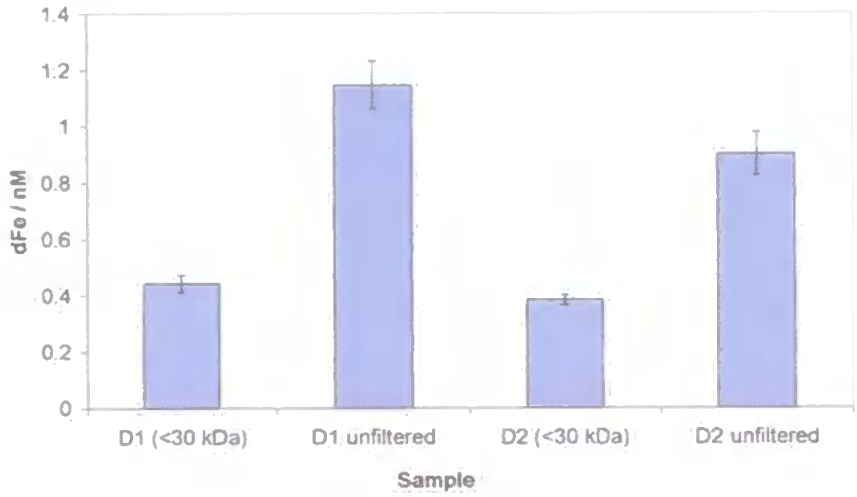

DFe concentrations in unfiltered samples D1 and D2 were 1.15 and 0.90 respectively whereas dFe concentrations in ultra-filtered seawater equilibrated with the same mass of dust were ~60 % lower (0.44 and 0.38 nM respectively) (Fig. 6.21). This showed that under the conditions of this experiment, the iron solubilities observed during these experiments were dependent on biotic and/or abiotic particle interaction. The samples were not handled under sterile conditions hence it is not possible to state that they are representative of natural seawater/aerosol equilibria. Nevertheless, the experimental data demonstrate that marine particle concentrations are another key variable that affect Fe solubility and dFe residence times in open ocean surface waters.

The maximum dFe concentrations found in this experiment and those of others are often greater than those reported for previous solubility experiments using the addition of iron salts to saturated seawater (e.g. refs [42-47]). If it is assumed that only physicochemical control existed for the

unfiltered samples, then the data imply that iron solubility in seawater can be controlled by equilibration between seawater and aerosol particle surfaces. This has major implications for basin-scale iron biogeochemical models.

6.8 Conclusions

1. dFe concentrations in the northern part of the 'Iron from Above' study area (cast station 10, 31.7 °N, 22.0 °W) varied from 0.3 – 0.4 nM in surface waters (0-150 m) to 0.5 – 0.6 nM. Intermediate and deep water concentrations compared well with historical data for nearby stations. [234,237] Fe(II) concentrations also increased with depth from 5 pM (detection limit for these analyses) - 21 pM in the euphotic zone to 10 - 40 pM at depth.

2. It is hypothesised that the dFe vertical distribution at station 10 was controlled by uptake in the upper water column (0 – 500 m) followed by regeneration and scavenging in intermediate and deep waters (500 – 5000 m). Correlations found for dFe with nitrate (R^2 = 0.80) and dAl (R^2 = 0.74) support this mechanism and demonstrate the dual role of iron as a nutrient and a scavenged element in these waters.

3. Surface depletion of dFe was mainly due to changes in soluble iron (<0.02 μm) concentrations, which varied from 0.14 nM at the surface to 0.32 nM at 1300 m. According to the soluble iron binding ligand data of Wu *et al.*, [272] an alternative to biota controlling soluble dFe concentrations in surface waters could be that soluble iron binding ligand concentrations increase with depth.

4. In the euphotic zone (0-150 m) of the study area, dFe concentrations ranged from 0.1 to 1.0 nM (mean of 0.42 nM (n = 71). Small colloidal iron concentrations (0.02 – 0.2 μm) were a major fraction of dFe (ca. 25 – 60%, mean of 38.9%) and did not vary significantly with depth between 0

– 1300 m depth (mean ± σ = 0.18 ±0.06 nM) at station 10. Soluble and small colloidal iron had mean concentrations of 0.281 and 0.170 nM respectively (n = 60). Fe(II) minima were observed at the chlorophyll maxima of 4 of the stations in the sampling grid. This was hypothesised to be due to either higher uptake and/or oxidation rates at these depths.

5. dFe concentrations in surface waters (3-6 m) varied between 0.15 and 0.95 nM over the sampling grid, whereas Fe(II) concentrations were generally negligible (below the LOD to 20 pM) except following rain showers and during the mid day solar maxima (~10 – 60 pM).

6. An inverse logarithmic relationship between dFe concentrations in surface waters (3-6 m) of the sample grid and the distance from the North West African coast was observed (R^2 = 0.66). A similar relationship was found for mean integrated dFe concentrations between 0 – 150 m depth, although the gradient was ca. half that of surface water dFe versus distance from the coast. This was attributed to the different biogeochemistry and residence times of dFe in surface waters compared with that of the entire euphotic zone.

7. No covariance between dFe and dAl was observed, nor any indication of high aerosol fluxes influencing this area. Therefore, it is hypothesised that the dFe gradient was a result of the continual advection of Fe enriched shelf and coastal waters. Further examination of nutrient and physical data for the study area will allow the validity of this hypothesis to be accessed.

8. The solubility of Fe in a Turkish dust equilibrated with seawater was found to be 0.002 %. This compared well with the % soluble Fe found for Saharan soil in seawater. [288] Kinetic dust dissolution experiment showed similar increases in dFe for ultra-filtered and unfiltered seawater and reached a pseudo steady state in less than one hour, whereas Fe(II) concentrations doubled (<15 pM to ca. 30 pM) after 6 – 8 h and continued to increase over 24 h. It was found that cells and particles in the surface seawater did not play an active role in the kinetics of dissolution of Fe(II) or dFe species.

9. When unfiltered seawater was equilibrated with dust for several months, it was found that dFe concentrations increased linearly with dust particle concentration (R^2 = 0.994 and 0.857, for dFe(<0.2 μm) and dFe(<0.02 μm, respectively) and a negative logarithmic relationship between % Fe solubility (for <0.02 and <0.2 μm size fractions) and amount of dust added was observed, as reported by other workers.

10. dFe concentrations in ultra-filtered seawater equilibrated with the same amount of dust were ~60 % lower than in unfiltered seawater, showing that dFe concentrations are dependent on biotic and/or abiotic particle interaction and that iron solubility in seawater (as defined by conventional filtration cut offs i.e. using filters with a 0.2 or 0.45 μm pore) can be controlled by equilibration between seawater and aerosol particle surfaces.

CHAPTER 7.

Conclusions and suggestions for future work

7.1 Conclusions

The distribution of dFe in seawater and its availability to primary producers has a significant impact on global climate. Both variables affect the growth and community composition of marine phytoplankton and bacteria and the utilization and transport of nutrients from the euphotic zone. There is a paucity in regional dFe data which is required for oceanographic data bases in order to improve ecosystem and climate models. Furthermore, the chemical speciation of iron speciation has similar importance as iron acquisition by plankton is likely to be kinetically controlled by its speciation.

The most plausible mechanism for Fe uptake by phytoplankton is the assimilation of labile dissolved inorganic species. Due to the higher stability of solid state ferric hydroxides and Fe(III) chelates, the steady state concentrations of these species is greatly increased by the reduction of the ferric forms to the more labile and soluble ferrous analogues. In order to gain insight into the role of Fe(II) in open ocean and shelf waters, a highly sensitive FI-CL method for the *in situ* determination of dissolved iron redox species was optimised, evaluated and tested in the field.

The FI-CL method was later used to determine the dissolved iron redox speciation and distribution in two study areas in the North East Atlantic Ocean. The study illustrated the diversity in the dissolved iron distribution and biogeochemistry that occurs in the surface and intermediate waters of open ocean provinces close to continental margins. The following conclusions summarise the findings of the studies reported in this thesis.

7.1.1 Optimisation, trials and evaluation of an FI-CL method for the ship-board determination of dissolved Fe(II) in seawater.

The automated method for determining Fe(II) in seawater by FI-CL [ref] was found to be more sensitive than other methods reported in the literature (e.g. references [162, 190, 204-207]). A limit of detection of 12 pM was determined during shipboard trials (Chapter 2) and following optimisation, this was improved to 5-12 pM in later studies. Due to its high sensitivity, the system was capable of detecting changes in Fe(II) concentrations of >1-2 % of typical open ocean dFe concentrations (i.e. assuming a concentration of ~0.5 nM).

The automated system was continuously operated at sea for long durations (>4 weeks) and was found to be sufficiently robust and portable; suitable for operation in a ship's laboratory or clean container. In addition, the method was fast (3 min for one analytical cycle), produced data with good precision for replicate analyses (0.9 - 6.2 %) and calibrations were linear over the range required (typical r^2 >0.98, 0-5 nM).

7.1.2 Potential interferences from dissolved organic molecules to the FI-CL method.

Studies conducted using a pure water matrix, showed that the individual effects of sub-micromolar concentrations of 17 model organic compounds on the CL signals of the FI-CL method (both with and without preconcentration on an 8-HQ column) were negligible. However, organic compounds, such as reductants (e.g. ascorbic acid) and chelating ligands (e.g. Desferrioxamine-B and EDTA) altered the sensitivity of the method to nanomolar concentrations of Fe(II) by >15 %.

Interference to Fe(II) signals from Fe(III) (20 nM) with organic compounds (200 nM) was assessed for seawater samples (pH 8.1) and positive interference was found (~10 – 150 pM relative Fe(II) signal). However, the maximum interference for both FI-CL methods from Fe(III) in the presence of natural organic ligands in seawater was found to be <1% of the total iron concentration.

Furthermore, unlike the solutions used in the study reported in Chapter 3, dissolved organic carbon concentrations are found to be in the micromolar range in seawater and this fraction is likely to contain a broad range of molecule sizes and functionalities.

7.1.3 Distribution of dissolved iron and redox speciation in two study areas in the north east Atlantic Ocean.

Vertical dFe distributions in the North East Atlantic Ocean

Vertical dFe distributions for three stations in the north of the Bay of Biscay are described as follows: dFe concentrations were 0.1 – 0.6 nM in surface waters (0 - 500 m), 0.5 – 1.4 nM in intermediate waters (1000 – 2500 m) and 0.5 – 0.8 nM in deep waters (2500 – 4500 m). It was hypothesised that the high variability in intermediate waters was due to patches of small colloids advected from the shelf slope, whereas deep water concentrations were less variable and consistent with the data of other workers for nearby stations.

Open ocean dFe concentrations in the northern part of the 'Iron from Above' study area (cast station 10, 31.7 °N, 22.0 °W) varied from 0.3 – 0.4 nM in surface waters (0-150 m) to 0.5 – 0.6 nM in intermediate and deep waters (150 – 4000 m) and showed oceanographic consistency with physico-chemical parameters (temperature, salinity and nutrients). This station was situated >1000 km from the North West African shelf and hence dFe concentrations in intermediate waters were less variable than those observed for the Bay of Biscay and deep water concentrations compared well with historical data for nearby stations. [234,237]

Due to the correlation of dFe with dAl ($R^2 = 0.74$) and the high annual aerosol fluxes in the area, it was hypothesised that the dFe vertical distribution in this region was principally controlled by scavenging in the upper water column (0 – 500 m). This was likely to be

linked to biological production and export as dFe concentrations also correlated well with nitrate concentrations ($R^2 = 0.80$).

Dissolved iron redox speciation

Surface water Fe(II) concentrations in the open ocean regions of the Canary Basin and the Bay of Biscay were between the limit of detection of the FI-CL method (<5- 12 pM) and 35 pM and hence interpretation of this data was limited. Elevated Fe(II) concentrations in the open ocean were only observed occasionally following rain showers and mid day solar maxima (Fe(II) ~10 – 60 pM). Fe(II) minima were observed at the chlorophyll maxima of 4 of the stations in the Canary Basin. This was hypothesised to be due to either higher uptake and/or oxidation rates at these depths.

Intermediate and deep water (1000 – 4500 m) Fe(II) concentrations varied from 10 - 40 pM in the Canary Basin (Station 10) to ca. 20 - 75 pM in the Bay of Biscay. Similar to the data for surface waters, Fe(II) was observed as a small fraction of dFe throughout the water column (mean = 5.5 %, $\sigma = 2.6$ %).

The results of a thermodynamic equilibrium model (based on electron activity, see Chapter 4) demonstrate that Fe complexes would require a standard reduction potential of > +0.65 V to stabilize a 5 % Fe(II) fraction in the dissolved iron pool, at equilibrium under the conditions observed. It is hypothesised that either the Fe(II) fraction in these waters was stabilised by unknown ligands or the redox state was controlled by kinetic processes such as dissolution and remineralization of particles and colloids. There was no indication of Fe redox speciation being significantly affected by changes in dissolved oxygen concentration within the range found for North East Atlantic (170 – 250 μM).

The data for the English Channel and North Sea waters show the significance of photoreduction and sediment dissolution as sources of Fe(II) in shelf waters. Fe(II) concentrations in the shelf

waters of the English Channel were 20 – 200 pM with the highest concentrations in the near-bottom waters on the shelf break and Fe(II) was observed as a constant fraction of dFe (mean = 5.0 %, σ = 2.7 %). A diurnal trend was observed during a solar maximum in the shelf waters that caused the %Fe(II) to rise to ca. 10%. Using a simple kinetic model, an upper limit for a conditional first order photo-reduction rate constant (k_{hv}^{cond}) was calculated as ~2.5 x 10^{-3} s^{-1} for these waters.

Effect of continental margins and hydrography on dissolved iron distributions on the European Continental Shelf

Evidence of the large-scale impact of sediment resuspension and benthic diffusion on the iron biogeochemistry of the European Continental Shelf region in early springtime was found (March 2002, Chapter 5). Elevated dFe concentrations were observed in near bottom waters at the shelf break (0.75 – 1.0 nM), which coincided with high Fe(II) concentrations (> 100 pM). A minimum flux of 12 µM Fe(II) m^{-2} d^{-1} was calculated for these sediments using a simple kinetic model. Intermediate waters near the shelf slope (1000 – 3000 m) also contained high dFe concentrations (>0.8 nM) and it was hypothesised that this was caused by the direct advection of colloidal material from the shelf rather than from biological regeneration.

A 'trace metal front' caused by mixing between Fe depleted open ocean surface waters (0.2 nM dFe) and enriched shelf waters (ca. 0.8 nM dFe) was observed for both dFe and Fe(II) in the surface waters between the English Channel and the Bay of Biscay (3-6 m depth, 7.0 – 4.0 °W). The overall relationship between dFe and salinity observed between the North Sea and the European Continental Shelf slope was non-linear signifying that factors such as benthic inputs and scavenging controlled dFe concentrations in shelf waters. However, a twofold increase in dFe with a decrease in salinity was seen in the coastal waters of the southern North Sea, suggesting high freshwater dFe inputs in this region.

In the surface waters of the Canary Basin (3-6 m depth, October 2002), dFe concentrations varied between 0.15 and 0.95 nM and an inverse logarithmic relationship between dFe concentrations in surface waters and the distance from the North West African coast was observed ($R^2 = 0.66$). This relationship was attributed to the continuous advection of Fe enriched shelf and coastal waters, as no evidence of high aerosol fluxes affecting the area were found (based on satellite aerosol data and no covariance between dFe and dAl). Concentrations of dFe in the euphotic zone (0-150 m) were similar to those of surface waters (0.1 to 1.0 nM, mean of 0.42 nM (n = 71)).

The dFe gradient (0.2 - 0.8 nM) in the Canary Basin occurred over ~1000 km illustrating the large-scale effect of the North East trade winds and upwelling areas on the propagation of dFe from continental and coastal sources. In contrast, the dFe gradient between the Bay of Biscay and the English Channel occurred over a distance of <200 km and the mixing of open ocean and shelf waters occurred in the shallow waters of the shelf. The short distance propagation of dFe may have been caused by the low level of entrainment of the shelf waters caused by near bottom currents that run parallel to the slope [249,250] and the wind driven eastward surface current.

7.1.4 The significance of small colloidal iron (0.02 - 0.2 μm) in the dissolved iron pool of the euphotic zone of the Canary Basin.

Soluble and small colloidal iron were determined in the euphotic zone (0-150 m) of the Canary Basin and the mean concentrations where 0.281 and 0.170 nM respectively (n = 60). In the northern part of the study area (31.7 °N, 22.0 °W), soluble iron increased with depth (0.1 to 0.3 nM) between 25 and 1500 m. Small colloidal iron (0.02 – 0.2 μm) was a major fraction of dFe in the euphotic zone of the Canary Basin (ca. 25 – 60%, mean of 38.9%), whereas in deeper waters (0 – 1300 m depth) this fraction was smaller and less variable (mean ± σ = 0.18 ±0.06 nM, station 10). Possible sources of small colloidal iron were from aerosol deposition and iron bound to

colloidal organic matter.

7.1.5 Potential variables that affect the dissolution of iron from aerosol dusts in seawater.

The solubility of Fe in a Turkish dust equilibrated with seawater was found to be 0.002 % (at a dust concentration 20 mg/L). This compared well with the % soluble Fe found for Saharan soil in seawater. [288] Kinetic dust dissolution experiment demonstrated that dFe and Fe(II) concentrations for ultra-filtered and unfiltered seawater reached a pseudo steady state in <48 h and that cells and particles in the surface seawater did not play an active role in the kinetics of dissolution of Fe(II) or dFe species.

dFe concentrations (<0.02 and <0.2 μm size fractions) increased linearly with dust particle concentration (R^2 = 0.994 and 0.857) in equilibrated unfiltered seawater and a negative relationship between % Fe solubility and amount of dust added was observed, suggesting that lower dust loadings increase the % soluble Fe from aerosols. dFe concentrations in ultra filtered seawater were ~60 % lower than in unfiltered seawater and hence dFe concentrations were dependent on biotic and/or abiotic particle interaction.

7.2 Future work

There are several ways in which the work reported here can be taken further, these include:

Method development

The FI-CL method is highly suited for shipboard and field measurements and has been used to determine dFe and TDFe species in several open ocean studies (e.g. refs [21,189,232,244]) in addition to those reported here. The accuracy of the method for determining dissolved iron in acidified

samples has been assessed by analysing standard reference materials (e.g. CASS and NASS seawaters) [163] and during several international intercomparison exercises. [290-292]

Despite good agreement between the dFe data produced using the FI-CL method reported here and those of other laboratories (e.g. certified reference seawater), uncertainties remain concerning the effects of the variation of seawater matrices on dFe determination . In Chapter 3 of this work it was demonstrated that with sufficient concentrations of iron binding ligands, it is possible to mask Fe even when the sample is acidified to pH 2 and reduced with sodium sulphite. Furthermore, when the reduction of dFe from a coastal sample was monitored over a period of several weeks, Fe(II) continued to be released from colloids in the sample (Fig. 3.8). Hence further evaluation of the method and investigation into improving the sample pre-treatment is required.

Due to the lack of reference material and the sensitivity of redox species, evaluation of Fe(II) determination is more challenging. The FICL shipboard method reported here has the advantages of a low limit of detection (5 – 12 pM), low analysis time (allowing high temporal and spatial resolution) and solid phase extraction of the analyte to remove a large portion of aqueous phase species. It is possible that with improved instrumental design and reduction of the blank signal the sensitivity and limit of detection can be optimised further. However, it remains unknown whether variation in the sensitivity of the method to different Fe(II) and Fe(III) complexes and charge transfer reactions can cause significant interference.

In Chapter 3 it was demonstrated that interference from Fe(III) species in seawater was only significant when the ambient Fe(II) concentrations were ~1 % of the total iron concentration. However, as demonstrated in Chapters 5 and 6 the %Fe(II) determined in most samples was ~ 5% of the dFe concentration hence this interference could become significant in these waters. It may be possible to assess this further using Fe(II) or Fe(III) specific ligands (e.g. ferrozine) to mask Fe(II) signals and assess the analytical blank further but the chemistry of these experiments must be carefully investigated as blanks of this kind are likely to further alter the ambient redox speciation.

Other suggestions for further evaluation of the FI-CL method for the determination of Fe(II) are to examine the sensitivity of the method to different inorganic and organic Fe(II) species under anaerobic conditions (i.e. using nitrogen purged solutions and 8-HQ column to remove anoxic matrix). This type of experiment would prevent the oxidation of Fe(II) species and allow sufficient time for complexation to occur with the ferrous species at ambient pH (e.g. 5 - 8.1) . Furthermore, it would evaluate the use of the method for use with anoxic samples. In addition, further Fe(II) interference studies could be conducted by adding pre-complexed Fe(III) to seawater and freshwater matrices.

Micro-scale biogeochemistry

A well-defined knowledge of iron speciation is required in order to improve our knowledge of cell surface uptake and to integrate iron speciation field data with models. Current uptake models often only assume the equilibrium of truly dissolved species (e.g. Fe' and FeL). However, reported dissolved iron concentrations from field data are usually acidified and often contain colloidal iron within the 'dissolved' size fraction (e.g. < 0.2 μm). Furthermore, the equilibrium between dissolved and particulate Fe phases is likely to be influenced by the adsorption and desorption of particulate iron species that are removed by filtration and will be affected by physico-chemical variables such as temperature and pH. Hence a suggestion for future work is to continue to examine the complexation kinetics and equilibria of Fe(II) and Fe(III) species between different model phases and dissolved iron complexes under controlled conditions.

Basin-scale biogeochemistry

Further understanding of basin-scale iron cycling and more accurate estimates of Fe residence times can be gained by improving estimates of iron fluxes to and within the water column of the open ocean. It is necessary to determine Fe transport over shelf margins in order to quantify the fluxes from terrestrial and shelf sources to the open ocean. Further insight into the transport of dFe

from shelf processes may be achieved by studying iron transport via particle and colloidal fluxes using particle filtration, sediment traps, benthic flux chambers and moorings near shelf areas. If the main enrichment of dFe occurs via advection of colloids then a steady state dissolved/particulate model could be combined with water column downward particle fluxes obtained via field studies. In addition, differences in isotopic ratios may also help to track lithogenic iron originating from the shelf.

Integration of real-time satellite aerosol data and iron deposition may be possible in the future but a better understanding of the dissolution of Fe from aerosols is required. According to the work reported here and the recent work of Bonnet and Guieu, [288] Fe dissolution from particles takes place within the residence time of aerosols in surface waters (e.g. ~ 20 days [105]) and the % Fe solubility of aerosol dusts is not constant and increases at low particulate loading and higher marine particle concentrations.

Variability due to the structure and origin of aerosols and the atmospheric processing they are exposed to is more difficult to examine and requires access to a large and varied collection of samples. Improved knowledge of atmospheric derived fluxes can also be obtained using improved sampling strategies that allow an iron budget to be calculated. An example being an eddy-scale time series experiments where atmospheric and water column particulate fluxes are determined in combination with dissolved iron measurements.

In addition to Fe fluxes, another important research area is the quantification and characterization of iron binding ligands. Ligand concentrations have been identified as a key variable in the global iron budget [5,124,125,248] and may control the dissolved iron concentrations in large oceanic regions. An improved understanding of the chemical structure and distribution in the oceans is required in order to determine the sources, sinks and transport of these molecules.

Redox speciation

Several of the variables that were hypothesised to influence iron redox speciation were examined during this study but more incite into water column redox chemistry may be obtained by studying the temporal and spatial changes redox cycling of Fe(II) with hydrogen peroxide. In addition to this the evaluation of kinetic parameters for redox reactions under aerobic and anaerobic conditions at ambient seawater pH will improve kinetic models.

References

[1] J. H. Martin, K. H. Coale, K. S. Johnson, S. E. Fitzwater, R. M. Gordon, S. J. Tanner, C. N. Hunter, V.A. Elrod, *et al.*, *Nature* **1994**, 371, 123.

[2] P. G. Falkowski, *Photosyn. Res.* **1994**, 39, 235.

[3] P. G. Falkowski, J. A. Raven, *Aquatic Photosynthesis* **1997** (Blackwell Science: Oxford).

[4] A. Jacobs, M. Worwood, *Iron in Biochemistry and Medicine* **1974** (Academic: London).

[5] J. K. Moore, S. C. Doney, D. M. Glover, I. Y. Fung, *Deep-Sea Res.* Part II **2002**, 49, 463.

[6] T. J. Hart, *Discovery Rep.* **1942**, 11, 261.

[7] H. W. Harvey, *The Chemistry and Fertility of Sea Waters* **1957** (Cambridge University Press: Cambridge).

[8] W. M. Landing, K. W. Bruland, *Geochim. Cosmochim. Acta* **1987**, 51, 29.

[9] J. H. Martin, R. M. Gordon, *Deep-Sea Res.* **1988**, 35, 177.

[10] J. H. Martin, R. M. Gordon, S. E. Fitzwater, W. W. Broenkow, *Deep-Sea Res.* **1989**, 36, 649.

[11] K. W. Bruland, R. P. Franks, G. A. Knauer, J. H. Martin, *Anal. Chim. Acta* **1979**, 105, 233.

[12] J. H. Martin, R. M. Gordon, S. E. Fitzwater, *Limnol. Oceanogr.* **1991**, *36*, 1793.

[13] J. H. Martin, R. M. Gordon, S. E. Fitzwater, *Nature* **1990**, *345*, 156.

[14] J. H. Martin, *Paleoceanography* **1990**, *5*, 1.

[15] N. Lefevre, A. J. Watson, *Global Biogeochem. Cycles* **1999**, *13*, 727.

[16] J. Watson, D. C. E. Bakker, A. J. Ridgwell, P. W. Boyd, C. S. Law, *Nature* **2000**, *407*, 730.

[17] Maher, P. F. Dennis, *Nature* **2001**, *411*, 176.

[18] K. H. Coale, K. S. Johnson, S. E. Fitzwater, S. P. G. Blain, T. P. Stanton, T. L. Coley, *Deep-Sea Res. Part II* **1998**, *45*, 919.

[19] R. M. Gordon, K. S. Johnson, K. H. Coale, *Deep-Sea Res. Part II* **1998**, *45*, 995.

[20] K. H. Coale, K. S. Johnson, S. E. Fitzwater, R. M. Gordon, S. Tanner, F. P. Chavez, L. Ferioli, C. Sakamoto, *et al.*, *Nature* **1996**, *383*, 495.

[21] P. W. Boyd, A. J. Watson, C. S. Law, E. R. Abraham, T. Trull, R. Murdoch, D. C. E. Bakker, A. R. Bowie, *et al.*, *Nature* **2000**, *407*, 695.

[22] K. H. Coale, K. S. Johnson, F. P. Chavez, K. O. Buesseler, R. T. Barber, M. A. Brzezinski, W. P. Cochlan, F. J. Millero, *et al.*, *Science* **2004**, *304*, 408.

[23] A. Tsuda, S. Takeda, H. Saito, J. Nishioka, Y. Nojiri, I. Kudo, H. Kiyosawa, A. Shiomoto, *et al.*, *Science* **2003**, *300*, 958.

[24] D. A. Hutchins, K. W. Bruland, *Nature* **1998**, *393*, 561.

[25] K. W. Bruland, E. L. Rue, G. J. Smith, *Limnol. Oceanogr.* **2001**, *46*, 1661.

[26] G. F. Firme, E. L. Rue, D. A. Weeks, K. W. Bruland, D. A. Hutchins, *Global Biogeochem. Cycles* **2003**, *17*, 1016.

[27] D. A. Hutchins, C. E. Hare, R. S. Weaver, Y. Zhang, G. F. Firme, G. R. DiTullio, M. B. Alm, S. F. Riseman, *et al.*, *Limnol. Oceanogr.* **2002**, *47*, 997.

[28] M. T. Maldonado, P. W. Boyd, P. J. Harrison, N. M. Price, *Deep-Sea Res. Part II* **1999**, *46*, 2475.

[29] S. Takeda, A. Kamatani, K. E. Kawanobe, *Mar. Chem.* **1995**, *50*, 229.

[30] R. Bowie, M. T. Maldonado, R. D. Frew, P. L. Croot, E. P. Achterberg, R. F. C. Mantoura, P. J. Worsfold, C. S. Law, *et al.*, *Deep-Sea Res. Part II* **2001**, *48*, 2703.

[31] Q. Schiermeier, *Nature* **2003**, *421*, 109.

[32] J. A. Fuhrman, D. G. Capone, *Limnol. Oceanogr.* **1991**, *36*, 1951.

[33] M. Markels, R. T. Barber, in *ACS Natl. Meet., Fuel Chemistry Division* **2001** (ACS: Washington, DC).

[34] R. McKie, in *The Observer*, 12 January **2003**.

[35] S. R. Taylor, *Geochim. Cosmochim. Acta* **1964**, *28*, 1273.

[36] S. F. Mason, *Chemical Evolution* **1991** (Clarendon Press: Oxford).

[37] D. R. Turner, K. A. Hunter, H. J. W. de Baar, in *The Biogeochemistry of Iron in Seawater* (Eds D. R. Turner, K. A. Hunter) **2001** (John Wiley: New York, NY).

[38] N. N. Greenwood, A. Earnshaw, *Chemistry of the Elements* **1984** (Pergamon: New York, NY).

[39] W. Stumm, J. J. Morgan, *Aquatic Chemistry, 3rd edn* **1996** (John Wiley: New York, NY).

[40] J. Gobler, J. R. Donat, J. A. Consolvo, S. A. Sanudo-Wilhelmy, *Mar. Chem.* **2002**, *77*, 71.

[41] J. Nishioka, S. Takeda, C. S. Wong, W. K. Johnson, *Mar. Chem.* **2001**, *74*, 157.

[42] X. Liu, F. J. Millero, *Geochim. Cosmochim. Acta* **1999**, *63*, 3487.

[43] R. H. Byrne, D. R. Kester, *Mar. Chem.* **1976**, *4*, 255.

[44] F. J. Millero, W. Yao, J. Aicher, *Mar. Chem.* **1995**, *50*, 21.

[45] K. Kuma, J. Nishioka, K. Matsunaga, *Limnol. Oceanogr.* **1996**, *41*, 396.

[46] R. H. Byrne, Y.-R. Luo, R. W. Young, *Mar. Chem.* **2000**, *70*, 23

[47] X. Liu, F. J. Millero, *Mar. Chem.* **2002**, *77*, 43.

[48] M. Gledhill, C. M. G. van den Berg, *Mar. Chem.* **1994**, *47*, 41.

[49] M. G. Van den Berg, *Mar. Chem.* **1995**, *50*, 139.

[50] E. L. Rue, K. W. Bruland, *Mar. Chem.* **1995**, *50*, 117.

[51] J. Wu, G. W. Luther, *Mar. Chem.* **1995**, *50*, 159.

[52] R. T. Powell, J. R. Donat, *Deep-Sea Res. Part II* **2001**, *48*, 2877.

[53] A. Witter, D. A. Hutchins, A. Butler, G. W. Luther, *Mar. Chem.* **2000**, *69*, 1.

[54] K. Kuma, A. Katsumoto, H. Kawakami, F. Takatori, K. Matsunaga, *Deep-Sea Res. I* **1998**, *45*, 91.

[55] J. E. Huheey, E. A. Keiter, R. L. Keiter, *Inorganic Chemistry. 4th edn* **1993** (Harper Collins: CITY).

[56] A. Cotton, G. Wilkinson, *Advanced Inorganic Chemistry* **1988** (John Wiley: New York, NY).

[57] M. M. Morel, J. G. Hering, *Principles and Applications of Aquatic Chemistry* **1993** (John Wiley: New York, NY).

[58] H. Boukhalfa, A. Crumbliss, *Biometals* **2002**, *15*, 325.

[59] D. L. Huffman, M. M. Rosenblatt, K. S. Suslick, *J. Am. Chem. Soc.* **1998**, *120*, 6183.

[60] E. J. Roekens, R. E. Van Grieken, *Mar. Chem.* **1983**, *13*, 195.

[61] F. J. Millero, S. Sotolongo, M. Izaguirre, *Geochim. Cosmochim. Acta* **1987**, *51*, 793.

[62] F. J. Millero, S. Sotolongo, *Geochim. Cosmochim. Acta* **1989**, *53*, 1867.

[63] A. L. Rose, T. D. Waite, *Environ. Sci. Technol.* **2002**, *36*, 433.

[64] T. Holland, *Ph.D. Thesis* **2001** (University of Plymouth: Plymouth).

[65] D. W. King, H. A. Lounsbury, F. J. Millero, *Environ. Sci. Technol.* **1995**, *29*, 818.

[66] D. W. King, *Environ. Sci. Technol.* **1998**, *32*, 2997.

[67] D. W. King, R. Farlow, *Mar. Chem.* **2000**, *70*, 201.

[68] W. T. Welch, Z. Davis, S. D. Aust, *Arch. Biochem. Biophys.* **2002**, *397*, 360.

[69] T. L. Theis, P. C. Singer, *Environ. Sci. Technol.* **1974**, *8*, 569.

[70] C. J. Miles, P. L. Brezonik, *Environ. Sci. Technol.* **1981**, *15*, 1089.

[71] M. Santana-Casiano, M. Gonzalez-Davila, M. J. Rodriguez, F. J. Millero, *Mar. Chem.* **2000**, *70*, 211.

[72] D. L. Sedlak, J. Hoigne, *Atmos. Environ.* **1993**, *27A*, 2173.

[73] D. W. King, R. A. Aldrich, S. E. Charnecki, *Mar. Chem.* **1993**, *44*, 105.

[74] J. Sima, J. Makanova, *Coord. Chem. Rev.* **1997**, *160*, 161.

[75] K. Barbeau, E. L. Rue, K. W. Bruland, A. Butler, *Nature* **2001**, *413*, 409.

[76] W. G. Sunda, S. A. Huntsman, *Mar. Chem.* **1995**, *50*, 189.

[77] W. L. Miller, D. Kester, *J. Mar. Res.* **1994**, *52*, 325.

[78] M. L. Wells, L. M. Mayer, *Deep-Sea Res.* **1991**, *38*, 1379.

[79] K. A. Barbeau, J. W. Moffet, *Environ. Sci. Technol.* **1998**, *32*, 2969.

[80] K. S. Johnson, K. H. Coale, V. A. Elrod, N. W. Tindale, *Mar. Chem.* **1994**, *46*, 319.

[81] T. D. Waite, R. Szymczak, Q. I. Espey, M. J. Furnas, *Mar. Chem.* **1995**, *50*, 79.

[82] S. Glasauer, P. G. Weidler, S. Langley, T. J. Beveridge, *Geochim. Cosmochim. Acta* **2003**, *67*, 1277.

[83] J. Chen, B. Gu, R. A. Royer, W. D. Burgos, *Sci. Tot. Environ.* **2003**, *307*, 167.

[84] E. E. Roden, J. M. Zachara, *Environ. Sci. Technol.* **1996**, *30*, 1618.

[85] B. M. Voelker, F. M. M. Morel, B. Sulzberger, *Environ. Sci. Technol.* **1997**, *31*, 1004.

[86] R. F. Stallard, J. M. Edmond, *J. Geophys. Res.* **1983**, 88, 9671.

[87] J. M. Martin, M. Whitfield, in *Trace Metals in Seawater* (Eds C. S. Wong, E. Boyle, K. W. Bruland, J. D. Burton, E. D. Goldberg) **1983** (Plenum Press: New York, NY).

[88] J. M. Bewers, P. A. Yeats, *Nature* **1977**, *268*, 595.

[89] T. D. Jickells, L. J. Spokes, in *The Biogeochemistry of Iron in Seawater* (Eds D. R. Turner, K. A. Hunter) **2001** (John Wiley: New York, NY).

[90] E. R. Sholkovitz, *Geochim. Cosmochim. Acta* **1976**, *40*, 831.

[91] R. M. Moore, J. D. Burton, P. J. Williams, M. L. Young, *Geochim. Cosmochim. Acta* **1979**, *43*, 919.

[92] A. Turner, G. E. Millward, *Estuar. Coast. Shelf Sci.* **1994**, *39*, 45.

[93] S. A. Sanudo-Wilhelmy, I. Riviera-Duarte, A. R. Flegal, *Geochim. Cosmochim. Acta* **1996**, *60*, 4933.

[94] R. Chester, *Marine Geochemistry, 2nd edn* **2000** (Blackwell: London).

[95] H. Elderfield, A. Schultz, *Annu. Rev. Earth Planet. Sci.* **1996**, *24*, 191.

[96] R. A. Duce, N. W. Tindale, *Limnol. Oceanogr.* **1991**, *36*, 1715.

[97] G. Zhuang, R. A. Duce, D. R. Kester, *J. Geophys. Res.* **1990**, *95*, 16207.

[98] C. Guieu, Y. Bozec, S. Blain, C. Ridame, G. Sarthou, N. Leblond, *Geophys. Res. Lett.* **2001**, *29*, 1911.

[99] X. Zhu, J. M. Prospero, F. J. Millero, D. L. Savoie, G. W. Brass, *Mar. Chem.* **1992**, *38*, 91.

[100] R. J. Kieber, K. Williams, J. D. Willey, S. Skrabal, G. B. Avery, *Mar. Chem.* **2001**, *73*, 83.

[101] C. Guieu, R. Chester, M. Nimmo, J. M. Martin, S. Guerzoni, E. Nicolas, J. Mateu, S. Keyse, *Deep-Sea Res. Part II* **1997**, *44*, 655.

[102] N. Kubilay, A. C. Saydam, *Atmos. Environ.* **1995**, *29*, 2289.

[103] L. J. Spokes, T. D. Jickells, B. Lim, *Geochim. Cosmochim. Acta* **1994**, *58*, 3281.

[104] G. Zhuang, Z. Yi, R. A. Duce, P. R. Brown, *Global Biogeochem. Cycles* **1992**, *6*, 161.

[105] T. D. Jickells, *Mar. Chem.* **1999**, *68*, 5.

[106] R. J. Kieber, J. D. Willey, G. Brooks Avery, *J. Geophys. Res.* **2003**, *108*, C8 3277.

[107] J. D. Willey, R. J. Kieber, K. H. Williams, J. S. Crozier, S. A. Skrabal, G. B. Avery, *J. Atmos. Chem.* **2000**, *37*, 185.

[108] R. J. Kieber, B. Peake, J. D. Willey, B. Jacobs, *Atmos. Environ.* **2001**, *35*, 6041.

[109] Y. Erel, S. O. Pehkonen, M. R. Hoffman, *J. Geophys. Res.* **1993**, *98*, 18423.

[110] B. Sulzberger, H. Laubsher, *Mar. Chem.* **1995**, *50*, 103.

[111] C. Saydam, H. Z. Senyuva, *Geophys. Res. Lett.* **2002**, *29*, 1524.

[112] G. Zhuang, Z. Yi, R. A. Duce, P. R. Brown, *Nature* **1992**, *355*, 537.

[113] R. M. Moore, J. E. Milley, A. Chatt, *Oceanol. Acta* **1984**, *7*, 221.

[114] K. V. Desboeufs, R. Losno, F. Vimeux, S. Cholbi, *J. Geophys. Res.* **1999**, *104*, 21287.

[115] L. J. Spokes, T. D. Jickells, *Aquat. Geochem.* **1996**, *1*, 355.

[116] T. Ozsoy, A. C. Saydam, *J. Atmos. Chem.* **2001**, *40*, 41.

[117] R. Edwards, *Ph.D. Thesis* **1999** (University of Tasmania: Hobart).

[118] G. Zhuang, Z. Yi, G. T. Wallace, *Mar. Chem.* **1995**, *50*, 41.

[119] K. L. Von Damm, J. M. Edmond, C. I. Measures, B. Grant, *Geochim. Cosmochim. Acta* **1985**, *49*, 2221.

[120] R. Chester, S. R. Aston, in *Chemical Oceanography* (Eds J. P. Riley, R. Chester) **1976**, Vol. 6, pp. 281–390 (Academic Press: London).

[121] R. R. Haese, in *Marine Geochemistry* (Eds H. D. Shulz, M. Zabel) **2000** (Springer: Heidelberg).

[122] D. R. Lovely, *FEMS Microbiol. Rev.* **1997**, *20*, 305.

[123] M. Konig, M. Haeckel, E. Drodt, A. Suess, X. Trautwein, *Geochim. Cosmochim. Acta* **1999**, *63*, 1517.

[124] K. S. Johnson, R. M. Gordon, K. H. Coale, *Mar. Chem.* **1997**, *57*, 137.

[125] D. E. Archer, K. Johnson, *Global Biogeochem. Cycles* **2000**, *14*, 269.

[126] G. W. Luther, J. Wu, *Mar. Chem.* **1997**, *57*, 173.

[127] E. Boyle, *Mar. Chem.* **1997**, *57*, 163.

[128] D. A. Hutchins, G. R. Di Tullio, K. W. Bruland, *Limnol. Oceanogr.* **1993**, *38*, 1242.

[129] B. Neilands, in *Inorganic Biogeochemistry* (Ed. G. L. Eichhorn) **1973** (Elsevier: Amsterdam).

[130] T. Maldonado, N. M. Price, *Deep-Sea Res. Part II* **1999**, *46*, 2447.

[131] D. A. Hutchins, A. E. Witter, A. Butler, G. W. Luther, *Nature* **1999**, *400*, 858.

[132] E. L. Rue, K. W. Bruland, *Limnol. Oceanogr.* **1997**, *42*, 901.

[133] B. L. Lewis, P. D. Holt, S. W. Taylor, S. W. Wilhelm, C. G. Trick, A. Butler, G. W. Luther III, *Mar. Chem.* **1995**, *50*, 179.

[134] K. Barbeau, E.L. Rue, C.G. Trick, K.W. Bruland and A. Butler, Limnol. Oceanogr., **2003**, *48*, 1069.

[135] H. M. Macrellis, C. G. Trick, E. L. Rue, G. Smith, K. W. Bruland, *Mar. Chem.* **2001**, *76*, 175.

[136] T. Yoshida, K. Hayashi, H. Ohmoto, *Chem. Geol.* **2002**, *184*, 1.

[137] G. Haygood, P. D. Holt, A. Butler, *Limnol. Oceanogr.* **1993**, *38*, 1091.

[138] G. Xu, J. S. Martinez, J. T. Groves, A. Butler, *J. Am. Chem. Soc.* **2002**, *124*, 13408.

[139] J. S. Martinez, G. P. Zhang, P. D. Holt, H. T. Jung, C. J. Carrano, M. G. Haygood, A. Butler, *Science* **2000**, *287*, 1245.

[140] J. S. Martinez, M. G. Haygood, A. Butler, *Limnol. Oceanogr.* **2003**, *46*, 420.

[141] J. Granger, N. M. Price, *Limnol. Oceanogr.* **1999**, *44*, 541.

[142] M. Gledhill, P. McCormack, S. Ussher, E. P. Achterberg, R. F. C. Mantoura and P. J. Worsfold, *Mar. Chem.* **2004.** *88,* 75.

[143] W. G. Sunda, in *The Biogeochemistry of Iron in Seawater* (Eds D. R. Turner, K. A. Hunter) **2001** (John Wiley: New York, NY).

[144] R. J. M. Hudson, *Sci. Tot. Environ.* **1998**, *219*, 95.

[145] A. Anderson, F. M. M. Morel, *Limnol. Oceanogr.* **1982**, *27*, 789.

[146] F. M. M. Morel, R. J. M. Hudson, N. M. Price, *Limnol. Oceanogr.* **1991**, *36*, 1742.

[147] R. J. M. Hudson, F. M. M. Morel, *Limnol. Oceanogr.* **1990**, *35*, 1002.

[148] R. J. M. Hudson, F. M. M. Morel, *Deep-Sea Res.* **1993**, *40*, 129.

[149] M. T. Maldonado, N. M. Price, *Mar. Ecol. Prog. Ser.* **1996**, *141*, 161.

[150] M. T. Maldonado, N. M. Price, *Limnol. Oceanogr.* **2000**, *45*, 814.

[151] M. T. Maldonado, N. M. Price, *J. Phycol.* **2001**, *37*, 298.

[152] M. A. Anderson, F. M. M. Morel, *Mar. Biol. Lett.* **1980**, *1*, 263.

[153] C. Soria-Dengg, U. Horstmann, *Mar. Ecol. Prog. Ser.* **1995**, *127*, 269.

[154] K. Kuma, K. Matsunaga, *Mar. Biol.* **1995**, *122*, 1.

[155] M. L. Wells, N. G. Zorkin, A. G. Lewis, *J. Mar. Res.* **1983**, *41*, 731.

[156] K. Barbeau, J. W. Moffett, D. A. Caron, P. L. Croot, D. L. Erdner, *Nature* **1996**, *380*, 61.

[157] R. Maranger, D. F. Bird, N. M. Price, *Nature* **1998**, *396*, 248.

[158] P. MacLaurin, K. N. Andrew, P. J. Worsfold, in *Process Analytical Chemistry* (Eds F. McLennan, B. R. Kowalski.), **1995** (Blackie, Glasgow).

[159] S. Vink, E. A. Boyle, C. I. Measures, J. Yuan, *Deep-Sea Res. I* **2000**, *47*, 1141.

[160] C. M. Sakamoto-Arnold, K. S. Johnson, *Anal. Chem.* **1987**, *59*, 1789.

[161] H. Zamzow, K. H. Coale, K. S. Johnson, C. M. Sakamoto, *Anal. Chim. Acta* **1998**, *377*, 133.

[162] V. A. Elrod, K. S. Johnson, K. H. Coale, *Anal. Chem.* **1991**, *63*, 893.

[163] A. R. Bowie, E. P. Achterberg, R. F. C. Mantoura, P. J. Worsfold, *Anal. Chim. Acta* **1998**, *361*, 189.

[164] H. Obata, H. Karatani, M. Matsui, E. Nakayama, *Mar. Chem.* **1997**, *56*, 97.

[165] J. T. de Jong, J. den Das, U. Bahtmann, M. H. Stoll, G. Kattner, R. F. Nolting, H. J. de Baar, *Anal. Chim. Acta* **1998**, *377*, 113.

[166] T. P. Chapin, K. S. Johnson, K. H. Coale, *Anal. Chim. Acta* **1991**, *249*, 469.

[167] J. L. Nowicki, K. S. Johnson, K. H. Coale, V. A. Elrod, S. H. Lieberman, *Anal. Chem.* **1994**, *66*, 2732.

[168] D. Price, R. F. C. Mantoura, P. J. Worsfold, *Anal. Chim. Acta* **1998**, *371*, 205.

[169] A. R. J. David, T. McCormack, A. W. Morris, P. J. Worsfold, *Anal. Chim. Acta* **1998**, *361*, 63.

[170] R. T. Masserini, K. A. Fanning, *Mar. Chem.* **2000**, *68*, 323.

[171] J. Floch, S. Blain, D. Birot, P. Treguer, *Anal. Chim. Acta* **1998**, *377*, 157.

[172] T. D. Clayton, R. H. Byrne, *Deep-Sea Res.* **1993**, *40*, 2115.

[173] R. G. J. Bellerby, D. R. Turner, G. E. Millward, P. J. Worsfold, *Anal. Chim. Acta* **1995**, *309*, 259.

[174] L. K. Shpigun, I. Y. Kolotyrkina, Y. A. Zolotov, *Anal. Chim. Acta* **1992**, *261*, 307.

[175] J. F. Wu, E. A. Boyle, *Anal. Chim. Acta* **1998,** *367,* 183.

[176] M. L. Wells, K. W. Bruland, *Mar. Chem.* **1998,** *63,* 145.

[177] C. I. Measures, J. Yuan, J. A. Resing, *Mar. Chem.* **1995,** *50,* 3.

[178] H. Obata, C. M. G. Van den Berg, *Anal. Chem.* **2001,** *73* 2522.

[179] E. P. Achterberg, T. W. Holland, A. R. Bowie, R. F. C. Mantoura, P. J. Worsfold, *Anal. Chim. Acta* **2001,** *442,* 1.

[180] G. Merenyi, J. Lind, T. E. Eriksen, *J. Biolumin. Chemilumin.* **1990,** *5,* 53-56.

[181] A. L. Rose, D. Waite, *Anal Chem.* **2001,** *73,* 5909.

[182] D. W. O'Sullivan, A. K. Hanson D. R. Kester, *Mar. Chem.* **1995,** *49,* 65.

[183] H. Obata, H. Karatani, E. Nakayama, *Anal. Chem.* **1993,** *65,* 1524.

[184] W. R. Seitz, D. M. Hercules, *Anal. Chem.* **1972,** *44,* 2143.

[185] L. L. Klopf, T. A. Nieman, *Anal Chem.* **1983,** *55,* 1080.

[186] E. G. Sarontonis, A. Townsend, *Anal. Chim. Acta* **1986,** *184,* 311.

[187] A. Alwarthan, A. Townsend, *Anal. Chim. Acta* **1987,** *196,* 135.

[188] R. T. Powell, D. W. King, W. M. Landing, *Mar. Chem.* **1995,** *50,* 13.

[189] A. R. Bowie, E. P. Achterberg, P. N. Sedwick, S. Ussher, P. J. Worsfold, *Environ. Sci. Technol.* **2002,** *36,* 4600.

[190] P. L. Croot, P. Laan, *Anal. Chim. Acta* **2002,** *466,* 261.

[191] H. Hirata, Yoshihara, M. Aithara, *Talanta* **1999,** *49,* 1059.

[192] A.R. Bowie, E.P. Achterberg, S. Ussher and P.J. Worsfold, Journal of Automated Methods and Management in Chemistry, (in press).

[193] Http://Sine.Ni.Com/Apps/We/Nioc.Vp?Cid=1381&Lang=Us

[194] V. Cannizzaro, A. R. Bowie, A. Sax, E. P. Achterberg, P. J. Worsfold, *Analyst* **1999,** *125,* 51.

[195] E. P. Achterberg, C. B. Braungardt, R. C. Sandford, P. J. Worsfold, *Anal. Chim. Acta* **2001,** *440,* 27.

[196] Http://Www.Jhu.Edu/~Scor/Wg109front.Htm

[197] P. N. Sedwick, P. R. Edwards, D. J. Mackey, F. B. Griffiths, J. S. Parslow, *Deep-Sea Research Part I* **1997**, *44*, 1239.

[198] H. J. W. de Baar, J.T.M. de Jong, in *The Biogeochemistry Of Iron In Seawater* (Eds D. R. Turner, K. A. Hunter) **2001** (John Wiley: New York, NY).

[199] P. L. Croot, A.R. Bowie, R.D. Frew, M.T. Maldonado, J.A. Hall, K.A. Safi, J. LaRoche, P.W. Boyd, C.S. Law, *Geophys.Res.Lett.* **2001**, *28*, 3425.

[200] H. Hong, D.R. Kester, *Limnol.Oceanogr.* **1986**, *31*, 512.

[201] Y. Sohrin, S. Iwamoto, M. Matsui, H. Obata, E. Nakayama, K. Suzuki, N. Handa M. Ishii, *Deep-Sea Res. I* **2000**, *47*, 55.

[202] M. Yaqoob, S. J. Ussher, A. Nabi, A. P. Achterberg, P. J. Worsfold, *J. Flow Injection Anal.* **2003**, *20*, 183.

[203] E. P. Achterberg, T. W. Holland, A. R. Bowie, R. F. C. Mantoura, P. J. Worsfold, *Anal. Chim. Acta* **2001**, *442*, 1.

[204] M. Gledhill, C. M. G. van den Berg, *Mar. Chem.* **1995**, *50*, 51.

[205] D. W. King, J. Lin, D. R. Kester, *Anal. Chim. Acta* **1991**, *247*, 125.

[206] S. Blain, P. Treguer, *Anal. Chim. Acta* **1995**, *308*, 425.

[207] R. D. Waterbury, W. Yao, R. H. Byrne, *Anal. Chim. Acta* **1997**, *357*, 99.

[208] C. M. G. Van den Berg, *Mar. Chem.* **1995**, *50*, 139.

[209] C. Xiao, D. A. Palmer, D. J. Wesolowski, S. B. Lovitz, D. W. King, *Anal. Chem.* **2002**, *74*, 2210.

[210] Z. Lan, H. A. Mottola, *Analyst* **1996**, *121*, 211.

[211] R. J. M. Hudson, D. T. Covault, F. M. M. Morel, *Mar. Chem.* **1992**, *38*, 209.

[212] A. L. Rose, T. D. Waite, *Mar. Chem.* **2003**, *84*, 85.

[213] L. G. Sillen, *Section II: Stability Constants of Metal-Ion Complexes*, **1964**, (Chemical Society: London).

[214] E. Martell, R. M. Smith, *Volume 5: Critical Stability Constants,* **1982,** (Plenum, New York).

[215] L. Spasojevic, S. K. Amstrong, T. J. Brickman, A. L. Crumbliss, *Inorg. Chem.* **1999,** *38,* 449.

[216] D. Welch, T. Z. Davis, S. D. Aust, *Arch. Biochem. Biophys.* **2002,** *397,* 360.

[217] T. D. Waite, in *The Biogeochemistry of Iron in Seawater,* (Ed.s; D. R. Turner, K. A. Hunter) **2001** (John Wiley: New York, NY).

[218] M. L. Adams, K. J. Powell, *Anal. Chim. Acta* **2001,** *433,* 289.

[219] M. A. Anderson, F. M. M. Morel, *Limonol. Oceanogr.* **1982,** *27,* 263.

[220] N. M. Price, F. M. M. Morel, in *Metals in Biological Systems: Vol. 35,* (Eds A. Siegel, H. Siegel) **1998** (Marcel Dekker, New York).

[221] M. Boye, A. P. Aldrich, C. M. G. van den Berg, J. T. M. de Jong, M. Veldhuis, H. J. W. de Baar, *Mar. Chem.* **2003,** *80(2-3),* 129.

[222] D. W. O'Sullivan, A. K. Hanson, W. L. Miller, D. R. Kester, *Limnol. Oceanogr.* **1991,** *36(8),* 1727.

[223] W. L. Miller, D. W. King, J. Lin, D. R. Kester, *Mar. Chem.* **1995,** *50,* 63.

[224] K. Kuma, S. Nakabayashi, Y. Suzuki, I. Kudo, K. Matsunaga, *Mar. Chem.* **1992,** *37,* 15.

[225] G. J. Jones, F. M. M. Morel, *Plant Physiol.* **1988,** *87,* 143.

[226] R. Taylor, R. C. Chow, *Plant Cell Environ.* **2001,** *24,* 749.

[227] J. T. Berman-Frank, Y. Cullen, *et al., Limnol Oceanogr.* **2001,** *46(6),* 1249.

[228] M. Ozturk *et al., Deep Sea Res. II* **2004,** *51,* 2841.

[229] K. W. Bruland, J. R. Donat, D. A. Hutchins, *Limnol Oceanogr.* **1991,** *36(8),* 1555.

[230] K. W. Bruland, K. J. Orians, J. P. Cowen, *Geochim. Cosmochim. Acta,* **1994,** *58(15),* 3171.

[231] M. Tsuchiya, L. D. Talley, M. S. McCartney, *Deep Sea Res.* **1992,** *39,* 1885.

[232] A. R. Bowie, D. J. Whitworth, E. P. Achterberg, R. F. C. Mantoura, P. J. Worsfold, *Deep Sea Res. I* **2002,** *49,* 605.

[233] S. Vink, C. I. Measures, *Deep Sea Res. II* **2001,** *48,* 2787.

[234] J. Wu, E. Boyle, *Global Biogeochem. Cycles* **2002,** *16(4),* 1086, doi:10.1029/2001GB001453

[235] P. M. Saager, H. J. W. de Baar, J. T. M. de Jong, R. F. Nolting, J. Schijf, *Mar. Chem.* **1997,** *57,* 195.

[236] M. S. McCartney, L. D. Talley, *J. Phys. Oceanogr.* **1982,** *12,* 1169.

[237] J. H. Martin, S. E. Fitzwater, R. M. Gordon, C. N. Hunter, S. J. Tanner, *Deep Sea Res. II* **1993,** *40,* 115.

[238] A. Laes, S. Blain, P. Laan, E. P. Achterberg, G., Sarthou, H. J. W., de Baar, *Geophys. Res. Lett.* **2003,** *30 (17),* art. no. 1902.

[239] J. L. Reid, *Deep Sea Res.* **1979,** *26,* 1199.

[240] B. M. Loscher, H. J. W. de Baar, J. T. M. de Jong, C. Veth, F. Dehairs, *Deep Sea Res. II* **1997,** *44,* 143.

[241] A. W. Mantyla, J. L. Reid, *Deep Sea Res.* **1983,** *30,* 805.

[242] J. F. Wu, G. W. Luther, *Limnol Oceanogr.* **1994,** *39(5),* 1119.

[243] J. T. M. de Jong, M. Boye, V. F. Shoemann, R. F. Nolting, H. J. W. de Baar, *J. Environ. Monit.* **2000,** *2,* 496.

[244] G. Sarthou, A. R. Baker, S. Blain, E. P. Achterberg, M. Boye, A. R. Bowie, P. Croot, P. Laan, H. J. W. de Baar, T. D. Jickells, P. J. Worsfold, *Deep Sea Res. II* **2003,** *50,* 1339.

[245] R. T. Powell, D. W. King, W. M. Landing, *Mar. Chem.* **1995,** *50,* 1323.

[246] F. J. Millero, *Chemical Oceanography,* **1996** (CRC Press, Boca Raton, FL).

[247] H. Stommel, *Deep Sea Res.* **1958,** 5, 80.

[248] P. Parekh, M. J. Follows, E. Boyle, *Global Biogeochem. Cycles* **2004,** 18, doi:10.1029/2003GB002061

[249] R. Wollast, L. Chou, *Deep Sea Res. II* **2001,** *48,* 2971.

[250] J. M. Huthnance, *et al. Deep Sea Res. II* **2001,** *48,* 2979.

[251] K. S. Johnson, F. P. Chavez, G. E. Friederich, *Nature* **1999,** *398,* 697.

[252] D. J. Hydes, *et al. Deep Sea Res. II* **2001,** *48,* 3023.

[253] R. Schlitzer, Ocean Data View, http://awi-bremerhaven.de/GEO/ODV, **2004.**

[254] C. Le Gall, P. J. Statham, N. H. Morley, D. J. Hydes, C. H. Hunt, *Mar. Chem.* **1999,** *68,* 97.

[255] P. W. Balls, *Estuar. Coast. Shelf Sci.* **1985,** *20,* 717.

[256] F. L. L. Muller, A. D. Tappin, P J. Statham, J. D. Burton, D. J. Hydes, *Oceanologica Acta* **1994,** *17(4),* 383.

[257] G. R. Fones, W. Davison, J. Hamilton-Taylor, *Cont. Shelf Res.* **2004,** *24(13-14),* 1485.

[258] N. Antia, J. Maaβen, P. Herman, M. Voβ, J. Scholten, S. Groom, P. Miller, *Deep-Sea Res. II* **2001,** *48,* 3083.

[259] K. Kremling, C. Pohl, *Mar. Chem.* **1989,** *27,* 43.

[260] P. L. Croot, K. A. Hunter, *Mar. Chem.* **1998,** *62,* 185.

[261] A. D. Tappin, G. E. Millward, P. J. Statham, J. D. Burton, A. W. Morris, *Estuar. Coast. Shelf Sci.* **1999,** *41,* 275.

[262] National Oceanographic Data Center, MD, USA, http://www.nodc.noaa.gov

[263] A. Crumbliss, in *CRC handbook on microbial iron chelates,* (Ed. G. Winkelmann) **1991** (CRC Press, London).

[264] C. H. R., Heip, *et al.*, *Deep-Sea Res. II* **2001,** *48,* 3223.

[265] V. A. Elrod, W. M. Berelson, K. H. Coale, K. S. Johnson, *Geophys. Res. Lett.* **2004,** *31,* L12307, doi:10.1029/2004GL020216.

[266] J. W. Moffet, in *The Biogeochemistry of Iron in Seawater* (Eds D. R. Turner, K. A. Hunter) **2001** (John Wiley: New York, NY).

[267] E. D. Barton, in *The Sea -Volume 11 The global coastal ocean : regional studies and syntheses* (Ed.s A. Robinson K. Bri) **1998** (Wiley, NY).

[268] M. E. Torres-Padron *et al.*, *Deep Sea Research II* **2002,** *49(17),* 3455.

[269] J. Kuss, K. Kremling, *Deep-Sea Res. I* **46,** 1999, 149.

[270] K. Kremling, P. Streu, *Deep-Sea Res. I* **1993**, *40*, 1155.

[271] J. Kuss, K. Kremling, *Mar. Chem.* **1999**, *68*, 71.

[272] J. Wu, E. Boyle, W. Sunda, L. Wen, *Science* **2001**, *293*, 847.

[273] J. Wu, (pers. comm.), IARC, University of Alaska Fairbanks, USA. April **2002**

[274] N. N. Kubilay, (pers. comm.), IMS, Middle East Technical University, Turkey. **2003**

[275] A. Biscombe, Ph.D. Thesis, **2001** (University of Plymouth: UK).

[276] J. Kramer P. Laan, G. Sarthou, K. R. Timmermans, H. J. W. de Baar, *Mar. Chem.* **2004**, *88*, 85.

[277] K. J. Orians, K. W. Bruland, *Nature* **1985**, *316*, 427.

[278] K. H., Wedepohl, *Geochim. Cosmochim. Acta* **1995**, *59(7)*, 1217.

[279] H. U. Sverdrup, M. W. Johnson, R. H. Flemming, *The Oceans : Their Physics, Chemistry and General Biology*, **1942**, (Prentice Hall, NJ, USA).

[280] E. Helmers, *Mar. Chem.* **1996**, *53*, 51.

[281] C. I. Measures, J. M. Esmond, T. D. Jickells, *Geochim. Cosmochim. Acta* **1986**, *50*, 1423

[282] C. I. Measures, J. M. Esmond, *J. Geophys. Res.*, **1990**, *95*, 5331.

[283] C. I. Measures, *Mar. Chem.* **1995**, *49*, 267.

[284] E. Helmers, M. Rutgers van der Loeff, *J. Geophys. Res.* **1993**, *98*, 20261.

[285] K. J. Orians, K. W. Bruland, *Earth. Planet. Sci. Lett.* **1986**, *78*, 397.

[286] K. S. Johnson *et al.*, *Global Biogeochem. Cycles* **2003**, 17(2), 1063, doi :10.1029/2002GB002004.

[287] A. Baker and T. Jickells, (pers. comm.), University of East Anglia, Norwich, UK. **2005**

[288] S. Bonnet, C. Guieu, *Geophys. Res. Lett.* **2004**, *31*, L03303, doi :10.1029/2003Gl018423.

[289] M. Orif, (pers. comm.), University of Plymouth, Plymouth, UK. **2005**

[290] A. R. Bowie, P. N. Sedwick, P. J. Worsfold, *Limnol. Oceanogr. : Methods* **2004**, *2*, 42

[291] A. R. Bowie *et al.*, *Mar. Chem.* **2003**, *84*, 19.

[292] SCOR/IUPAC Working Group 109, Biogeochemistry of Iron in Seawater, Committee on Reference Materials for Ocean Science, *The National Academies Press* **2002**

Publications

CSIRO PUBLISHING

Review

www.publish.csiro.au/journals/env

S. J. Ussher et al., *Environ. Chem.* **2004**, *1*, 67–80. doi:10.1071/EN04053

Marine Biogeochemistry of Iron

Simon J. Ussher,[A] *Eric P. Achterberg*,[A] *and Paul J. Worsfold*[A,B]

[A] School of Earth, Ocean and Environmental Sciences (SEOES) and Plymouth Environmental Research Centre (PERC), University of Plymouth, Plymouth PL4 8AA, UK.

[B] Corresponding author. Email: pworsfold@plymouth.ac.uk

Environmental Context. *Several trace elements are essential to the growth of microorganisms, iron being arguably the most important. Marine microorganisms, which affect the global carbon cycle and consequently indirectly influence the world's climate, are therefore sensitive to the presence of iron. This link means iron-related oceanic processes are a significant ecological and political issue.*

Abstract. The importance of the role of iron as a limiting micronutrient for primary production in the World Ocean has become increasingly clear following large-scale in situ iron fertilization experiments in high-nutrient, low-chlorophyll (HNLC) regions.[1] This has led to intensive international research with the aim of understanding the marine biogeochemistry of iron and quantifying the spatial distribution and transport of the element in the oceans. Recent studies have benefited from improved trace metal handling protocols and sensitive analytical techniques, but uncertainties remain concerning fundamental processes such as redox transfer, solubility, adsorption, biological uptake, and remineralization.

This review summarizes our present knowledge of iron biogeochemistry. It begins with a discussion of the effects of the physicochemical speciation of iron in seawater from a thermodynamic perspective, including important topics such as inorganic and organic complexation and redox chemistry. This is followed by an overview of the fluxes of iron to the ocean interface and a description of iron cycling within the open ocean water column. Current uncertainties of iron biogeochemistry are highlighted and suggestions of future work provided.

Keywords. aerosols — biogeochemistry — iron — marine chemistry — redox reactions

Manuscript received: 30 June 2004.
Final version: 3 August 2004.

Introduction

An estimated 40% of photosynthesis on Earth occurs in aquatic environments[2] and the turnover time for marine plant biomass is nearly three orders of magnitude faster than that of terrestrial biomass.[3] Hence, the nutrients that regulate primary production in the marine environment have a significant effect on the global carbon cycle and consequently play a key role in controlling the world's climate.

Protein-bound iron complexes act as vital electron mediators for many metabolic processes in living systems. Iron complexes have important functions in intracellular respiration, oxygenic and non-oxygenic photosynthesis, and the element is further utilized by respiring higher organisms for oxygen transport.[4] Within aquatic photosynthetic organisms, iron is found as an essential component in photosynthetic apparatus (i.e. photosystems (PSI, PSII) and cytochromes) and for ATP synthase.[3] It is also required for nitrogen fixation and reduction of nitrate, nitrite, and sulphate.

In most oceanic regions, primary production is limited by light and macro-nutrients (i.e. nitrate, phosphate, and silicate) but approximately 40% of the world's surface waters are replete with major nutrients.[5] These regions have been named HNLC areas, the most important regions being the Southern Ocean, the Equatorial Pacific, and the Subarctic Pacific.

The observation that neritic waters near these regions often sustained far greater phytoplankton communities compared to the nearby open ocean waters led early workers to hypothesize that trace elements are essential for phytoplankton growth.[6] For example, Harvey[7] suggested that iron and manganese could become growth-limiting to phytoplankton, based on experiments that showed increased growth of diatoms and dinoflagellates after additions of iron and manganese to Southern Ocean seawater that was rich in phosphate and nitrate. Despite these early observations, there were few major advances in the knowledge of the significance of iron in these areas until the late 1980s when the first reliable iron determinations were made in the Pacific Ocean as part of the VERTEX programme.[8–10] These measurements were made possible by the sampling and analytical techniques previously developed by Bruland et al.[11]

1448-2517/04/020067

In addition to the vertical concentration profiles obtained at this time, ship-board experiments using iron additions to fresh seawater samples revealed that iron-limited regimes existed in the nutrient-rich, upwelling areas of the Subarctic and Equatorial Pacific.[12] Using the same methodology, it was also confirmed that there was also a definite relationship between ambient iron concentrations and phytoplankton growth in the Southern Ocean, when neritic (coastal) and pelagic (open ocean) waters were compared.[13]

In accordance with this, Martin published the 'Iron Hypothesis' in 1990.[14] This was based on an inverse correlation found between carbon dioxide and iron concentrations (inferred from aluminium data) in the Vostok ice cores. It was found that the trends corresponded with glacial and interglacial transitions. Martin proposed that an increase of iron input to HNLC oceanic regions, by means of higher dust loading, could stimulate primary production. Furthermore, it was suggested that this phenomenon had the potential to cause intense drawdown of carbon dioxide, reduce atmospheric temperatures, and hence cause significant global climate change.

The validity of this hypothesis has since been contested. Models based on global iron data and data from fertilization experiments estimated that realistic iron forcing could cause a maximum of ~50% of the CO_2 change expected during glacial–interglacial periods[15,16] but the remaining change was predicted to be due to other mechanisms, such as changes in ocean circulation and sea-ice extent. In addition, examination of sediment cores in the North Atlantic Ocean indicated that dust deposition fluxes in the Northern Hemisphere at the time of the penultimate deglaciation do not correlate with the change in CO_2 concentration in the Vostok ice cores.[17] However the affirmation of iron-limited HNLC areas, combined with the correlations observed in the Vostok ice cores, provide evidence that iron distribution is at least potentially an important control for global primary productivity and climate.

The fact that bottle experiments did not represent large-scale biological processes in the ocean, along with the development of artificial conservative tracers (i.e. SF_6) led to the instigation of in situ iron fertilization experiments. These have now been conducted in the Equatorial Pacific (e.g. IronEx I and IronEx II[1,18–20]), the Southern Ocean (e.g. SOIREE[21] and SOFeX[22]) and the Subarctic Pacific (e.g. SEEDS[23]), showing that primary productivity is iron-limited in these areas. In recent years, it has also become apparent that iron may play a vital intermediary role in nutrient cycling in low and mid-latitudes due to its involvement in nutrient cycling processes, such as nitrogen fixation. Iron-limited growth has been found in coastal upwelling areas[24–27] and iron co-limitation has been observed in areas such as the Northeast Pacific Ocean[28] and the Northwest Indian Ocean.[29]

General conclusions about HNLC waters drawn from these experiments were:

Certain phytoplankton species benefited more from iron addition (usually large diatoms and flagellates).
The efficiency of iron cycling depends on the conditions and ecology of the area.[30]
Zooplankton grazers were often quick to respond to increased numbers of phytoplankton.
The long-term fate of sequestered carbon remains uncertain, i.e. no evidence of significant carbon export to deep waters has been observed.

There is increasing evidence that the extent of iron limitation in a given water mass is likely to vary according to the species of organisms present in natural assemblages. This variation contributes to the increasing complexity of defining 'nutrient limitation' when discussing marine ecosystems.

Following the success of iron fertilization experiments, the possibility of industrial-scale iron fertilization of the oceans has been discussed as a means of reducing atmospheric CO_2 concentrations.[31] However, a number of possible ecological

Simon Ussher is completing his Ph.D. thesis on iron(II) biogeochemistry in the Northeast Atlantic as part of the EU-funded IRONAGES project. This work has involved four cruises (CLIVAR Transect, Southern Ocean, R.V. Aurora Australis, Oct–Dec 2001; IRONAGES Cruise, European Continental Shelf, R.V. Pelagia, Mar–Apr 2002; IRONAGES Cruise, Canary Basin, R.V. Pelagia, Oct 2002; Sargasso Sea, R.V. Weatherbird, Jul–Aug 2003).

Eric Achterberg has been at the School of Environmental Sciences, University of Plymouth, since 1994. His interests are the aquatic biogeochemistry of trace metals (including speciation), nutrients, and their interaction with organisms. Current projects include iron uptake by marine phytoplankton, the application of in situ voltammetric trace metal monitors for biogeochemical studies, and the development and application of spectroscopy-based monitoring equipment. During the last six years, he has attracted about £1 million in research income.

Paul Worsfold has 25 years research experience. He has been Professor of Analytical Science at the UoP since 1990 and Director of the Plymouth Environmental Research Centre since 1995. He has authored over 200 research papers and supervised 36 Ph.D. completions. His major research interests are the design and deployment of instrumentation for monitoring of environmental processes, and the use of this high quality data to elucidate biogeochemical cycles, trends, and transient events. Recent projects include techniques for measuring trace metals in marine waters, advancements in global iron simulations, detection and characterization of iron complexes in seawater, and site characterization of the Southwest European marine sites. Paul Worsfold is a member of the Editorial Advisory Board of Environmental Chemistry.

effects caused by large-scale iron fertilization have been predicted, such as denitrification and nitrate reduction, production of climate changing gases, and anoxia.[32] Furthermore, although CO_2 drawdown has been observed in many of the iron fertilization studies mentioned above, there is at present no conclusive evidence that fertilization increases carbon burial fluxes over long timescales.

Recent attempts to implement international emission targets (such as the Kyoto Agreement) have created the potential for an industry based on the reduction of greenhouse gases. This controversial industry would allow emission targets to be exceeded by a country if it could prove that the excess gases, such as CO_2, were actively being removed from the atmosphere. Due to this, certain organizations, which have foreseen the economic gain from ocean fertilization, have been requesting authorization to begin regular large-scale fertilization[31,33] even though there is no proof that fertilization will cause long-term drawdown of CO_2. The possibility of industrial-scale ocean fertilization has initiated considerable response from the scientific community, including public warnings of the unknown ecological effects and protests against countries assuming the right to 'use the world's oceans to resolve its domestic problems'.[34]

Clearly, the study of iron and macronutrients in marine biogeochemical cycles has become of great scientific, ecological, and political significance. It follows that to improve our understanding of important issues, such as the physicochemical transformations of iron occurring in seawater and the large-scale biological feedback mechanisms that may influence global climate, a detailed knowledge of iron biogeochemistry, transport, and distribution is required.

Iron Speciation in Seawater

The Crustal Abundance of Iron

Iron is the fourth most abundant element in the Earth's crust, exceeded only by oxygen, silicon, and aluminium. Its high relative abundance of 5.6%[35] in the Earth's crust can be attributed to the highly stable ^{56}Fe nucleus. This is the largest nucleus formed exothermically by nuclear fission during planetary formation and is known to have the highest nuclear binding energy per nucleon of all nuclei.[36] Iron has six known isotopes, from ^{54}Fe to ^{59}Fe. The percentage abundances of the more common isotopes ^{54}Fe, ^{56}Fe, and ^{57}Fe are 5.82, 91.66, and 2.19% respectively, resulting in a relative atomic mass of 55.847 amu.[37] Due to its high crustal abundance, iron compounds make up a large proportion of the Earth's rocks and soils. Iron forms salts with most inorganic anions in the solid phase but exists predominantly as oxides and carbonates, stabilized by their negative Gibbs free energies of formation (Fig. 1).

The most commonly occuring compounds in iron ores are haemetite (Fe_2O_3), magnetite (Fe_3O_4), limonite ($2Fe_2O_3 \cdot 3H_2O$), siderite ($FeCO_3$), and pyrite (FeS_2).[38] Due to the high stability of these compounds, efficient separation of iron from its ores requires highly energetic and strongly reducing conditions. Further still, it goes some way in explaining why, despite being ubiquitous in the Earth's crust, iron is found at trace concentrations within many aqueous environments.

The physicochemical speciation of iron in seawater is dependent on the heterogeneous equilibrium between various particulate and dissolved phases (see Fig. 2). The concentration of iron in the solid and particulate phases is therefore dependent on the rate of each process and the composition of the seawater. These processes are further complicated by the existence of redox transitions between the ferric and the more soluble ferrous forms.

In order to understand the processes that control iron marine biogeochemistry, the species that are investigated must be clearly defined. Size fractionation is particularly important due to the broad variety of iron species that

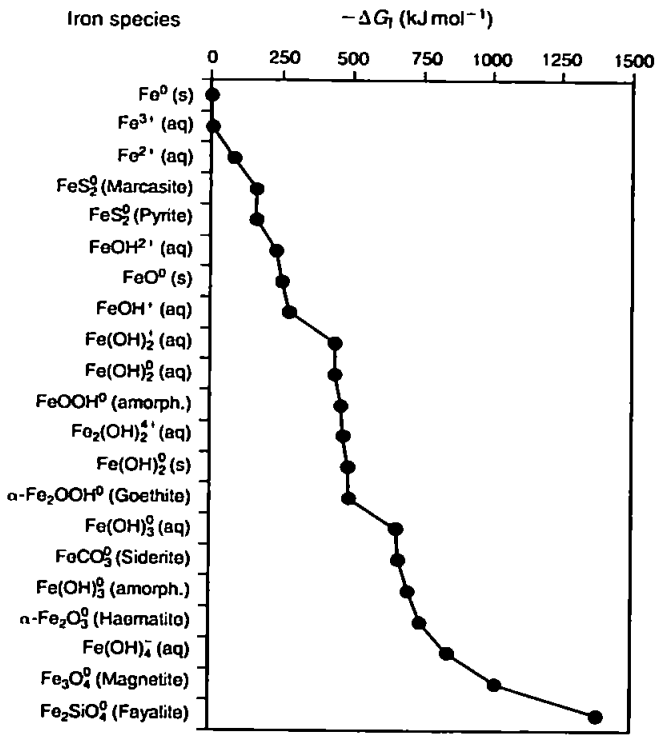

Fig. 1. Gibbs free energies of formation ($-\Delta G_f$) for common inorganic iron compounds. Plotted using tabulated values from Stumm and Morgan.[39]

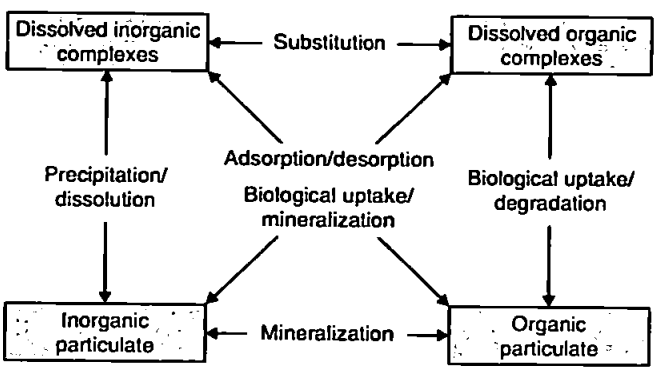

Fig. 2. Phase transfers of iron and related processes in seawater.

are thought to exist in seawater, including colloidal phases and macromolecules. Historically, dissolved iron has been defined as that which passes through a 0.2–0.45 μm filter membrane, but the recent development of ultra-filtration techniques allows improved characterization of different size fractions.[40,41]

Dissolved Inorganic Iron Speciation

Under most natural conditions, iron is found in the +2 and +3 oxidation states and forms salts with the majority of common anions. In aerated aqueous solutions at circumneutral pH the hexaaqua iron(III) cation becomes hydrolyzed, followed by the formation of polynuclear oxy-hydoxides. As a result, when the pH of an acidic solution is increased the solubility of the ions decreases, reaching a minimum at around pH 8. A solubility value of $\sim 10^{-11}$ M has been reported for 0.7 M NaCl solutions (pH 8.1, 25°C) where soluble iron was defined as that which passed through a 0.02 μm filter.[42] The solubility of iron(II) far exceeds that of iron(III). Under anoxic conditions, iron(II) is often found at millimolar concentrations but in air-saturated solutions and at high pH (>5) it becomes unstable and oxidizes rapidly.

The dissolved inorganic speciation of iron in seawater can be estimated using experimentally determined equilibrium constants (conditional stability constants), found for the most common inorganic iron species in seawater.[43–47] The speciation diagrams (Figs 3 and 4) show the calculated proportions of inorganic iron(III) and iron(II) species in seawater at 25°C; recently reported hydrolysis constants were used.

An ambient seawater chloride concentration (0.55 M) was used in the iron(III) model (Fig. 3) to represent an example of one of the simple anions that exist at high concentrations in seawater and associate with iron(III). At low pH, sulphate and fluoride behave in a similar manner. The most important trend to note is that the hydrolysis species are predicted to dominate when the pH value of the solution is greater than 4. This is due to the increase in activity of hydroxide anions at higher pH and the strong affinity of iron(III) for charged oxygen species as ligands.

Iron(II) behaves very differently, having relatively weak associations at pH values less than 7. At higher pH, inorganic complexation occurs when carbonate and hydroxy anions are more abundant. Interestingly, the solubility of iron(II) is predicted to be dependant on whether the seawater is in equilibrium with the atmosphere due to the formation of the insoluble $FeCO_3$ (siderite) species. Fig. 4 shows an open system in which there is considered to be continuous CO_2 exchange.

Dissolved Organic Iron Complexes in Seawater

Iron(III) has been found to be >99% complexed by strong organic ligands in seawater, even in intermediate and deep waters,[48–52] and two classes of strong iron-binding ligands (L_1, L_2) have been characterized and determined in open ocean seawaters. The complexing ability of iron-binding ligands is measured under ambient conditions and is expressed using conditional stability constants $K_{Fe^{3+}L}$ from the equilibrium of Eqn 1:

$$K_{Fe^{3+}L} = \frac{[FeL]}{[Fe^{3+}][L]} \quad (1)$$

A recent study of iron binding ligand stability constants in seawater summarized constants for all classes of ligands obtained in nine different oceanic regions.[53] The overall mean ($\pm 1\sigma$) $\log_{10} K_{Fe^{3+}L}$ for all the data reported was 21.4 ± 1.5 and the range of ligand concentrations [L] was 0.31–39.2 nM. All workers used similar methodologies; therefore it can be assumed that these values are representative iron-binding ligands in most oceanic regions. The consistency of these values with other thermodynamic data can be validated with the inorganic iron speciation model (Fig. 3). For example, if a theoretical ligand concentration [L_1] of 1 nM and the mean reported value of $\log_{10} K_{Fe^{3+}L}$ (shown above) are used, 99.8% of the total iron(III) is predicted to be bound by organic ligands at pH 8.0, similar to that observed in seawater samples (>99%). Therefore the presence of strong organic chelation has a significant effect on the speciation and solubility of iron in seawater.

Evidence that organic complexation increases iron solubility in seawater has been reported for 0.7 M NaCl solutions after the addition of humic acid and EDTA[42] and for seawater exposed to ultraviolet (UV) light. Furthermore, Kuma

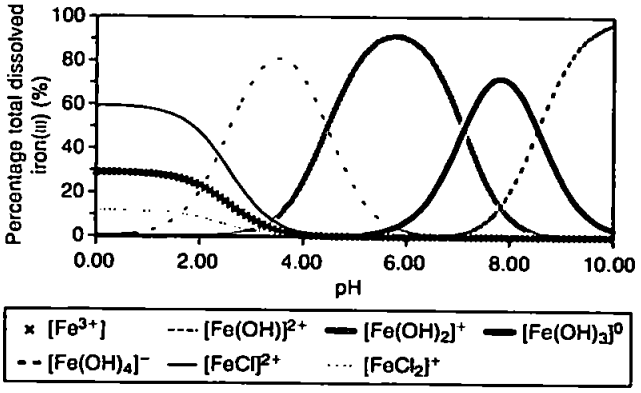

Fig. 3. Inorganic speciation model of Fe(III) in seawater. Calculated using the hydrolysis stability constants of Liu and Millero[47] measured in seawater and the chloride stability constants of Millero et al.[44]

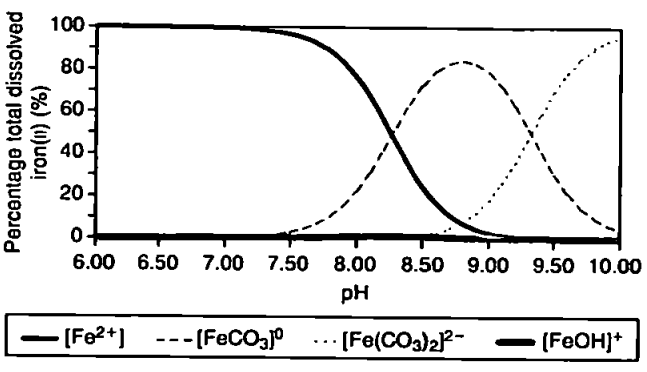

Fig. 4. Inorganic speciation model of Fe(II) in seawater. Calculated using the hydrolysis stability constants of Millero et al.[44] measured in seawater. Dissolved inorganic carbon modelled as an open system in equilibrium with the atmosphere under ambient conditions.

et al. found that the solubility of iron in oceanic water exposed to UV for 3 h was reduced by one order of magnitude. A comparison of the effect of UV treatment on coastal and open ocean waters as well as surface waters and deep waters was also described. The results indicate that although the binding constants of strong organic iron ligands are similar, some are more resistant to UV radiation.[54,55]

Dissolved Iron Complexation and Redox Transitions

The chemistry of the ferrous and ferric cations is extensive and a broad range of stereochemistries have been observed for natural and synthesized iron(II) and (III) complexes with coordination numbers from four to ten.[38] Iron(II) and (III) cations share similar characteristics but the effect of the difference of a single electron on the chemistry of both cations is considerable (i.e. difference in d^5 and d^6 configurations). One example is the effect on the size of their ionic nuclei; iron(II) has reported ionic radii of 75–106 pm whereas iron(III) is 63–92 pm.[56] Furthermore, the differences in their aqueous chemistry are best explained in terms of the free energies of the cations themselves and the ligand field stabilization energies (LFSE) of their bonding orbitals.

With a few exceptions (such as distorted complexes found with some stronger ligands) both cations are most often found in high- and low-spin octahedral states. The importance of the variation in LFSE should be emphasized as it can be used to explain the stability of oxidation states in different ligand fields. This is particularly true when comparing high- and low-spin compounds. For example, iron(II) in a high-spin state has a LFSE of $\Delta^\circ = 2/5$, whereas in a low spin state it has a LFSE of $\Delta^\circ = 12/5$, therefore gaining considerable stability in higher ligand fields where the effect of spin-pairing energy becomes less significant.

Iron(III) retains a high-spin, octahedral configuration in most of its complexes except with ligands that are high in the spectrochemical series. The high LFSE generated when bonding with ligands of this kind can cause spin-pairing in the t_{2g} orbitals (e.g. with bipyridyl and cyanide anions).[57] Iron(III) is a hard metal ion, acidic in nature, and forms its strongest complexes with O, N, and F donor ligands, particularly when they are negatively charged. Most iron(III) complexes absorb photons in the UV end of the spectrum and are often colourless due to the spin-forbidden nature of the d–d transitions. Iron(III) also forms strong chelates and a large variety of cluster compounds either with other iron(III) atoms or other transition metals directly or through oxo and hydroxo bridges.

Iron(II) is a borderline metal ion, between hard and soft cations, and forms complexes that are often coloured. It therefore gains stability in complexation with both soft bases, such as P or S ligands, as well as the stronger electron-pair donating ligands that bind strongly with iron(III). Similar to iron(III), iron(II) is most commonly found in the high-spin state but forms fewer complexes with O-donor ligands. Iron(II) gains the greatest LFSE in low-spin octahedral complexes with strong π-acceptor ligands such as cyanide and 1,10-phenanthroline.

To understand the redox equilibrium between aqueous inorganic iron species in seawater, both redox states must be considered with varying pH and electron activity (pE).[58] Oxic inorganic solutions at seawater pH, are predicted to contain negligible iron(II) concentrations at equilibrium.[39] However, due to the high percentage of organically complexed iron species in seawater, the dissolved iron redox speciation may not be controlled by the pH-dependant equilibria of free hydrolysis species but by the effect of pH and pE on the organic complexes formed in seawater. This type of thermodynamic control would mean that the iron redox speciation in seawater is dependant on the physicochemical properties of the organic complexes present.

The reduction potentials of individual iron complexes can be used to estimate the equilibrium ratio of iron(II) and (III) species under different conditions. Complexes with high reduction potentials will favour iron(II) whereas those with low reduction potentials will favour iron(III) (see Fig. 5). The redox speciation of individual iron species under oxic conditions can be calculated using Eqn 2:

$$pE_{O_2/H_2O} = pE^\circ_{Fe(II)/Fe(III)} - \log \frac{[Fe(II)]}{[Fe(III)]} \qquad (2)$$

Using this Equation and assuming a seawater pE of 12–14, the standard reduction potential (E°_H) required to give an equilibrium ratio of 0.01 for [Fe(II)L]/[Fe(III)L] in seawater would be greater than 0.65 V, which is higher than the reduction potentials of most natural iron-binding chelates (e.g. Fig. 5).

Indeed, recent thermodynamic data have shown that a large proportion of naturally occurring strong iron-binding ligands (such as porphyrins and siderophore–iron complexes) have reduction potentials that are significantly lower than 0.65 V[59,60] and are unlikely to stabilize iron in the ferrous form in oxygenated seawater. However many of these complexes are more reactive and soluble than the inorganic hydrolysis species, and therefore may be reduced by processes such as Haber–Weiss cycling and photoreduction,

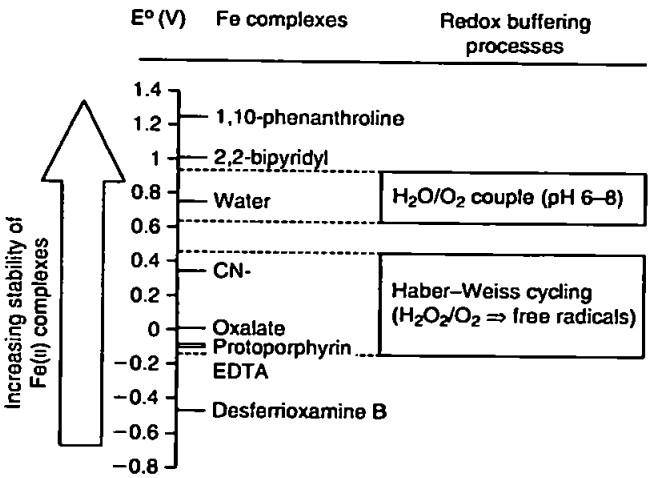

Fig. 5. Standard redox potentials of well-known iron complexes and redox buffering reactions that occur in oxic waters.

hence kinetic models are often adopted to estimate iron redox speciation.

The Kinetics of Iron(II) Oxidation

The kinetics of oxidation of iron(II) have been investigated in natural[61–65] and artificial seawaters.[58] Millero and coworkers[62] confirmed that oxidation rate constants have a positive relationship with pH and temperature, and all workers have found the pseudo-first-order half-life of iron(II) in natural and artificial seawater at ambient conditions (pH 8, 25°C) to be in the order of minutes (see Table 1).

The oxidation of iron(II) is reported to proceed predominantly according to the Haber–Weiss mechanism,

$$\mathrm{Fe(II)} + \mathrm{O_2} \xrightarrow{k_1} \mathrm{Fe(III)} + \mathrm{O_2^{\bullet -}}$$

$$\mathrm{Fe(II)} + \mathrm{O_2^{\bullet -}} + 2\mathrm{H^+} \xrightarrow{k_2} \mathrm{Fe(III)} + \mathrm{H_2O_2}$$

$$\mathrm{Fe(II)} + \mathrm{H_2O_2} \xrightarrow{k_3} \mathrm{Fe(III)} + \mathrm{HO^{\bullet}} + \mathrm{OH^-}$$

$$\mathrm{Fe(II)} + \mathrm{HO^{\bullet}} \xrightarrow{k_4} \mathrm{Fe(III)} + \mathrm{OH^-}$$

for which Eqn 3 expresses the rate equation for a solution of defined pH, temperature, and salinity:

$$-\frac{\mathrm{d[Fe(II)]}}{\mathrm{d}t} = 2K_1[\mathrm{O_2}][\mathrm{Fe(II)}] + 2K_3[\mathrm{H_2O_2}][\mathrm{Fe(II)}] \quad (3)$$

The Haber–Weiss mechanism illustrates the importance of dissolved oxygen and hydrogen peroxide on iron(II) oxidation rates. Other inorganic side reactions, such as those of superoxide and redox-active transition metals (e.g. copper), have also been shown to be important but the most significant rate-determining step in the oxidation mechanism remains the reaction of inorganic and organically complexed iron with molecular oxygen.[64]

The relationship between the speciation of iron(II) and its oxidation rate has gained considerable attention. King et al.[67,68] and Millero et al.[62,63] have described the effects of inorganic speciation, focussing mainly on the common inorganic iron complexes in seawater. Results show that species such as $FeCl^+$ alter the oxidation rate but the most striking observation was the increase in the rate for carbonate and hydroxy species, which form a significant fraction of the inorganic ferrous species at higher pH (>7). Similar to the thermodynamic treatment above, an estimation of whether a complexed ligand will decrease or increase the oxidation rate of iron(II) can be estimated by comparing the equilibrium constants, ΔG_F values, or reduction potentials of the iron(II) and (III) species.

In accordance with this, organic ligands have been found to both stabilize and promote the oxidation of iron(II). Generally, oxygen ligands that form highly stable iron(III) complexes (e.g. EDTA, NTA, citric acid, desferrioxamine) are found to increase the rate of iron(II) oxidation whereas nitrogen or sulfur ligands inhibit it.[69] At circumneutral pH, organic compounds commonly found from biological decay have been seen to retard the oxidation of iron(II) for up to several days.[70,71] A study of the effects of some common amino acids on iron(II) oxidation at pH 6–8 revealed cysteine to be among these compounds,[72] whereas naturally occurring strong iron-binding ligands such as fulvic acid and oxalate have shown an accelerating effect.[64,73]

Table 1. Reported half-lives for iron(II) oxidation in natural and artificial seawater
Measured at 25°C

Medium	pH	$t_{1/2}$ [min]	Ref.
North Sea Seawater	8.0	~1.5	[61]
Gulf Stream Seawater	8.0	~1.2	[62]
Australia (NSW), Coastal Water	8.09	~3.5	[64]
0.7 M NaCl	7.83	~1	[66]

Reduction of Iron(III) in Seawater

Despite thermodynamic redox speciation calculations predicting negligible concentrations of iron(II), the dynamic and variable chemistry of seawater means that this is not always the case. Physicochemical reduction processes of iron in seawater have been observed to cause significant pseudo-steady-state concentrations to persist under natural oxic conditions. The most studied physicochemical process of iron(II) production in surface seawater is photoreduction. This occurs when UV irradiation causes direct and indirect photoreduction of colloidal and dissolved ferric species. Indirect photoreduction results from the reaction of iron(III) with reducing species produced during irradiation, whereas direct photoreduction refers to ligand–metal charge transfer (LMCT) reactions caused by photon absorption by iron complexes. Direct photoreduction is known to reduce the monohydroxide ferric species[74] and a number of organically complexed dissolved species via LMCT reactions (see ref. [75] and references therein), including certain siderophore chelates.[76]

Reduction of iron complexes is important in surface seawater as most of the dissolved iron is organically complexed, and reductive dissociation in the presence of phytoplankton may provide a source of bioavailable iron to phytoplankton.[50,77] In addition, several studies have shown the importance of the photoreduction of colloidal iron in seawater[78–81] although the nature of the colloids that promote photoreduction in seawater is unknown.

Diel variations of subnanomolar (0.1–1 nM) concentrations of iron(II) in naturally irradiated coastal water have been observed.[82] However, according to the model formulated by Johnson et al.[81] photo-produced concentrations of iron(II) in fully irradiated surface waters of open ocean gyres are likely to be in the picomolar range or less (assuming dissolved iron concentrations are ~0.15 nM, which is typical in the Equatorial Pacific).

Biomediated reduction is another process that can generate iron(II) in seawater, although it is unlikely to be as efficient as photoreduction in surface waters. The bioreduction of ferric species is a well-known phenomenon of subsurface

bacteria found in terrestrial and marine sediments. Laboratory studies using cultured bacterial strains (e.g. *Shewanella putrefaciens*[83,84] and *S. alga*[85]) have shown significant reduction rates of ferric colloids under anaerobic conditions. In addition, recent evidence of cell surface reduction has been found for several species of marine phytoplankton (see below) and the chemical reduction of iron by natural organic matter (NOM) has also been observed at pH 3–6, in the absence and presence of light[86] and in the presence of bacteria.[84] Further laboratory and in situ studies are required to confirm whether or not the chemical and biomediated processes mentioned above produce iron(II) at rates that are rapid enough to maintain significant steady-state concentrations of iron(II) in oxic seawater.

Iron Inputs to the Oceans

Iron is transported to the ocean via three major pathways: fluvial (riverine) input, atmospheric deposition, and processes occurring on the sea floor such as hydrothermal venting, sediment resuspension, and diagenesis (see Fig. 6).

To be transported by any of these pathways, iron must firstly become mobilized from the lithosphere by either mechanical action (i.e. erosion) or by thermal and chemical reactions (i.e. leaching, anoxia, or geothermal activity). Once in a mobile phase, many physicochemical processes can occur, altering properties such as solubility and chemical speciation, between the source–ocean interface. Further understanding of the global iron cycle will be gained by determining fluxes of iron to/in the water column of the open ocean and by assessing its transport in marine ecosystems.

Fluvial Inputs

Fluvial inputs transport iron to the coastal zone, following mobilization from soils and rocks. Particulate and dissolved iron concentrations in rivers are typically in the order of 1 mM and 1 μM respectively (the estimated global mean for dFe in major rivers is 0.7 μM[87]). Upon mixing with seawater, both dissolved and particulate iron are scavenged when flocculation occurs within the salinity/pH gradient.[91–94] Estuarine mixing reduces the global dissolved iron flux to the ocean by about 70–95%.[95] Rivers and land run-off are estimated to deliver approximately half of the surface global iron input to the oceans (see Fig. 6), despite a high percentage of mobilized iron being lost in estuaries. Riverine inputs of iron to the oceans are extremely variable and dominated by occasional flood events. Although this pathway is likely to provide the main source of bioavailable iron to many coastal and shelf waters, it remains unknown what proportion of suspended/soluble iron originating from land run-off is transported to open ocean gyres.

Atmospheric Inputs

The importance of the transport of atmospheric iron to the ocean surface is high. Firstly, because it accounts for a major portion of the global iron input to the World Ocean (see Fig. 6) but also because this pathway is considered the principle source of soluble and bioavailable iron to remote open ocean surface waters, often thousands of miles from the aerosol origin.[90] The majority of aeolian iron received by the ocean arrives via wind-transported dust originating from arid and semi-arid landmasses, important areas being North Africa, the Asian deserts, and the Middle East. Due

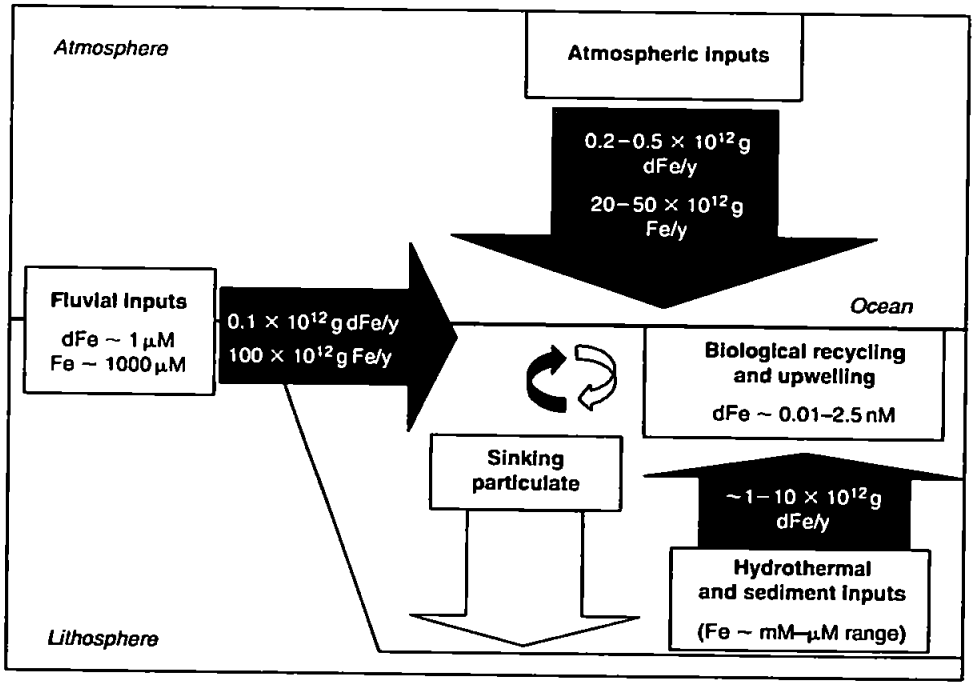

Fig. 6. Global iron transport. Ambient concentrations of dissolved iron (dFe) and particulate iron (Fe) are in white boxes, and approximate annual fluxes are shown in black and white arrows. Approximate values are deduced from refs [87–90,95,96]. Riverine flux is estimated on the basis of 90% loss from estuarine mixing.

to their dependence on meteorological events, rates of dust production and wet/dry deposition to the ocean are sporadic.

Approximate models for global and regional aerosol iron fluxes have been calculated using available field data.[5,97] These demonstrate the magnitude of dust flux to the ocean and the large-scale regional effects of the aforementioned arid areas. The overall annual dust flux to the oceans using the data compiled by Duce et al. has been estimated to be in the region of 500×10^{12} g yr^{-1}.[90] The atmospheric flux of iron to surface waters and its oceanic residence time depend on several factors, the most important being the percentage iron content of the mineral aerosols (for crustal aerosols this is usually assumed to be its abundance in soils and rocks, about 3.5%) and the soluble percentage of iron in aerosols.

At present, a representative global average for the fraction of soluble iron (i.e. <0.2 or <0.45 μm filtered) from aerosols has not been reported, although a value of 2% was used for a recent global biogeochemical model.[5] Laboratory protocols (i.e. leaching conditions) used for dissolution experiments are often different, making results difficult to compare. However, there are trends seen in the data such as the apparent lower solubility of crustal aerosols in comparison with marine and anthropogenic aerosols (see Table 2).

Particulate loading is known to affect iron solubility in seawater. Leaching experiments using marine aerosols in North Pacific surface water gave saturation concentrations of 10–17 nM (dFe).[98] More recently, supporting evidence for this phenomenon was an observed relationship between dust concentration and percentage iron solubility for Saharan dust dissolution in Mediterranean surface water.[99] The authors of this study reported higher solubilities for lower dust inputs and by modelling the relationship they were able to estimate iron solubility for the low ambient dust concentrations in their study area.

Aerosol iron solubility is also dependent on dust composition,[100] meteorological phenomena,[101] and the degree of cloud processing that the aerosol undergoes. Considerable differences have been seen between trace metal enrichment for aerosols of crustal and anthropogenic origin,[102,103] and simulated atmospheric conditions have been observed to cause chemical and photoinduced dissolution of aerosol iron.[104] Due to this, the solubilities of iron in wet precipitation from different study areas are also variable (approximately 10–50%) even when the mean values of each dataset are compared (see Table 3).

Redox speciation changes during the lifetime of wet and dry aerosols are known to enhance iron solubility. This is due to the high solubility of iron(II) compared to iron(III) and the subsequent oxidation of iron(II) to more labile amorphous species on the surface of aerosols.[105] At cloud/rainwater pH values, chemical- or photoproduced iron(II) has been observed to have a half-life in the order of hours to days, and it has been postulated that iron(II) in aerosols is stabilized by organic complexation,[106,107] although little evidence has been reported to confirm this. However, there is increasing evidence that a major portion of dissolved iron in rainwater is organically complexed with ligands such as oxalate.[108]

Due to scavenging, total iron concentrations in wet deposition can be relatively high and are usually between 5–1500 nM (see ref. [101] and references therein). Reported iron(II) percentages of the dissolved iron in precipitation also show high variability (see Table 4). The broad range of iron(II) fractions can be explained in terms of the variables discussed above for total iron dissolution (i.e. aerosol origin, cloud processing). In addition, there is strong proof that iron photoreduction in atmospheric water is closely related to light-induced diurnal cycling, including the redox cycling of other species such as copper, acetate, oxalate, sulfur(IV)/(VI), and hydrogen peroxide.[110–113] The reactions with sulfur are considered particularly important due to the link with dimethyl sulphide (DMS) production as a potential feedback mechanism for atmospheric exchange with phytoplankton.[114]

Hydrothermal Inputs

In the past few decades, high- and low-temperature hydrothermal systems have been identified at spreading centres

Table 2. Percentage soluble iron in collected aerosols

Percentage solubility [%]	Medium	Aerosol	Ref.
		Marine aerosols	
5–50	Seawater, pH 8.11	Central Pacific Islands marine aerosols	[98]
~10	Seawater, pH 5.4–8	Nova Scotia, Canada marine aerosols	[115]
		Crustal origin	
~0.05	Water, pH 3.8–5.3	Capo Verdi, North East Atlantic (Sahara, Niger)	[116]
~0.4	Seawater, pH 8.11	Saharan soil, small grain size	[99]
<0.013–0.2	Water, pH 8	Laboratory acid-cycled Saharan dust	[117]

Table 3. Percentage soluble iron in collected precipitation
Results averaged over several measurements

Percentage solubility [%]	Medium	Precipitation	Ref.
9.6	Rainwater, pH 3–8	Erdemli, Turkey	[118]
26	Rainwater	Wilmington, USA	[101]
37.8	Rainwater	Dunedin, New Zealand	[109]
41	Snow	Eastern Antarctica	[119]

Table 4. Redox speciation of iron in collected precipitation
Results averaged over several measurements marked with*

Percentage Fe(II) in dissolved Fe fraction [%]	Medium	Precipitation	Ref.
24*	Rainwater	Coastal: Dunedin, New Zealand	[109]
60*	Rainwater	Coastal: Wilmington, USA	[101]
25–55	Rainwater	Coastal: Boston, USA	[120]
25–74	Snow		
2–55	Fog, pH 2.2–7.1	Coastal and inland: Los Angeles, Bakersfield, and Delaware Bay, USA	[110]

of mid-ocean ridges. The physicochemical effects of these sources are localized (e.g. high temperatures, low pH, enrichment and depletion of different elements) but seawater end-members produced by these systems are known to have very high iron concentrations, in the region of 1 mM.[121]

The global flux of dissolved iron from hydrothermal activity is estimated to be in the region of $1–10 \times 10^{12}$ g yr^{-1}. This indicates that this pathway is potentially the largest supplier of dFe to deep waters. Nevertheless, it should be noted that sediments in the vicinity of hydrothermal areas have been found to be highly enriched in iron, suggesting that the majority of the dFe precipitates and therefore is not transported away from these areas.

Sediment Inputs

Within marine sediments, iron is generally found to have an abundance of 1–20% (by weight) with the highest enrichment found near hydrothermal areas and ferromanganese nodules.[122] The upper sediments are often found to be areas of high chemical activity where early diagenesis occurs, causing the oxidation of organic matter and, consequently, the utilization of oxidants. The resulting chemical and biologically mediated conditions mean that most particulate iron species are potentially reducible and therefore can be reintroduced into the overlying waters in a more bioavailable form.[123] Recent studies have shown that even highly refractory iron species are reducible by certain bacteria.[124]

As a result of these redox reactions, solubilized iron(II) is often found to accumulate in marine sediments and pore waters under anoxic conditions, often at micromolar concentrations. An example of this was seen over the tan-green colour change in pelagic sediment cores collected from the Peru Basin,[125] which contained iron(II) at 10–40% of the total iron content. However, on account of the rapid oxidation of iron(II) in oxic seawater, it is unlikely to be released into the overlying waters in an inorganic form unless the bottom water is anoxic or there is only a short oxygen penetration depth.[123] Hence dissolved iron(II) and (III) inputs from sediments are only expected to be important in anoxic areas, in areas where there is a significant degree of turbidity, or if there is a gradual release of iron in a chemically stabilized form (e.g. organically complexed).

Iron Cycling in the Oceans

Vertical Distribution

Iron generally has a nutrient-type vertical distribution in open ocean HNLC waters, with depleted dissolved (<0.4 μm) concentrations of less than 0.3 nM in surface waters, increasing to 0.4–1.5 nM below 500 m depth. In oligotrophic areas where the sources of iron are more prominent, surface and intermediate waters are often less depleted in iron and concentrations can be more variable (see Fig. 7). Interestingly, similar deep-water dissolved iron concentrations have been reported for a number of ocean basins (average concentration of 0.76 nM, $n = 30$) and these show little inter-ocean fractionation.[126] This phenomenon is surprising, considering the variability in iron sources and a relatively short residence time in deep waters (~70–200 yr). The consistent solubility observed may be controlled by either equilibrium between dissolved and suspended particulate and/or by the association of iron with strong organic ligands (see above). A model fitted to global datasets has been reported and supports the latter hypothesis,[127] but for it to be valid the complexation reactions must be rapid ($> 10^{-4}$ M^{-1} s^{-1}) and the dissociation slow ($< 10^{-4}$ M^{-1} s^{-1}).[128] Further open ocean studies are required to validate this hypothesis, and hence steady-state control of dissolved iron by association and dissociation of dissolved iron from particles should not be disregarded as an important mechanism for controlling iron solubility in deep waters.[129]

Iron transport in the upper water column is far more dynamic due to intensified biological activity and mixing processes,[130] and the estimated residence times for iron reflect this. For example, residence times for dissolved and particulate iron in the upper 100 m of the Sargasso Sea have been calculated to be about 250 and 18 days, respectively.[106]

The recent global model of Moore et al.[5] indicates that the main processes exporting dissolved iron from the mixed layer in the open ocean to be detrainment and sinking detritus, whereas the main inputs are entrainment and atmospheric deposition, although it should be noted that regional processes such as upwelling are highly significant in certain areas. Within the euphotic zone, iron is also cycled within the biological pool. This has a significant effect on iron transport through the upper water column, and rates of iron uptake by marine organisms and remineralization are estimated to be of the same order as the input and export fluxes, where surface mixed layer global fluxes are in the order of 10^{12} g(Fe) yr^{-1} ($\equiv 2 \times 10^{10}$ mol(Fe) yr^{-1}).[5]

Iron Uptake by Marine Organisms

Marine microorganisms acquire iron by either ion membrane transporters or siderophore systems. Siderophore systems have been observed for terrestrial bacteria and fungi[131] and, more recently, for marine bacteria. They function by the excretion of low molecular weight (300–1000 Da) iron

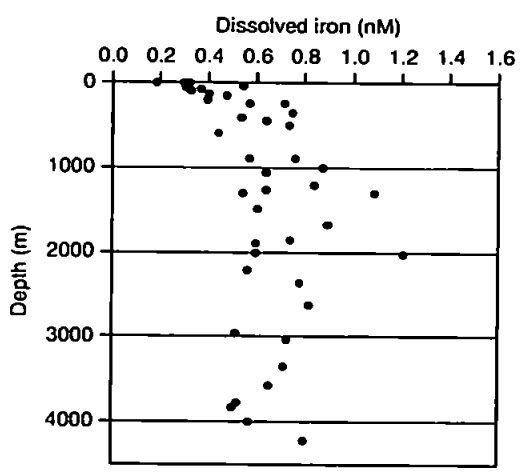

Fig. 7. Dissolved iron (<0.2 μm) profiles from the North-East Atlantic Ocean (IRONAGES Cruises II and III, 2002).

chelators, often found to have hydroxamate or catecholate functional groups, which selectively bind iron(III) and are then transported back into cells via chelate specific transport proteins. Siderophore production is known to be used as an iron uptake mechanism for heterotrophic and cyano bacteria but at present there is no conclusive proof that these systems are used by eukaryotic marine phytoplankton, although they have been observed to utilize siderophore-bound iron.[132,133]

There is growing evidence that siderophore compounds excreted by marine bacteria form a major component of the strong iron-binding ligand pool. For example, production of two classes of ligands (L_1, L_2) were observed during the IronEx II mesoscale iron enrichment experiment following iron addition.[134] These had conditional stability constants in the order of $K_{Fe'L_1L} = 10^{12}\ M^{-1}$ and $10^{11}\ M^{-1}$, respectively (where the constant is calculated for all inorganic iron (Fe′) rather than free Fe^{3+}). The binding constants of these ligands were similar to the binding constants of catecholate and hydroxamate marine siderophores produced by laboratory cultures and low molecular weight ligands extracted from coastal seawater ($K_{Fe'L,Fe} = 10^{11.5}$–$10^{12.5}\ M^{-1}$ [135–137]). The presence of these compounds and their high affinity for iron has been predicted to have significant effects on dissolved iron speciation, such as increased dissolution rates and solubilities of ferric hydroxides.[138]

Marine siderophores that have been characterized are reported to have high cellular membrane affinities or are produced by bacteria associated with particles.[139–142] Repressed siderophore production has been observed under iron-replete conditions[143] but production of characterized siderophores have also been observed in iron-rich coastal waters.[144] Thus, the significance of siderophore production in different regions is unknown, although it is thought to be favoured in low turbulence areas with high concentrations of biomass and dissolved iron.[145]

Ion membrane transporters are used by both marine bacteria and phytoplankton but, unlike siderophore species, iron uptake is directly related to the concentration of free inorganic iron species ([Fe′]). These free species represent charged hydrolysis and mono-substituted inorganic species which are in equilibrium with the less-labile organic species reported for seawater.

It is uncertain whether specific free iron species are preferentially utilized by ion membrane transporters (i.e. free iron(II) or (III)). Furthermore, there is evidence that cell surface mechanisms increase [Fe′] by accessing organically complexed iron (see below). Nevertheless, workers investigating iron uptake by cells often use the 'free ion model', Eqn 4,[146] to interpret data:

$$ML_{org} \longrightarrow M'_{inorg} \underset{k_2}{\overset{k_1}{\rightleftharpoons}} MX_{trans} \xrightarrow{k_{in}} M_{cell} \qquad (4)$$

In this model, k_1 and k_2 are the association and dissociation rate constants, respectively, for free iron binding with trans-membrane ligands, and k_{in} is the rate constant for uptake across a cell membrane. The model assumes that only free inorganic iron becomes bound to transport proteins on the cell membrane, from where it either dissociates back into solution or is transported into the cell. Iron membrane transport is thought to be driven by ATP or electrochemical gradients.[147]

The rate of iron uptake can operate under equilibrium or kinetic control. The former implies that k_1 and $k_2 \gg k_{in}$, whereas kinetic control implies that k_2 is slow and k_1 and k_{in} are fast. Based on experiments on coastal phytoplankton, the rate-determining step is kinetically controlled by the binding of Fe′ to the transporter site. This is ultimately dependent on the loss of water from the Fe′ inner coordination sphere.[146,148,149]

Comparisons of several phytoplankton species revealed that, when normalized to cell surface areas, they all had a similar maximum limit of iron uptake based on the kinetics of iron exchange with transport proteins and the space available on the cell membrane.[149,150] Further interpretation of this phenomenon shows that the surface area to volume ratio of cells becomes important with regards to iron uptake, when diffusion limitation ceases to dominate (cell diameters less than 60 μm).[145]

In situ studies have shown that the uptake of iron by smaller cells is far more efficient when normalized to unit cell volumes. In addition, open ocean phytoplankton are able to reduce their cell sizes to cope with iron limitation and even adapt their metabolism to cope with lower cellular iron requirement for growth.[151,152]

Additional Sources of Bioavailable Iron

Ferric reduction is an important process for organisms that use ion membrane transporters, as it provides a further source of bioavailable Fe′ species for marine organisms and can recycle otherwise refractory iron species. Reduction occurs in marine waters via physicochemical processes (such as photochemical and thermochemical reduction of particle-bound iron or iron chelates) and various forms of biological reduction (see above). However, there is growing evidence that in the absence of sufficient external sources of Fe′, iron-deficient phytoplankton are able to reduce iron(III) chelates, including siderophores, using trans-membrane reductases (e.g. NADH, NADPH). Models relating cell surface reduction to cell radius show that, unlike siderophore systems, larger cells benefit more from this process whereas small cells benefit from the resulting increase of Fe′ in the bulk seawater.[145]

Cell surface reduction of iron chelates has been observed for several species of marine diatoms including *Thalassiosira oceanica*,[153,154] *T. weissflogii*,[155] and *Phaeodactylum tricornutum*.[156] In the case of *T. oceanica*, evidence suggests that iron(II) production can be faster than the cell uptake rate (allowing for a large proportion to diffuse away from the cell) and that it is the resulting oxidized Fe(III)′ species that is taken up by the cell. Furthermore it was observed that the reduction rate was proportional to the logarithm of the ratio of the ferric and ferrous binding constants for individual complexes, i.e. $\log_{10}(K_{Fe(III)L}/K_{Fe(II)L})$.[154]

Particulate iron is another source of Fe′ that can be used by certain marine organisms to satisfy their iron requirements. It has been demonstrated that Fe′ can be obtained by phytoplankton from amorphous iron hydroxides[157,158] and iron bound to natural marine colloids.[84] This can occur either by thermal- or siderophore-mediated dissolution and by plasma membrane reductase mechanisms, such as those described above. Another important pathway for the creation of bioavailable iron is the digestion of colloids and biogenic particles. It has been estimated that the production of bioavailable iron from ingested colloids during protozoan grazing exceeds that of photoreduction when the entire water column is considered.[159] In addition, mixotrophic flagellates can also obtain iron through ingestion of bacteria and this pathway has been estimated to account for to up to ~50% of the total iron uptake by autotrophs in the Equatorial Pacific.[160]

Conclusions

Iron plays a critical role as a limiting micronutrient for primary production in the World Ocean. This review considered the marine biogeochemistry of the element in relation to modelling iron transport and biological utilization in the marine environment. Specific issues that need to be addressed to improve our understanding include the following five items.

Analytical Constraints. In the past decade analytical techniques with picomolar detection limits have been developed for the determination of dissolved iron, but inconsistencies remain between reported dissolved iron datasets (e.g. for aerosol iron solubility and open ocean concentrations). This demonstrates a clear need for a sub-nanomolar iron certified reference material and more reliable protocols for sample collection and filtration, pre-treatment (e.g. acidification), and storage. Consistency between workers will only be achieved by continued international collaboration and rigorous intercomparison exercises, both at sea and in the laboratory.

Sources and Fate of Marine Iron. To improve regional and global iron flux estimates, further temporal and spatial studies of iron distribution and speciation in the open ocean are required. These should include surveys that ascertain the sources and magnitude of iron inputs, e.g. by determining aerosol input fluxes, isotopic abundances, and elemental ratios (Fe/Al for example), as well as tracer studies that target specific processes that transport the element in the water column.

Significance of Iron-Binding Ligands. Speciation studies and global models highlight the importance of experiments that characterize and quantify iron-binding ligands in seawater. Organic complexation strongly influences the thermodynamics of iron and hence its redox state and solubility. In addition, it is predicted that the kinetics of important processes, such as phase transitions, biological uptake, and scavenging, are perturbed by organic complexation. Hence, further laboratory and in situ studies that investigate the effects of complexation on all of these processes are required. In particular, there is a need for data relating to iron(II) complexation.

Kinetics of Complexation. Reported conditional stability constants for natural ligands are becoming more available but there is also a need for conditional kinetic constants for the complexation of iron(II) and (III) with dissolved organic and particle-bound ligands in seawater. This will help to determine the timescales of such reactions and whether they can compete with important mesoscale processes such as precipitation and biological uptake.

Bioavailability and Phase Transitions. Current iron bioavailability models are constrained by the lack of well-defined iron speciation data. Most iron uptake models consider only 'free iron species' (i.e. truly dissolved, unbound species) or biologically produced siderophore species that are targeted by membrane receptor sites, but iron concentrations determined during field and laboratory studies are operationally defined fractions. Therefore obtaining near real-time data describing the fractionation of the iron pool (qualified by size and complexation coefficients) will help to integrate theoretical uptake models with experimental data and better describe the chemistry of iron at cell membranes.

Acknowledgements

The authors would like to thank the Natural Environment Research Council for supporting this work through grant NER/A/S/2003/00489.

References

[1] J. H. Martin, K. H. Coale, K. S. Johnson, S. E. Fitzwater, R. M. Gordon, S. J. Tanner, C. N. Hunter, V. A. Elrod, et al., *Nature* **1994**, *371*, 123. doi:10.1038/371123A0
[2] P. G. Falkowski, *Photosyn. Res.* **1994**, *39*, 235.
[3] A. Jacobs, M. Worwood, *Iron in Biochemistry and Medicine* **1974** (Academic: London).
[4] P. G. Falkowski, J. A. Raven, *Aquatic Photosynthesis* **1997** (Blackwell Science: Oxford).
[5] J. K. Moore, S. C. Doney, D. M. Glover, I. Y. Fung, *Deep-Sea Res. Part II* **2002**, *49*, 463. doi:10.1016/S0967-0637(01)00074-7
[6] T. J. Hart, *Discovery Rep.* **1942**, *11*, 261.
[7] H. W. Harvey, *The Chemistry and Fertility of Sea Waters* **1957** (Cambridge University Press: Cambridge).
[8] W. M. Landing, K. W. Bruland, *Geochim. Cosmochim. Acta* **1987**, *51*, 29. doi:10.1016/0016-7037(87)90004-4
[9] J. H. Martin, R. M. Gordon, *Deep-Sea Res.* **1988**, *35*, 177. doi:10.1016/0198-0149(88)90035-0
[10] J. H. Martin, R. M. Gordon, S. E. Fitzwater, W. W. Broenkow, *Deep-Sea Res.* **1989**, *36*, 649. doi:10.1016/0198-0149(89)90144-1
[11] K. W. Bruland, R. P. Franks, G. A. Knauer, J. H. Martin, *Anal. Chim. Acta* **1979**, *105*, 233. doi:10.1016/S0003-2670(01)83754-5
[12] J. H. Martin, R. M. Gordon, S. E. Fitzwater, *Limnol. Oceanogr.* **1991**, *36*, 1793.
[13] J. H. Martin, R. M. Gordon, S. E. Fitzwater, *Nature* **1990**, *345*, 156.
[14] J. H. Martin, *Paleoceanography* **1990**, *5*, 1.
[15] N. Lefevre, A. J. Watson, *Global Biogeochem. Cycles* **1999**, *13*, 727. doi:10.1029/1999GB900034
[16] A. J. Watson, D. C. E. Bakker, A. J. Ridgwell, P. W. Boyd, C. S. Law, *Nature* **2000**, *407*, 730. doi:10.1038/35037561
[17] B. A. Maher, P. F. Dennis, *Nature* **2001**, *411*, 176. doi:10.1038/35075543

[18] K. H. Coale, K. S. Johnson, S. E. Fitzwater, S. P. G. Blain, T. P. Stanton, T. L. Coley, *Deep-Sea Res. Part II* **1998**, *45*, 919. doi:10.1016/S0967-0645(98)00019-8
[19] R. M. Gordon, K. S. Johnson, K. H. Coale, *Deep-Sea Res. Part II* **1998**, *45*, 995. doi:10.1016/S0967-0645(98)00012-5
[20] K. H. Coale, K. S. Johnson, S. E. Fitzwater, R. M. Gordon, S. Tanner, F. P. Chavez, L. Ferioli, C. Sakamoto, et al., *Nature* **1996**, *383*, 495. doi:10.1038/383495A0
[21] P. W. Boyd, A. J. Watson, C. S. Law, E. R. Abraham, T. Trull, R. Murdoch, D. C. E. Bakker, A. R. Bowie, et al., *Nature* **2000**, *407*, 695. doi:10.1038/35037500
[22] K. H. Coale, K. S. Johnson, F. P. Chavez, K. O. Buesseler, R. T. Barber, M. A. Brzezinski, W. P. Cochlan, F. J. Millero, et al., *Science* **2004**, *304*, 408. doi:10.1126/SCIENCE.1089778
[23] A. Tsuda, S. Takeda, H. Saito, J. Nishioka, Y. Nojiri, I. Kudo, H. Kiyosawa, A. Shiomoto, et al., *Science* **2003**, *300*, 958. doi:10.1126/SCIENCE.1082000
[24] D. A. Hutchins, K. W. Bruland, *Nature* **1998**, *393*, 561. doi:10.1038/31203
[25] K. W. Bruland, E. L. Rue, G. J. Smith, *Limnol. Oceanogr.* **2001**, *46*, 1661.
[26] G. F. Firme, E. L. Rue, D. A. Weeks, K. W. Bruland, D. A. Hutchins, *Global Biogeochem. Cycles* **2003**, *17*, 1016. doi:10.1029/2001GB001824
[27] D. A. Hutchins, C. E. Hare, R. S. Weaver, Y. Zhang, G. F. Firme, G. R. DiTullio, M. B. Alm, S. F. Riseman, et al., *Limnol. Oceanogr.* **2002**, *47*, 997.
[28] M. T. Maldonado, P. W. Boyd, P. J. Harrison, N. M. Price, *Deep-Sea Res. Part II* **1999**, *46*, 2475. doi:10.1016/S0967-0645(99)00072-7
[29] S. Takeda, A. Kamatani, K. E. Kawanobe, *Mar. Chem.* **1995**, *50*, 229. doi:10.1016/0304-4203(95)00038-S
[30] A. R. Bowie, M. T. Maldonado, R. D. Frew, P. L. Croot, E. P. Achterberg, R. F. C. Mantoura, P. J. Worsfold, C. S. Law, et al., *Deep-Sea Res. Part II* **2001**, *48*, 2703. doi:10.1016/S0967-0645(01)00015-7
[31] Q. Schiermeier, *Nature* **2003**, *421*, 109. doi:10.1038/421109A
[32] J. A. Fuhrman, D. G. Capone, *Limnol. Oceanogr.* **1991**, *36*, 1951.
[33] M. Markels, R. T. Barber, in *ACS Natl. Meet., Fuel Chemistry Division* **2001** (ACS: Washington, DC).
[34] R. McKie, in *The Observer*, 12 January **2003**.
[35] S. R. Taylor, *Geochim. Cosmochim. Acta* **1964**, *28*, 1273. doi:10.1016/0016-7037(64)90129-2
[36] S. F. Mason, *Chemical Evolution* **1991** (Clarendon Press: Oxford).
[37] D. R. Turner, K. A. Hunter, H. J. W. de Baar, in *The Biogeochemistry of Iron in Seawater* (Eds D. R. Turner, K. A. Hunter) **2001** (John Wiley: New York, NY).
[38] N. N. Greenwood, A. Earnshaw, *Chemistry of the Elements* **1984** (Pergamon: New York, NY).
[39] W. Stumm, J. J. Morgan, *Aquatic Chemistry, 3rd edn* **1996** (John Wiley: New York, NY).
[40] C. J. Gobler, J. R. Donat, J. A. Consolvo, S. A. Sanudo-Wilhelmy, *Mar. Chem.* **2002**, *77*, 71. doi:10.1016/S0304-4203(01)00076-7
[41] J. Nishioka, S. Takeda, C. S. Wong, W. K. Johnson, *Mar. Chem.* **2001**, *74*, 157. doi:10.1016/S0304-4203(01)00013-5
[42] X. Liu, F. J. Millero, *Geochim. Cosmochim. Acta* **1999**, *63*, 3487. doi:10.1016/S0016-7037(99)00270-7
[43] R. H. Byrne, D. R. Kester, *Mar. Chem.* **1976**, *4*, 255. doi:10.1016/0304-4203(76)90012-8
[44] F. J. Millero, W. Yao, J. Aicher, *Mar. Chem.* **1995**, *50*, 21. doi:10.1016/0304-4203(95)00024-L
[45] K. Kuma, J. Nishioka, K. Matsunaga, *Limnol. Oceanogr.* **1996**, *41*, 396.
[46] R. H. Byrne, Y.-R. Luo, R. W. Young, *Mar. Chem.* **2000**, *70*, 23. doi:10.1016/S0304-4203(00)00012-8
[47] X. Liu, F. J. Millero, *Mar. Chem.* **2002**, *77*, 43. doi:10.1016/S0304-4203(01)00074-3
[48] M. Gledhill, C. M. G. van den Berg, *Mar. Chem.* **1994**, *47*, 41. doi:10.1016/0304-4203(94)90012-4
[49] C. M. G. van den Berg, *Mar. Chem.* **1995**, *50*, 139. doi:10.1016/0304-4203(95)00032-M
[50] E. L. Rue, K. W. Bruland, *Mar. Chem.* **1995**, *50*, 117. doi:10.1016/0304-4203(95)00031-L
[51] J. Wu, G. W. Luther, *Mar. Chem.* **1995**, *50*, 159. doi:10.1016/0304-4203(95)00033-N
[52] R. T. Powell, J. R. Donat, *Deep-Sea Res. Part II* **2001**, *48*, 2877. doi:10.1016/S0967-0645(01)00022-4
[53] A. E. Witter, D. A. Hutchins, A. Butler, G. W. Luther, *Mar. Chem.* **2000**, *69*, 1. doi:10.1016/S0304-4203(99)00087-0
[54] K. Kuma, J. Nishioka, K. Matsunaga, *Limnol. Oceanogr.* **1996**, *41*, 396.
[55] K. Kuma, A. Katsumoto, H. Kawakami, F. Takatori, K. Matsunaga, *Deep-Sea Res. Part I* **1998**, *45*, 91. doi:10.1016/S0967-0637(97)00067-8
[56] J. E. Huheey, E. A. Keiter, R. L. Keiter, *Inorganic Chemistry, 4th edn* **1993** (Harper Collins: New York, NY).
[57] F. A. Cotton, G. Wilkinson, *Advanced Inorganic Chemistry* **1988** (John Wiley: New York, NY).
[58] F. M. M. Morel, J. G. Hering, *Principles and Applications of Aquatic Chemistry* **1993** (John Wiley: New York, NY).
[59] H. Boukhalfa, A. Crumbliss, *Biometals* **2002**, *15*, 325. doi:10.1023/A:1020218608266
[60] D. L. Huffman, M. M. Rosenblatt, K. S. Suslick, *J. Am. Chem. Soc.* **1998**, *120*, 6183. doi:10.1021/JA9704545
[61] E. J. Roekens, R. E. Van Grieken, *Mar. Chem.* **1983**, *13*, 195. doi:10.1016/0304-4203(83)90014-2
[62] F. J. Millero, S. Sotolongo, M. Izaguirre, *Geochim. Cosmochim. Acta* **1987**, *51*, 793. doi:10.1016/0016-7037(87)90093-7
[63] F. J. Millero, S. Sotolongo, *Geochim. Cosmochim. Acta* **1989**, *53*, 1867. doi:10.1016/0016-7037(89)90307-4
[64] A. L. Rose, T. D. Waite, *Environ. Sci. Technol.* **2002**, *36*, 433. doi:10.1021/ES0109242
[65] T. Holland, *Ph.D. Thesis* **2001** (University of Plymouth: Plymouth).
[66] D. W. King, H. A. Lounsbury, F. J. Millero, *Environ. Sci. Technol.* **1995**, *29*, 818.
[67] D. W. King, *Environ. Sci. Technol.* **1998**, *32*, 2997. doi:10.1021/ES980206O
[68] D. W. King, R. Farlow, *Mar. Chem.* **2000**, *70*, 201. doi:10.1016/S0304-4203(00)00026-8
[69] W. T. Welch, Z. Davis, S. D. Aust, *Arch. Biochem. Biophys.* **2002**, *397*, 360. doi:10.1006/ABBI.2001.2694
[70] T. L. Theis, P. C. Singer, *Environ. Sci. Technol.* **1974**, *8*, 569.
[71] C. J. Miles, P. L. Brezonik, *Environ. Sci. Technol.* **1981**, *15*, 1089.
[72] J. M. Santana-Casiano, M. Gonzalez-Davila, M. J. Rodriguez, F. J. Millero, *Mar. Chem.* **2000**, *70*, 211. doi:10.1016/S0304-4203(00)00027-X
[73] D. L. Sedlak, J. Hoigne, *Atmos. Environ.* **1993**, *27A*, 2173.
[74] D. W. King, R. A. Aldrich, S. E. Charnecki, *Mar. Chem.* **1993**, *44*, 105. doi:10.1016/0304-4203(93)90196-U
[75] J. Sima, J. Makanova, *Coord. Chem. Rev.* **1997**, *160*, 161. doi:10.1016/S0010-8545(96)01321-5
[76] K. Barbeau, E. L. Rue, K. W. Bruland, A. Butler, *Nature* **2001**, *413*, 409. doi:10.1038/35096545
[77] W. G. Sunda, S. A. Huntsman, *Mar. Chem.* **1995**, *50*, 189. doi:10.1016/0304-4203(95)00035-P
[78] W. L. Miller, D. Kester, *J. Mar. Res.* **1994**, *52*, 325.
[79] M. L. Wells, L. M. Mayer, *Deep-Sea Res.* **1991**, *38*, 1379. doi:10.1016/0198-0149(91)90012-5
[80] K. A. Barbeau, J. W. Moffet, *Environ. Sci. Technol.* **1998**, *32*, 2969. doi:10.1021/ES9802549
[81] K. S. Johnson, K. H. Coale, V. A. Elrod, N. W. Tindale, *Mar. Chem.* **1994**, *46*, 319. doi:10.1016/0304-4203(94)90029-9
[82] T. D. Waite, R. Szymczak, Q. I. Espey, M. J. Furnas, *Mar. Chem.* **1995**, *50*, 79. doi:10.1016/0304-4203(95)00028-P

[83] S. Glasauer, P. G. Weidler, S. Langley, T. J. Beveridge, *Geochim. Cosmochim. Acta* **2003**, *67*, 1277. doi:10.1016/S0016-7037(02)01199-7
[84] J. Chen, B. Gu, R. A. Royer, W. D. Burgos, *Sci. Tot. Environ.* **2003**, *307*, 167. doi:10.1016/S0048-9697(02)00538-7
[85] E. E. Roden, J. M. Zachara, *Environ. Sci. Technol.* **1996**, *30*, 1618. doi:10.1021/ES9506216
[86] B. M. Voelker, F. M. M. Morel, B. Sulzberger, *Environ. Sci. Technol.* **1997**, *31*, 1004. doi:10.1021/ES9604018
[87] R. F. Stallard, J. M. Edmond, *J. Geophys. Res.* **1983**, *88*, 9671.
[88] J. M. Martin, M. Whitfield, in *Trace Metals in Seawater* (Eds C. S. Wong, E. Boyle, K. W. Bruland, J. D. Burton, E. D. Goldberg) **1983** (Plenum Press: New York, NY).
[89] J. M. Bewers, P. A. Yeats, *Nature* **1977**, *268*, 595.
[90] T. D. Jickells, L. J. Spokes, in *The Biogeochemistry of Iron in Seawater* (Eds D. R. Turner, K. A. Hunter) **2001** (John Wiley: New York, NY).
[91] E. R. Sholkovitz, *Geochim. Cosmochim. Acta* **1976**, *40*, 831. doi:10.1016/0016-7037(76)90035-1
[92] R. M. Moore, J. D. Burton, P. J. Williams, M. L. Young, *Geochim. Cosmochim. Acta* **1979**, *43*, 919. doi:10.1016/0016-7037(79)90229-1
[93] A. Turner, G. E. Millward, *Estuarine, Coastal Shelf Sci.* **1994**, *39*, 45. doi:10.1006/ECSS.1994.1048
[94] S. A. Sanudo-Wilhelmy, I. Riviera-Duarte, A. R. Flegal, *Geochim. Cosmochim. Acta* **1996**, *60*, 4933. doi:10.1016/S0016-7037(96)00284-0
[95] R. Chester, *Marine Geochemistry, 2nd edn* **2000** (Blackwell: London).
[96] H. Elderfield, A. Schultz, *Annu. Rev. Earth Planet. Sci.* **1996**, *24*, 191. doi:10.1146/ANNUREV.EARTH.24.1.191
[97] R. A. Duce, N. W. Tindale, *Limnol. Oceanogr.* **1991**, *36*, 1715.
[98] G. Zhuang, R. A. Duce, D. R. Kester, *J. Geophys. Res.* **1990**, *95*, 16207.
[99] C. Guieu, Y. Bozec, S. Blain, C. Ridame, G. Sarthou, N. Leblond, *Geophys. Res. Lett.* **2001**, *29*, 1911.
[100] X. Zhu, J. M. Prospero, F. J. Millero, D. L. Savoie, G. W. Brass, *Mar. Chem.* **1992**, *38*, 91. doi:10.1016/0304-4203(92)90069-M
[101] R. J. Kieber, K. Williams, J. D. Willey, S. Skrabal, G. B. Avery, *Mar. Chem.* **2001**, *73*, 83. doi:10.1016/S0304-4203(00)00097-9
[102] C. Guieu, R. Chester, M. Nimmo, J. M. Martin, S. Guerzoni, E. Nicolas, J. Mateu, S. Keyse, *Deep-Sea Res. Part II* **1997**, *44*, 655. doi:10.1016/S0967-0645(97)88508-6
[103] N. Kubilay, A. C. Saydam, *Atmos. Environ.* **1995**, *29*, 2289. doi:10.1016/1352-2310(95)00101-4
[104] L. J. Spokes, T. D. Jickells, B. Lim, *Geochim. Cosmochim. Acta* **1994**, *58*, 3281. doi:10.1016/0016-7037(94)90056-6
[105] G. Zhuang, Z. Yi, R. A. Duce, P. R. Brown, *Global Biogeochem. Cycles* **1992**, *6*, 161.
[106] T. D. Jickells, *Mar. Chem.* **1999**, *68*, 5. doi:10.1016/S0304-4203(99)00061-4
[107] R. J. Kieber, J. D. Willey, G. B. Avery, *J. Geophys. Res.* **2003**, *108*, C8 3277. doi:10.1029/2001JC001031
[108] J. D. Willey, R. J. Kieber, K. H. Williams, J. S. Crozier, S. A. Skrabal, G. B. Avery, *J. Atmos. Chem.* **2000**, *37*, 185. doi:10.1023/A:1006421624865
[109] R. J. Kieber, B. Peake, J. D. Willey, B. Jacobs, *Atmos. Environ.* **2001**, *35*, 6041. doi:10.1016/S1352-2310(01)00199-6
[110] Y. Erel, S. O. Pehkonen, M. R. Hoffman, *J. Geophys. Res.* **1993**, *98*, 18423.
[111] D. L. Sedlak, J. Hoigne, *Atmos. Environ.* **1993**, *314*, 2173.
[112] B. Sulzberger, H. Laubsher, *Mar. Chem.* **1995**, *50*, 103. doi:10.1016/0304-4203(95)00030-U
[113] A. C. Saydam, H. Z. Senyuva, *Geophys. Res. Lett.* **2002**, *29*, 1524. doi:10.1029/2001GL013562
[114] G. Zhuang, Z. Yi, R. A. Duce, P. R. Brown, *Nature* **1992**, *355*, 537. doi:10.1038/355537A0
[115] R. M. Moore, J. E. Milley, A. Chatt, *Oceanol. Acta* **1984**, *7*, 221.
[116] K. V. Desboeufs, R. Losno, F. Vimeux, S. Cholbi, *J. Geophys. Res.* **1999**, *104*, 21287. doi:10.1029/1999JD900236
[117] L. J. Spokes, T. D. Jickells, *Aquat. Geochem.* **1996**, *1*, 355.
[118] T. Ozsoy, A. C. Saydam, *J. Atmos. Chem.* **2001**, *40*, 41. doi:10.1023/A:1010602026579
[119] R. Edwards, *Ph.D. Thesis* **1999** (University of Tasmania: Hobart).
[120] G. Zhuang, Z. Yi, G. T. Wallace, *Mar. Chem.* **1995**, *50*, 41. doi:10.1016/0304-4203(95)00025-M
[121] K. L. Von Damm, J. M. Edmond, C. I. Measures, B. Grant, *Geochim. Cosmochim. Acta* **1985**, *49*, 2221. doi:10.1016/0016-7037(85)90223-6
[122] R. Chester, S. R. Aston, in *Chemical Oceanography* (Eds J. P. Riley, R. Chester) **1976**, Vol. 6, pp. 281–390 (Academic Press: London).
[123] R. R. Haese, in *Marine Geochemistry* (Eds H. D. Shulz, M. Zabel) **2000** (Springer: Heidelberg).
[124] D. R. Lovely, *FEMS Microbiol. Rev.* **1997**, *20*, 305. doi:10.1016/S0168-6445(97)00013-2
[125] I. Konig, M. Haeckel, M. Drodt, E. Suess, A. X. Trautwein, *Geochim. Cosmochim. Acta* **1999**, *63*, 1517. doi:10.1016/S0016-7037(99)00104-0
[126] K. S. Johnson, R. M. Gordon, K. H. Coale, *Mar. Chem.* **1997**, *57*, 137. doi:10.1016/S0304-4203(97)00043-1
[127] D. E. Archer, K. Johnson, *Global Biogeochem. Cycles* **2000**, *14*, 269. doi:10.1029/1999GB900053
[128] G. W. Luther, J. Wu, *Mar. Chem.* **1997**, *57*, 173. doi:10.1016/S0304-4203(97)00046-7
[129] E. Boyle, *Mar. Chem.* **1997**, *57*, 163. doi:10.1016/S0304-4203(97)00044-3
[130] D. A. Hutchins, G. R. Di Tullio, K. W. Bruland, *Limnol. Oceanogr.* **1993**, *38*, 1242.
[131] J. B. Neilands, in *Inorganic Biogeochemistry* (Ed. G. L. Eichhorn) **1973** (Elsevier: Amsterdam).
[132] M. T. Maldonado, N. M. Price, *Deep-Sea Res. Part II* **1999**, *46*, 2447. doi:10.1016/S0967-0645(99)00071-5
[133] D. A. Hutchins, A. E. Witter, A. Butler, G. W. Luther, *Nature* **1999**, *400*, 858. doi:10.1038/23680
[134] E. L. Rue, K. W. Bruland, *Limnol. Oceanogr.* **1997**, *42*, 901.
[135] B. L. Lewis, P. D. Holt, S. W. Taylor, S. W. Wilhelm, C. G. Trick, A. Butler, G. W. Luther III, *Mar. Chem.* **1995**, *50*, 179. doi:10.1016/0304-4203(95)00034-O
[136] K. Barbeau, E. L. Rue, K. W. Bruland, A. Butler, *Nature* **2001**, *413*, 409. doi:10.1038/35096545
[137] H. M. Macrellis, C. G. Trick, E. L. Rue, G. Smith, K. W. Bruland, *Mar. Chem.* **2001**, *76*, 175. doi:10.1016/S0304-4203(01)00061-5
[138] T. Yoshida, K. Hayashi, H. Ohmoto, *Chem. Geol.* **2002**, *184*, 1. doi:10.1016/S0009-2541(01)00297-2
[139] M. G. Haygood, P. D. Holt, A. Butler, *Limnol. Oceanogr.* **1993**, *38*, 1091.
[140] G. Xu, J. S. Martinez, J. T. Groves, A. Butler, *J. Am. Chem. Soc.* **2002**, *124*, 13408. doi:10.1021/JA026768W
[141] J. S. Martinez, G. P. Zhang, P. D. Holt, H. T. Jung, C. J. Carrano, M. G. Haygood, A. Butler, *Science* **2000**, *287*, 1245. doi:10.1126/SCIENCE.287.5456.1245
[142] J. S. Martinez, M. G. Haygood, A. Butler, *Limnol. Oceanogr.* **2003**, *46*, 420.
[143] J. Granger, N. M. Price, *Limnol. Oceanogr.* **1999**, *44*, 541.
[144] M. Gledhill, P. McCormack, S. Ussher, E. P. Achterberg, R. F. C. Mantoura, P. J. Worsfold, *Mar. Chem.* **2004**, *88*, 75. doi:10.1016/J.MARCHEM.2004.03.003
[145] W. G. Sunda, in *The Biogeochemistry of Iron in Seawater* (Eds D. R. Turner, K. A. Hunter) **2001** (John Wiley: New York, NY).
[146] R. J. M. Hudson, *Sci. Tot. Environ.* **1998**, *219*, 95. doi:10.1016/S0048-9697(98)00230-7
[147] M. A. Anderson, F. M. M. Morel, *Limnol. Oceanogr.* **1982**, *27*, 789.

[148] F. M. M. Morel, R. J. M. Hudson, N. M. Price, *Limnol. Oceanogr.* **1991**, *36*, 1742.
[149] R. J. M. Hudson, F. M. M. Morel, *Limnol. Oceanogr.* **1990**, *35*, 1002.
[150] R. J. M. Hudson, F. M. M. Morel, *Deep-Sea Res.* **1993**, *40*, 129. doi:10.1016/0967-0637(93)90057-A
[151] W. G. Sunda, S. A. Huntsman, *Mar. Chem.* **1995**, *50*, 189. doi:10.1016/0304-4203(95)00035-P
[152] M. T. Maldonado, N. M. Price, *Mar. Ecol. Prog. Ser.* **1996**, *141*, 161.
[153] M. T. Maldonado, N. M. Price, *Limnol. Oceanogr.* **2000**, *45*, 814.
[154] M. T. Maldonado, N. M. Price, *J. Phycol.* **2001**, *37*, 298. doi:10.1046/J.1529-8817.2001.037002298.X
[155] M. A. Anderson, F. M. M. Morel, *Mar. Biol. Lett.* **1980**, *1*, 263.
[156] P. C. Soria-Dengg, U. Horstmann, *Mar. Ecol. Prog. Ser.* **1995**, *127*, 269.
[157] K. Kuma, K. Matsunaga, *Mar. Biol.* **1995**, *122*, 1.
[158] M. L. Wells, N. G. Zorkin, A. G. Lewis, *J. Mar. Res.* **1983**, *41*, 731.
[159] K. Barbeau, J. W. Moffett, D. A. Caron, P. L. Croot, D. L. Erdner, *Nature* **1996**, *380*, 61. doi:10.1038/380061A0
[160] R. Maranger, D. F. Bird, N. M. Price, *Nature* **1998**, *396*, 248. doi:10.1038/24352

High temporal and spatial resolution environmental monitoring using flow injection with spectroscopic detection

Grady Hanrahan, Simon Ussher, Martha Gledhill, Eric P. Achterberg, Paul J. Worsfold*

Department of Environmental Sciences, Plymouth Environmental Research Centre, University of Plymouth, Plymouth PL4 8AA, UK

This article describes the use of flow-injection techniques combined with molecular spectroscopic detection (spectrophotometry, fluorescence and chemiluminescence) for the rapid determination of chemical parameters in environmental matrices. The emphasis is on field deployment in order to obtain high temporal and spatial resolution data without the need for discrete sample collection and storage. Specific examples considered are the determination of phosphorus in river water and dissolved iron in open ocean water. The environmental drivers for these determinations are presented and the analytical capabilities of flow-injection instrumentation for remote deployment are discussed. © **2002 Published by Elsevier Science B.V. All rights reserved.**

Keywords: Chemiluminescence; Environmental monitoring; Flow injection; Fluorescence; Molecular spectroscopic detection; Spatial resolution; Spectrophotometry; Temporal resolution

1. Introduction

Global water and elemental (for example carbon and phosphorus) cycles are controlled by long-term, cyclical processes and are perturbed on much shorter timescales by anthropogenic activities. A schematic diagram of some of the major global environmental processes controlling these cycles is shown in Fig. 1.

In order to elucidate the mechanistic and kinetic aspects of the processes and to investigate element-specific biogeochemical cycling in particular environmental compartments [1], the acquisition of high-quality analytical data is a pre-requisite. Because of the rapid dynamics of many environmental processes, such as in-stream dynamics of phosphorus exchange in freshwater systems, and spatial variations in concentrations, such as oceanic-scale iron and catchment-scale nutrient distributions, high temporal and spatial resolution data are often required.

Laboratory methods require targets to be met for accuracy (and hence must be free from contamination), precision and detection limits, and possibly sample throughput, cost per sample and waste minimization. Field-based methods pose additional challenges, including the need for robust and reliable instrumentation, fully automated (unattended) operation and data acquisition, on-line sample conditioning (such as filtration), on-board calibration and long term operation [2]. The exact nature of each goal will depend on the location and on the analytical and environmental requirements of the application.

This article discusses the suitability of flow injection (FI) for the continuous monitoring of specific chemical parameters in natural waters. The need for high-quality environmental data with good temporal and/or spatial resolution is discussed with reference to two specific examples: the determination of phosphorus in rivers with high temporal resolution; and, the determination of iron in open ocean waters with high spatial resolution.

*Corresponding author. E-mail: pworsfold@plymouth.ac.uk

0165-9936/02/$ - see front matter
PII: S0000-0000(00)00-

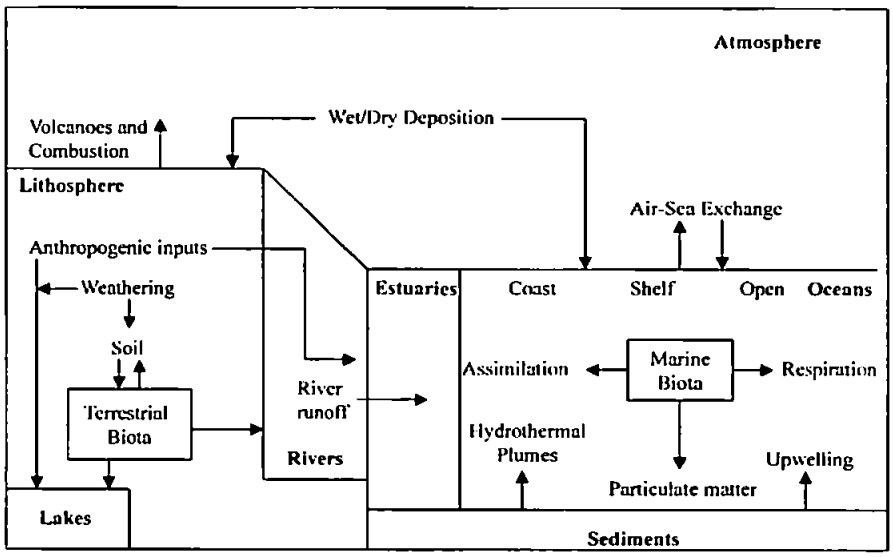

Fig. 1. Schematic diagram of the major global environmental processes.

2. Flow injection

The FI technique is now an established analytical tool for automating wet chemical analyses and facilitating on-line sample treatment (physical and chemical) for a range of detection systems. It is also used in process analysis [3], but this article emphasizes its potential for *in-situ* environmental monitoring. The attractive features of FI for this purpose are shown in Table 1 and a schematic diagram of a 'field' FI analyzer is presented in Fig. 2.

3. Freshwater processes

The behavior of trace elements in freshwater systems is often complex because of the variety of physical, chemical and biological processes involved. In the case of phosphorus, its dynamics in rivers and streams can be very rapid and the rate of cycling between biological, dissolved and particulate compartments (Fig. 3) must be considered [4].

Transformation between the different phosphorus fractions occurs during transport through the catchment and depends upon such processes as desorption, dissolution, extraction and mineralization from soil, plant, stream bed and aquatic biota [5]. Although there are extensive data on phosphorus concentrations in rivers, there is a paucity of information on short-term changes in phosphorus concentrations (and fluxes) during rain events. A critical period for such changes is the onset of high flows in autumn and winter, when terrestrial and sediment-bound phosphorus is rapidly flushed into stream channels.

Continuous monitoring is essential to characterize the nature, magnitude and frequency of these discontinuous inputs of phosphorus into river systems. This will allow a more accurate calculation of fluxes and improved dynamic modeling of in-stream processes. Consequently, the acquisition of high-quality, *in-situ* analytical

Table 1
Attractive features of FI for *in-situ* environmental monitoring

- High temporal and spatial resolution
- Rugged, portable, automated instrumentation
- Contamination-free, enclosed environment
- Sensitive and selective detection
- In-line removal of matrix interferences, such as sea salts
- Long-term stability (reagents, standards, pumps, detector)
- In-line filtration to remove suspended particulate matter
- In-line treatment (for example acid wash) to prevent internalbiofouling
- On-board calibration and quality control (for accuracy)
- Simple, rapid field maintenance

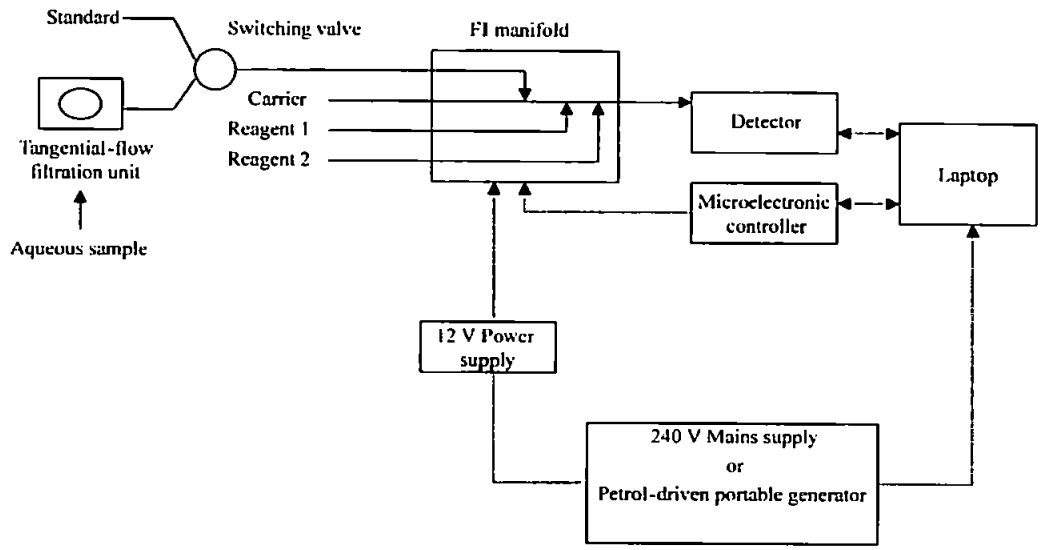

Fig. 2. Block diagram of a flow-injection system for remote environmental deployment.

data with good temporal resolution is required in order to improve our understanding of the biogeochemistry of phosphorus and other trace elements in freshwater systems.

3.1. Monitoring

Table 2 [6–11] lists examples of FI instrumentation that have been used for the *in-situ* determination of nutrients in freshwaters. Historically, field systems have typically incorporated solid-state detection based on light-emitting diodes (LEDs) and photodiodes. Such solid-state detection devices are low cost and rugged [12] but are limited in that they can provide an integrated response only over the spectral bandwidth of the LED (typically 20–30 nm).

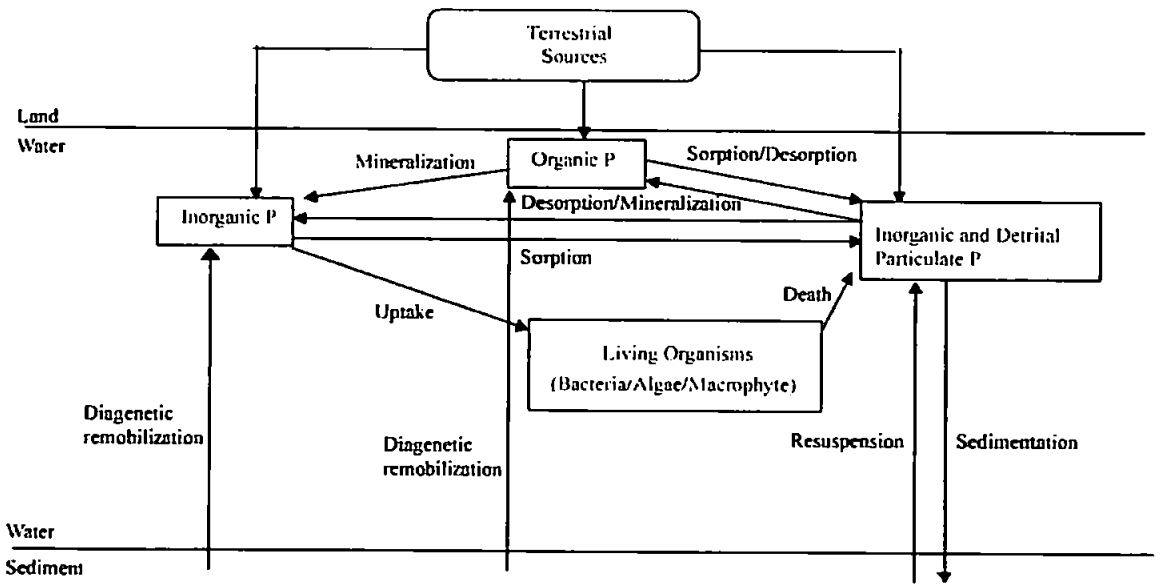

Fig. 3. Phosphorus cycling in freshwater environments.

Table 2
Field deployment of flow-injection instrumentation with spectrophotometric detection for monitoring freshwater environments

Analyte	Matrix	LOD (uM)	Detection	Comments	Ref.
FRP	Riverine	0.67	Miniature CCD		[6]
FRP	Riverine	0.40	LED	Dual photometric detector	[7]
TP	Riverine, wastewater	4.84	LED	UV photooxidation/thermal digestion	[8]
NO_3-N	Riverine	1.71	LED		[9]
NO_3-N	Riverine	0.50	Miniature CCD		[10]
FRP, NO_3-N	Riverine	0.30, 0.70	Spectrophotometry	Micro-flow injection system	[11]

FRP: filterable reactive phosphorus; TP: total phosphorus.

More recently, instrumentation incorporating miniature array detectors has provided enhanced information through full spectral acquisition and signal processing [6,10] but it requires more sophisticated interfacing hardware and software. In this regard, graphical programming packages, such as LabVIEW, have been able to provide excellent control and data-processing capabilities. The use of micro-analytical systems that incorporate miniature solenoid-type pumps and valves for lower reagent consumption and ease of operation is another recent and important development [6,10,11].

4. Marine processes

The carbon cycle is of particular biogeochemical importance, as it acts as a generic indicator of the health of the biosphere [13]. An aspect of the carbon cycle that has attracted considerable attention is oceanic primary productivity, which results in fixation of carbon by photosynthesis and acts as a crucial link in CO_2 exchange between atmosphere and seawater [14]. The rate of primary production depends on the concentration of macronutrients (such as nitrogen, silicon and phosphorus) and micronutrients (such as Co, Zn, Cu and Fe), and, in certain regions, such as the Southern Ocean, iron has been shown to be the limiting nutrient. A detailed understanding of iron-seawater biogeochemistry (Fig. 4) is therefore important for the accurate prediction of net primary production in the world's oceans.

This in turn requires analytical techniques for mapping iron at sub-nanomolar concentrations across ocean and local scale transects, determining its chemical speciation (for example redox states) and studying its uptake by living organisms. Iron, like all nutrients, is distributed across particulate and dissolved phases *via* a variety of biogeochemical processes. The kinetics of these processes are often rapid and sample integrity cannot be guaranteed during storage. Therefore, environmentally relevant measurements can be made only in the field, thus requiring reliable ship-board or *in-situ* analytical techniques.

4.1. Monitoring

For the study of dynamic marine environments, such as estuaries, the high temporal resolution of FI is an attractive feature. Monitoring phosphate concentrations during a tidal cycle, with subsequent flux calculations, is a good example of this application [15]. However, for the study of open-ocean environments, such as the ship-board mapping of dissolved iron, the high spatial resolution and the rapid response of FI are the most important features. As stated above, this is particularly important when sample composition is likely to change during preservation and storage, for example Fe(II)/Fe(III) redox states [19–22]. Because FI effectively isolates the sample from the surrounding environment, contamination from the ship's laboratory is minimized, particularly when the FI analyzer is housed within a portable, laminar flow hood. Other important features of FI for

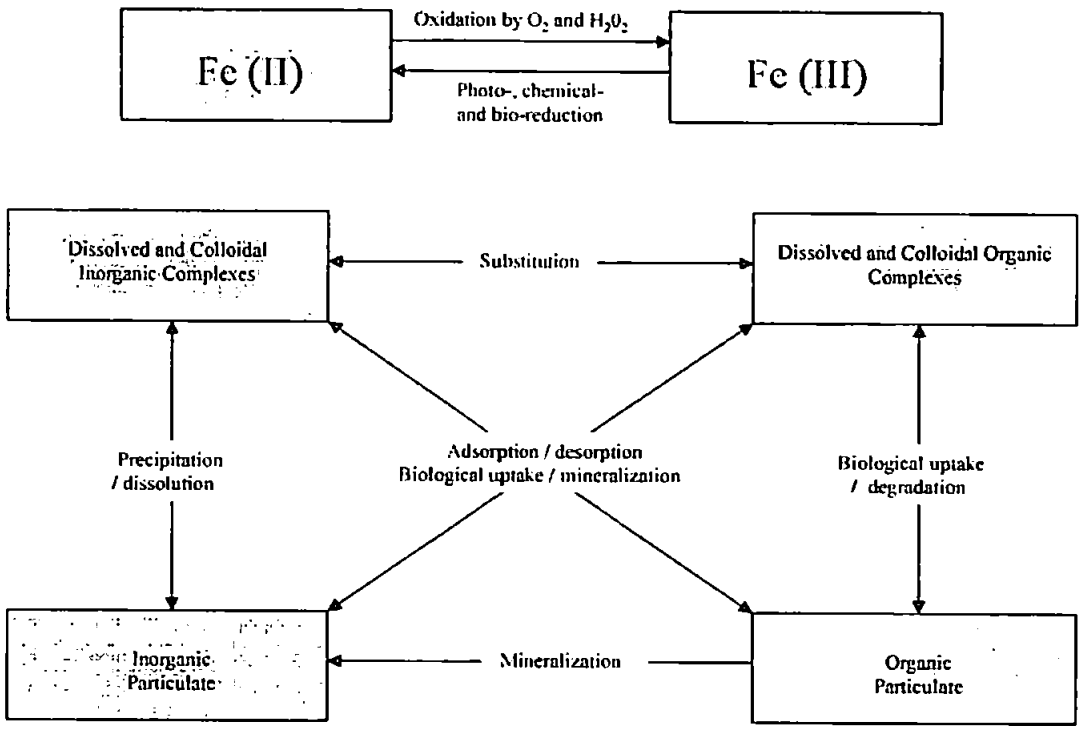

Fig. 4. Speciation of iron in the marine environment.

ship-board monitoring are low reagent consumption, waste containment, high reliability and ease of maintenance.

Current ship-board flow systems use a variety of detection methods in order to maximize the sensitivity, precision and selectivity for individual trace elements. Table 3 lists FI methods that have been used for shipboard measurements of chemical parameters in marine waters. Spectrophotometry, fluorescence and chemiluminescence have all been used for detection, and a common feature of many of the reported methods is the incorporation of a solid-phase micro-column containing an immobilized

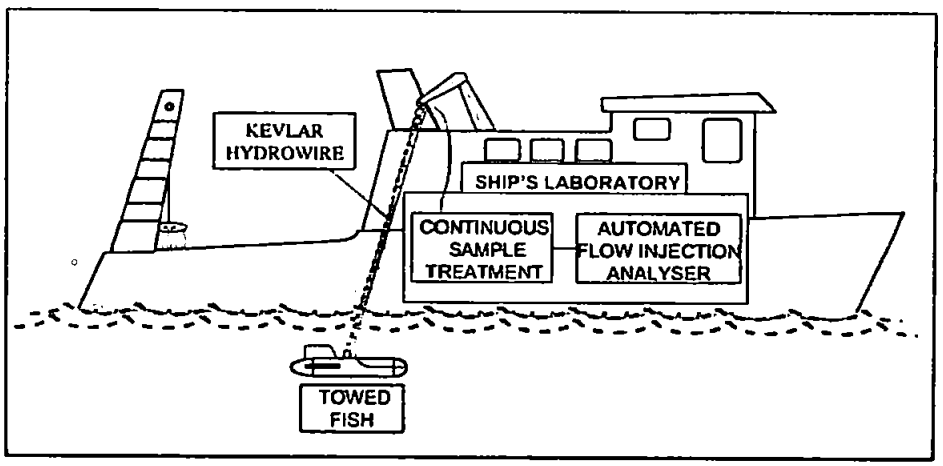

Fig. 5. Schematic diagram of clean, ship-board, sampling and analysis approach.

Table 3
Ship-board and submersible deployment of flow-injection instrumentation with spectroscopic detection for monitoring marine environments

Analyte	Location	LOD (nM)	Detection	Comments	Ref.
Al(III)	Open ocean	0.15	Fluorescence	Lumogallion, Brij-35	[16]
Co(II)	Open ocean	0.5	Chemiluminescence	Gallic acid, hydrogen peroxide	[17]
Cu(II)	Coastal waters	0.1	Chemiluminescence	Hydrogen peroxide, 1,10-phenanthroline	[18]
Fe(II)	Open ocean	0.45	Chemiluminescence	Brilliant sulfoflavin, hydrogen peroxide	[19]
Fe(II)	Open ocean	0.04	Chemiluminescence	Luminol, dissolved oxygen	[20]
Fe(III)	Open ocean	0.01 0.02	Chemiluminescence	Hydrogen peroxide, luminol	[21] [22]
Mn(II)	Coastal waters	0.1	Chemiluminescence	7,7,8,8-Tetracyano-quinodimethane	[23]
Zn(II)	Open ocean	0.1	Fluorescence	*P*-tosyl-8-aminoquinoline	[24]
H_2O_2	Open ocean	10.6	Chemiluminescence	Cobalt(II), luminol	[25]
NO_x	Open ocean	100	Spectrophotometry (with LED)	N1NED, suphanilimide, cadmium reduction, submersible	[26]
NO_2^-, NO_3^-	Open ocean	4.6	Fluorescence	Aniline, imidazole, cadmium reduction	[27]
NH_3,	Open ocean	1	Fluorescence	OPA, dialysis temperature controlled	[27]
$Si(OH)_4$	Coastal waters	300	Spectrophotometry	Ammonium molybdate, tin chloride, submersible analyzer	[28]
pH	Open ocean	-	Spectrophotometry	m-Cresol purple, temperature controlled	[29]
	Open ocean	-	Spectrophotometry	Phenol red, temperature controlled	[30]

chelating ligand for preconcentration of the analyte and matrix removal (such as the major ions in sea salt). One of the most popular ligands is 8-hydroxyquinoline [16,18–24]. With direct spectrophotometric methods, that is no micro-column, care must be taken to minimize refractive index (Schlieren) effects [28].

Typical on-line treatments with such methods include reductor columns for redox speciation, such as NO_2^-/NO_3^-, and filtration to remove suspended particulate matter. On-line seawater supplies (Fig. 5) from towed fish can be coupled with filtration units and FI to provide near-real-time analysis, for example of dissolved or total macro-nutrient and micro-nutrient concentrations in surface waters [16,22]. Another option, particularly for transient species, is the deployment of a submersible FI analyzer [26,28].

Ship-board FI techniques are not restricted to measuring macro-nutrients and micro-nutrients. Methods for determining other fundamental parameters that require high temporal and spatial resolution measurements (such as pH, pCO_2, TCO_2 [29,30] and H_2O_2 [25]) have also been adapted for high-precision ship-board use in a FI system. The small size and weight of FI instruments also permits simultaneous multi-analyte measurements [27,31].

5. Monitoring atmospheric processes

FI instrumentation for environmental monitoring has been applied principally to aquatic environments but it has also been used, albeit less frequently, to monitor atmospheric processes. Surveying the large-scale fluxes of gases and aerosols transported in the atmosphere requires high temporal resolution because of the extreme seasonal and diurnal variability. Gas-diffusion FI has been used successfully to measure gases, such as ammonia [32], sulphur dioxide [32] and nitrogen dioxide [33]. This instrumentation is based on the use of permeation denuders to transfer the atmospheric sample into the FI manifold, which provides the opportunity for preconcentration and continuous monitoring. Direct aerosol analysis is more difficult because long sample-collection times are required and because a high percentage of aerosols, including terrestrial dusts, exist in the solid phase.

6. Future trends

FI instrumentation and chemistries for field monitoring have evolved by a combination of technology-driven advances, such as miniature detectors and novel pumping devices, and environmental process requirements, such as the need for low-level, ship-board iron determinations. The key to future developments is an even closer interaction between analytical chemists and environmental scientists so that the technique can be targeted at applications where the lack of high-quality analytical measurements are currently limiting our understanding of biogeochemical processes.

In terms of instrumentation, there will be continuing advances in hardware and software, but important issues that need to be addressed include sample presentation (for example filtration), instrument design (including suitable housings), miniaturization (but not necessarily nanotechnology), reductions in reagent consumption and remote communication. The chemistries and the method protocols used with such hardware will also need to be improved and standardized. For example, operational protocols for on-line sample treatments, such as acidification and removal of suspended particulate matter, methods for determining speciation and particular operational fractions, and validation of field data, through intercomparison exercises and the use (and availability) of suitable certified reference materials.

References

[1] S.S. Butcher, R.J. Charlson, G.H. Orins, G.V. Wolfe, Global Biogeochemical Cycles, Harcourt Brace & Company, London, 1992.
[2] K.N. Andrew, N.J. Blundell, D. Price, P.J. Worsfold, Anal. Chem. 66 (1994) 916A.
[3] P. MacLaurin, K.N. Andrew, P.J. Worsfold, Flow Injection Analysis, in: F. McLennan, B.R. Kowalski (Editors), Process Analytical Chemistry, Blackie, Glasgow, 1995, pp. 159–182.
[4] K. Robards, I.D. McKelvie, R.L. Benson, P.J. Worsfold, N.J. Blundell, H. Casey, Anal. Chim. Acta 287 (1994) 147.
[5] A.N. Sharpley, M.J. Hedley, E. Sibbesen, A. Hillbricht-Ilkowska, W.A. House, L. Ryszkowski, Phosphorus Transfers From Terrestrial To Aquatic Ecosystems, In: H. Tiessen (Editor), Phosphorus In The Global Environment: Transfers, Cycles and Management, Scientific Committee on Problems of the Environment (SCOPE), John Wiley & Sons, Chichester, 1995, pp. 171–200.
[6] G. Hanrahan, M. Gledhill, P.J. Fletcher, P.J. Worsfold, Anal. Chim. Acta - In press.
[7] P.J. Worsfold, J.R. Clinch, H. Casey, Anal. Chim. Acta 197 (1987) 43.
[8] R.L. Benson, I.D. McKelvie, B.T. Hart, Y.B. Truong, I.C. Hamilton, Anal. Chim. Acta 326 (1996) 29.
[9] J.R. Clinch, P.J. Worsfold, H. Casey, Anal. Chim. Acta 200 (1987) 523.
[10] S. Coles, M. Nimmo, P.J. Worsfold, Lab. Robotics Automat. 12 (2000) 183.
[11] S. Motomizu, M. Oshima, L. Ma, Anal. Sciences 13 (1997) 401.
[12] M. Trojanowicz, P.J. Worsfold, J.R. Clinch, Trends Anal. Chem. 7 (1988) 301.
[13] W.H. Schlesinger, An Analysis of Global Change (2nd Ed.), Academic Press, San Diego, 1997.
[14] R. Chester, Marine Geochemistry (2nd Ed.), Blackwell Science, Oxford, 2000.
[15] S. Auflitsch, D.M.W. Peat, I.D. McKelvie, P.J. Worsfold, Analyst 122 (1997) 1477.
[16] S. Vink, E.A. Boyle, C.I. Measures, J. Yuan, Deep-Sea Res. I 45 (2000) 1141.
[17] C.M. Sakamoto-Arnold, K.S. Johnson, Anal. Chem. 59 (1987) 1789.
[18] H. Zamzow, K.H. Coale, K.S. Johnson, C.M. Sakamoto, Anal. Chim. Acta 377 (1998) 133.
[19] V.A. Elrod, K.S. Johnson, K.H. Coale, Anal. Chem. 63 (1991) 893.
[20] A.R. Bowie, E.P. Achterberg, R.F.C. Mantoura, P.J. Worsfold, Anal. Chim. Acta 361 (1998) 189.
[21] H. Obata, H. Karatani, M. Matsui, E. Nakayama, Mar. Chem. 56 (1997) 97.
[22] J.T. de Jong, J. den Das, U. Bahumann, M.H. Stoll, G. Kattner, R.F. Nolting, H.J. de Baar, Anal. Chim. Acta 377 (1998) 113.
[23] T.P. Chapin, K.S. Johnson, K.H. Coale, Anal. Chim. Acta 249 (1991) 469.
[24] J.L. Nowicki, K.S. Johnson, K.H. Coale, V.A. Elrod, S.H. Lieberman, Anal. Chem. 66 (1994) 2732.
[25] D. Price, R.F.C. Mantoura, P.J. Worsfold, Anal. Chim. Acta 371 (1998) 205.
[26] A.R.J. David, T. McCormack, A.W. Morris, P.J. Worsfold, Anal. Chim. Acta 361 (1998) 63.
[27] R.T. Masserini, K.A. Fanning, Mar. Chem. 68 (2000) 323.
[28] J. Floch, S. Blain, D. Birot, P. Treguer, Anal. Chim. Acta 377 (1998) 157.
[29] T.D. Clayton, R.H. Byrne, Deep-Sea Res. 40 (1993) 2115.
[30] R.G.J. Bellerby, D.R. Turner, G.E. Millward, P.J. Worsfold, Anal. Chim. Acta 309 (1995) 259.
[31] L.K. Shpigun, I.Y. Kolotyrkina, Y.A. Zolotov, Anal. Chim. Acta 261 (1992) 307.
[32] W. Frenzel, Anal. Chim. Acta 291 (1994) 305.
[33] W. Frenzel, Anal. Chim. Acta 308 (1995) 109.

Environ. Sci. Technol. 2002, 36, 4600–4607

Real-Time Monitoring of Picomolar Concentrations of Iron(II) in Marine Waters Using Automated Flow Injection-Chemiluminescence Instrumentation

ANDREW R. BOWIE,[†,‡] ERIC P. ACHTERBERG,[‡] PETER N. SEDWICK,[†,§] SIMON USSHER,[†] AND PAUL J. WORSFOLD*,[‡]

Antarctic CRC, GPO Box 252-80, Hobart, Tasmania 7001, Australia, Department of Environmental Sciences, Plymouth Environmental Research Centre, University of Plymouth, Plymouth PL4 8AA, United Kingdom, and Bermuda Biological Station for Research, St. George's, GE01, Bermuda

A shipboard-deployable, flow-injection (FI) based instrument for monitoring iron(II) in surface marine waters is described. It incorporates a miniature, low-power photon-counting head for measuring the light emitted from the iron-(II)-catalyzed chemiluminescence (CL) luminol reaction. System control, signal acquisition, and data processing are performed in a graphical programming environment. The limit of detection for iron(II) is in the range 8–12 pmol L^{-1} (based on 3s of the blank), and the precision over the range 8–1000 pmol L^{-1} varies between 0.9 and 7.6% (n = 4). Results from a day–night deployment during a north-to-south transect of the Atlantic Ocean and a daytime transect in the Sub-Antarctic Front are presented together with ancillary temperature, salinity, and irradiance data. The generic nature of the components used to assemble the instrument make the technology readily transferable to other laboratories and the modular construction makes it easy to adapt the system for use with other CL chemistries.

Introduction

In much of the open-ocean, the major nutrients (nitrate, phosphate, and silicate) control primary production by phytoplankton, but in vast areas of the Southern and Pacific Oceans, iron has been shown to be growth limiting (*1–3*). Accurate determination of iron in seawater is therefore fundamentally important to our understanding of the dynamics of marine ecosystems and their role in global climate change. However, despite its abundance in the Earth's crust, dissolved iron is present at extremely low levels (<1.0 nmol L^{-1}) in the open ocean (*4*), which is primarily the result of its low solubility in seawater.

* Corresponding author phone: +44 1752 233006; fax: +44-1752-233009; e-mail: pworsfold@plymouth.ac.uk.
† Antarctic CRC.
‡ University of Plymouth.
§ Bermuda Biological Station for Research.

It is particularly important to determine the lower redox state, iron(II), because of its greater solubility and potential bioavailability (*5, 6*). However, iron(II) is a transient species in oxygenated waters, existing at low picomolar concentrations, and therefore making measurements that do not perturb the redox balance is extremely difficult. At seawater pH, iron(II) is rapidly oxidized by O_2 and H_2O_2 to the more thermodynamically favored iron(III) form (*7, 8*). Iron(II) persists due to a combination of photochemical (*9, 10*), thermal, enzymatic, and microbial cycling pathways (*11, 12*). Its oxidation rate is retarded at low temperatures (*7*), and although there is no direct evidence for the presence of iron-(II)-specific ligands in marine waters, organic complexation may promote iron(III) photoreduction and thus slow oxidation rates further (*10, 12*). Moreover, iron(II) may be supplied to the ocean through atmospheric deposition (*13*) and diffusion from reducing sediments (*14*). The ratio of iron(II) to "total" dissolved iron(II+III) in surface seawater is thus a balance between the strength of the sources of iron(II), rates of reduction and oxidation, and complexation of each redox state by (in)organic ligands.

Due to the short half-life (several minutes) of iron(II) species in seawater, measurements are best performed in situ or immediately after underway sampling, by delivering seawater directly from the ocean to the analyzer. Discrete vertical sampling for iron(II) using Go-Flo bottles is problematic because during collection, retrieval, and analysis, the redox speciation may change due to oxidation to iron-(III), hydrolysis, and precipitation to form colloidal and oxyhydroxide species. Alternatively, the analyte can be stabilized in situ using strong iron(II) chelators (e.g. ferrozine) (*15, 16*) for later analysis, but this may promote a redox shift toward the reduced form (*17, 18*). Ferrozine can also be used without preconcentration by incorporating long path length capillaries (2–5 m) to achieve moderate detection limits (100–200 pM) with absorbance spectroscopy (*19, 20*). It is important to appreciate that all iron speciation results are essentially operationally defined.

Existing techniques for iron determinations in seawater can be broadly categorized into "land-based" (graphite furnace atomic absorption spectrometry (GFAAS) (*21*) or inductively coupled plasma mass spectrometry (ICP-MS)) (*22*) and "ship-based" (flow injection (FI) with chemiluminescence (CL) (*23*) or spectrophotometric (*24*) detection or cathodic stripping voltammetry (CSV)) (*25*) methods. The advantages of shipboard systems are near real-time data with increased temporal and/or spatial resolution and the ability to modify research strategies in response to environmental change or inadvertent contamination.

In this paper, we describe a portable FI-CL instrument for the on-line monitoring of iron(II) in surface seawater, based on the catalytic effect of iron(II) on the luminol reaction in the absence of added oxidant (*26–29*). The method can also be used for dissolved iron(II+III) measurements, after minor modification to the manifold and software (*23*). FI-CL systems for dissolved iron determinations in discrete samples (*30–32*) and for investigating iron(II) oxidation rates in synthetic media (*33*) and eutrophic lakes (*34*) have been reported. The mechanism of the two step luminol oxidation chemiluminescence reaction has recently been described in detail (*35, 36*). An automated FI-spectrophotometric system has previously been described (*37*) for underway determination of dissolved iron in the surface ocean (5 min resolution), but the reaction, based upon the catalytic oxidation of *N,N*-dimethyl-*p*-phenylenediamine dihydrochloride (DPD), cannot be used for iron redox speciation studies. The automated

10.1021/es020045v CCC: $22.00
Published on Web 09/21/2002

instrumentation reported here, however, can be used for the continuous underway measurement of ambient iron(II) in seawater. The system incorporates a miniature, low-power (5 V) photon-counting head detector and is controlled through graphical user software programmed in National Instruments LabVIEW. Performance characteristics and analytical figures of merit are presented, together with results of shipboard deployment and evaluation over several day–night cycles during a north–south transect through the subtropical Atlantic Ocean and a daytime transect in the Sub-Antarctic Front south of Australia.

Experimental Section

Instrumentation. The system was designed as a multipurpose instrument which facilitates computer control of mains-powered peristaltic pumps, low voltage microsolenoid pumps and microelectronic switching, injection and autosampler valves, while simultaneously acquiring measurement data from one or two photomultipliers (PMTs), and up to 14 other unspecified analogue units. The instrument consists of two enclosures: a main control unit houses the power supply and power control sections, and a separate smaller, isolated enclosure houses the photomultiplier interface and associated electronics.

Instrument control is performed using a type II PCMCIA DAQCard-DIO-24 input/output (I/O) card (National Instruments Corp., Newbury, UK) providing 24 digital transistor-transistor logic (TTL) lines. Signal acquisition is achieved through a multifunction NI DAQCard-700, incorporating a 16 channel, 12 bit analogue-to-digital converter. In addition, eight digital TTL outputs on this card provide supplementary lines used in switched gain amplification of the PMT signals (four modes). Both cards are operated through a Toshiba Satellite 310CDS Pentium laptop computer (Toshiba Information Systems Ltd., Weybridge, UK). Communications software was written in LabVIEW version 5.1 (National Instruments Corp.). A generic LabVIEW *VI* (virtual instrument subroutine), produced by Ruthern Instruments Ltd. (Bodmin, UK), provides basic control of the instrument acquisition and output functions. This *VI* was later integrated within a secondary routine for automation, display, and data processing functions. In combination, the two *VIs* provide a fully functional virtual instrument designed for a variety of trace metal analyses based on incorporation of CL chemistries into FI manifolds (*38*).

A LabVIEW *VI* consists of two component windows: the front panel and the wiring diagram. The front panel is where the program is designed and contains ready-to-use switches, buttons, controls, and graphical displays of detector readings. The connections between each element in the front panel appear in a wiring diagram, which also includes additional functions for mathematical operations, file management, and I/O of data and controls via acquisition cards.

Figure 1 shows the flow-through design used for the sampling and determination of iron(II) in surface seawater. The pumps, valves, and detector used for the online iron(II) FI manifold (shown on the right-hand side of Figure 1) were coupled to the automated instrument described above. The FI manifold is a modification of that described in Bowie et al. (*23*) for the determination of "total" dissolved iron(II+III). For shipboard use, where additional space was available, conventional peristaltic pumps (Gilson Minipuls 3, Anachem Ltd., Luton, UK) were used to minimize flow pulsing. These pumps could be replaced by solenoid operated self-priming micropumps to miniaturize the system further for remote field deployments, although in-line filtration is essential with such devices to remove particulate material and prevent blockages inside the pumps (*39*). Injection valves I1 and I2 are 6-port Cheminert low-pressure valves (model C22, Valco Instruments Co., Houston, U.S.A.) with microelectronic two position actuators and $^1/_4$-28 fittings. Electronic switching valves are 3-way, 2-position direct lift solenoid valves, containing PTFE wetted parts and zero dead volumes (model EW-01367-72, Cole-Parmer Instrument Co., Hanwell, UK). Switching valves are set by default to normally open-common (NO/COMM) when de-energized and to the normally closed-common (NC/COMM) position when power is supplied. Pumps and switches are operated at 5 V DC (TTL) and 12 V DC, respectively, supplied from the main control unit. A power saver relay was used to reduce the input voltage from 12 to 8 V DC when energizing the solenoids for extended (>2 min) periods, to prevent coil damage.

The detection system consists of a flow cell constructed from coiled transparent PVC tubing (1.0 mm i.d., Altec, Hants, UK) and mounted on the window of a side-on photon-counting head (model H6240-01, Hamamatsu Photonics, Welwyn Garden City, UK). This compact unit incorporated a low-noise PMT and internal high-voltage power supply. It is supplied with a low voltage (5 V DC) source from the main control unit. The photon counting circuitry produces a TTL output pulse train, modulated by the light intensity received at the PMT window. This pulse train is integrated in a resistor-capacitor network to produce a low-level voltage, which in turn is amplified and filtered, resulting in a clean signal suitable for collection at the analogue-to-digital converter of the DAQCard-700.

All manifold tubing is 0.75 mm i.d. PTFE tubing (Fisher Scientific, Loughborough, UK), except peristaltic pump tubing which is flow-rated PVC (Elkay, Basingstoke, UK). Preconcentration, matrix elimination, and sample buffer cleanup was performed using in-line microcolumns (*23*) containing 8-hydroxyquinoline (8HQ) immobilized on a vinyl copolymer resin, synthesized according to a modified version of Landing et al. (*40*).

Shipboard Field Trials and Sampling. Shipboard trials were conducted during expedition ANT XIII/1 (September 29–October 23, 2000) aboard PS *Polarstern*. A north–south transect of the Atlantic Ocean was undertaken during the cruise from Bremerhaven (Germany) to Cape Town (South Africa). The regions of the open Atlantic Ocean covered during this voyage receive trace metal inputs dominated in the tropics and subtropics by wet and dry atmospheric deposition, predominantly due to episodic, long-range transport of Saharan dust, and precipitation through the migrating Inter-Tropical Convergence Zone. Moreover, high daytime irradiance levels experienced through large sections of this transect meant that this was an interesting area in which to study the possible effects of photochemistry on iron redox speciation.

A further shipboard trial was conducted in a contrasting environment aboard RSV *Aurora Australis* as part of the CLIVAR SR3 expedition in the Southern Ocean south of Australia (October 28–December 12, 2001). Cold seawater temperatures and low H_2O_2 concentrations may lead to extended iron(II) oxidation half-lives in these waters (*12*). During the return voyage to Hobart (Australia) a north–south transect was undertaken across a filament of the Sub-Antarctic Front (SAF). In contrast to the open Atlantic Ocean, this is an area of extremely low atmospheric iron deposition and extended daylight periods, although irradiance levels are variable due to persistent cloudy skies, even during the austral summer.

Continuous underway sampling of surface (1–2 m) seawater was performed using a towed torpedo-shaped fish (left-hand side of Figure 1) deployed off the crane arm of a hydrographic winch at a distance of ~5 m from the ship's starboard side (*32*, *41*). For the Atlantic Ocean survey, seawater was pumped on-board using a variable speed high volume peristaltic pump (model 7591-00, Cole Palmer Instrument Co.), fitted with silicone pump tubing and filtered

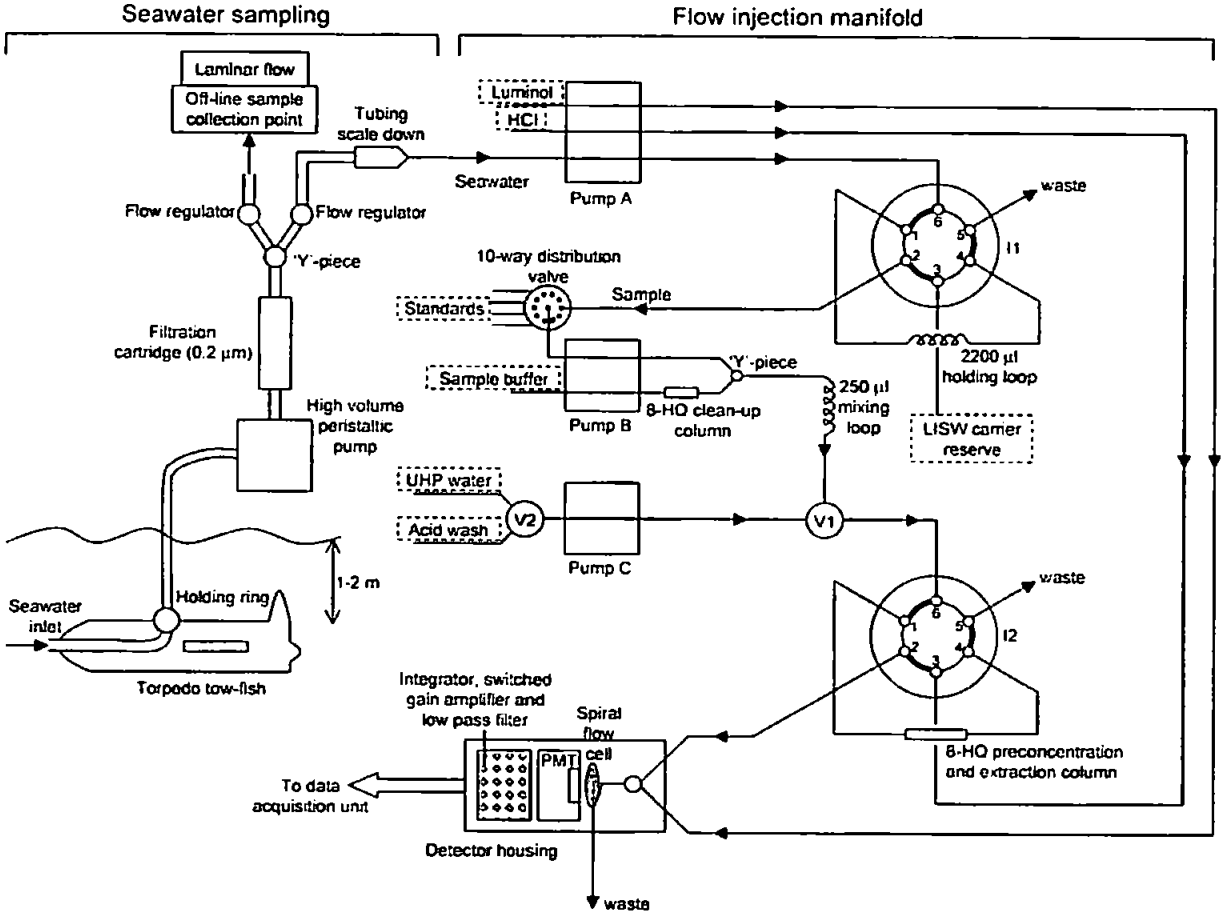

FIGURE 1. Schematic of the flow design used for the online determination of iron(II) in surface seawater. The left-hand side shows the in situ torpedo fish, high volume pumping and filtration system, while the right-hand side shows the components and tubing within the FI manifold. Pump A delivers a continuous stream of surface seawater and CL reagents, pump B delivers sample solution and sample buffer, and pump C delivers UHP water and acid wash solutions. Seawater from the LISW carrier reserve is not preconcentrated onto the 8HQ column and is simply used to prevent air entering the holding loop when sample solution is drawn up by pump B. The holding loop consists of 5 m of 0.75 mm i.d. PTFE tubing. V1 and V2 are solenoid switching valves, I1 and I2 are 6-port, 2-way injection valves. Boxes shown as dotted lines indicate the solution is sealed from the atmosphere within double zip-lock bags.

through a Sartobran-P polypropylene cartridge unit with a 0.2 μm cellulose acetate filter membrane (Sartorius Ltd., Epsom, UK). For the Southern Ocean survey, seawater was pumped on-board using a pneumatic PVDF double-diaphragm pump (model P.025, Wilden) and filtered through a Whatman Polycap (model 150TC) filter with 0.2 μm polysethersulfone filter membrane. Water from the sampling tubing entered a clean container laboratory positioned on the ship's aft deck, passed through a flow regulator, and was split into two channels. Seawater from one line was fed directly to the FI-CL iron(II) analyzer (Figure 1), while the other line provided a collection point for discrete samples which were later analyzed for dissolved iron(II+III) by FI-CL.

Elevated signals were observed for the first few (2−3) sample injections of each automated run of the iron(II) analyzer. This phenomenon was believed to be due to either low level contamination from the Cheminert injection valves or photoreduction of iron in seawater sitting in the transparent PTFE flow lines contained within the laboratory van. Thus data from the initial peaks for each run are not considered. The timing of each sample injection was determined by back calculation from the time (in UTC, Coordinated Universal Time) each data file was written to disk, and this time was adjusted for lag time delays due to surface water pumping and analysis (5.5 min on the Atlantic Ocean survey, 13.0 min on the Southern Ocean survey). The iron(II) concentration data were then merged with the ship's position and underway surface water parameters recorded on the ship's data logger system.

Reagents and Standards. Reagents were prepared as described previously (*23*, *42*) for the determination of "total" dissolved iron (II+III). One liter volumes of buffered luminol reagent and HCl eluent were prepared in order to allow continuous determination of iron(II) species over a >10 h period. Low-level iron impurities in these reagents contributed to the detector baseline, which was above the background PMT noise level recorded in the absence of reagent flow. Blank correction was performed by subtracting the signal that was generated due to one load and elution cycle, without seawater sample present (i.e. sample buffer load plus ultrahigh purity (UHP) water rinse). To obtain this blank measurement, the sample line was stopped at the 'Y'-piece (to the right of pump B in Figure 1) and the associated pump tubing disconnected. A 1 s load can be used to differentiate the blank contribution from the 8HQ microcolumn and the switching of the injection valve, which were not negligible, from the reagent (sample buffer plus UHP water) contribution.

System calibration was performed as follows: low-iron seawater, which had been previously collected and allowed to age in the dark, was adjusted to pH 2.0 with triple quartz-distilled hydrochloric acid (Q-HCl) and 100 μM sodium sulfite added to ensure the iron in the sample was present in the reduced, ferrous form. Standards prepared at pH 2.0 in the presence of a reducing agent were necessary in order to prevent reoxidation of iron(II) which may have occurred at a higher pH. After a >8 h reduction period, standard additions of iron(II) in the range 0−1.0 nmol L^{-1} were made to this solution and immediately introduced into the FI-CL analyzer. The sensitivity of the system to iron(II) was ascertained from the slope of the standard curve.

System Operation. Prior to use, the PTFE flow lines, fittings, connectors and 8HQ microcolumns of the FI manifold were cleaned with 0.5 M Q-HCl and UHP water for >8 h. The system was calibrated at the start and end of each batch of reagents and also after any change in sensitivity (e.g. after change in temperature). For sample analysis, filtered (0.2 μm) ambient pH seawater was continually pumped from the towed torpedo fish into a 5 m (2.2 mL) holding loop (Figure 1) contained within injection valve I1. If air bubbles form in the holding loop (e.g. due to the degassing that may occur when very cold seawater enters a warm container laboratory) (*37*), the injection valve I1 can be replaced by a polyethylene bottle or PTFE debubbling vial that temporarily stores a small volume (e.g. 2 mL) of seawater pumped from the tow-fish for subsequent subsampling using a PTFE tube from the FI system. On switching I1 to the elute position, 1.6 mL of sample was drawn into the FI manifold where it was buffered in-line to pH 5.5 on passing through a 0.57 m (250 μL) mixing coil. The iron(II) in the buffered sample was preconcentrated and separated from the seawater matrix as it passed for 1 min over the 8HQ microcolumn contained within injection valve I2 (see *Method Chemistry* below). A distribution valve allows the system to be switched from sample analysis mode to calibration mode whereby up to 9 flow lines may be fed to spiked standard solutions. During calibration, seawater from the fish is continually pumped through the holding loop in injection valve I1 and to waste.

One complete analytical cycle was completed within 3 min. During this time, injection valve I1 was returned to the load position and seawater continually pumped through the holding loop ready for the next sample load. Using one batch of reagents, two blank measurements (in triplicate), two calibration curves (seawater standard plus two additions, in triplicate), and up to 8 h (160 peaks) of continuous online determination of 8HQ-reactive iron(II) can be performed. With a sampling and analysis sequence taking place every 3 min, a measurement is made every 0.9 km of the ship's track if the cruising speed is ~10 knots (18 km h^{-1}).

Results and Discussion

Analytical Performance. Instrumental drift was monitored during the Atlantic Ocean shipboard trials by regularly measuring the CL background emission and background peak-to-peak noise, blank signals, and calibration slopes. Sensitivity variations may result from temperature fluctuations (affecting both the PMT detector and CL chemistry), differences in reagent composition between batches, reagent aging, and degradation of pump tubing (affecting flow rates). The effect of temperature on the CL background noise and analyte signal generated using a 2.0 nmol L^{-1} iron(II) standard prepared in UHP water with the FI system in direct injection mode (i.e. 8HQ microcolumn removed; see *Method chemistry* below) was studied over a 24 h period. No significant changes in CL background noise (<2% drift, one measurement made each second, n > 80 000) or analyte signal (<6%, 86 ± 5 mV, n = 36) were observed, despite a 5.5 °C change in laboratory temperature. However, to minimize the risk of possible changes in sensitivity with temperature, the complete system was housed in an air conditioned clean air laboratory container.

A switched gain amplifier (gain on the PMT anode current) contained within the PMT interface provided four settings, ×100, ×1000, ×2000, and ×5000, which were selectable by the control *VI* software. Signal-to-noise ratio was proportional to gain, and therefore the highest gain setting (×5000) was used for most open-ocean applications. A lower PMT gain setting can be used for the higher concentration ranges expected in coastal and estuarine waters.

The sensitivity of the system was evaluated by comparing the slopes of calibration curves for standards prepared in low iron seawater (LISW), collected from the Southern Ocean Iron RElease Experiment (SOIREE) site (61°S 140°E) at a depth of approximately 500 m (*41*). Standard additions of 0.2, 0.4, 0.6, 0.8, and 1.0 nmol L^{-1} iron(II) were made. System sensitivity varied <5% on a single day (800 ± 40 mV per nmol L^{-1}, r^2 = 0.998) but varied up to 10% between days (typically 775 ± 73 mV per nmol L^{-1}, r^2 = 0.995). The precision for the standard addition solutions was in the range 0.9−6.2% RSD (n = 4). The iron(II) blank was typically 24 ± 4 pmol l^{-1} (n = 4), resulting in a limit of detection of 12 pmol L^{-1} (defined as three times the standard deviation of the blank).

Method Chemistry. In-line adjustment of sample pH was necessary to ensure optimum preconcentration of iron(II) species onto the 8HQ resin, while minimizing the effect of any interfering species which bind to 8HQ at higher pH (e.g. Mn) (*31*). Many other species are also known to catalyze the luminol reaction in the absence of selective analyte extraction and preconcentration (*43*). As such, these iron(II) measurements represent the operationally defined fraction that is extracted onto an 8HQ microcolumn after short (1 min) in-line buffering of sample to pH 5.5. These iron(II) measurements are hereafter referred to as 8HQ-reactive iron(II), recognizing that the iron(II) oxidation rate will be retarded and stability enhanced at lower pH (*7*, *9*). Ideally, iron(II) measurements should follow a sampling and pretreatment protocol that maintains speciation integrity as closely as possible.

The iron(II) detected using this approach is not an artefact of the analytical method. Since the residence time of the sample in the 8HQ microcolumn is short (<1.7 s), no significant reduction of iron(III) was observed in aged, filtered Southern Ocean seawater solutions spiked with up to 5.0 nmol L^{-1} iron(III) (<7% of analyte signal obtained for equimolar spiked iron(II) standards). Direct injection iron-(II) measurements without the preconcentration protocol (and hence not operationally defined) are also possible by removing the 8HQ microcolumn and sample buffer line. To achieve this, the 8HQ column within injection valve I2 is replaced with a sample loop (typically 100−150 μL). UHP water is used as carrier instead of an HCl eluent stream, and the column wash step (see Figure 1) is eliminated. In this manifold, injection valve I1 is not required, as seawater is fed directly to the loop within valve I2. The detection limit of this method is an order of magnitude higher than with the 8HQ column manifold (~0.2 nmol L^{-1}) and thus unsuitable for open-ocean iron(II) measurements where dissolved iron-(II+III) concentrations are extremely low (<0.1 nmol L^{-1}). However, this no-preconcentration version of the iron(II) system is particularly useful as a tracer for rapid underway mapping during iron fertilization experiments (e.g. SOIREE) (*3*), although it is important that the protocols described above are followed when determining the analytical blank. Any small positive matrix interference from Co(II) (*23*) can be removed by adding dimethylglyoxime (20 μM) to the luminol stream.

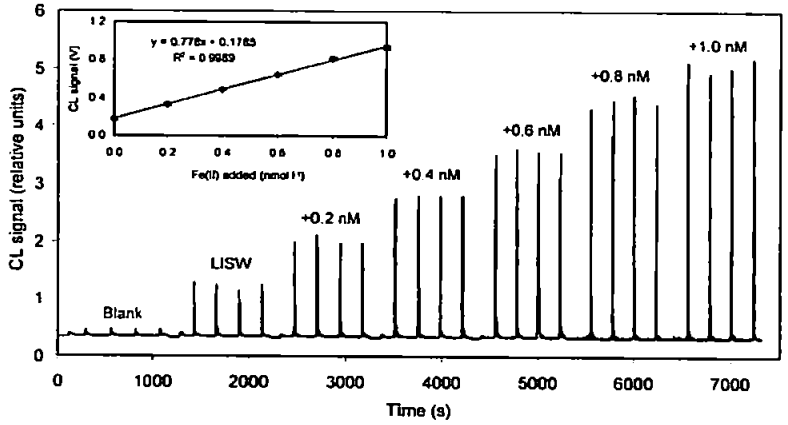

FIGURE 2. Shipboard calibration peaks and corresponding graph (inset) for iron(II) in the range 0−1.0 nmol L^{-1}.

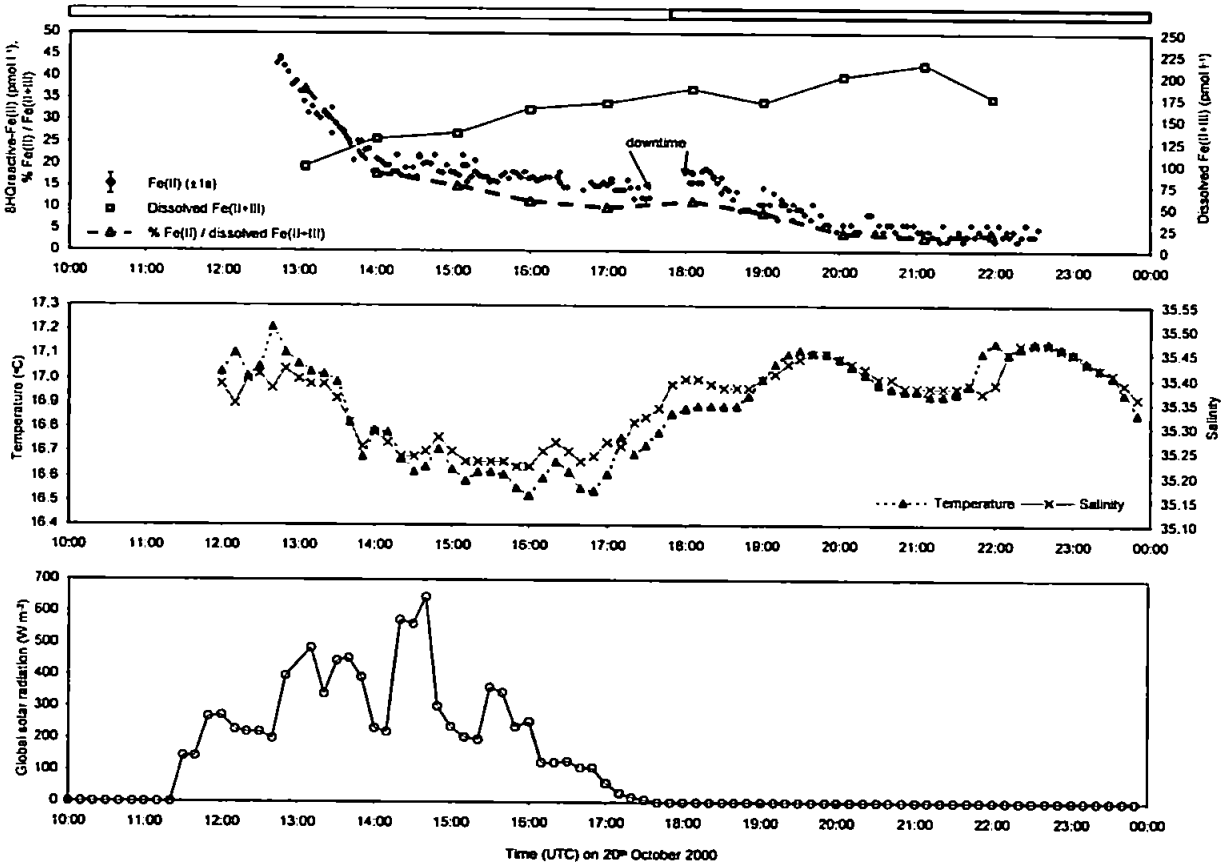

FIGURE 3. (a) Concentration of 8HQ-reactive iron(II), dissolved iron(II+III), and the iron(II)/iron(II+III) ratio during a 10 h shipboard deployment in the Atlantic Ocean, (b) surface temperature and salinity (10 min resolution), and (c) global solar radiation (10 min resolution) over the period 10:00−00:00 (UTC) on October 20, 2000. A typical error bar (1s) for the iron(II) concentrations is shown. The horizontal black bar represents the dark period during the survey.

Shipboard Trials. *Atlantic Ocean Survey.* Shipboard calibrations were performed at the beginning and end of each reagent batch (10 h periods). Figure 2 shows a typical set of peaks and corresponding standard curve for the blank solution and calibration standards prepared in LISW, with 0.2, 0.4, 0.6, 0.8, and 1.0 nmol L^{-1} additions of iron(II). Four replicates of each solution were made. The CL background noise showed good stability and reproducibility between replicate ($n = 4$) injections was typically <3%.

Figure 3 shows the results from the continuous determination of iron(II) in surface waters of the southeast Atlantic Ocean during one 10 h day−night period. Concurrent sea-surface temperature, salinity, and incident solar radiation are also shown. The online system was calibrated prior to switching to fully automated mode at 12:40 UTC on October 20, 2000. Continuous analyses were conducted until 22:34, except between 17:33 and 18:03 when a flow problem through the filtration cartridge needed to be rectified. The ship transited between 23°17′ S, 8°39′ E and 24°48′ S, 9°59′ E during the trial. During daylight hours, light cloud cover was present. Dusk occurred between 17:45−18:15 UTC. Subsamples were also taken hourly from the online system during the trial.

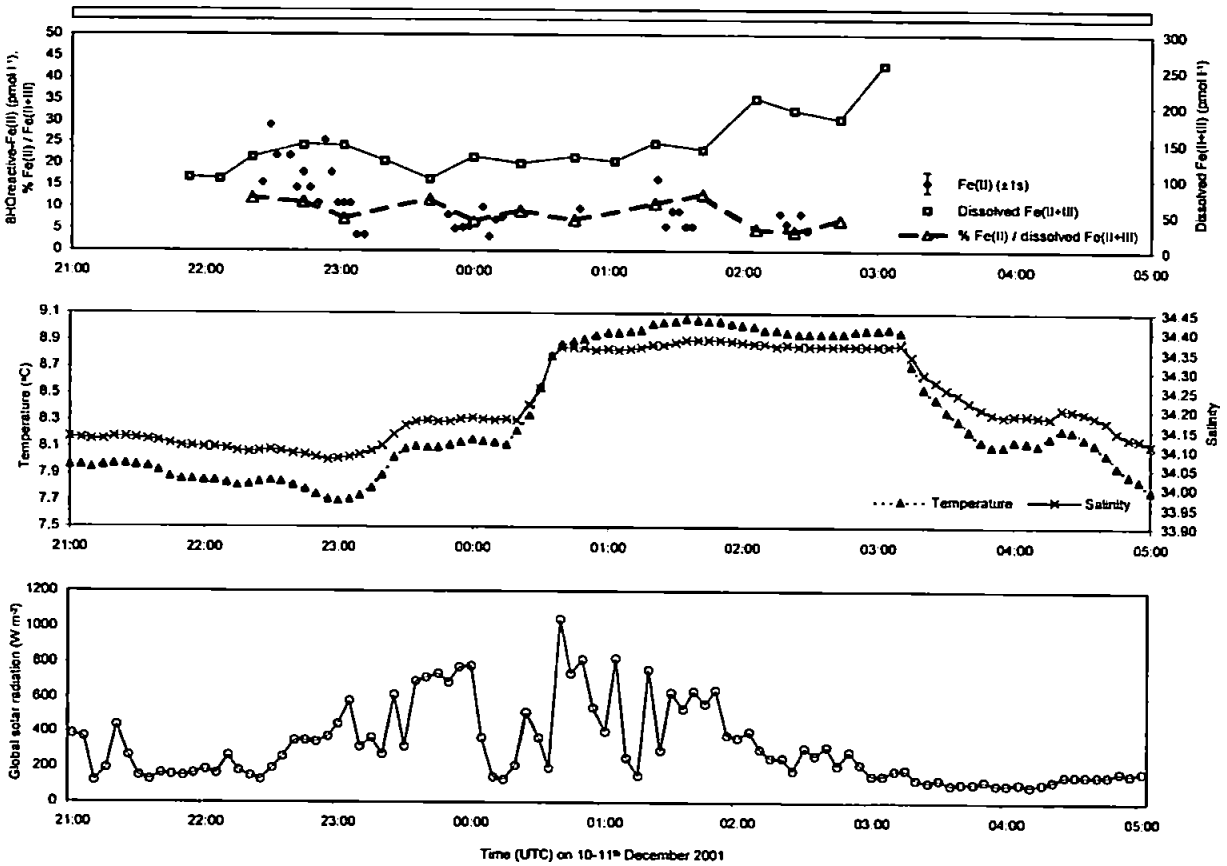

FIGURE 4. (a) Concentration of 8HQ-reactive iron(II), dissolved iron(II+III) and the iron(II)/iron(II+III) ratio during a 5 h shipboard deployment in the Southern Ocean, (b) surface temperature and salinity (5 min resolution), and (c) global solar radiation (portside, 5 min resolution) over the period 21.00 on December 10, 2001 to 05.00 (UTC) on December 11, 2001. A typical error bar (1s) for the iron(II) concentrations is shown. The horizontal white bar represents the daytime period during the survey.

acidified, reduced (0.01 M Q-HCl, 100 μM Na_2SO_3), and analyzed at sea by FI-CL for dissolved iron(II+III) (*23*).

The results (Figure 3) for 8HQ-reactive iron(II) showed concentrations in the subtropical, oligotrophic Atlantic Ocean ranging from below the detection limit (< 12 pmol L^{-1}) during darkness up to 45 pmol L^{-1} at 12:50 UTC, at which time the solar intensity was close to the maximum experienced during the trial. The concentration of dissolved iron(II+III) in surface waters generally increased during the survey, but was low compared to other data (*4*) for the Atlantic Ocean (164 ± 35 pmol L^{-1}, $n = 10$). Dissolved iron(II) or iron(II+III) distributions are not correlated with subtle changes in temperature and salinity. Interestingly, the iron(II) to iron(II+III) ratio decreased steadily from 37% at 13:05 to 3% at 21:07, suggesting that the iron(II) concentration was independent of changes in water mass. These data are consistent with earlier work that suggests photochemical reduction of iron(III) to be the dominant mechanism for iron(II) production in the Southern Ocean (*12*), offshore waters of Peru (*14*), and northern Australian shelf waters (*44*). Our data also support previous results demonstrating diurnal cycling between total "reducible" (dissolved/bioavailable) and "nondetectable" (colloidal/particulate) iron concentrations in natural seawater incubations spiked with added iron (*10*). The reduction of iron(III) to transient iron(II) species, either photochemically or involving marine microorganisms, may increase the solubility and bioavailability of iron in seawater.

Southern Ocean Survey. A short (5 h) trial was also undertaken in the Australian sector of the Southern Ocean between 50°92′ S, 143° 38′ E and 51°25′ S, 143°03′ E, in the Sub-Antarctic Front (SAF). The objective here was to demonstrate the generic capability of the instrumentation by deploying it in a contrasting marine environment. Iron(II) was measured from 21.00 on December 10, 2001 to 05.00 UTC on December 11, 2001 (local daytime) during austral summer. Conditions were partly overcast. Calibration standards were prepared as described above, and three replicates of each solution were made. The mean detection limit from daily shipboard calibrations was 8.7 pmol L^{-1}, and reproducibility between replicate ($n = 3$) blank injections was RSD <7.6%. A debubbler polyethylene subsampling bottle replaced injection valve II during this survey, as described in *System Operation*. Unfortunately, there are several short periods where no data were recorded. This was due to a problem with the continuous supply of surface water from the tow-fish, which was a deployed in increasingly rough seas.

The results (Figure 4) show concentrations ranging from below the detection limit up to 29 pmol L^{-1} for 8HQ-reactive iron(II). Dissolved iron(II+III) concentrations generally increased during the transect from 99 pmol L^{-1} at 22:06 to 257 pmol L^{-1} at 03:03 UTC, although total dissolvable iron (i.e. unfiltered and acidified, TDFe) levels (not shown) were fairly constant (399 ± 33 pmol L^{-1}, $n = 16$). These data are consistent with the low surface dissolved iron concentrations (0.1−0.2 nmol L^{-1}) observed in previous studies of this region (*45, 46*). In the period 00:40 to 03:10, a significant shift in temperature (1.0 °C) and salinity (0.2 units) was observed, suggesting the intrusion of a different water mass, although this resulted in no clear trend in iron(II), dissolved iron-

(II+III) or TDFe concentrations. The iron(II) to iron(II+III) ratio was variable and ranged from 4 to 13%. The Southern Ocean 8HQ-reactive iron(II) concentrations are also in the same range as the southeast Atlantic data, but are closer to the detection limit, have greater temporal variation, and are out of phase with the variable solar irradiance profile, suggesting that photochemically mediated reduction of iron(III) to iron(II) was not dominant. Earlier work by O'Sullivan et al. (*9*) showed that iron(II) concentrations may be highest in the early morning and lower in the late afternoon, due to the photochemical production of significant steady-state concentrations of transient oxidants of iron(II), such as H_2O_2. Unfortunately, we have no iron(II) data during the nighttime period for comparison in this region.

Our contrasting Atlantic and Southern Ocean observations highlight the need for further shipboard studies on the cycling of iron(II) at ambient surface ocean concentrations. Such surveys should examine changes in iron(II) concentrations through complete 24 h periods in warm, temperate, and polar oceans and should address which processes (e.g. photoredox, thermal, microbial) are necessary for the transient production of iron(II). The FI-CL instrument reported here would facilitate the high resolution, ultratrace level investigations necessary to address these important questions.

Other Applications. The shipboard FI-CL instrument described here is a low cost, portable, rugged system suitable for online determination of iron(II) in surface marine waters. Moreover, the generic nature of system components and graphical programming software make it easily adaptable to other CL-detectable analytes (e.g. Co, Cu, Mn, H_2O_2). The performance and reliability of the instrument and the analytical figures of merit are sufficient to allow iron(II) to be determined at picomolar concentrations in real-time over long (>10 h) periods, without user intervention.

In open-ocean environments, iron(II) measurements and observations of iron redox cycling are inherently difficult due to the extremely low dissolved iron(II+III) concentrations, but our preliminary results show that the FI-CL approach can provide acceptable high resolution data in such settings. This instrument would also be particularly useful for examining subtle changes in iron redox chemistry during in situ iron fertilization experiments or in coastal and freshwater environments where dissolved iron(II+III) concentrations are significantly higher. The system could also be used for monitoring biologically mediated redox cycling and uptake of iron(II) in laboratory culture experiments, deckboard incubations, or chemostats. Further development is planned to adapt the manifold for concurrent online determination of "total" dissolved iron(II+III), after an in-line HCl acidification and Na_2SO_3 reduction step.

Acknowledgments

The authors thank the Alfred-Wegener-Institut fur Polar- und Meeresforschung and the Australian National Antarctic Research Expeditions for providing the berths on-board PS *Polarstern* and RSV *Aurora Australis*. The Netherlands Institute for Sea Research and the Australian Antarctic Division supplied the "tow-fish" sampling systems. We thank John Wood (Ruthern Instruments) for constructing the main control and PMT interface units. This work was partly funded by the EU programs MEMOSEA (Trace Metal Monitoring in Surface Marine Waters and Estuaries, MAS3-CT97-0143) and IRONAGES (Iron Resources and Oceanic Nutrients – Advancement of Global Environment Simulations, EVK2-1999-00031), an Australian Research Council IREX Fellowship to A.B. (X00106765) and the Antarctic CRC.

Literature Cited

(1) Coale, K. H.; Johnson, K. S.; Fitzwater, S. E.; Gordon, R. M.; Tanner, S.; Chavez, F. P.; Ferioli, L.; Sakamoto, C. M.; Rogers, P.; Millero, F.; Steinberg, P.; Nightingale, P.; Cooper, D.; Cochlan, W. P.; Landry, M. R.; Constantinou, J.; Rollwagen, G.; Trasvina, A.; Kudela, R. *Nature* **1996**, *383*, 495.
(2) Behrenfeld, M. J.; Kolber, Z. S. *Science* **1999**, *283*, 840.
(3) Boyd, P. W.; Watson, A. J.; Law, C. S.; Abraham, E. R.; Trull, T.; Murdoch, R.; Bakker, D. C. E.; Bowie, A. R.; Buesseler, K. O.; Chang, H.; Charette, M.; Croot, P.; Downing, K.; Frew, R.; Gall, M.; Hadfield, M.; Hall, J.; Harvey, M.; Jameson, G.; LaRoche, J.; Liddicoat, M.; Ling, R.; Maldonado, M. T.; McKay, R. M.; Nodder, S.; Pickmere, S.; Pridmore, R.; Rintoul, S.; Safi, K.; Sutton, P.; Strzepek, R.; Tanneberger, K.; Turner, S.; Waite, A.; Zeldis, J. *Nature* **2000**, *407*, 695.
(4) de Baar, H. J. W.; de Jong, J. T. M. In: *The Biogeochemistry of Iron in Seawater*; Turner, D. R., Hunter, K. A., Eds.; SCOR-IUPAC: Baltimore, U.S.A., 2001; Chapter 5.
(5) Bruland, K. W.; Donat, J. R.; Hutchins, D. A. *Limnol. Oceanogr.* **1991**, *36*, 1555.
(6) Rich, H. W.; Morel, F. M. M. *Limnol. Oceanogr.* **1990**, *35*, 652.
(7) Millero, F. J.; Sotolongo, S.; Izaguirre, M. *Geochim. Cosmochim. Acta* **1987**, *51*, 793.
(8) Moffett, J. W.; Zika, R. G. *Environ. Sci. Technol.* **1987**, *21*, 804.
(9) O'Sullivan, D. W.; Hanson, A. K.; Miller, W. L.; Kester, D. R. *Limnol. Oceanogr.* **1991**, *36*, 1727.
(10) Johnson, K. S.; Coale, K. H.; Elrod, V. A.; Tindale, N. W. *Mar. Chem.* **1994**, *46*, 319.
(11) Tortell, P. D.; Maldonado, M. T.; Granger, J.; Price, N. M. *Fems Microbio. Ecol.* **1999**, *29*, 1.
(12) Croot, P. L.; Bowie, A. R.; Frew, R. D.; Maldonado, M. T.; Hall, J. A.; Safi, K. A.; LaRoche, J.; Boyd, P. W.; Law, C. S. *Geophys. Res. Lett.* **2001**, *28*, 3425.
(13) Zhuang, G. S.; Yi, Z.; Duce, R. A.; Brown, P. R. *Nature* **1992**, *355*, 537.
(14) Hong, H.; Kester, D. R. *Limnol. Oceanogr.* **1986**, *31*, 512.
(15) Blain, S.; Treguer, P. *Anal. Chim. Acta* **1995**, *308*, 425.
(16) King, D. W.; Lin, J.; Kester, D. R. *Anal. Chim. Acta* **1991**, *247*, 125.
(17) Hudson, R. J. M.; Covault, D. T.; Morel, F. M. M. *Mar. Chem.* **1992**, *38*, 209.
(18) Murray, J. W.; Gill, G. *Geochim. Cosmochim. Acta* **1978**, *42*, 9.
(19) Waterbury, R. D.; Yao, W. S.; Byrne, R. H. *Anal. Chim. Acta* **1997**, *357*, 99.
(20) Zhang, J. Z.; Kelbe, C.; Millero, F. J. *Anal. Chim. Acta* **2001**, *438*, 49.
(21) Bruland, K. W.; Franks, R. P.; Knauer, G. A.; Martin, J. H. *Anal. Chim. Acta* **1979**, *105*, 233.
(22) Wells, M. L.; Bruland, K. W. *Mar. Chem.* **1998**, *63*, 145.
(23) Bowie, A. R.; Achterberg, E. P.; Mantoura, R. F. C.; Worsfold, P. J. *Anal. Chim. Acta* **1998**, *361*, 189.
(24) Measures, C. I.; Yuan, J.; Resing, J. A. *Mar. Chem.* **1995**, *50*, 3.
(25) Obata, H.; van den Berg, C. M. G. *Anal. Chem.* **2001**, *73*, 2522.
(26) Seitz, W. R.; Hercules, D. M. *Anal. Chem.* **1972**, *44*, 2143.
(27) Klopf, L. L.; Nieman, T. A. *Anal. Chem.* **1983**, *55*, 1080.
(28) Sarantonis, E. G.; Townshend, A. *Anal. Chim. Acta* **1986**, *184*, 311.
(29) Alwarthan, A. A.; Townshend, A. *Anal. Chim. Acta* **1987**, *196*, 135.
(30) Powell, R. T.; King, D. W.; Landing, W. M. *Mar. Chem.* **1995**, *50*, 13.
(31) Obata, H.; Karatani, H.; Nakayama, E. *Anal. Chem.* **1993**, *65*, 1524.
(32) de Jong, J. T. M.; den Das, J.; Bathmann, U.; Stoll, M. H. C.; Kattner, G.; Nolting R. F.; de Baar, H. J. W. *Anal. Chim. Acta* **1998**, *377*, 113.
(33) King, D. W.; Lounsbury, H. A.; Millero, F. J. *Environ. Sci. Technol.* **1995**, *29*, 818.
(34) Emmenegger, L.; King, D. W.; Sigg, L.; Sulzberger, B. *Environ. Sci. Technol.* **1998**, *32*, 2990.
(35) Rose, A. L.; Waite, D. *Anal. Chem.* **2001**, *73*, 5909.
(36) Xiao, C.; Palmer, D. A.; Wesolowski, D. J. Lovitz, S. B.; King, D. W. *Anal. Chem.* **2002**, *74*, 2210.
(37) Vink, S.; Boyle, E. A.; Measures C. I.; Yuan, J. *Deep-Sea Res. I* **2000**, *47*, 1141.
(38) Bowie, A. R.; Sanders M. G.; Worsfold, P. J. *J. Biolum. Chemilum.* **1996**, *11*, 61.
(39) Hanrahan, G.; Gledhill, M.; Fletcher P. J.; Worsfold, P. J. *Anal. Chim. Acta* **2001**, *440*, 55.
(40) Landing, W. M.; Haraldsson C.; Paxeus, N. *Anal. Chem.* **1986**, *58*, 3031.

(41) Bowie, A. R.; Maldonado, M. T.; Frew, R. D.; Croot, P. L.; Achterberg, E. P.; Mantoura, R. F. C.; Worsfold, P. J.; Law C. S.; Boyd, P. W. *Deep-Sea Res. II* **2001**, *48*, 2703.
(42) Cannizzaro, V.; Bowie, A. R.; Sax, A.; Achterberg E. P.; Worsfold, P. J. *Analyst* **1999**, *125*, 51.
(43) Campbell, A. K. In *Chemiluminescence*; Ellis Horwood: Chichester, 1988; p 415.
(44) Waite, T. D.; Szymczak, R.; Espey Q. I.; Furnas, M. J. *Mar. Chem.* **1995**, *50*, 79.
(45) Sedwick, P. N.; Edwards, P. R.; Mackey, D. J.; Griffiths F. B.; Parslow, J. S. *Deep-Sea Res. I* **1997**, *44*, 1239.
(46) Sohrin, Y.; Iwamoto, S.; Matsui, M.; Obata, H.; Nakayama, E.; Suzuki, K.; Handa, N.; Ishii, M. *Deep-Sea Res. I* **2000**, *47*, 55.

Received for review February 28, 2002. Revised manuscript received August 5, 2002. Accepted August 8, 2002.

ES020045V

Direct Determination of Iron(II) in Acidified Seawater using a Matrix Matched Flow Injection Manifold with Chemiluminescence Detection

M. Yaqoob[1], S. J. Ussher[2], A. Nabi[1], E. P. Achterberg[2] and P. J. Worsfold[2*]

[1]Department of Chemistry, University of Balochistan, Quetta, Pakistan
[2]School of Environmental Sciences, Plymouth Environmental Research Centre, University of Plymouth, Drake Circus, Plymouth, PL4 8AA, UK

email pworsfold@plymouth.ac.uk

Abstract

A flow-injection method is reported for the determination of iron(II) in acidified seawater (pH 3.0) based on selective chemiluminescence detection using the luminol reaction with no added oxidant and no preconcentration column. The limit of detection (3 x standard deviation of the blank) was 0.1 nM and the time between injection and detection was 12 s. The calibration graph was linear (r^2 = 0.993, n = 5) over the range 2 – 10 nM with relative standard deviations (n = 4) in the range 1.0 – 3.7%. Analysis of a coastal water certified reference material (CASS-3) for iron(II), after reduction of iron(III) with sodium sulphite, gave good results (18.5 ± 5.2 nM compared with the certificate value of 22.56 ± 3.04 nM).

Keywords Flow injection, iron(II), total iron, chemiluminescence, seawater.

1. Introduction

Iron is an important element in biogeochemical processes. It is an essential micronutrient for living organisms and plays a key role in oceanic plankton productivity. Iron also has a regulatory role in micro-organisms as an inhibitor and promoter of citrate and antibiotic syntheses respectively [1, 2].

Despite the high abundance of iron in the earth's crust (5.6%) its concentration in coastal waters is usually in the nM range (e.g. 0.4 - 28 nM in the North Sea) and is typically very low in open ocean environments (0.05 - 2 nM) [3]. In areas such as the Southern Ocean iron limits phytoplankton growth [4] and this has important implications for the air - sea exchange of carbon dioxide [5]. The speciation of iron in aquatic systems is very important for biogeochemical studies because of the influence of its chemical form on bioavailability, mobility and toxicological properties [6 - 8].

Flow-injection with chemiluminescence detection (FI-CL) has been widely used for the determination of trace metals in environmental, pharmaceutical, clinical, biochemical, food and beverage samples at very low (nM) concentrations [9 – 12]. Major advantages of FI-CL methods include robustness, nb portability and low cost of the instrumentation, rapid analysis, low contamination risk, low (nM) detection limits and excellent sensitivity.

A number of FI-CL methods have been reported for dissolved iron species in seawater. Elrod et al. [13] and Hirata et al. [14] utilised the iron(II)-specific reagent brilliant sulfoflavin (4-amino-*N*-*p*-tolyl)-naphthalimide-3-sulfonate) to determine iron(II). Elrod et al. preconcentrated iron on an 8-HQ microcolumn whilst Hirata et al. used an Amberlite XAD-4 resin functionalised with *N*-hydroxyethylenediamine (HEED). Total dissolved iron was measured by adding a reducing agent (ascorbic acid [13] or hydroxylammonium chloride [14]) to samples prior to analysis.

Luminol, (5-amino-2,3-dihydro-1,4-phthalazinedione) which is catalytically oxidised by iron to an excited state 3-aminophthalate di-anion, has also been widely used. The type of oxidant used with luminol influences which redox species of iron catalyses the reaction. Obata et al. [15, 16] used hydrogen peroxide as an added oxidant to determine iron(III). Samples were acidified to pH 3.0 and iron(III) was selectively preconcentrated on an 8-HQ column before detection. Determination of iron(II) required initial removal of iron(III) from the sample using this column and increasing sample pH to 6 in order to preconcentrate iron(II). Powell et al. [17] and Bowie et al. [18] utilised the oxidation of luminol by dissolved oxygen present in the reagents to selectively determine iron(II). Iron(III) was reduced to iron(II) using sulphite and then preconcentrated on-line using an 8-HQ microcolumn before measurement of total dissolvable iron in unfiltered samples. O'Sullivan et al. [19] also utilised this reaction with a stopped flow technique without preconcentration. Luminol chemiluminescence reactions offer the lowest detection limits for iron in seawater.

In the present study, we describe a FI-CL method for the rapid and selective determination of Fe(II) in acidified seawater by its catalytic effect on the oxidation of luminol in the absence of added oxidant and without a preconcentration column. The manifold used is similar to previously reported methods [20, 21] but uses a seawater carrier stream (rather than 0.7 M NaCl at pH 7.0 [20] or ultra-pure water [21]). Manifold parameters have

been optimised, several buffers have been investigated and the method applied to the determination of Fe(II) in a coastal seawater certified reference material.

2. Experimental

2.1. Materials and Methods

All plasticware used during the experiments and for storage of reagents and standards was cleaned with 50% HCl for 48 h, thoroughly rinsed with ultra high purity (UHP) deionised water (18.2 MΩ cm^{-1}, Elgastat, Maxima, England) and stored in re-sealable plastic bags to prevent contamination. All reagents and standards were of analytical grade (supplied by VWR unless stated otherwise), were prepared in UHP water and further diluted immediately prior to use. Low nutrient seawater (LNS, salinity 35) was obtained from Ocean Scientific International, Wormley, England and used as received for the optimisation and interference studies. For the calibration and accuracy experiments LNS was pre-cleaned to reduce trace metal contamination as described in section 3.3.

An iron(II) stock solution (0.01 M) was prepared by dissolving 0.196 g of $Fe(NH_4)_2(SO_4)_2.6H_2O$ in 50 mL of HCl (0.01 M, prepared every 15 days). The standards were prepared daily in LNS adjusted to pH 3.0 to prevent oxidation of Fe(II). Standard solutions of Mn(II), Cu(II), Ni(II), Zn(II), Pb(II), Co(II) and Cr(III) were prepared from atomic absorption standards (Spectrosol, BDH, England) in LNS (pH 3.0). Iron(III) standard was prepared directly from $NH_4Fe(SO_4)_2.12H_2O$.

Luminol stock solution (0.01 M) was prepared by dissolving 0.089 g of luminol (5-amino-2, 3-dihydro-1, 4-phthal-zinedione, Fluka) in 50 mL of borate buffer followed by sonicating for 30 min. A working luminol solution (1 x 10^{-3} M) was prepared by diluting 10.0 mL of the stock solution in 100 mL of borate buffer (0.1 M) and adjusting to pH 10.4 with sodium hydroxide (2 M). The following buffer solutions were used for luminol solution preparation; NH_3/NH_4, Tris/NaOH, carbonate/NaOH and borate/NaOH (all 0.1 M, pH 10.5).

2.2. Instrumentation and Procedures

The FI-CL manifold used for the determination of Fe(II) is shown in Fig. 1. A 4 channel peristaltic pump (Minipuls 3, Gilson, France) was used to propel the sample carrier and reagent solutions at a flow rate of 2.0 mL min^{-1}. A rotary injection valve (Rheodyne 5020, UK, 270 µL sample loop) was used to inject Fe(II) standards into the LNS (pH 8.0) stream and was merged at a T-piece with the CL reagent stream. The merged streams travelled 3.0 cm before passing through a quartz glass spiral flow cell (1.1 mm i.d., 130 µL internal volume) placed directly in front of an end window photomultiplier tube (PMT, Thorn EMI, 9798QA). Aluminium foil was placed behind the coil to reflect light onto the photo-cathode. The PMT, glass coil and T-piece were enclosed in a light tight housing [18]. The PMT was attached to a 1 kV power supply (Thorn EMI, PM20NS, England) and an integral amplifier was powered from an independent 15 V power supply (BBH Power Products, England). The detector output was recorded using a chart recorder (Kipp & Zonen, Delft, The Netherlands).

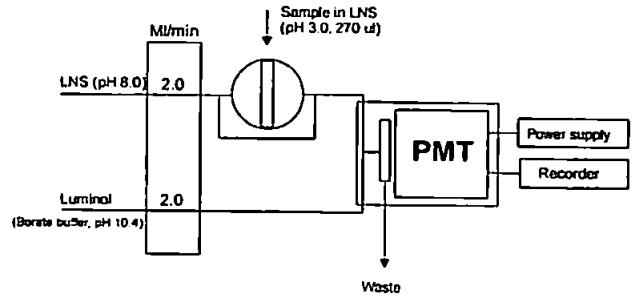

Fig. 1. Flow injection with chemiluminescence detection (FI-CL) manifold for the determination of Fe(II).

3. Results and Discussion

3.1. Optimisation of FI manifold

In order to establish optimum conditions for the determination of Fe(II), various parameters were investigated including buffer concentrations and pH, reagent concentrations, sample volume, reagent flow rates and photomultiplier voltage. All these studies were performed using a 100 nM Fe(II) standard. A univariate strategy was deliberately adopted in order to understand the effect of each variable on the reaction chemistry and the system response.

The efficiency of luminol chemiluminescence is particularly dependent on reaction conditions. In the proposed FI-CL system, different buffers were investigated (NH_3/NH_4, Tris/NaOH, carbonate/NaOH and borate/NaOH; 0.1 M, pH 10.5). The CL responses for 100 nM Fe(II) using these buffers were 5.0, 15.0, 20.0 and 350 mV (n =4) respectively. LNS formed a precipitate with the carbonate buffer and CL signals were irreproducible with an unsteady baseline. The CL responses were very small when using ammonia and Tris-HCl buffers and maximum CL response was obtained with borate buffer. The optimum pH for the luminol reaction with borate buffer was therefore investigated in the range 9.8 – 10.8. Maximum CL emission was observed at pH 10.4, as shown in Fig. 2, and was therefore used for all subsequent studies.

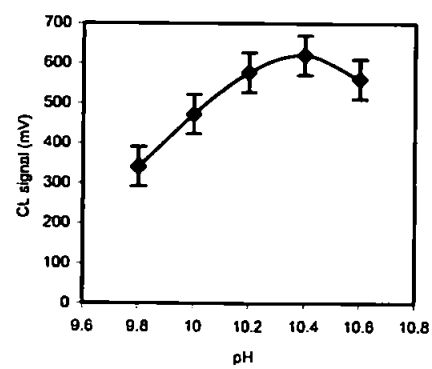

Fig. 2. Effect of borate buffer pH on the peak response of the luminol CL reaction.

The effect of the luminol concentration was then studied over the range $1x10^{-2}$ – $1x10^{-6}$ M using the optimised buffer conditions. As shown in Fig. 3, the CL response increased up to

$1x10^{-3}$ M luminol (used in all subsequent experiments), above which the response decreased due to photon quenching. Variation in reagent sensitivity was observed over time as the luminol solution aged, as found by other workers [20], and therefore it was always prepared 24 h before use.

Fig. 3. Effect of luminol concentration on the determination of Fe(II).

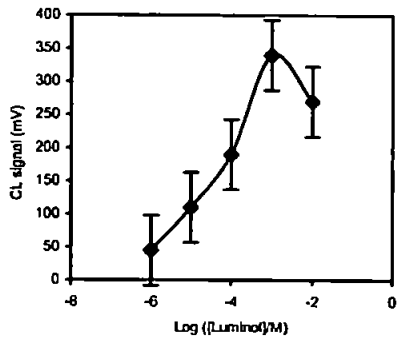

The effect of flow rate of the carrier and reagent streams was studied over the range 1.0–3.0 mL min^{-1} in terms of CL response, speed of analysis and reagent consumption (it is important to match the flow rates of the two streams for maximum efficiency). At a flow rate of 2.0 mL min^{-1} (used for all subsequent experiments), maximum CL intensity was observed with a steady base line and reproducible peak heights (Table 1). The effect of the sample volume on CL response was studied in the range of 45 – 450 µL. Maximum CL response was obtained at 270 µL (Table 1) and was selected for all subsequent experiments.

The effect of LNS pH on the determination of Fe(II) was investigated in the range 1.0 – 5.0. There was an increase in CL intensity up to pH 3.0 but a higher pH decreased the CL intensity (Table 1). Therefore, LNS at pH 3.0 was used for the preparation of all Fe(II) standard solutions to prevent oxidation of iron(II).

The effect of PMT voltage over the range 900 – 1300 V was optimised for maximum CL signal-to-noise (Table 1). CL response increased linearly with PMT voltage but 1050 V was used for all subsequent studies because it gave the best signal-to-noise ratio.

Table 1. Effect of various parameters on the CL peak response for the determination of 100 nM Fe(II). For each parameter the optimised conditions for all other parameters were used, i.e. flow rate 2.0 mL/min; sample volume 270 µL; PMT voltage 1050 V; LNS pH 3.0.

Flow Rate (mL/min)	1.0	1.5	2.0	2.5	3.0
CL signal (mV)*	300	450	760	755	750
Sample volume (µL)	90	180	270	360	450
CL signal (mV)*	250	460	510	500	500
PMT voltage (V)	900	1000	1100	1200	1300
CL signal (mV)*	32	90	250	580	1400
LNS pH	1.0	2.0	3.0	4.0	5.0
CL signal (mV)*	390	410	450	430	400

* Mean of four injections

3.2. Interferences

The effect of foreign metal ions on the determination of Fe(II) was studied by preparing standards at elevated concentrations (compared with typical seawater) in LNS (pH 3.0). The results are shown in Table 2. Cr(III), Ni(II), Pb(II) and Zn(II) had negligible effect, Cu(II) and Mn(II) had a small suppressive effect (similar to that reported previously by O'Sullivan et al. [19]) and Fe(III) and Co(II) had a small positive effect, However, the maximum Co(II) concentration in open sea waters typically range between 100 – 300 pM [22]. If necessary, Fe(III) and Co(II) can be masked by adding desferrioxamine B (1.0 µM, in UHP water) [14] and dimethylglyoxime (100 µM in methanol) [18], respectively, to the luminol stream.

Table 2. Effect of foreign ions on the CL peak response for the determination of Fe(II).

Metal ion	Concentration (nM)	CL signal (mV)*	Conc. (nM)	CL signal (mV)*
LNS	----	6.0 ± 1.0	----	6.0 ± 1.0
Fe(II)	10	24 ± 2.2	10	24 ± 2.2
Fe(III)	10	7.5 ± 1.4	100	9.2 ± 1.3
Co(II)	100	7.8 ± 1.2	1000	9.5 ± 1.5
Cu(II)	100	4.6 ± 1.5	1000	3.2 ± 1.3
Mn(II)	100	3.8 ± 1.0	1000	2.4 ± 0.8
Cr(III)	100	6.8 ± 1.0	1000	7.0 ± 1.2
Ni(II)	100	6.4 ± 1.1	1000	6.8 ± 1.0
Pb(II)	100	6.6 ± 1.0	1000	6.6 ± 1.1
Zn(II)	100	6.7 ± 1.2	1000	7.0 ± 1.0

* Mean of four injections

3.3. Calibration

To obtain the analytical blank for the calibration graph, LNS (pH 5.0), was first passed through a pre-cleaned 8-hydoxyquinoline column (8-HQ, 2.5 mm x 3.0 cm, washed with HCl (0.5 M) for 24 h, followed by a UHP water rinse) [18] at a flow rate of 0.3 mL min^{-1}. Thereafter, the LNS was adjusted to pH 3.0 with HCl (2.0 M) and used as a blank for the proposed FI-CL system. The blank signal was reduced by approximately 50% compared with the signal from untreated LNS at pH 3.0. This residual blank signal is due to (i) release of complexed iron from the seawater matrix on adjusting the pH of the LNS down to 3.0 and (ii) the pH gradient at the sample/carrier stream interface.

Using the optimum conditions described above, the calibration data of CL response versus Fe(II) concentration over the range 2.0 – 10 nM is shown in Table 3. The correlation coefficient was 0.993 (n=5) and the regression equation was $y = 2.65x - 2.10$ [y = CL response (mV), x = concentration (nM)]. The relative standard deviation of the method was 1.0 – 3.7% (n=4) over the range studied. The limit of detection (3 x standard deviation of the blank) was 0.1 nM Fe(II). The time between injection and detection with the optimised system was 12 s, which makes the method suitable for high resolution in situ monitoring of Fe(II) in marine waters.

Table 3. Calibration data (blank value 3.0 mV; all data are blank subtracted).

Iron Standards (nM)	2.0	4.0	6.0	8.0	10.0
CL intensity (mV)*	4.0	8.0	13.0	19.0	25.0
RSD (%)	3.7	2.7	3.7	1.0	1.3

* Mean of four injections

3.5. Accuracy

The accuracy of the proposed method was ascertained by analysing CASS-3 (Coastal Atlantic Surface Seawater) certified sea water obtained from the National Research Council of Canada (Marine Analytical Chemistry Standards Program). This solution was analysed using the proposed FI-CL system after addition of a 100 μM solution of high purity sodium sulphite for 4 h at room temperature (20 °C) and pH 3.0 to reduce Fe(III) into Fe(II). A value of 18.5 ± 5.2 nM was obtained for Fe(II) which is in good agreement with the certified value of 22.56 ± 3.04 nM. CASS-3 was also analysed without the reduction step and gave a result of 16.8 ± 4.5 nM Fe(II) which shows that the majority of the iron in the CRM is in the reduced Fe(II) form.

4. Conclusions

This manual FI-CL method is simple and rapid, with an analysis time of 12 s and a limit of detection of 0.1 nM for Fe(II) in acidified seawater. The method is based on enhancement of the luminol CL reaction with no added oxidant and does not need a preconcentration / matrix removal column.

The method was validated by quantifying total dissolved iron (Fe(II) +Fe(III)) in a certified reference coastal seawater (CASS-3) after reduction with sulphite. The result, 18.5 ± 5.2 nM, was in good agreement with the certified value 22.56 ± 3.04 nM. The speciation of iron in CASS-3 was over 90 % in the Fe(II) form. This method could therefore be used to examine iron speciation in stored, acidified samples as an aid to understanding the mechanisms of iron release from dissolved, colloidal and particulate material.

This method also has the potential to be used for real time Fe(II) monitoring in the field using natural seawater at ambient pH as the carrier stream. The use of a matrix matched carrier stream (after Fe(II) removal) should minimise analytical artefacts caused by mixing gradients at the sample/carrier stream interface.

Acknowledgement

Research was conducted at the School of Environmental Sciences, University of Plymouth, UK, and was supported by the Ministry of Science and Technology, Govt. of Pakistan in the form of a Post Doctoral Fellowship. Support from the EU IRONAGES Project (EVK2-CT1999-00031) is also acknowledged.

References

[1] A. Townshend (Ed) *Encyclopaedia of Analytical Science* Vol. 4, Academic Press, New York, 2369-88 (1995).

[2] M. Brewer and T. Scott (Eds) *Concise Encyclopaedia of Biochemistry*, de Gruyter, New York, 162 & 231 (1983).

[3] W. Davison, *Earth Sci. Rev.*, **34**, 119 (1993).

[4] J. H. Martin, R. M. Gordon and S. Fitzwater, *Nature*, **345**, 156 (1990).

[5] J. H. Martin, *Paleoceanography*, **5**, 1 (1990).

[6] T. M. Florence and G. E. Batley, *CRC Crit. Rev. Anal. Chem*, **9**, 259 (1980).

[7] T. M. Florence, *Talanta*, **29**, 345 (1982).

[8] E. Nakayama, Y. Suzuki, K. Fujiwara and Y. Kitano, *Anal. Sci.*, **5**, 129 (1985).

[9] P. Fletcher, K. N. Andrew, A. C. Calokerinos, S. Forbes and P. J. Worsfold, *Luminescence* **16**, 1 (2001).

[10] Y. F. Mestre, L. L. Zamore and J. M. Calatayud, *Luminescence*, **16**, 213 (2001).

[11] C. Dogeigne and L. T. R. Lejeune, *Talanta*, **50**, 425 (2000).

[12] E. P. Achterberg, T. W. Holland, A. R. Bowie, R. F. C. Mantoura and P. J. Worsfold, *Anal. Chim. Acta*, **442**, 1 (2001).

[13] V. A. Elrod, K. S. Johnson and K. H. Coale, *Anal. Chem.*, **63**, 893 (1991).

[14] S. Hirata, H. Yoshihara and M. Aithara, *Talanta*, **49**, 1059 (1999).

[15] H. Obata, H. Karatani and E. Nakayama, *Anal. Chem.*, **65**, 1524 (1993).

[16] H. Obata, H. Karatani, M. Matsui and E. Nakayama, *Mar. Chem.*, **56**, 97 (1997).

[17] R. T. Powell, D. W. King, W. M. Landing, *Mar. Chem.*, **50**, 13 (1995).

[18] A. R. Bowie, E. P. Achterberg, R. F. C. Mantoura and P. J. Worsfold, *Anal. Chim. Acta.*, **361**, 189 (1998).

[19] D. W. O'Sullivan, A. K. Hanson and D. R. Kester, *Mar. Chem.*, **49**, 65 (1995).

[20] D. W. King, H. A. Lounsbury and F. J. Millero, *Environ. Sci. Technol.*, **29**, 818 (1995).

[21] P. L. Croot and P. Laan, *Anal. Chim. Acta.*, **466**, 261 (2002).

[22] C. M. Sakamoto-Arnold, K. S. Johnson, *Anal. Chem.*, **59**, 1789 (1987).